NASA TECHNICAL NOTE

NASA TN D-8474

NASA TN D-8474

EFFECT OF WINGLETS ON A FIRST-GENERATION JET TRANSPORT WING

II - Pressure and Spanwise Load Distributions for a Semispan Model at High Subsonic Speeds

Lawrence C. Montoya
Dryden Flight Research Center
Edwards, Calif. 93523

and

Stuart G. Flechner and Peter F. Jacobs
Langley Research Center
Hampton, Va. 23665

NATIONAL AERONAUTICS AND SPACE ADMINISTRATION • WASHINGTON, D. C. • JULY 1977

1 Report No	2 Government Accession No	3 Recipient's Catalog No
NASA TN D-8474		

4 Title and Subtitle	5 Report Date
EFFECT OF WINGLETS ON A FIRST-GENERATION JET TRANSPORT WING. II - PRESSURE AND SPANWISE LOAD DISTRIBUTIONS FOR A SEMISPAN MODEL AT HIGH SUBSONIC SPEEDS	July 1977
	6 Performing Organization Code

7 Author(s)	8 Performing Organization Report No
Lawrence C. Montoya (Dryden Flight Research Center), Stuart G. Flechner, and Peter F. Jacobs (Langley Research Center)	L-11026
	10 Work Unit No
	505-11-16-08
9 Performing Organization Name and Address	11 Contract or Grant No
NASA Langley Research Center Hampton, VA. 23665	
	13 Type of Report and Period Covered
	Technical Note
12 Sponsoring Agency Name and Address	14 Sponsoring Agency Code
National Aeronautics and Space Administration Washington, D.C. 20546	

15 Supplementary Notes

16. Abstract

Pressure and spanwise load distributions on a first-generation jet transport semispan model at high subsonic speeds are presented. The data are given for the basic wing and for configurations with an upper winglet only, upper and lower winglets, and a simple wing-tip extension. Selected data are discussed to show the general trends and effects of the various configurations.

17 Key Words (Suggested by Author(s))	18 Distribution Statement
Winglets Pressure distributions Spanwise load distribution	Unclassified - Unlimited Subject Category 02

19 Security Classif. (of this report)	20 Security Classif. (of this page)	21 No. of Pages	22 Price*
Unclassified	Unclassified	209	$7.75

* For sale by the National Technical Information Service, Springfield, Virginia 22161

EFFECT OF WINGLETS ON A FIRST-GENERATION JET TRANSPORT WING

II - PRESSURE AND SPANWISE LOAD DISTRIBUTIONS FOR A SEMISPAN MODEL AT HIGH SUBSONIC SPEEDS

Lawrence C. Montoya
Dryden Flight Research Center

Stuart G. Flechner and Peter F. Jacobs
Langley Research Center

SUMMARY

Pressure and spanwise load distributions on a first-generation jet transport semispan model at high subsonic speeds are presented. The data were measured for the basic wing and for configurations with an upper winglet only, upper and lower winglets, and a simple wing-tip extension. Selected data are discussed to show the general trends and effects for the various configurations. The results show that the winglets mainly affected the pressure distributions on the outboard region of the wing near the tip. In general, the wing pressure coefficients become more negative on the aft region of the upper surface and more positive on the lower surface because of the winglets. At high angles of attack the winglet configurations show good trailing-edge pressure recovery near the wing tip, whereas the basic-wing configuration shows poor recovery. With the lower winglet on, the high induced velocities on the upper surface of the upper winglet near the leading edge are reduced, which in turn reduced the effects of the upper winglet on the wing. The effects of the lower winglet become more pronounced at high angles of attack and Mach numbers. The winglet and tip-extension configurations increased the loads near the wing tip and resulted in approximately the same root bending moment at the wing-fuselage juncture.

INTRODUCTION

Winglets, as described in reference 1, are intended to provide reductions in drag coefficient, at cruise conditions, substantially greater than those obtained with a simple wing-tip extension, which has been designed to impose the same bending increments on the wing structure as the winglets. The National Aeronautics and Space Administration has been conducting extensive experimental investigations of the effects of winglets on jet transport wings at high subsonic Mach numbers. (See refs. 2 and 3.)

This investigation was conducted to determine the effects of winglets and a simple wing-tip extension on the longitudinal aerodynamic characteristics, surface static-pressure distributions, and cross-flow velocities behind the wing tip of a first-generation jet transport. This paper, which is one of a series,

presents wing and winglet chordwise pressure distributions and spanwise loadings at high subsonic speeds only. Longitudinal aerodynamic characteristics and cross-flow velocities are presented in reference 4. Chordwise pressure and spanwise load distributions for the wing and winglets at a Mach number of 0.30 are presented in reference 5. Results are given herein for the basic wing and configurations with an upper winglet, upper and lower winglets, and a simple wing-tip extension.

Data are presented for wind-tunnel free-stream Mach numbers of 0.70, 0.75, 0.78, and 0.80 at a constant free-stream dynamic pressure of 41 kPa (850 psf) and an angle-of-attack range from about 0° to 7°. The Reynolds number varied slightly from 18.67×10^6 per m (5.69×10^6 per ft) at Mach 0.70 to 16.90×10^6 per m (5.15×10^6 per ft) at Mach 0.80.

SYMBOLS

Force and moment data have been reduced to coefficient form based on the exposed trapezoidal area of the basic wing. All dimensional values are given in both the International System of Units (SI) and U.S. Customary Units (ref. 6). All measurements and calculations were made in U.S. Customary Units.

Coefficients and symbols used herein are defined as follows:

b' exposed semispan of wing with basic tip, 124.26 cm (48.92 in.)

$\Delta b'$ incremental increase in exposed wing semispan (tip extension), 0.38 of span of upper winglet, 7.62 cm (3.00 in.)

c local chord, cm (in.)

$\bar{c}$ mean geometric chord of exposed basic wing, 39.98 cm (15.74 in.)

c_{av} average chord of exposed basic wing, S/b', 37.41 cm (14.73 in.)

c_t tip chord of basic wing, cm (in.)

$C_{B'}$ bending-moment coefficient of wing at wing-fuselage juncture, Bending moment/$q_\infty Sb'$

C_L lift coefficient, Lift/$q_\infty S$

C_m pitching-moment coefficient

C_N normal-force coefficient obtained from integration of spanwise load distribution

c_n section normal-force coefficient obtained from integration of pressure measurements

C_p pressure coefficient, $(p_l - p_\infty)/q_\infty$

$C_{p,sonic}$ pressure coefficient corresponding to local speed of sound

h span of upper winglet from chord plane of wing tip (see fig. 2(b)), cm (in.)

i incidence of winglet measured from free-stream direction, positive with leading edge inward for upper winglet, outward for lower winglet (see fig. 2(b)), deg

M_∞ free-stream Mach number

p_l local static pressure, Pa (psf)

p_∞ free-stream static pressure, Pa (psf)

q_∞ free-stream dynamic pressure, Pa (psf)

R Reynolds number per unit length, per m (per ft)

S exposed trapezoidal area of basic wing, 0.4648 m^2 (5.0034 ft^2)

x chordwise distance from leading edge, positive aft, cm (in.)

y spanwise distance from wing-fuselage juncture, positive outboard, cm (in.)

z vertical coordinate of airfoil, positive upward, cm (in.)

z' distance along winglet span from chord plane of wing, cm (in.)

α angle of attack, deg

η exposed wing semispan station (based on basic-wing panel), y/b'

Subscript:

basic reference configuration, model with no wing-tip devices

Abbreviations:

L.S. lower surface

U.S. upper surface

EXPERIMENTAL APPARATUS AND PROCEDURES

Test Facility

This investigation was conducted in the Langley 8-foot transonic pressure tunnel, a continuous single-return tunnel with a slotted rectangular test section. The longitudinal slots in the floor and ceiling of the test section

reduce tunnel wall interference and allow relatively large models to be tested through the subsonic speed range. Controls are available to permit independent variation of Mach number, stagnation pressure, temperature, and dew point. A more detailed description of the wind tunnel is given in reference 7.

Model Description

To obtain the highest possible winglet Reynolds number and sufficient winglet size in which to install surface pressure measurement tubes, a semispan model was utilized. The 0.07-scale semispan model used in this investigation was of the KC-135A transport aircraft. Photographs of the model in the wind tunnel are shown in figure 1, and drawings of the model in figure 2.

Fuselage.- The fuselage contours closely simulate the full-scale fuselage shape, with the exception of the wheel-well area. An enlargement of this area was necessary to enclose the model mounting apparatus. The fuselage midsection covers the balance and has a slot through which the wing protrudes. The fuselage is not attached to the balance, but it does rotate with the wing through the angle-of-attack range.

Wing.- The basic wing of the KC-135A model has 7° dihedral and 2° of incidence at the root chord. The wing has no geometric twist. A typical outboard airfoil section is shown in figure 3, with its coordinates presented in table I. The wing thickness ratio varies nonlinearly from 15 percent at the wing-fuselage juncture to 9 percent at the trailing-edge break and then remains constant at 9 percent to the wing tip. The trapezoidal planform of the total wing (extended to the fuselage center line) has a sweep at the quarter-chord of 35°, an aspect ratio of 7.0, and a taper ratio of 0.35. For all data analysis, the reference geometry parameters S, b', $\bar{c}$, and c_{av} are based on the exposed trapezoidal planform of the basic wing. The model wing stiffness was designed so that the relative model bending deflection at the tip was approximately the same as that for the actual airplane at cruise conditions.

Nacelles.- Flow-through nacelles were used with an inlet diameter of 5.64 cm (2.22 in.) and exit diameter of 3.45 cm (1.36 in.). The inlet diameter was maintained back to approximately 0.66 of the nacelle length and then tapered linearly to the exit.

Tip extension.- The 7.62-cm (3.00-in.) wing-tip extension (fig. 2(a)) had the same coordinates as the outboard wing section. The span was estimated so that the tip extension produced essentially the same increments in bending moment at the wing-fuselage juncture as the winglets.

Winglets.- The winglet configuration investigated were based on the design approach described in reference 1. A detailed drawing of the winglets used in this investigation is presented in figure 2(b). The winglets employed an 8-percent-thick general aviation airfoil. Winglet airfoil coordinates are presented in table II.

The upper winglet has a span equal to the wing-tip chord, a root chord equal to 65 percent of the wing-tip chord, a leading-edge sweep of 38°, a taper

ratio of 0.32, and an aspect ratio of 2.33. The planform area of the upper winglet is 3.8 percent of the exposed trapezoidal planform area of the basic wing. The upper winglet is canted outboard 15° from vertical (75° dihedral) and toed out 4° (leading edge outboard) relative to the fuselage center line. The upper winglet is untwisted and therefore has constant negative geometric incidence across its span. The "upper surface" of the upper winglet is the inboard surface.

The lower winglet has a span equal to 23 percent of the wing-tip chord, a root chord equal to 40 percent of the wing-tip chord, a leading-edge sweep of 52°, a taper ratio of 0.40, and an aspect ratio of 0.82. The planform area of the lower winglet is 0.6 percent of the exposed trapezoidal planform area of the basic wing. The lower winglet is canted outboard from vertical 36° (54° anhedral) and toed in 7° (trailing edge outboard for negative incidence) relative to the fuselage center line. The lower winglet was twisted about its leading edge with 4° washout at the tip. The "upper surface" of the lower winglet is the outboard surface.

To smooth the transition from the wing to the winglets, fillets were added to the inside corners at those junctures and the outside corners were rounded.

Boundary-Layer Transition Strips

Boundary-layer transition strips were placed on both surfaces of the wing and winglets. These strips were comprised of a 0.159-cm (0.06-in.) wide band of carborundum grains sized on the basis of reference 8 and set in a plastic adhesive. The transition strip patterns for the wing and winglets are shown in figure 4.

The transition strips on the lower surface of the winglets were located rearward in an attempt to simulate full-scale Reynolds number boundary-layer conditions. (See ref. 9.) The strips on the upper surface of the winglets were located forward to insure transition ahead of the shock wave for the various test conditions.

The fluorescent-oil-film flow-visualization technique described in reference 10 was employed to verify the presence of laminar flow ahead of the transition strip.

Test Conditions

Measurements were taken at Mach numbers of 0.70, 0.75, 0.78, and 0.80 with the model angle of attack ranging from approximately 0° to 7°. During the tests stagnation temperature was maintained at 322 K (120° F), and the air was dried until the dew point was sufficiently low to prevent condensation effects. The Reynolds numbers and dynamic pressures at which the data were obtained are presented in the following table:

M_∞	R		q_∞	
	per m	per ft	kPa	psf
0.70	18.67×10^6	5.69×10^6	41	850
.75	17.72	5.40	41	850
.78	17.22	5.25	41	850
.80	16.90	5.15	41	850

Measurements

Force and moment data were obtained using a five-component electrical strain-gage balance. Side-force measurements were not taken. An accelerometer attached to the wing mounting block inside the fuselage was used to measure angle of attack.

Chordwise static-pressure distributions were measured at the 0.26, 0.77, 0.92, and 0.99 semispan stations of the basic wing (fig. 5(a)). In addition, they were measured at three stations on the upper winglet and at one station on the lower winglet (fig. 5(b)), for the respective wing-tip configurations. These stations were located at 0.15, 0.50, and 0.80 of the upper-winglet span and at 0.50 of the lower-winglet span, which correspond, respectively, to the 1.01, 1.03, 1.05, and 1.01 wing semispan stations. (Note that semispan stations are defined as a fraction of the distance from the wing-fuselage juncture to the tip of the basic wing panel. As the upper and lower winglets extend beyond this distance, semispan stations can be greater than 1.0). The wing and winglet pressures were measured with pressure-scanning valves. The range of the pressure sensors in the valves was sized for the upper or lower wing or winglet surfaces and wind-tunnel test conditions.

Wing-tip deflections were determined from photographs of a chordwise line on the edge of the wing tip and are shown in figure 6.

Corrections

The slotted wind-tunnel test section is designed to reduce wall effects on lift. Data from this investigation show that the wing spanwise load distributions for all configurations at the same conditions are nearly identical over the major portion of the span. Therefore, wall effects on wing lift can be considered systematic, and no correction is made to the data for these effects. The wing semispan and the model frontal area were sufficiently small (1.5 percent of the test-section cross-sectional area) to avoid having to correct Mach number for wind-tunnel blockage effects (ref. 11). The angle of attack of the model was corrected for flow angularity in the wind tunnel.

PRESENTATION OF RESULTS

The results of this investigation are presented in the following figures:

DISCUSSION OF RESULTS

The discussion presented herein is limited to a few selected cases. The data discussed are considered to show trends which are generally representative of the various configurations. The data presented at $M_\infty = 0.78$ and $\alpha = 2.5^\circ$ are at the design cruise conditions of the basic wing.

Throughout the figures of this paper, an effort has been made to retain a particular symbol with each of the four configurations tested (basic wing, upper winglet, upper and lower winglets, and tip extension). This practice is intended to facilitate identification of a particular set of data. Also, for the pressure distributions (figs. 8 to 11), the configuration is indicated at the top of each page.

In figure 12, comparisons of the chordwise pressure distributions for the upper-winglet and basic-tip configurations are presented for two angles of attack at two Mach numbers. The comparison at $M_\infty = 0.70$ and $\alpha = 2.5^\circ$ (fig. 12(a)) shows no difference in the C_p variation for the two configurations at the two inboard wing stations but slightly more negative pressure coefficients on the wing upper surface for the upper-winglet configuration at $\eta = 0.92$. At the tip station ($\eta = 0.99$), the upper-winglet configuration has more negative pressure coefficients on the aft region of the wing upper surface and more positive pressure coefficients on the wing lower surface, with good pressure recovery ($C_p \approx 0$) at the trailing edge. At $\eta = 0.99$, the more negative pressure coefficients on the wing upper surface begin at about $x/c = 0.4$,

which is the approximate location of the intersection of the upper-winglet leading edge with the wing upper surface.

Figure 12(b) compares the data at $M_\infty = 0.70$ and $\alpha = 7.2^\circ$ and shows trends similar to those for $\alpha = 2.5^\circ$, with the exception of the trailing-edge pressure coefficients at $\eta = 0.99$. The data show that the basic wing has poor trailing-edge pressure recovery, while the upper-winglet configuration has good pressure recovery. Because the basic-tip configuration indicates good pressure recovery at $\eta = 0.92$, the poor recovery for this configuration at $\eta = 0.99$ is apparently due to vortex formation at the wing tip, which causes the pressure coefficients on the aft portion of the upper surface of the basic wing tip to become more negative. The upper winglet prevents this influence of the tip vortex on the upper-surface pressures, allowing the pressures to recover near the wing tip.

Comparison of figures 12(c) and 12(d) for $M_\infty = 0.78$ shows that the trends are similar to those at $M_\infty = 0.70$, with the exception that pressure coefficients indicate flow separation at the trailing edge of the basic configuration at $\eta = 0.92$ and $\alpha = 7.2^\circ$.

A comparison of the wing pressure distributions for the upper-winglet and upper-and-lower-winglet configurations is presented in figure 13. At $M_\infty = 0.70$ and $\alpha = 2.5^\circ$ (fig. 13(a)), the data show that the pressure coefficients for the two configurations are generally similar except at the tip station where the upper-and-lower-winglet configuration shows slightly higher pressure coefficients. The winglet pressure coefficients show that there are essentially no differences in the data except near the leading edge of the upper winglet at $\eta = 1.01$. The less negative pressure coefficients for the upper-and-lower-winglet configuration at $\eta = 1.01$ are due to the lower winglet reducing the high induced velocities on the inboard region of the upper surface of the upper winglet. At $\alpha \approx 7.2^\circ$ (fig. 13(b)), the wing pressure coefficients at $\eta = 0.99$ for the upper-and-lower-winglet configuration are more positive on the wing lower surface near the leading edge and less negative on the center portion of the wing upper surface than those for the upper winglet alone. The winglet pressure coefficients for $\alpha \approx 7.2^\circ$ show trends similar to those at $\alpha = 2.5^\circ$ in that the leading-edge pressure coefficients on the upper winglet are less negative with the lower winglet on.

Comparison of figures 13(c) and 13(d) shows that the data for $M_\infty = 0.78$ have the same trends as those for $M_\infty = 0.70$ (figs. 13(a) and 13(b)) with the exception that the upper-and-lower-winglet configuration has larger reductions of the high negative pressure coefficients on the aft portion of the wing upper surface at $\alpha \approx 7.2^\circ$. The pressure coefficients for the upper winglet (fig. 13(d)) show larger reductions due to installation of the lower winglet than those noted in figures 13(a), 13(b), and 13(c). Thus, the effect of the lower winglet becomes more pronounced at higher angles of attack and Mach numbers.

The comparison of the wing spanwise load distributions at the design cruise conditions of $M_\infty = 0.78$ and $\alpha = 2.5^\circ$, presented in figure 14(o), is used to discuss the general effects of the various configurations on the span loads. As is shown, the winglets and tip extension increase the wing loads near the tip.

These increased loads resulted in about 3.2-percent increase in bending-moment increment at the wing-fuselage juncture for the upper-winglet configuration and about 3.5 percent for the upper-and-lower-winglet and tip-extension configurations, as shown in figure 15 which was obtained from reference 1. The similar bending-moment increments between the winglet and tip-extension configurations were expected since the length of the tip extension was estimated to give the same increment in bending moment as the winglet configurations.

The winglet spanwise loads show slightly lower values on the inboard region of the upper winglet with the lower winglet installed. The integrated winglet spanwise loads have shown (fig. 16, taken from ref. 1) that the normal-force coefficients are nearly the same as the wing lift coefficients from the design lift coefficient to the lift coefficients at which the angle-of-attack and pitching-moment curves break. (See fig. 7.)

SUMMARY OF RESULTS

A wind-tunnel investigation of winglets mounted on the tip of a 0.07-scale KC-135A jet transport model wing has been conducted. Wing and winglet pressure and spanwise load distributions at high subsonic speeds have been presented for the basic wing and configurations with an upper winglet only, upper and lower winglets, and a simple wing-tip extension. An analysis of selected data which are considered to be representative of general trends for the various configurations tested indicate the following:

1. The winglets mainly affect the pressure distributions on the wing near the tip. In general, the wing pressure coefficients were more negative on the aft region of the upper surface and more positive on the lower surface.

2. The trailing-edge pressure coefficients at the wing tip show good pressure recovery for the winglet configurations but poor recovery for the basic-wing configuration at high angles of attack.

3. The lower winglet reduced the high induced velocities on the upper surface of the upper winglet near the leading edge which in turn reduced the effect of the upper winglet on the wing. The effects of the lower winglet were more pronounced at high angles of attack and Mach numbers.

4. The winglets and tip extension increased the wing loads near the tip, which resulted in approximately the same root bending moment at the wing-fuselage juncture, as expected.

Langley Research Center
National Aeronautics and Space Administration
Hampton, VA 23665
April 18, 1977

REFERENCES

1. Whitcomb, Richard T.: A Design Approach and Selected Wind-Tunnel Results at High Subsonic Speeds for Wing-Tip Mounted Winglets. NASA TN D-8260, 1976.

2. Flechner, Stuart G.; Jacobs, Peter F.; and Whitcomb, Richard T.: A High Subsonic Speed Wind-Tunnel Investigation of Winglets on a Representative Second-Generation Jet Transport Wing. NASA TN D-8264, 1976.

3. Jacobs, Peter F.; and Flechner, Stuart G.: The Effect of Winglets on the Static Aerodynamic Stability Characteristics of a Representative Second Generation Jet Transport Model. NASA TN D-8267, 1976.

4. Jacobs, Peter F.; Flechner, Stuart G.; and Montoya, Lawrence C.: Effect of Winglets on a First-Generation Jet Transport Wing. I - Longitudinal Aerodynamic Characteristics of a Semispan Model at Subsonic Speeds. NASA TN D-8473, 1977.

5. Montoya, Lawrence C.; Jacobs, Peter F.; and Flechner, Stuart G.: Effect of Winglets on a First-Generation Jet Transport Wing. III - Pressure and Spanwise Load Distributions for a Semispan Model at Mach 0.30. NASA TN D-8478, 1977.

6. Mechtly, E. A.: The International System of Units - Physical Constants and Conversion Factors (Second Revision). NASA SP-7012, 1973.

7. Schaefer, William T., Jr.: Characteristics of Major Active Wind Tunnels at the Langley Research Center. NASA TM X-1130, 1965.

8. Braslow, Albert L.; and Knox, Eugene C.: Simplified Method for Determination of Critical Height of Distributed Roughness Particles for Boundary-Layer Transition at Mach Numbers From 0 to 5. NACA TN 4363, 1958.

9. Blackwell, James A., Jr.: Preliminary Study of Effects of Reynolds Number and Boundary-Layer Transition Location on Shock-Induced Separation. NASA TN D-5003, 1969.

10. Loving, Donald L.; and Katzoff, Samuel: The Fluorescent-Oil Film Method and Other Techniques for Boundary-Layer Flow Visualization. NASA MEMO 3-17-59L, 1959.

11. Brooks, Joseph D.: Some Anomalies Observed in Wind-Tunnel Tests of a Blunt Body at Transonic and Supersonic Speeds. NASA TN D-8237, 1976.

TABLE I.- COORDINATES OF TYPICAL OUTBOARD WING SECTION

[Wing section at 2° incidence]

Upper surface		Lower surface	
x/c	z/c	x/c	z/c
0	0	0	0
.0011	.0042	.0020	-.0054
.0022	.0056	.0035	-.0063
.0034	.0071	.0061	-.0073
.0058	.0090	.0092	-.0081
.0095	.0116	.0201	-.0097
.0132	.0136	.0391	-.0116
.0180	.0161	.0631	-.0139
.0234	.0186	.0950	-.0168
.0324	.0221	.1016	-.0174
.0415	.0253	.1445	-.0212
.0536	.0291	.1826	-.0245
.0716	.0338	.2235	-.0284
.0897	.0377	.2597	-.0314
.0990	.0394	.2950	-.0341
.1132	.0417	.3326	-.0366
.1408	.0454	.3726	-.0391
.1589	.0471	.4276	-.0418
.1740	.0483	.4690	-.0429
.1861	.0492	.5110	-.0433
.2011	.0501	.5560	-.0430
.2192	.0510	.5967	-.0424
.2342	.0516	.6386	-.0414
.2584	.0522	.6818	-.0406
.3432	.0522	.7243	-.0397
.3729	.0524	.7620	-.0389
.4090	.0513	.7951	-.0381
.4572	.0489	.8308	-.0377
.5054	.0454	.8662	-.0371
.5416	.0420	.9029	-.0363
.5897	.0367	.9392	-.0358
.6379	.0304	.9790	-.0348
.6862	.0226	.9999	-.0350
.7343	.0153		
.7582	.0108		
.7823	.0065		
.8040	.0027		
.8344	-.0023		
.8642	-.0076		
.8874	-.0119		
.9223	-.0180		
.9492	-.0229		
.9718	-.0269		
.9920	-.0308		
1.0001	-.0347		

TABLE II.- AIRFOIL COORDINATES FOR WINGLETS

x/c	z/c for -	
	Upper surface	Lower surface
0	0	0
.0020	.0077	-.0032
.0050	.0119	-.0041
.0125	.0179	-.0060
.0250	.0249	-.0077
.0375	.0296	-.0090
.0500	.0333	-.0100
.0750	.0389	-.0118
.1000	.0433	-.0132
.1250	.0469	-.0144
.1500	.0499	-.0154
.1750	.0525	-.0161
.2000	.0547	-.0167
.2500	.0581	-.0175
.3000	.0605	-.0176
.3500	.0621	-.0174
.4000	.0628	-.0168
.4500	.0627	-.0158
.5000	.0618	-.0144
.5500	.0599	-.0122
.5750	.0587	-.0106
.6000	.0572	-.0090
.6250	.0554	-.0071
.6500	.0533	-.0052
.6750	.0508	-.0033
.7000	.0481	-.0015
.7250	.0451	.0004
.7500	.0419	.0020
.7750	.0384	.0036
.8000	.0349	.0049
.8250	.0311	.0060
.8500	.0270	.0065
.8750	.0228	.0064
.9000	.0184	.0059
.9250	.0138	.0045
.9500	.0089	.0021
.9750	.0038	-.0013
1.0000	-.0020	-.0067

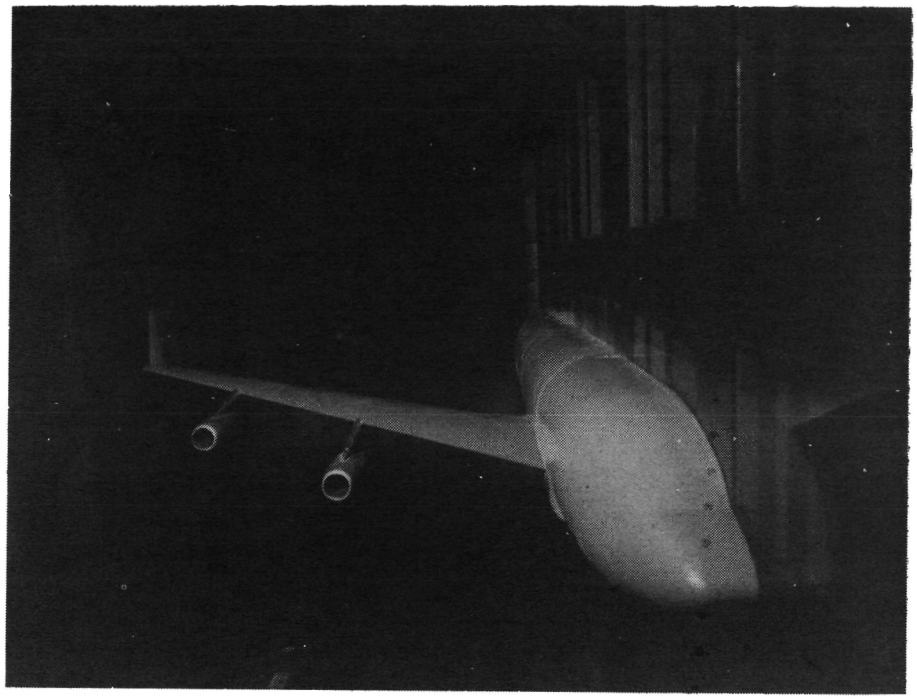

L-75-8430

(a) Complete configuration.

L-75-8429

(b) Winglets.

Figure 1.- Photographs of model.

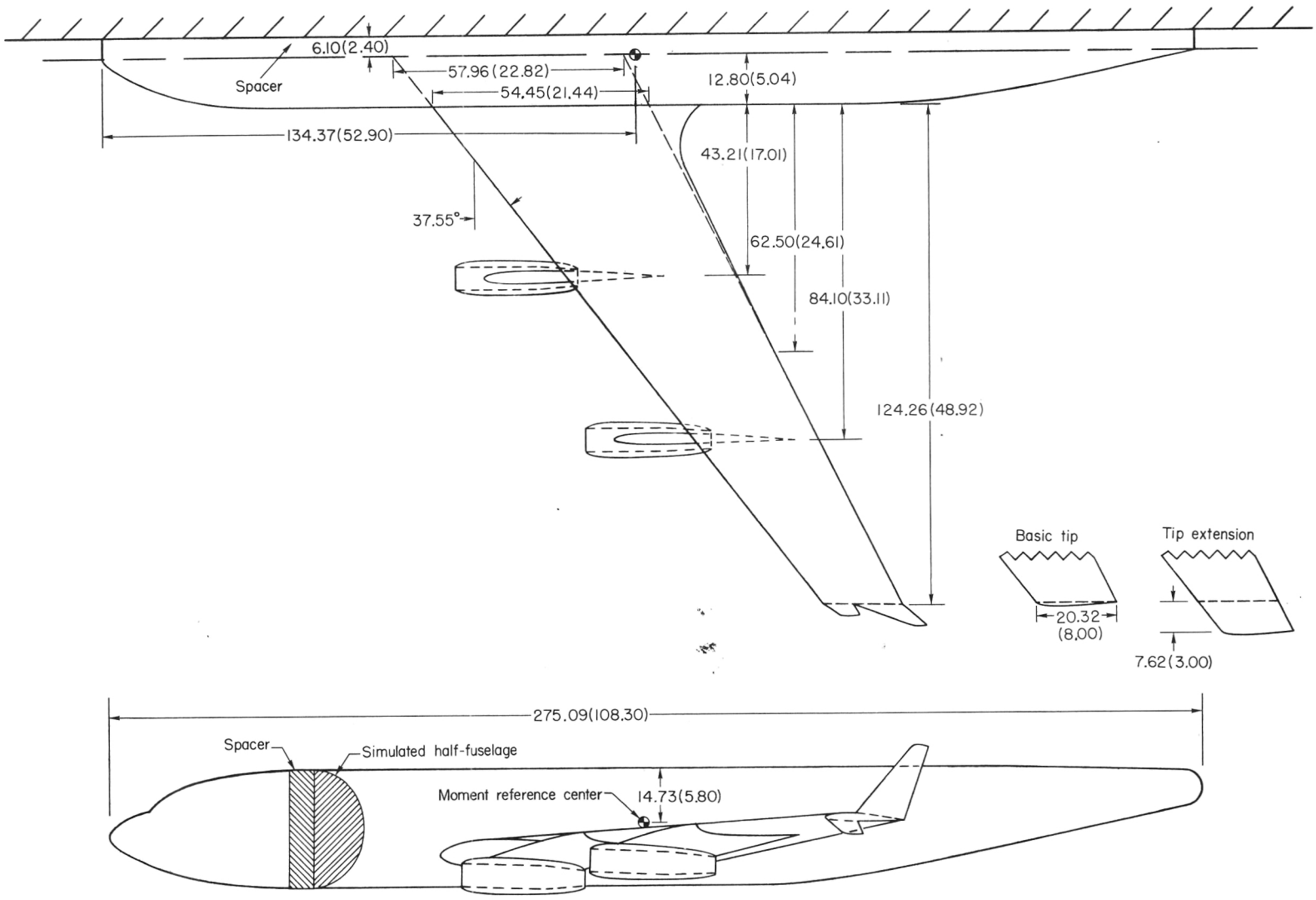

(a) General layout of model.

Figure 2.- Drawings of semispan model. Dimensions in centimeters (inches).

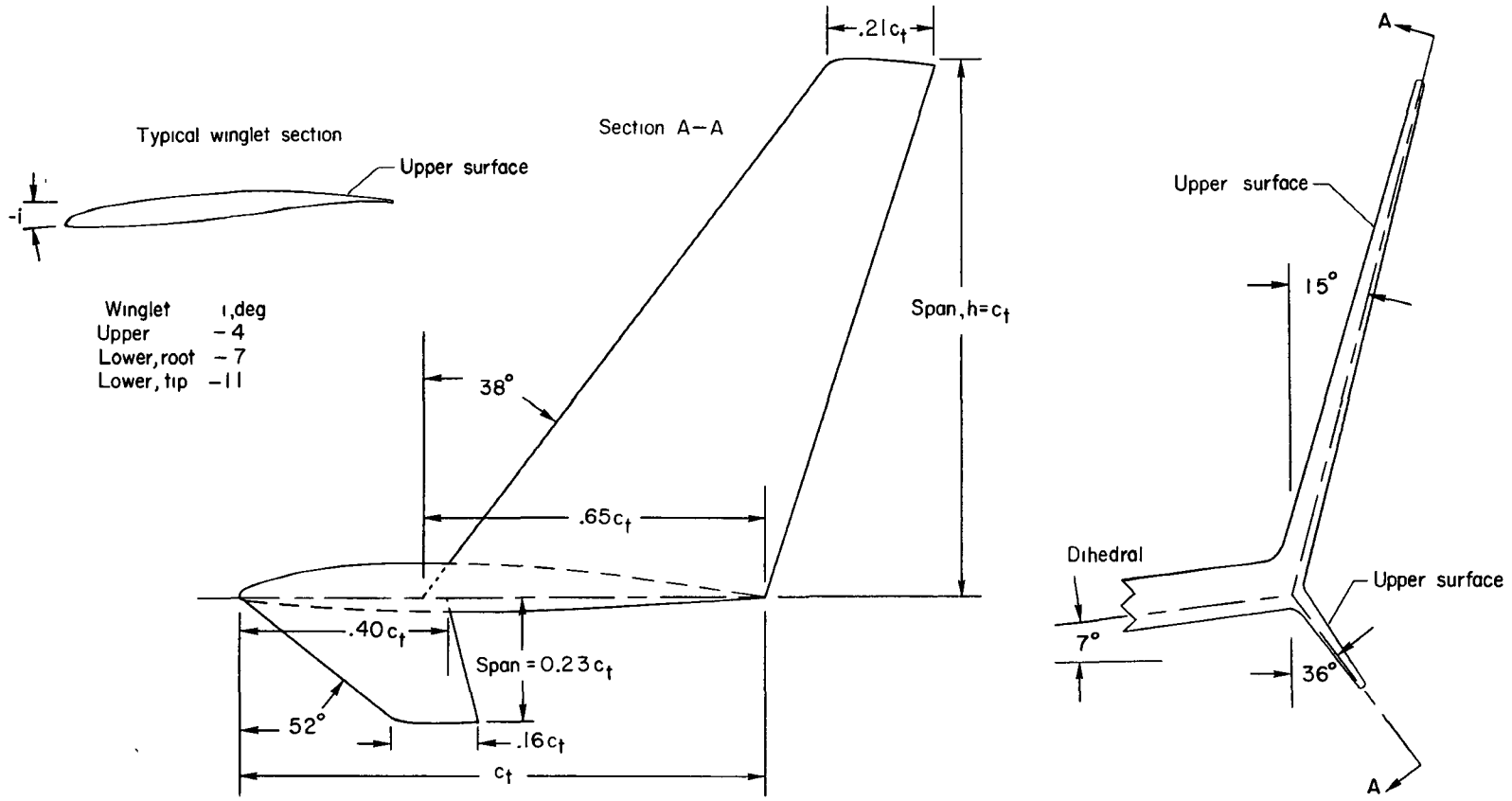

(b) Winglet details.

Figure 2.- Concluded.

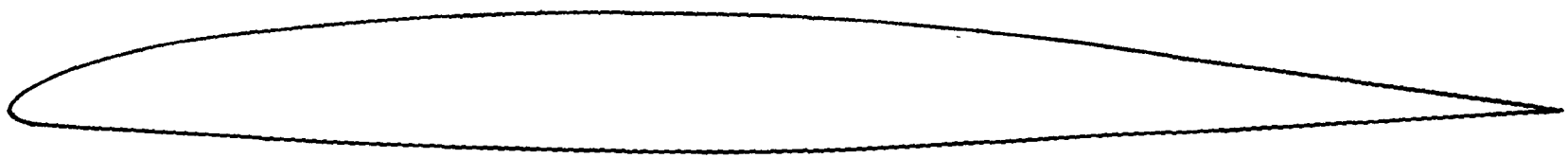

Figure 3.- Typical outboard wing airfoil section.

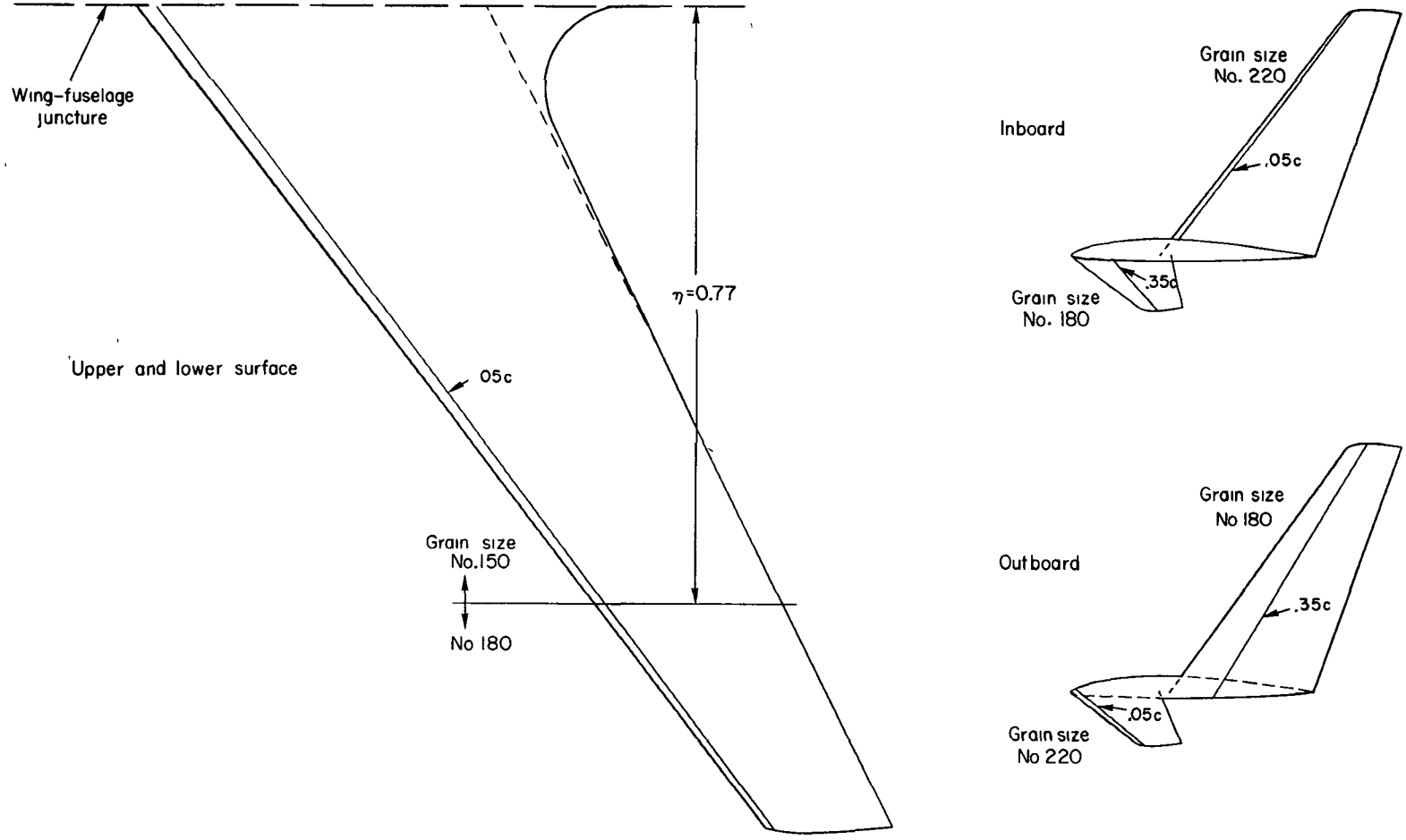

Figure 4.- Locations of boundary-layer transition strips.

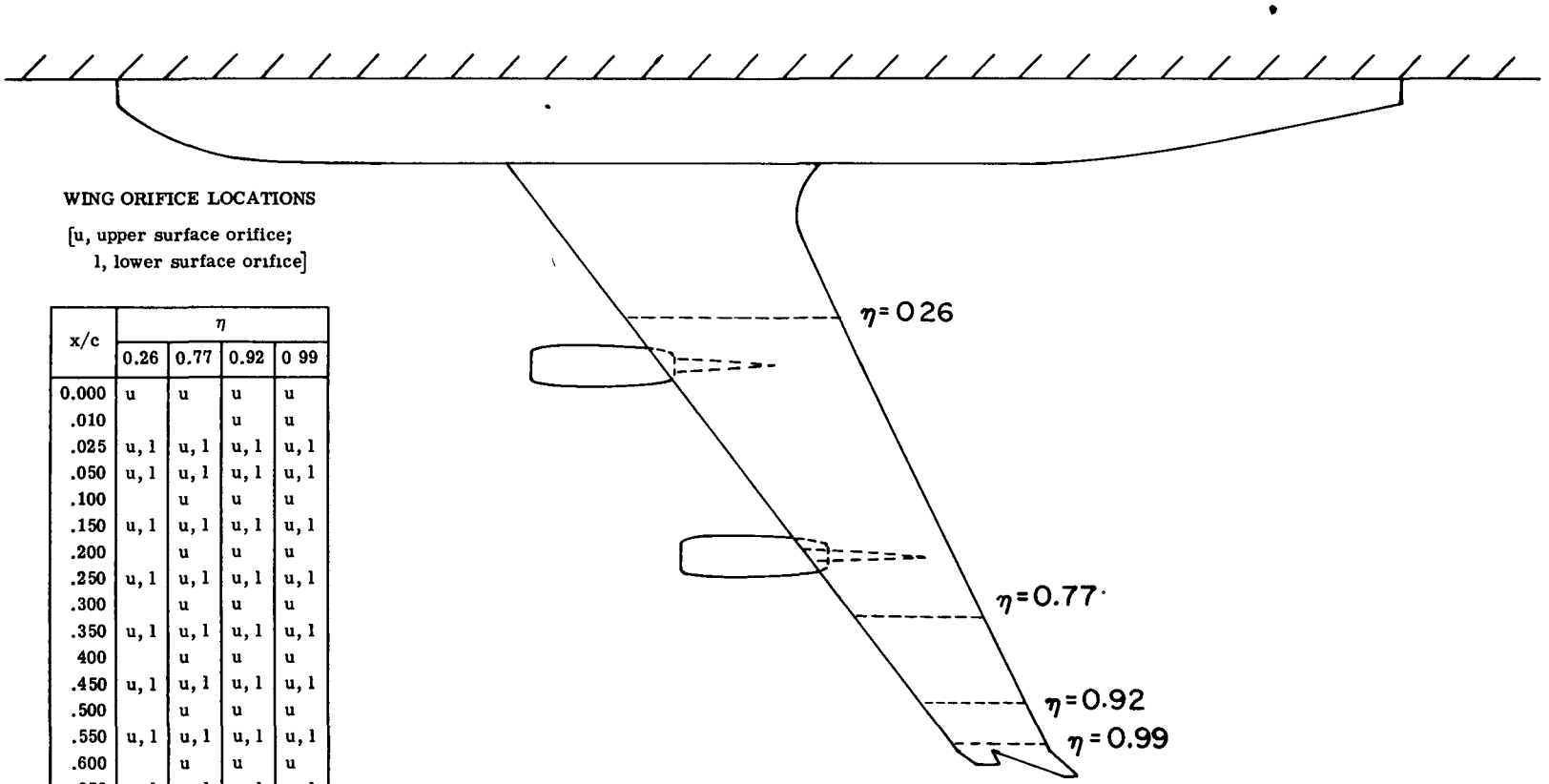

WING ORIFICE LOCATIONS

[u, upper surface orifice;
l, lower surface orifice]

x/c	η			
	0.26	0.77	0.92	0 99
0.000	u	u	u	u
.010			u	u
.025	u, l	u, l	u, l	u, l
.050	u, l	u, l	u, l	u, l
.100		u	u	u
.150	u, l	u, l	u, l	u, l
.200		u	u	u
.250	u, l	u, l	u, l	u, l
.300		u	u	u
.350	u, l	u, l	u, l	u, l
400		u	u	u
.450	u, l	u, l	u, l	u, l
.500		u	u	u
.550	u, l	u, l	u, l	u, l
.600		u	u	u
.650	u, l	u, l	u, l	u, l
.700		u	u	u
.750	u, l	u, l	u, l	u, l
.800		u	u	
.850	u	u, l	u, l	u, l
.900		u	u	u
.950	u, l	u, l	u, l	u, l

(a) On wing.

Figure 5.- Wing and winglet static-pressure orifice locations.

WINGLET ORIFICE LOCATIONS

[u, upper surface orifice;
l, lower surface orifice]

x/c	η			
	Upper winglet			Lower winglet
	1.01	1.03	1.05	1.01
0.000	u	u	u	u
.020	u, l	u, l	u, l	u, l
.050	u, l	l	u, l	u, l
.150	u, l	u, l	u, l	u, l
.250	u, l	u, l	u, l	u, l
.350	u, l	u	u, l	u, l
.450	u, l	u, l	u, l	u, l
.550	u, l	u, l	u, l	u, l
.650	u, l	u, l	u, l	u, l
.750	u, l	u, l	u, l	u, l
.850	u, l	u, l	u, l	u, l
.950	u, l	u, l	u, l	u, l

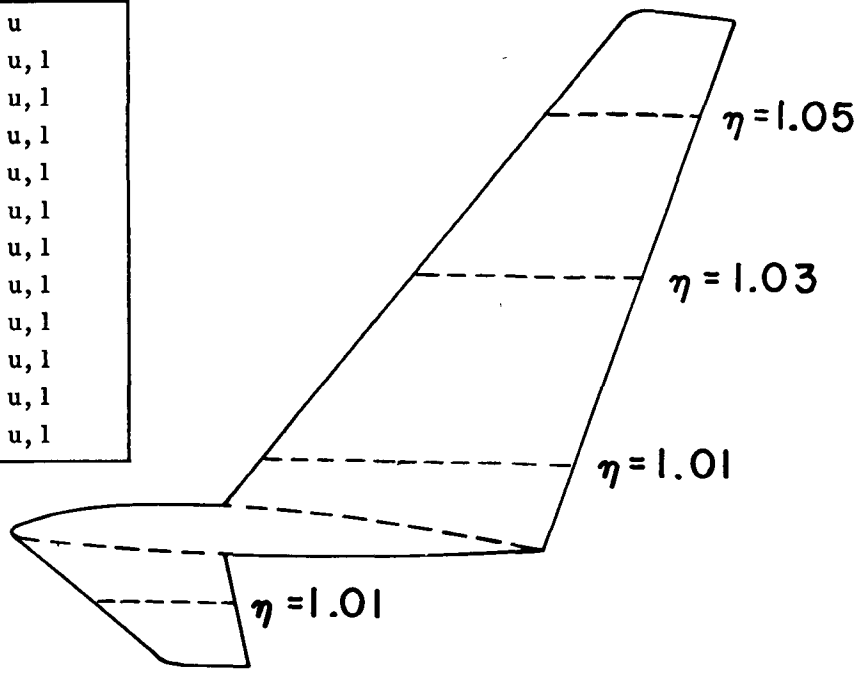

(b) On winglets.

Figure 5.- Concluded.

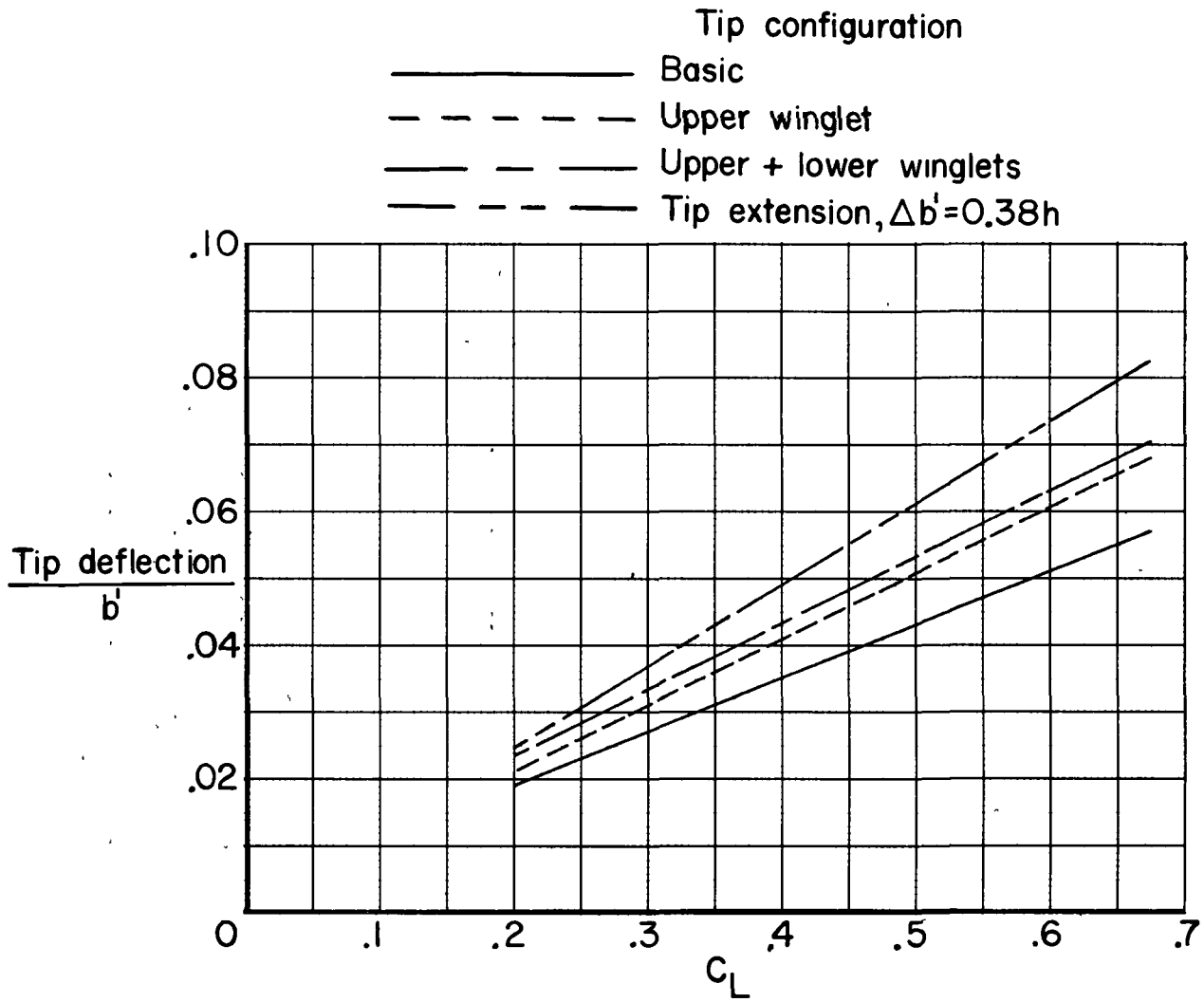

(a) $M_\infty = 0.70$.

Figure 6.- Wing-tip deflections.

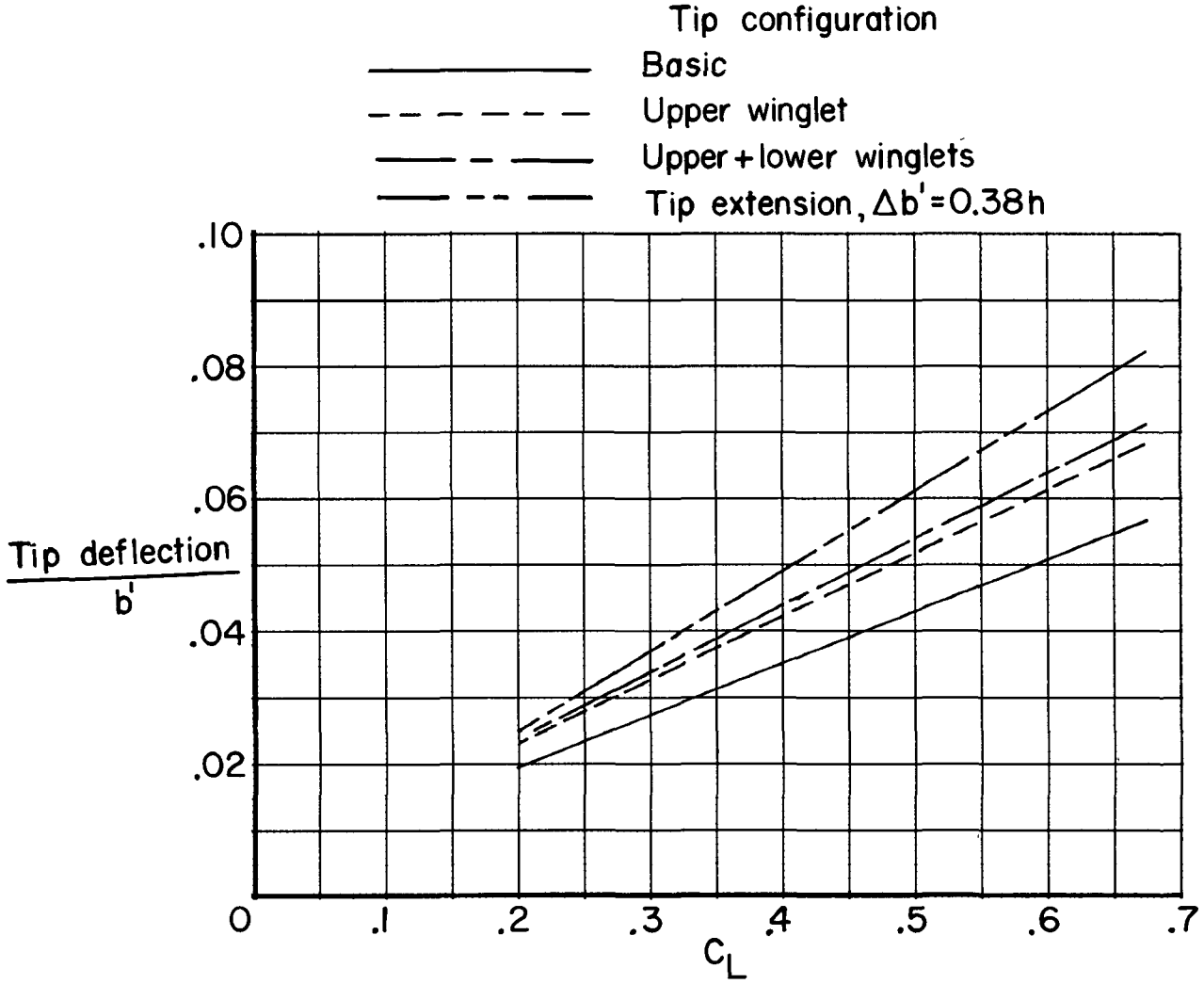

(b) $M_\infty = 0.75$.

Figure 6.- Continued.

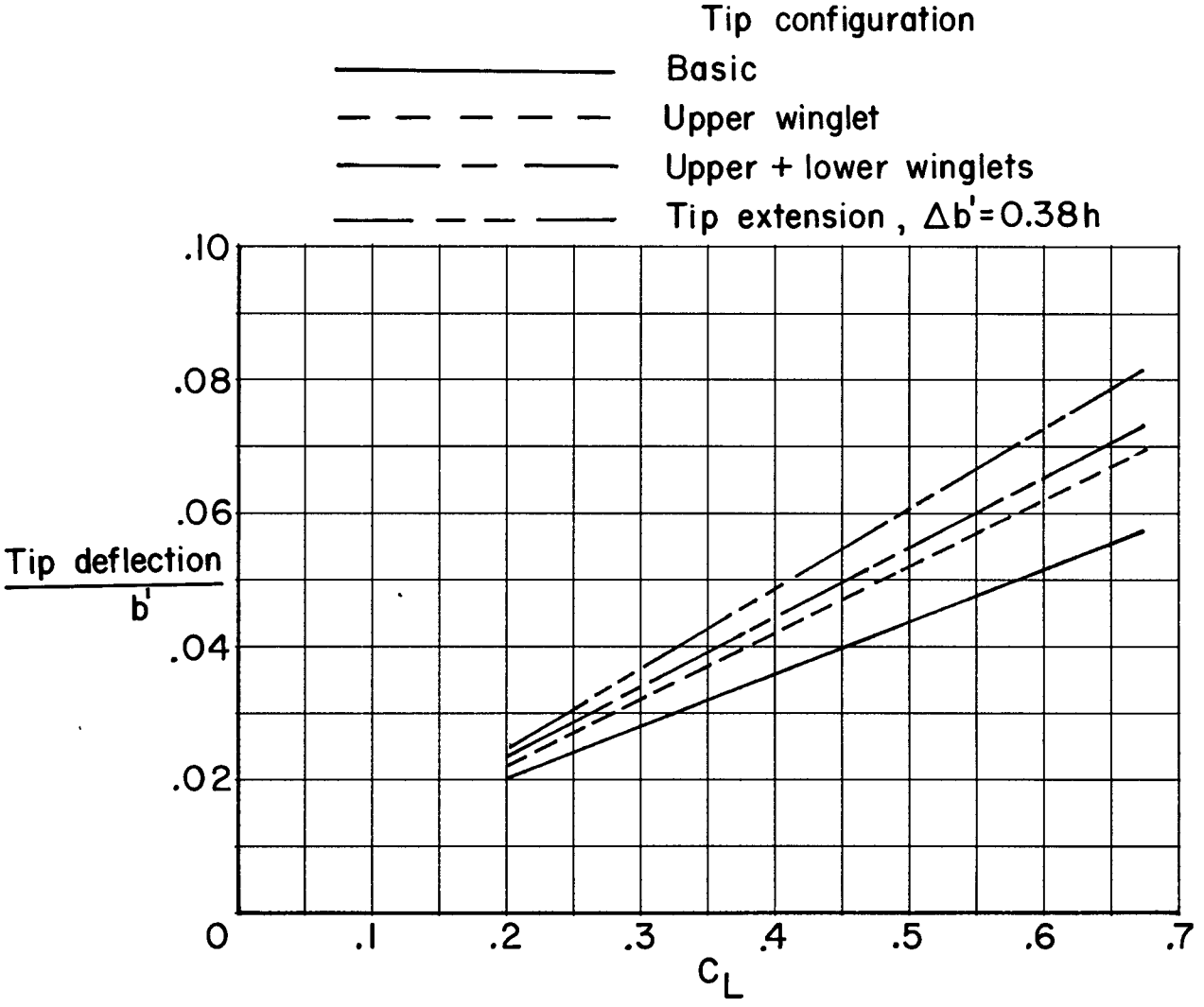

(c) $M_\infty = 0.78$.

Figure 6.- Continued.

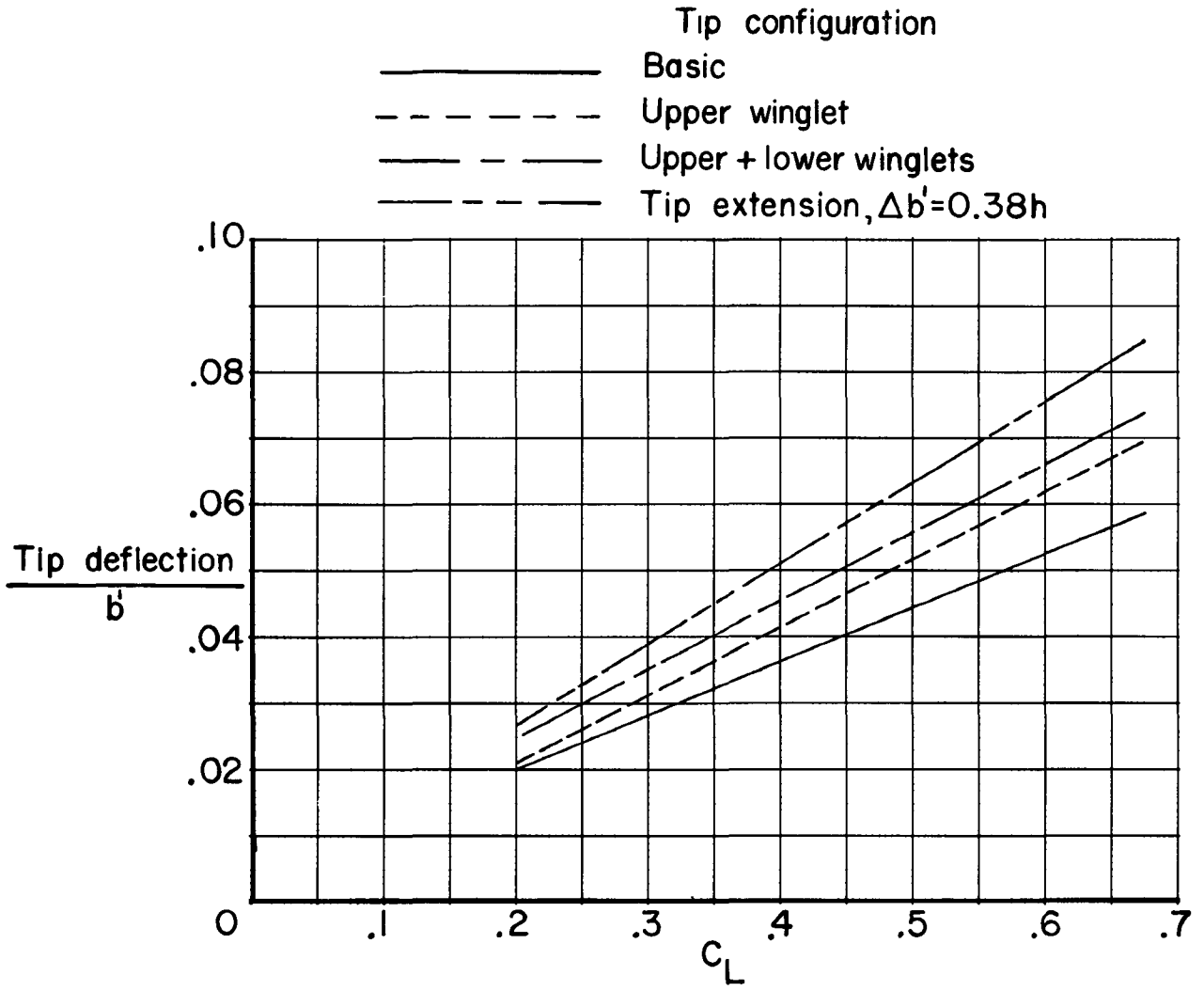

(d) $M_\infty = 0.80$.

Figure 6.- Concluded.

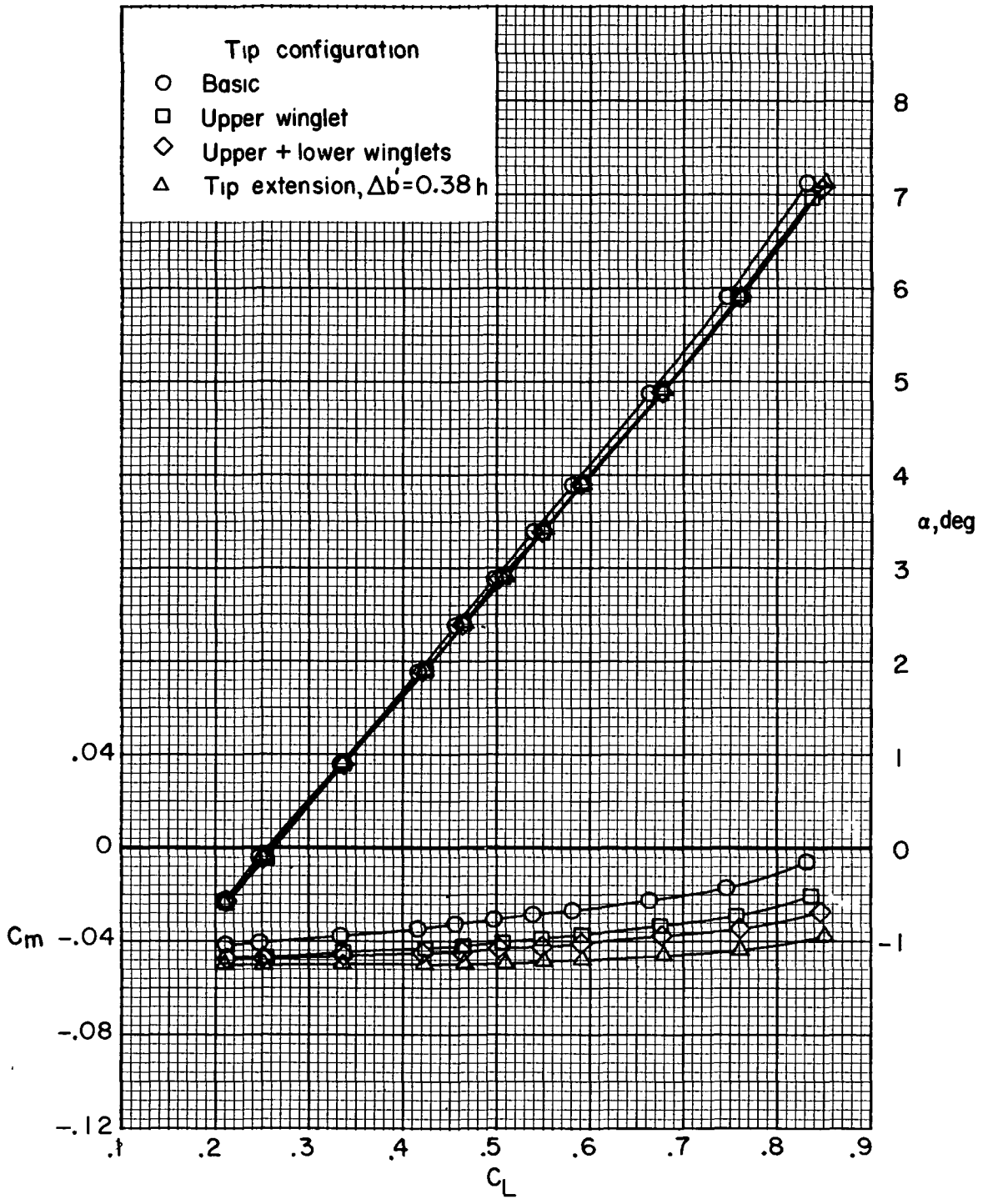

(a) $M_\infty = 0.70$.

Figure 7.- Variations of pitching-moment coefficient and angle of attack with lift coefficient.

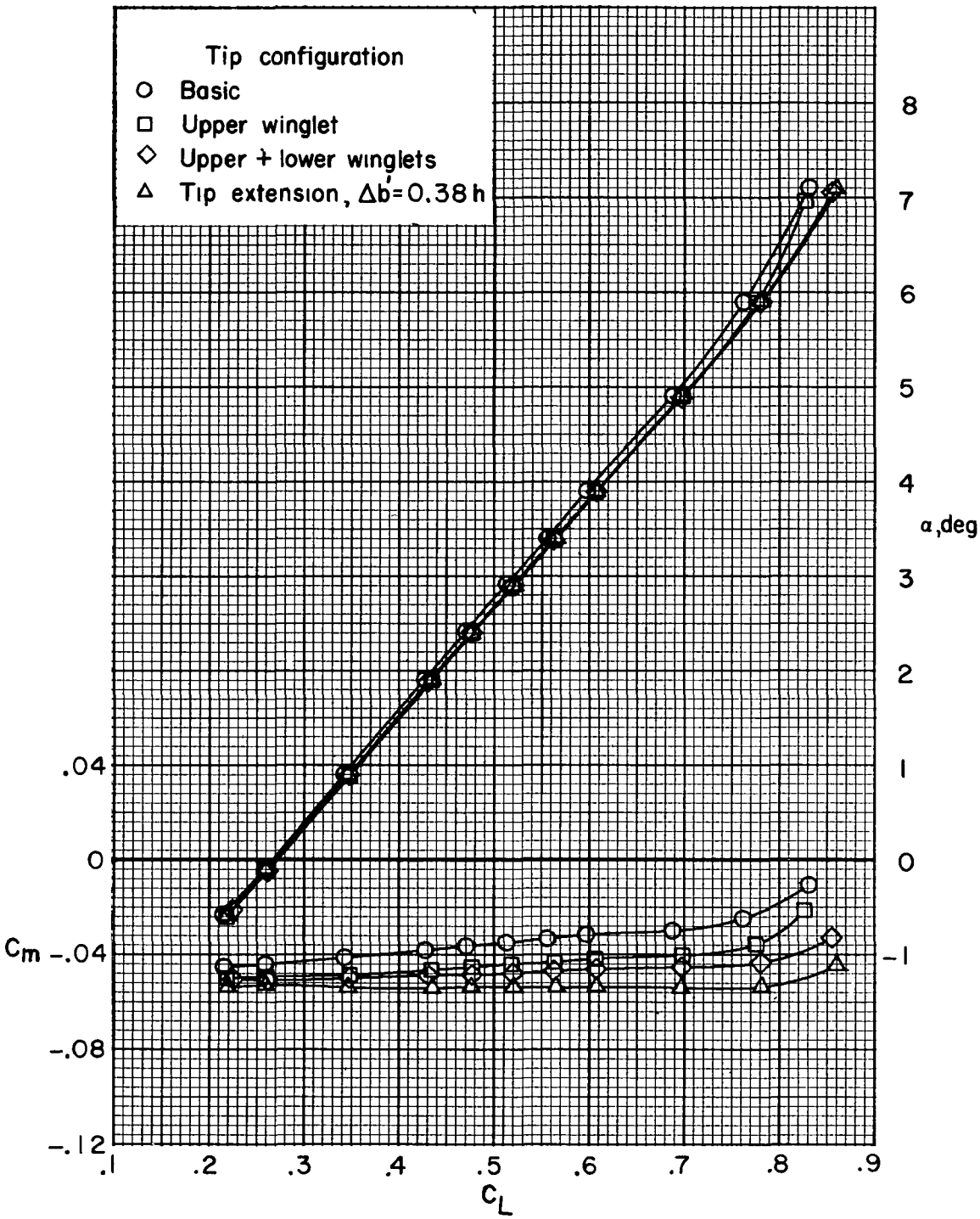

(b) $M_\infty = 0.75$.

Figure 7.- Continued.

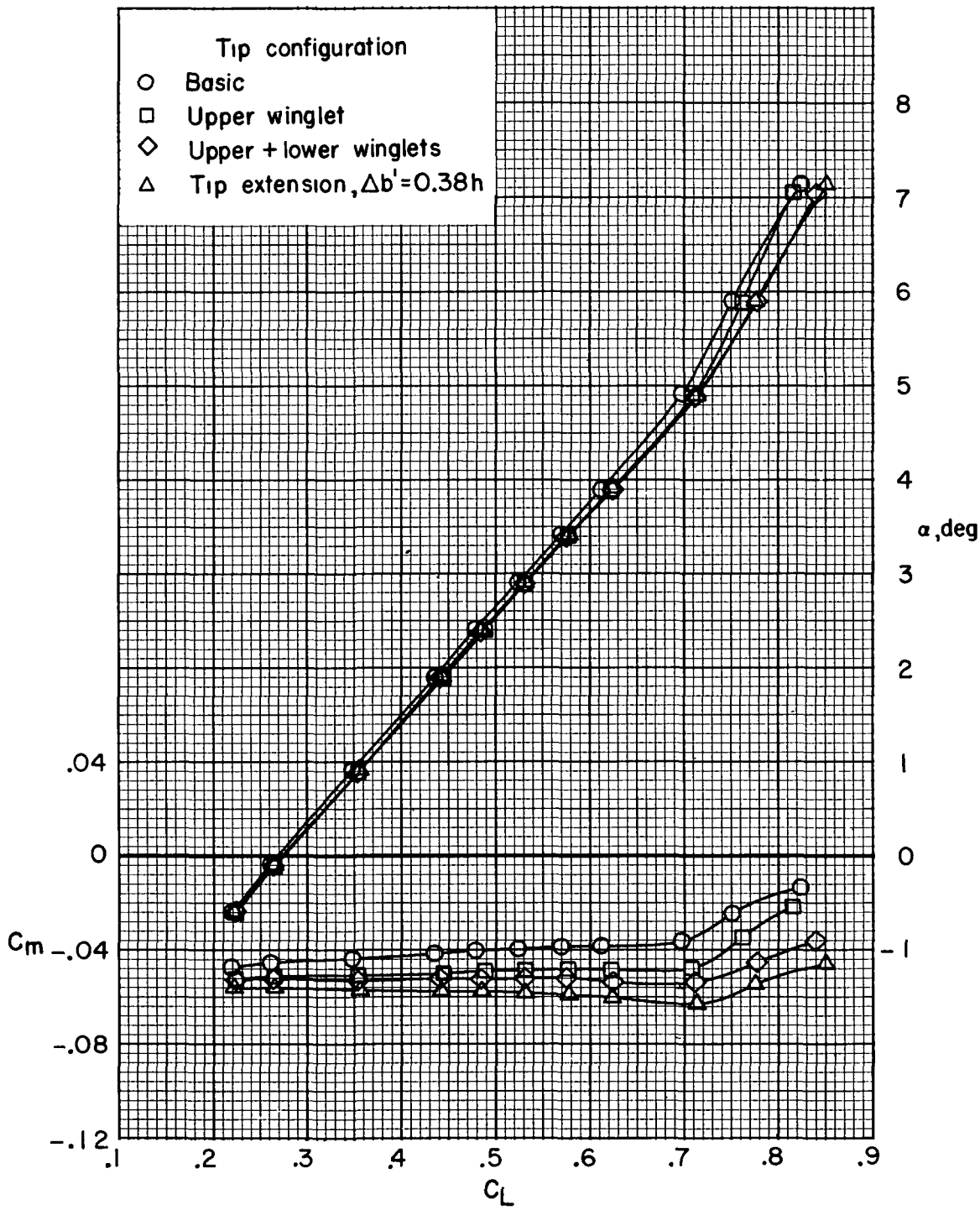

(c) $M_\infty = 0.78$.

Figure 7.- Continued.

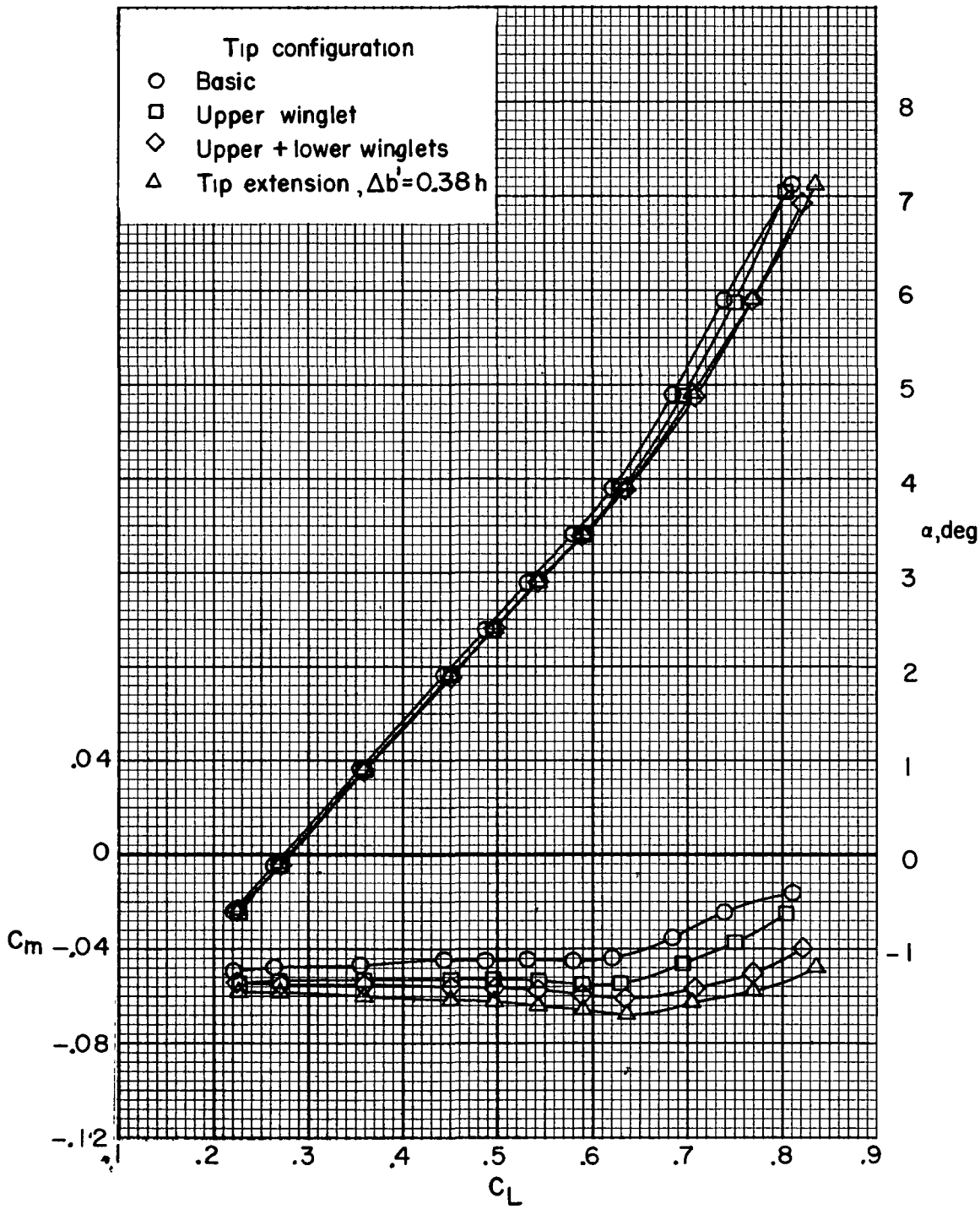

(d) $M_\infty = 0.80$.

Figure 7.- Concluded.

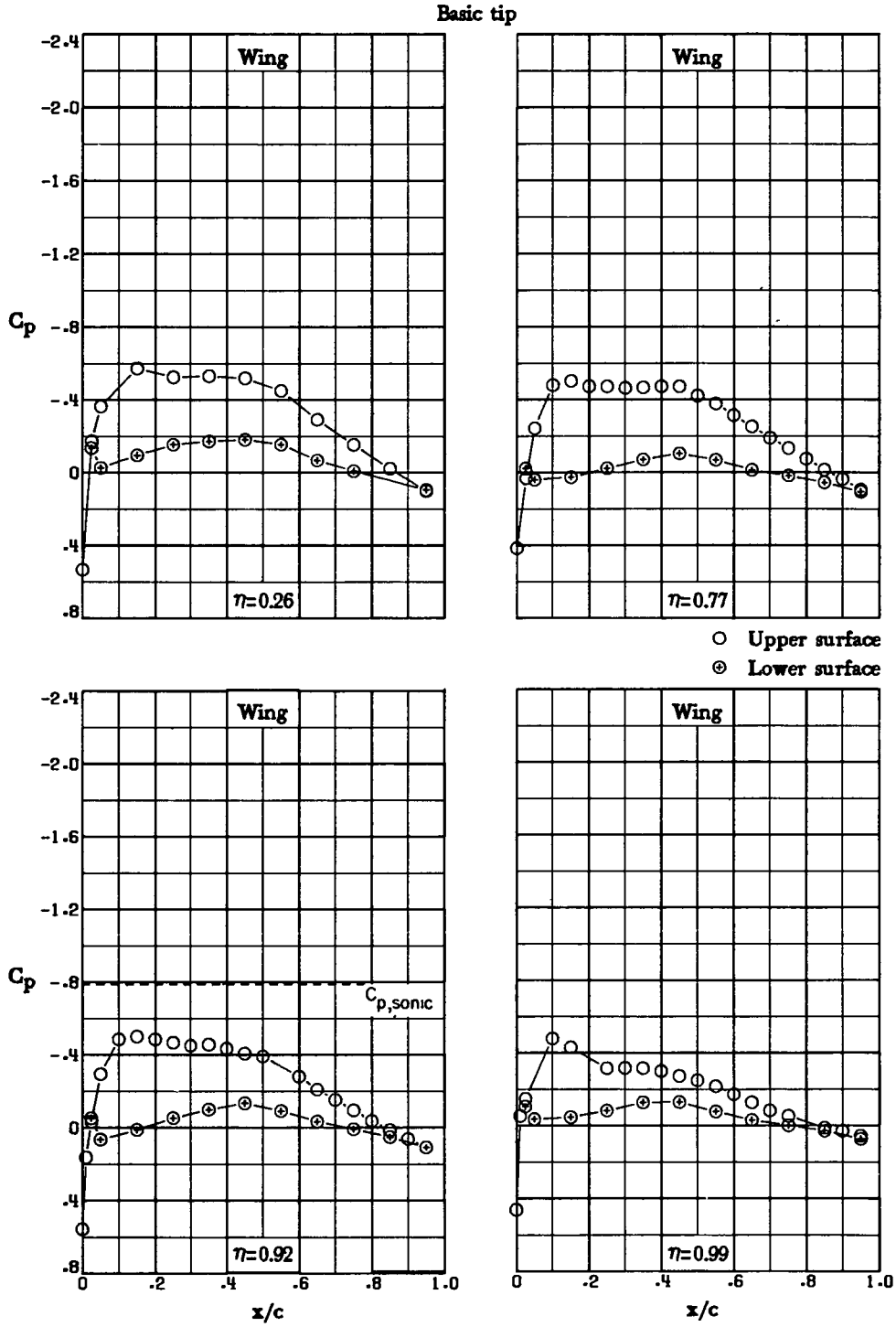

(a) $M_\infty = 0.70$; $\alpha = 0^o$.

Figure 8.- Pressure distributions for basic-tip configuration.

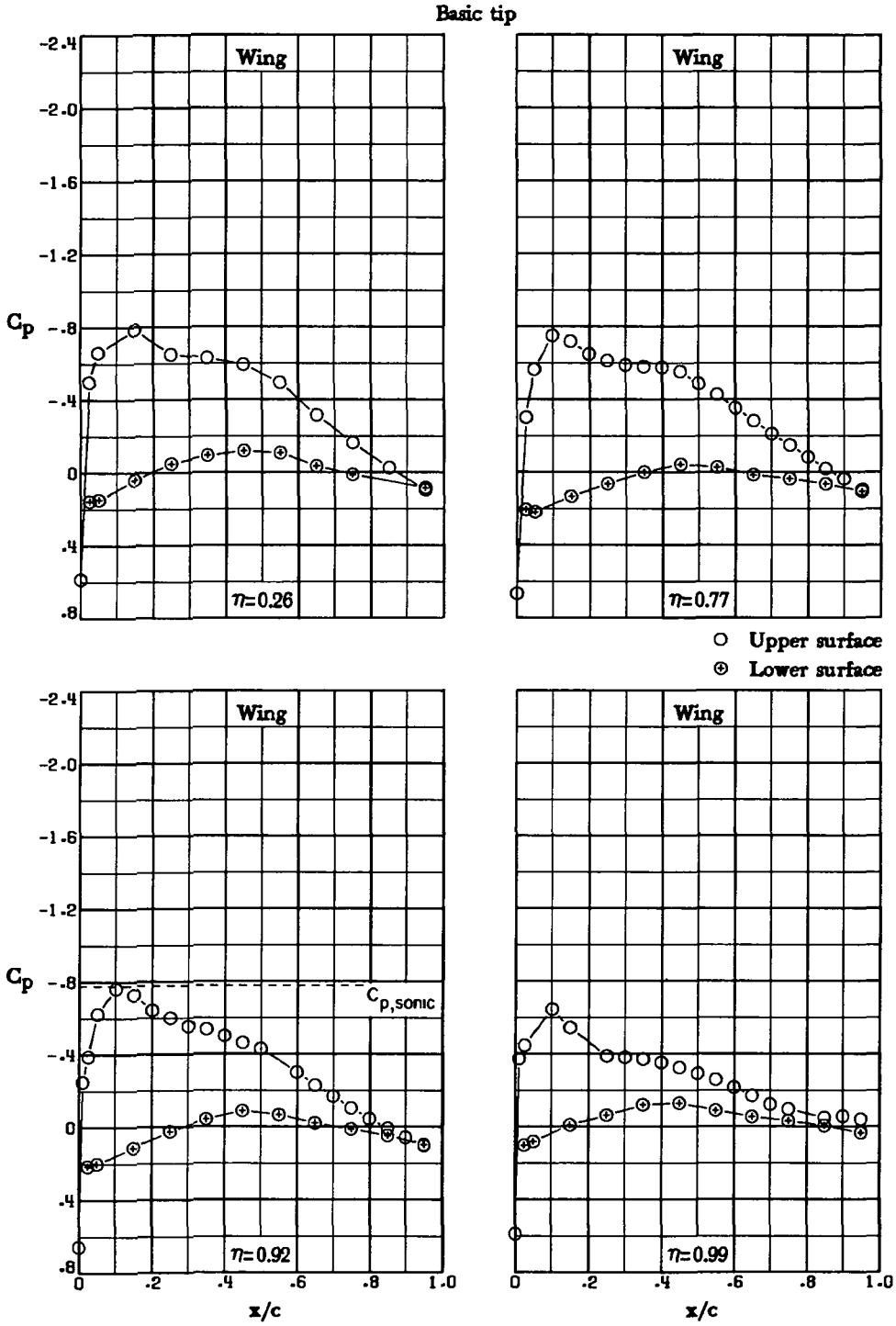

(b) $M_\infty = 0.70$; $\alpha = 2.0^\circ$.

Figure 8.- Continued.

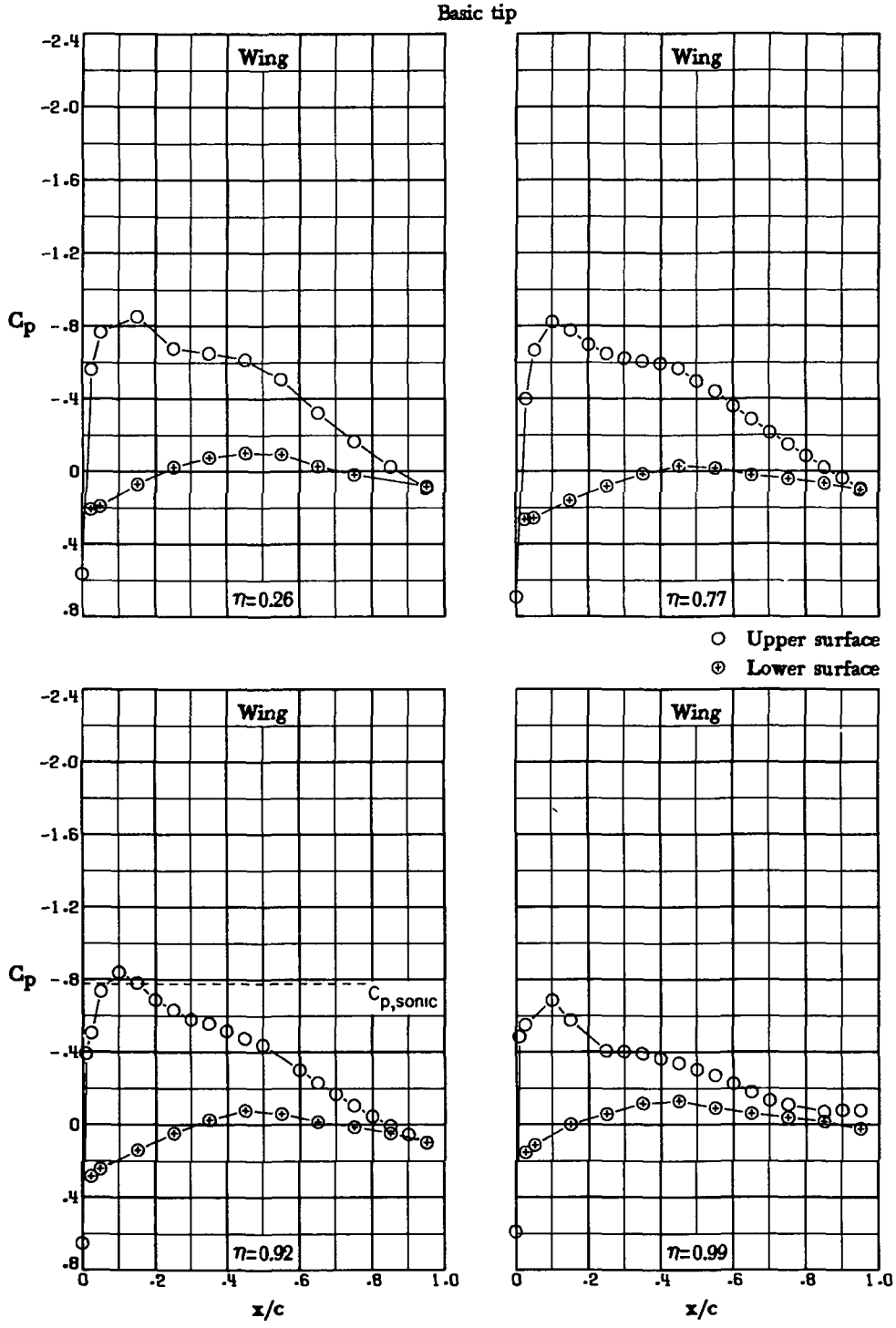

(c) $M_\infty = 0.70$; $\alpha = 2.5^\circ$.

Figure 8.- Continued.

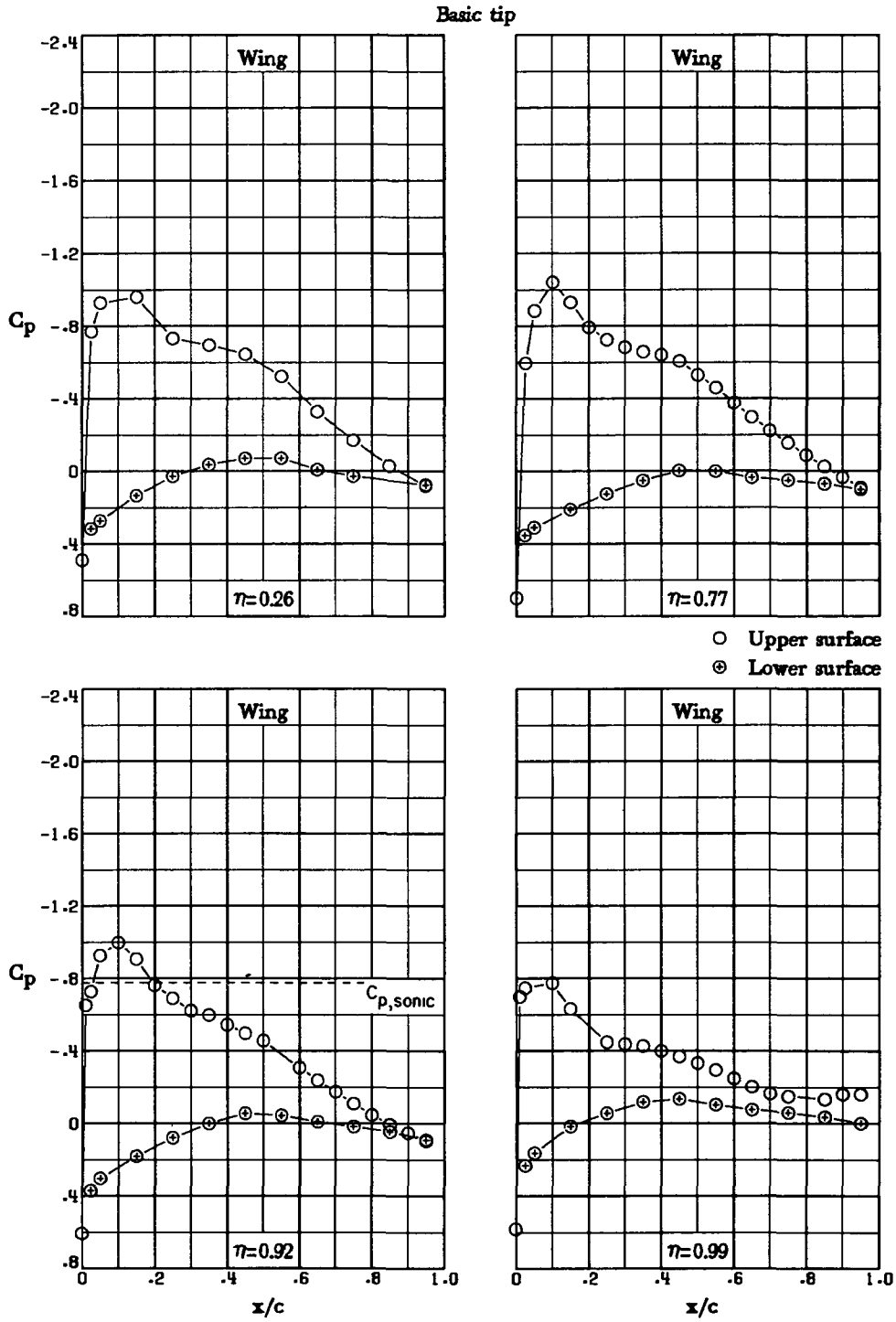

(d) $M_\infty = 0.70$; $\alpha = 3.5^o$.

Figure 8.- Continued.

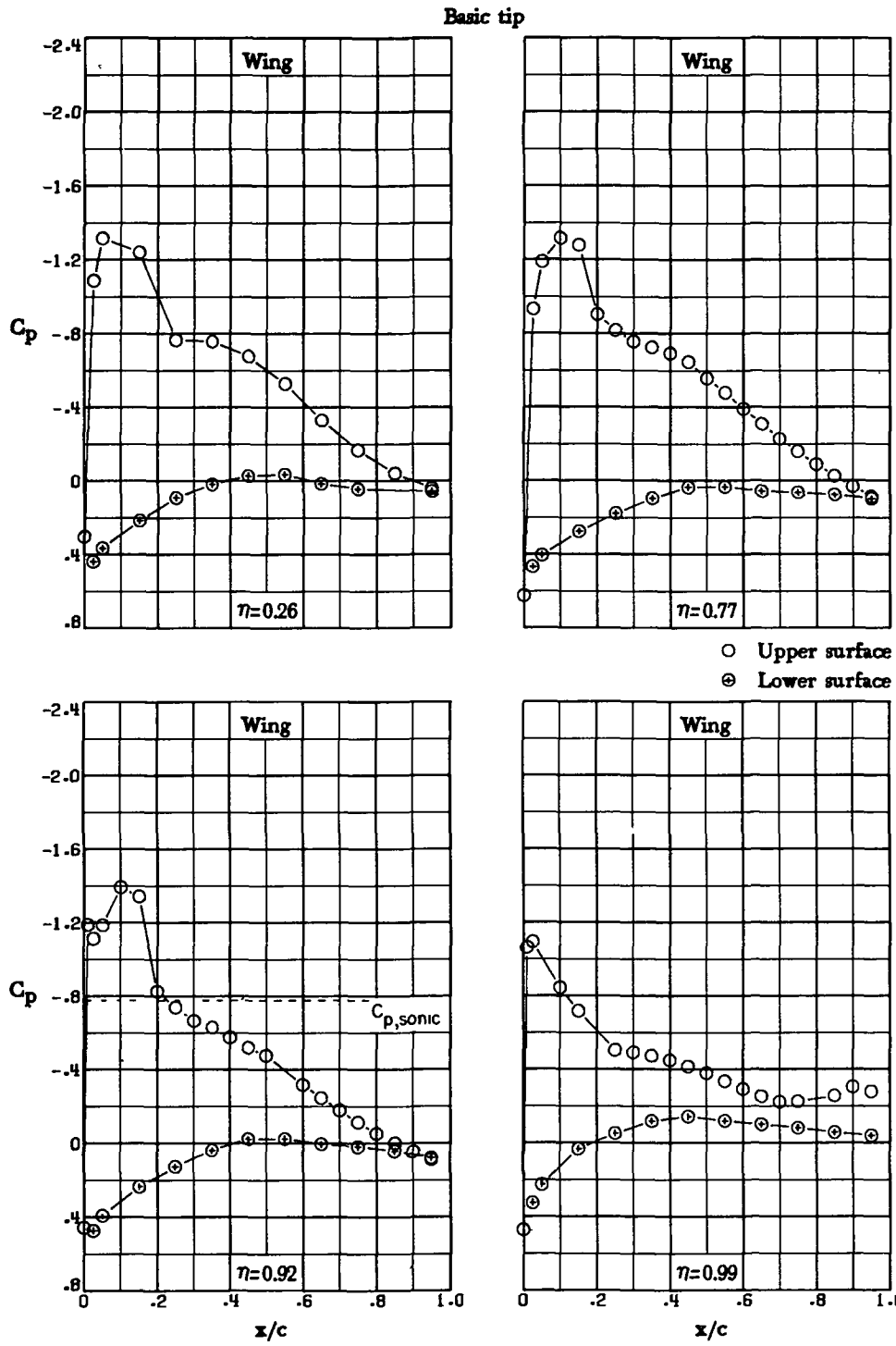

(e) $M_\infty = 0.70$; $\alpha = 5.0°$.

Figure 8.- Continued.

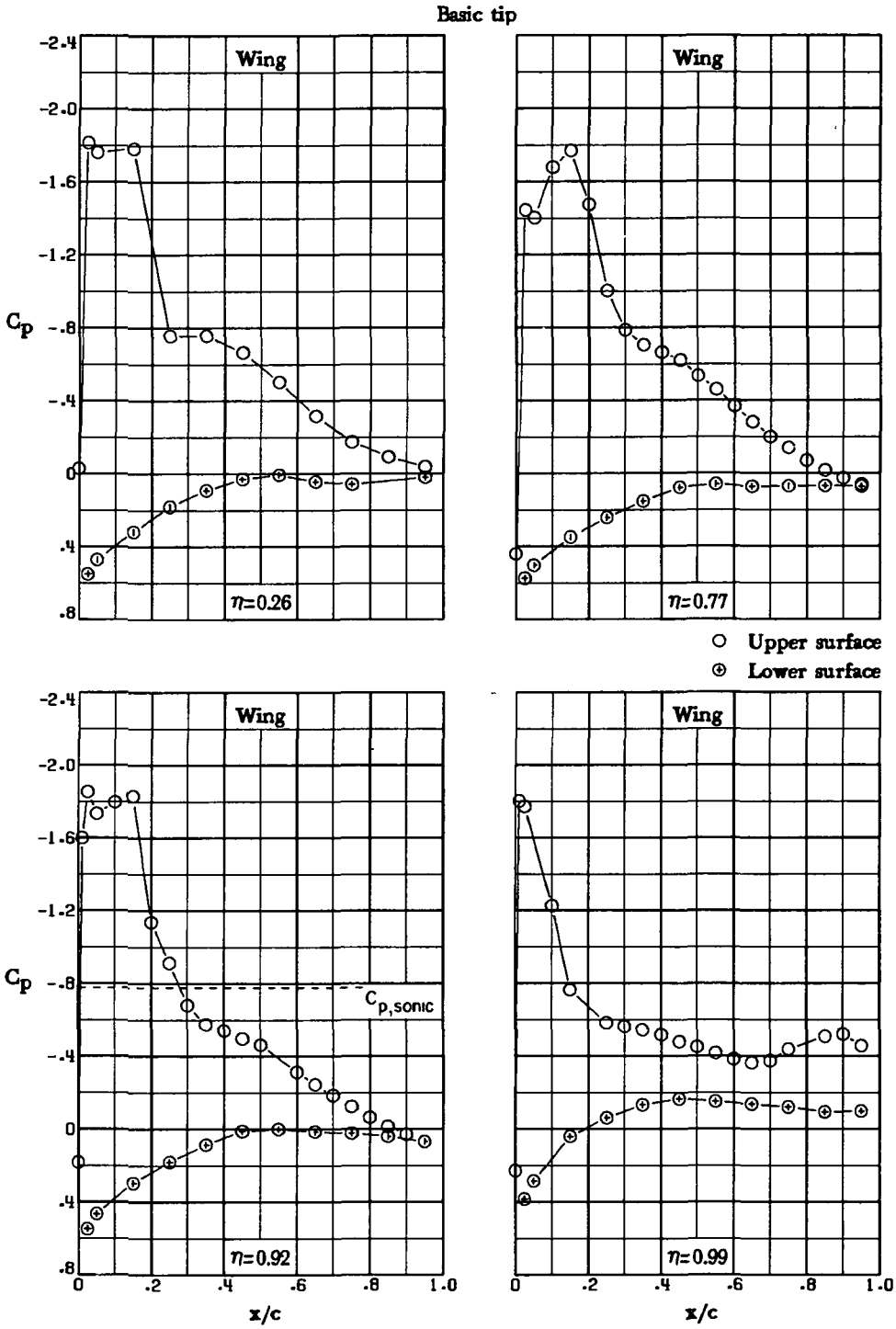

(f) $M_\infty = 0.70$; $\alpha = 7.2^\circ$.

Figure 8.- Continued.

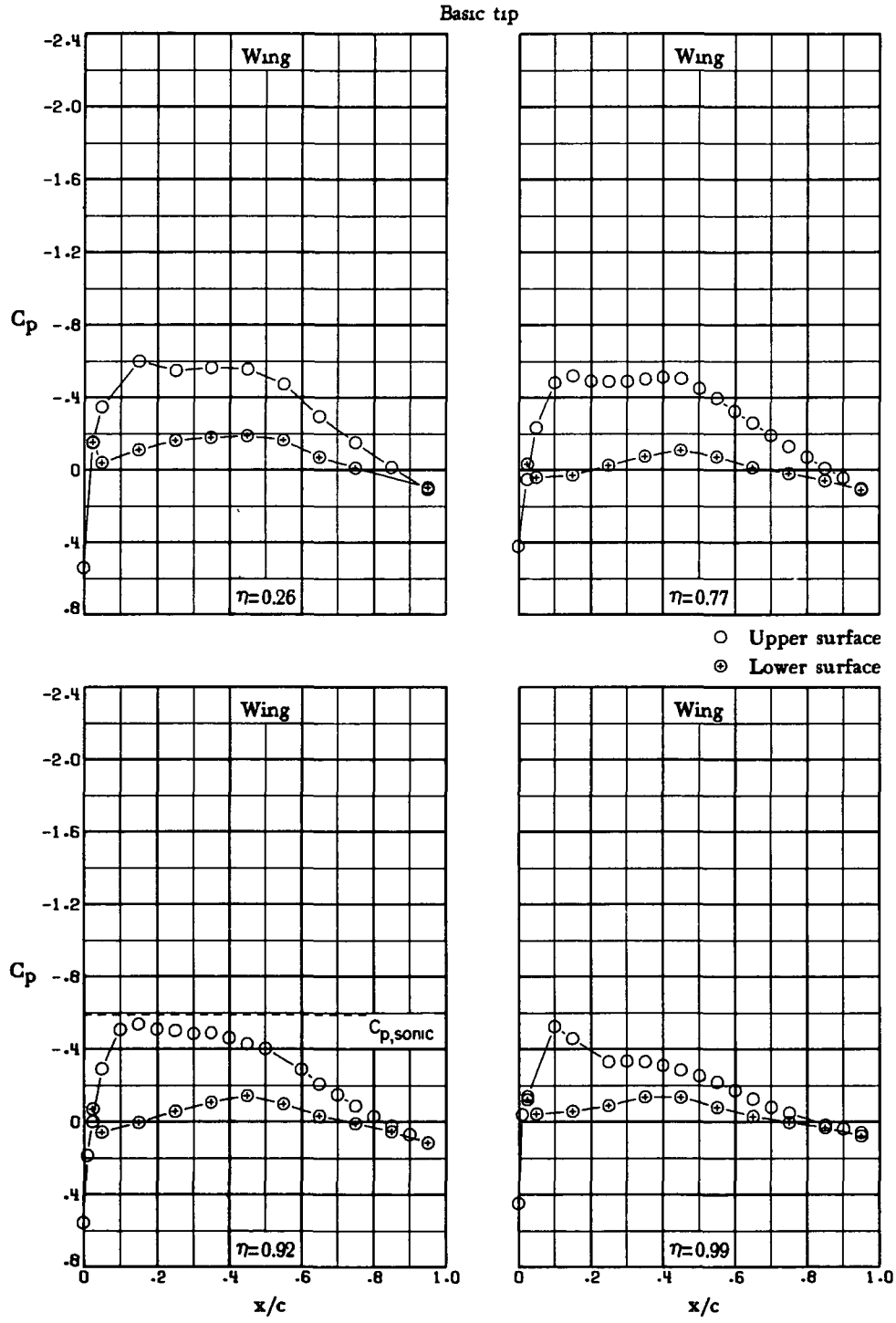

(g) $M_\infty = 0.75$; $\alpha = 0^\circ$.

Figure 8.- Continued.

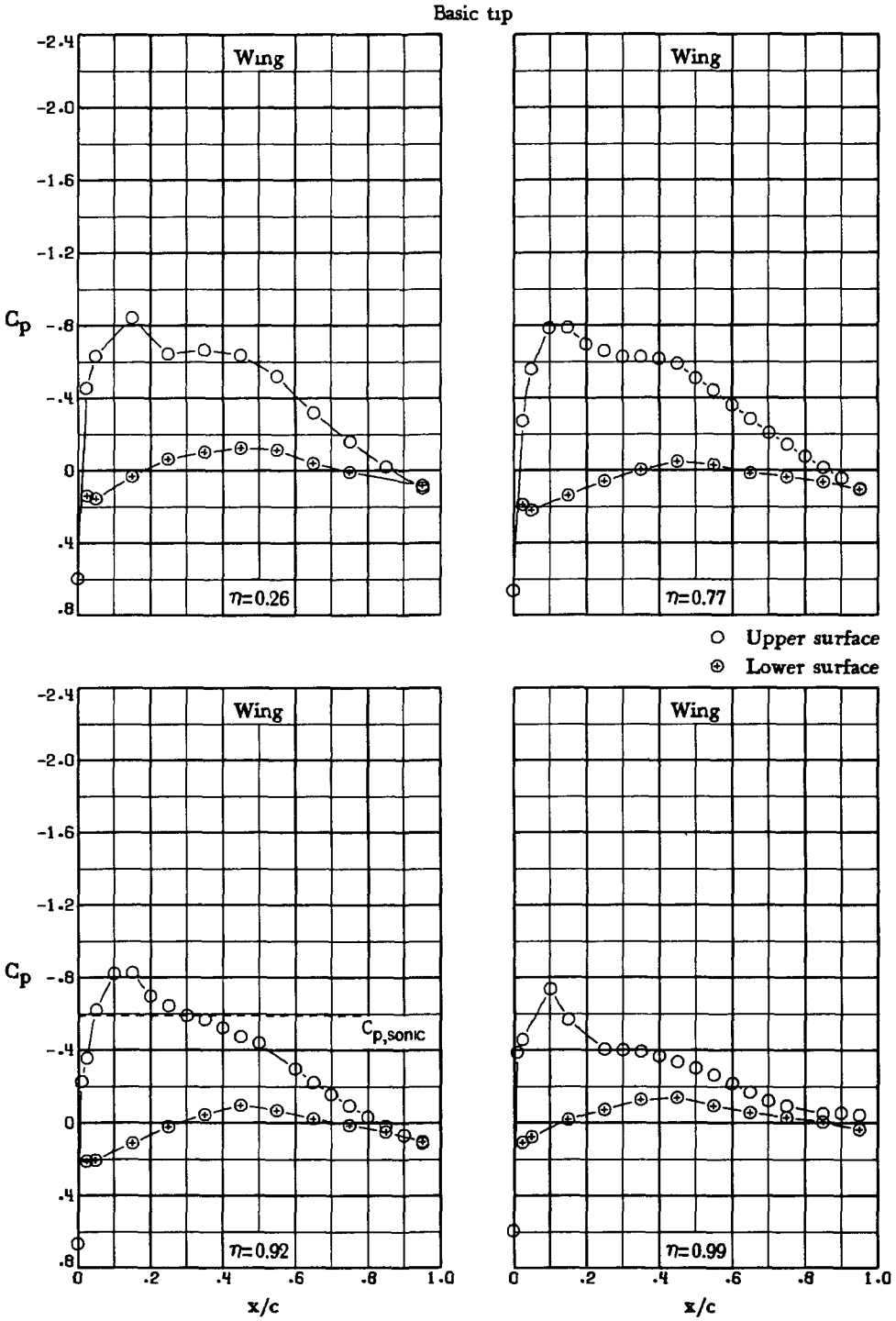

(h) $M_\infty = 0.75$; $\alpha = 2.0^\circ$.

Figure 8.- Continued.

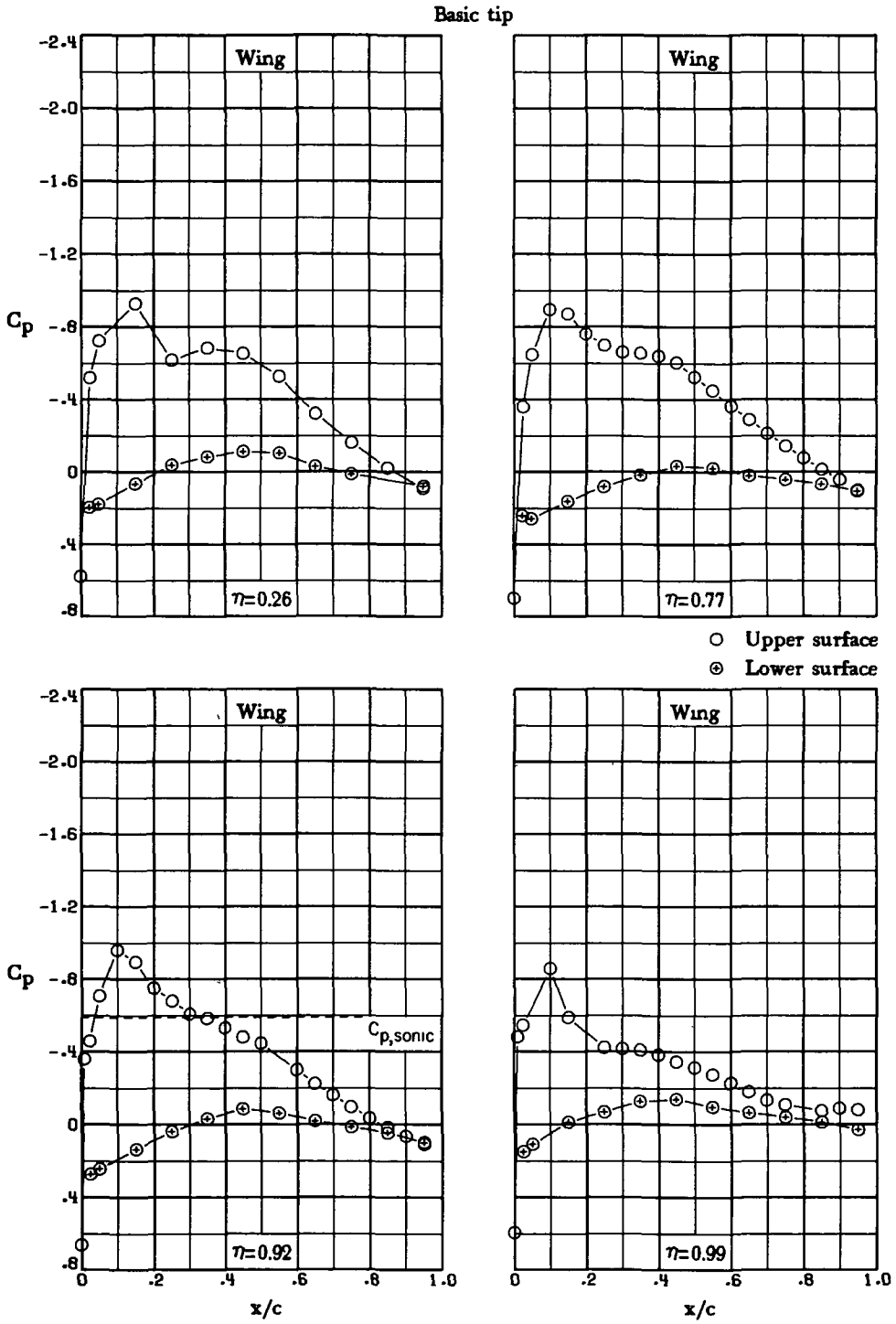

(i) $M_\infty = 0.75$; $\alpha = 2.5^\circ$.

Figure 8.- Continued.

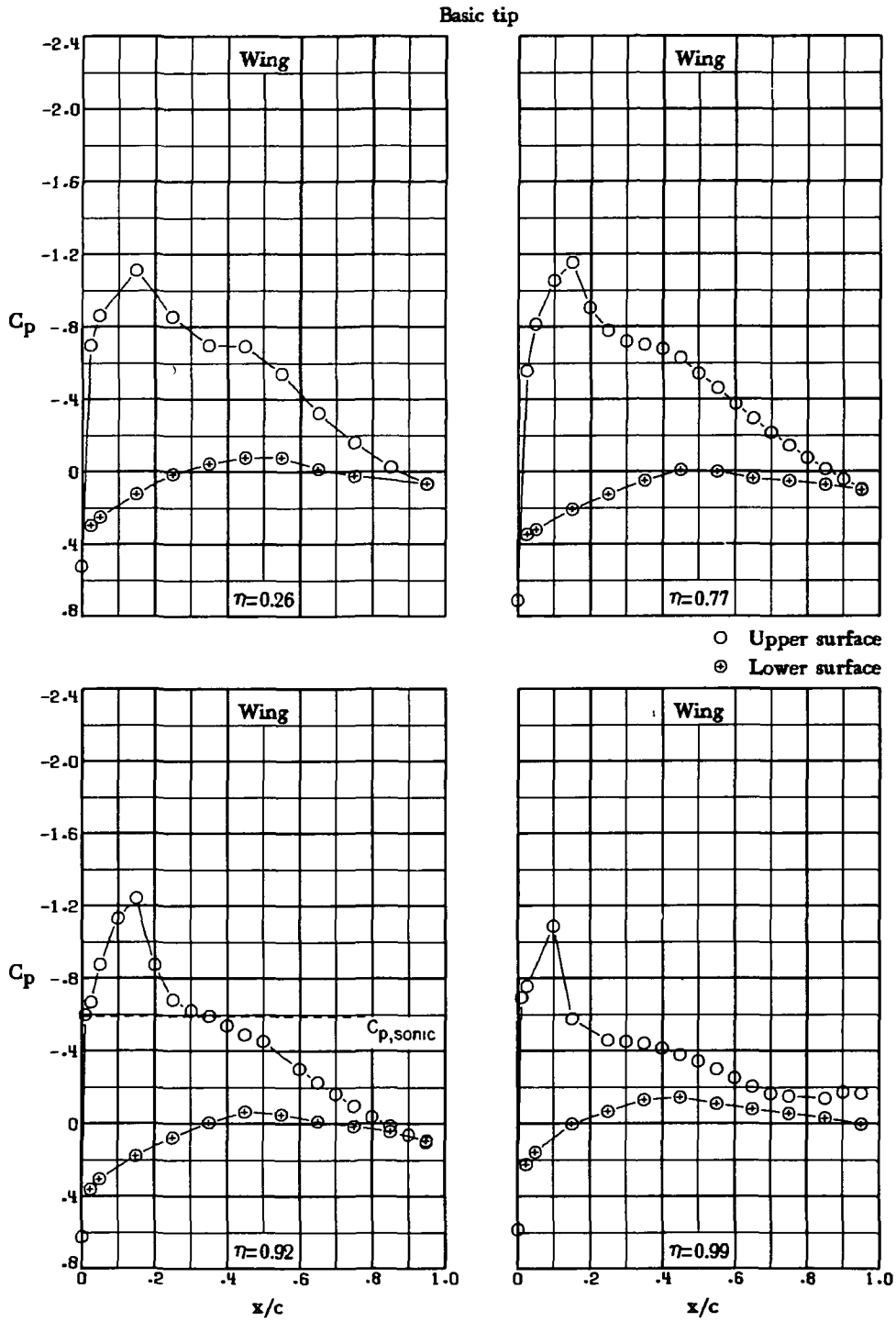

(j) $M_\infty = 0.75$; $\alpha = 3.5^\circ$.

Figure 8.- Continued.

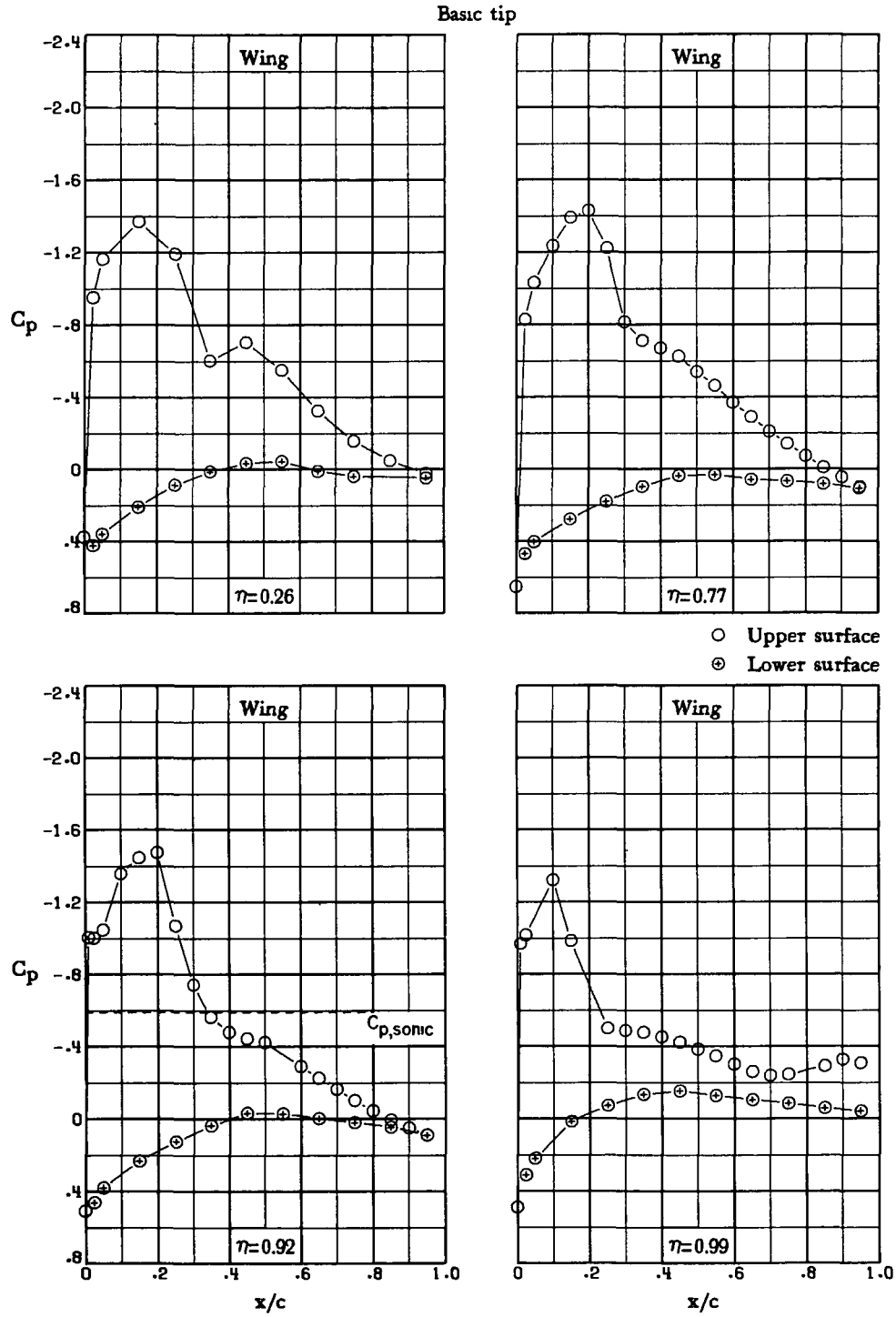

(k) $M_\infty = 0.75$; $\alpha = 5.0^\circ$.

Figure 8.- Continued.

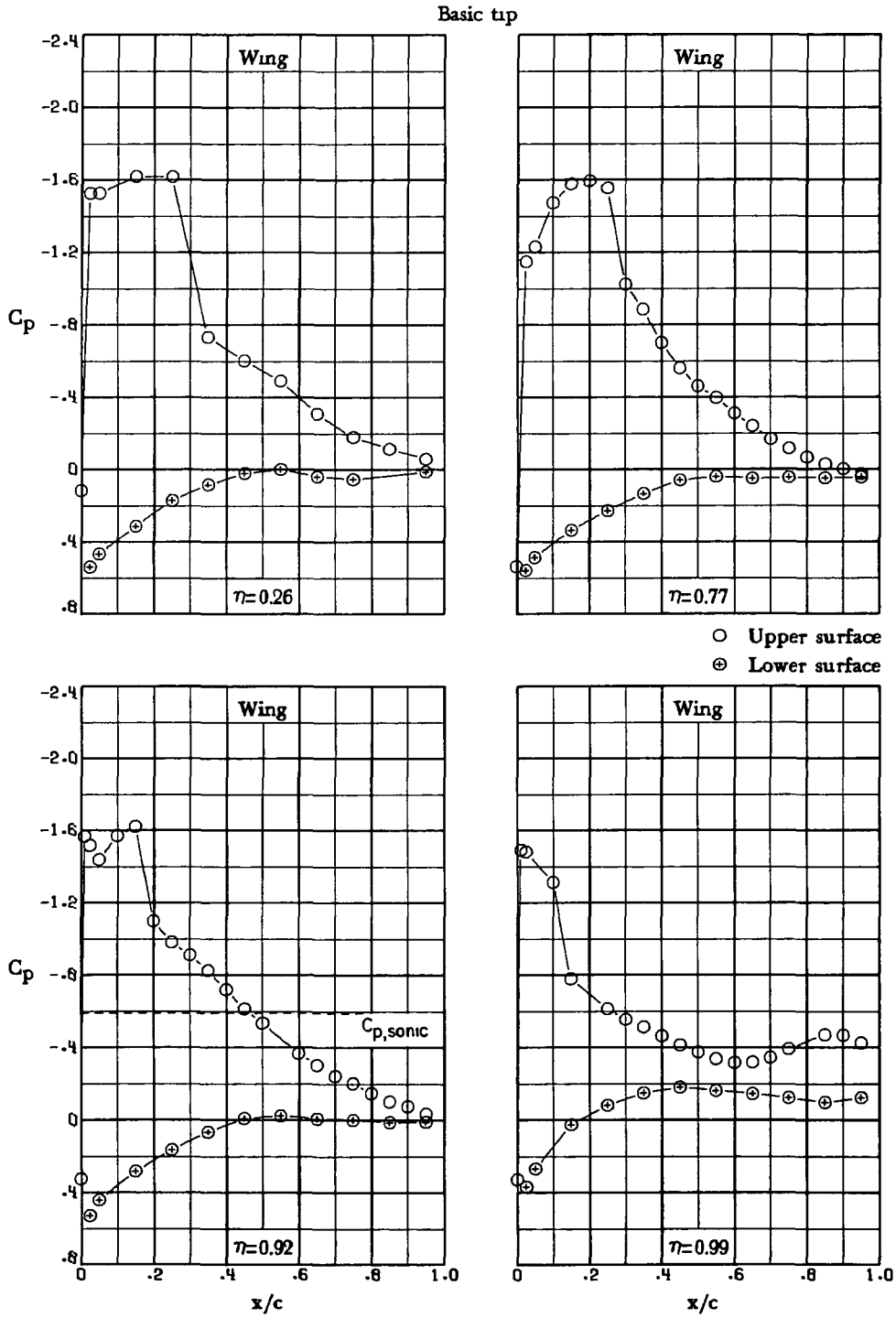

(1) $M_\infty = 0.75$; $\alpha = 7.3^\circ$.

Figure 8.- Continued.

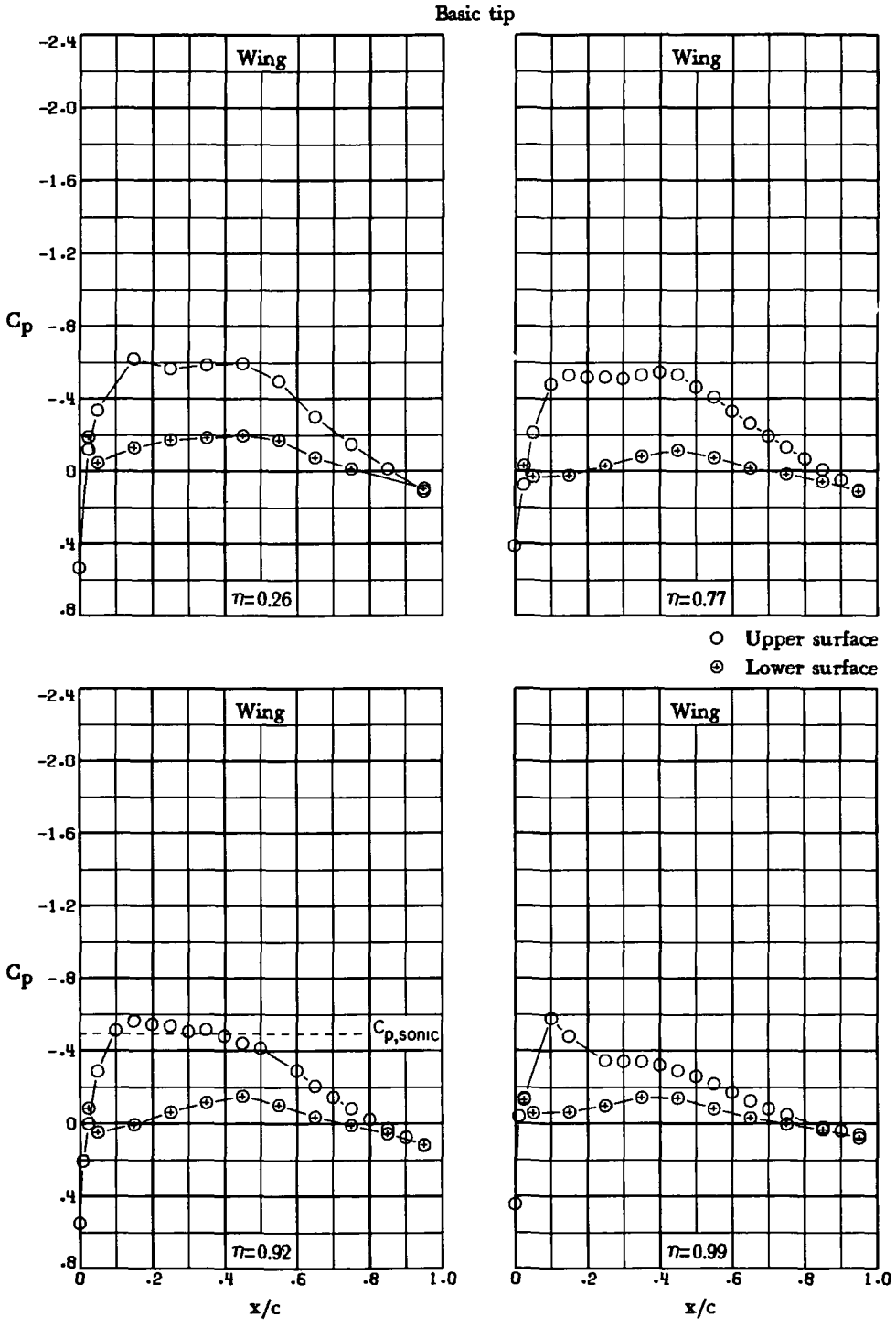

(m) $M_\infty = 0.78$; $\alpha = 0^o$.

Figure 8.- Continued.

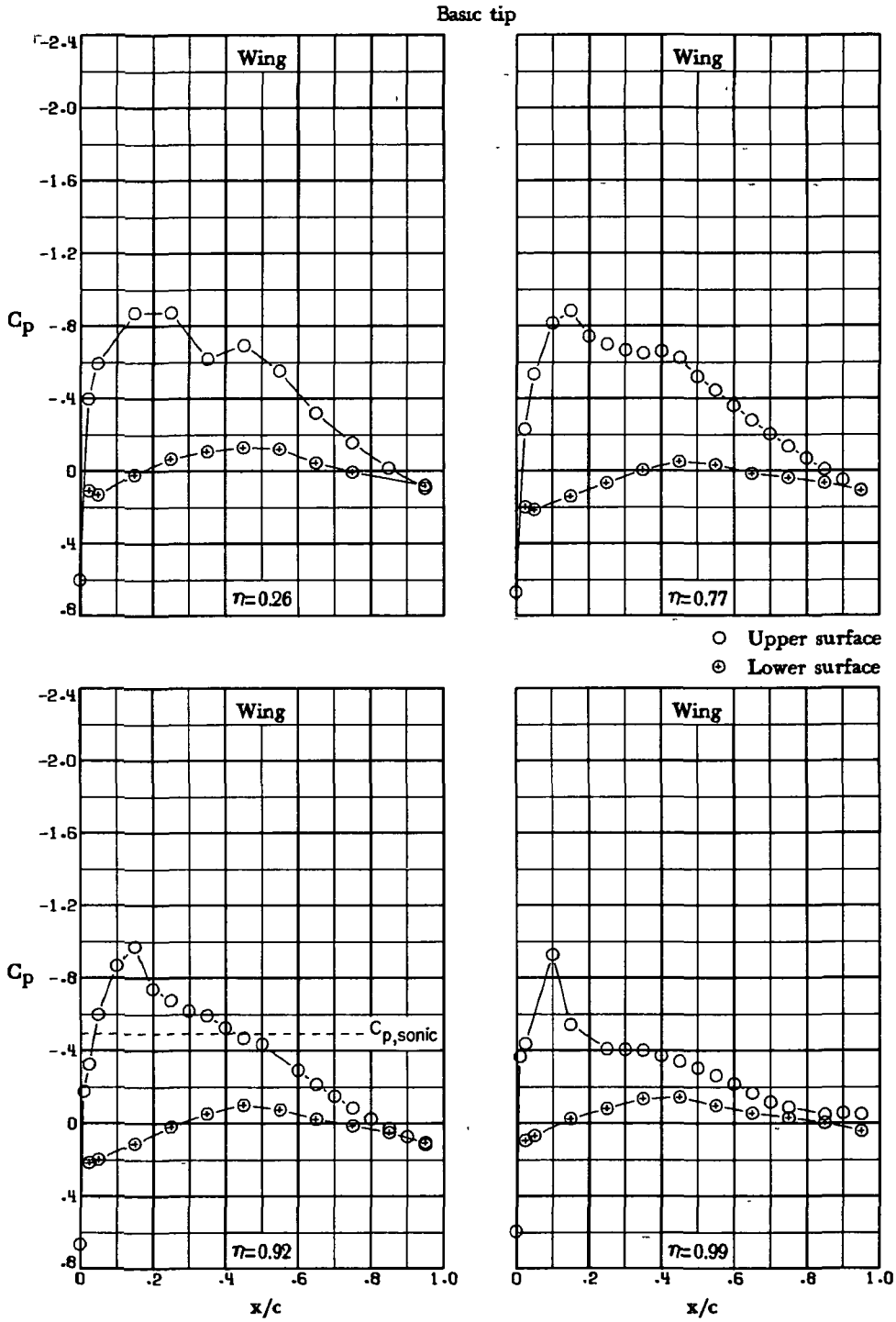

(n) $M_\infty = 0.78$; $\alpha = 2.0^\circ$.

Figure 8.- Continued.

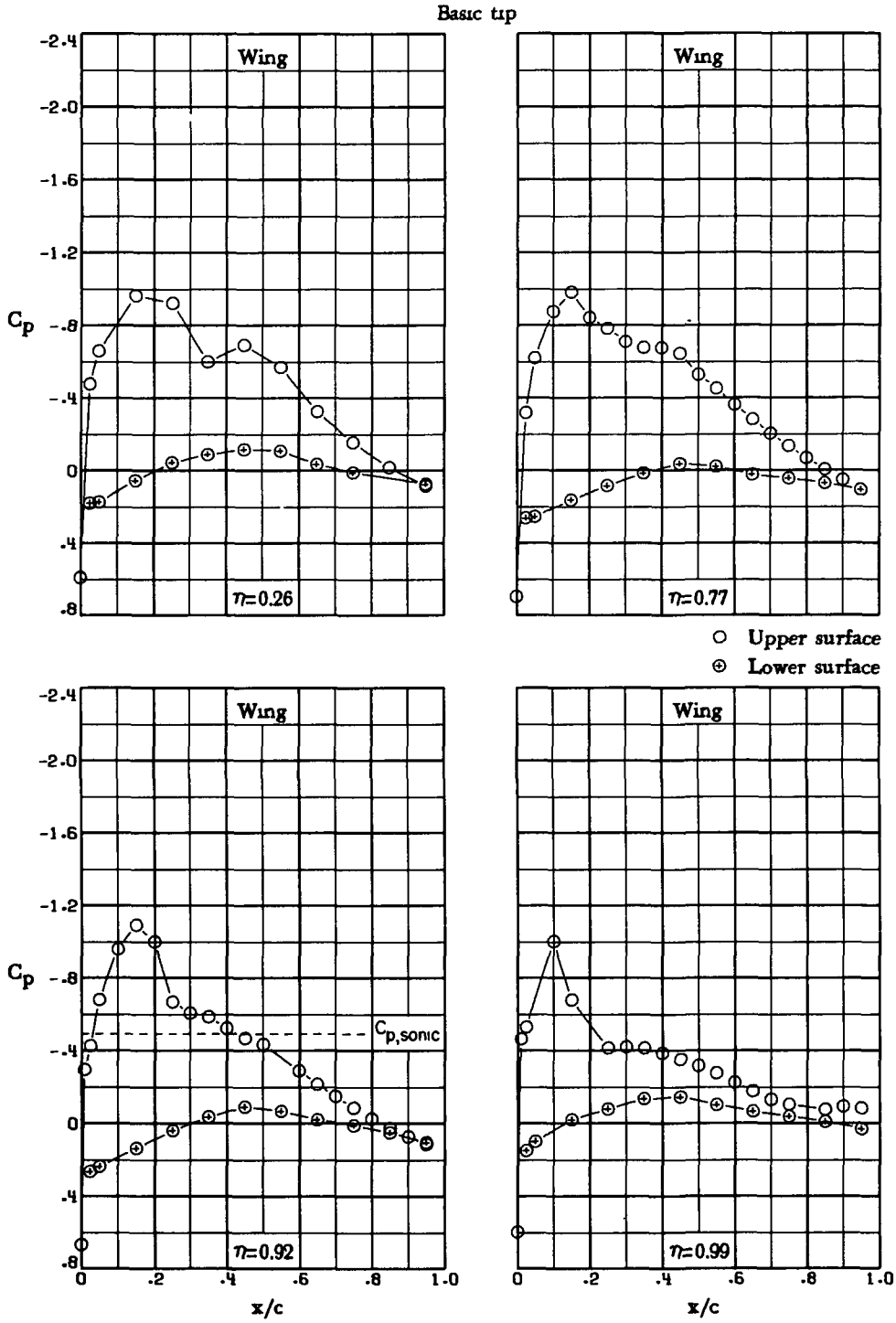

(o) $M_\infty = 0.78$; $\alpha = 2.5^\circ$.

Figure 8.- Continued.

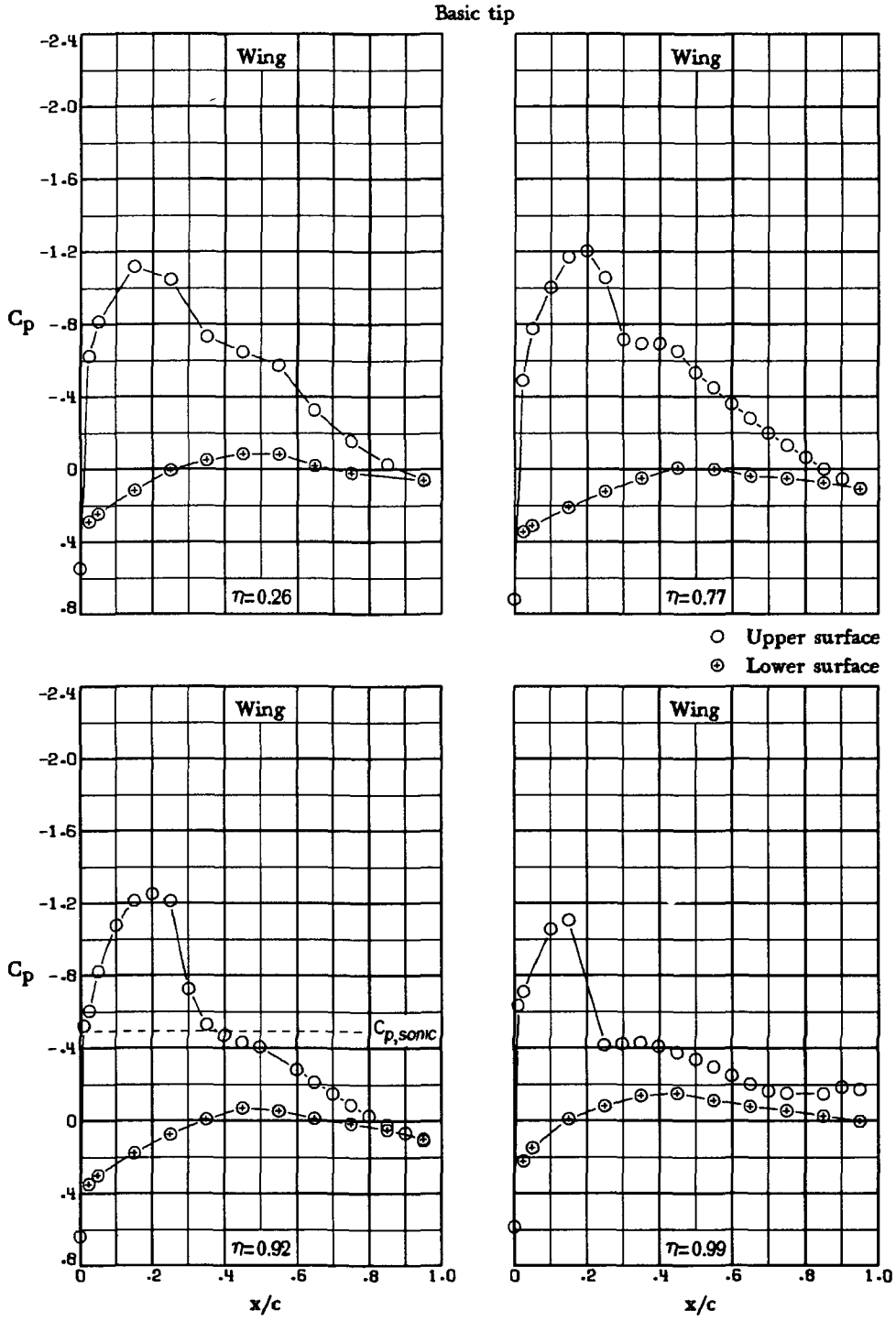

(p) $M_\infty = 0.78$; $\alpha = 3.5^\circ$.

Figure 8.- Continued.

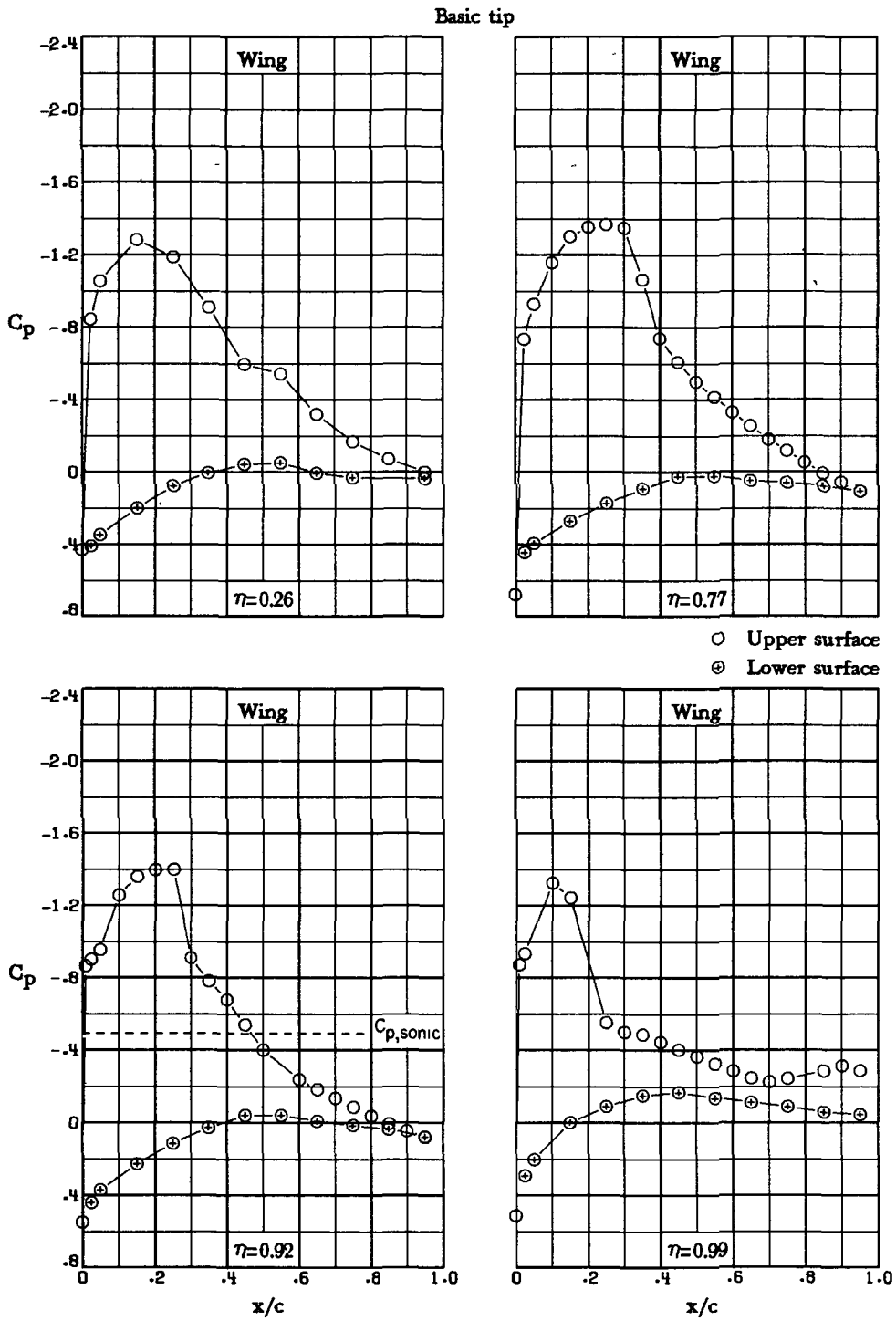

(q) $M_\infty = 0.78$; $\alpha = 5.0^\circ$.

Figure 8.- Continued.

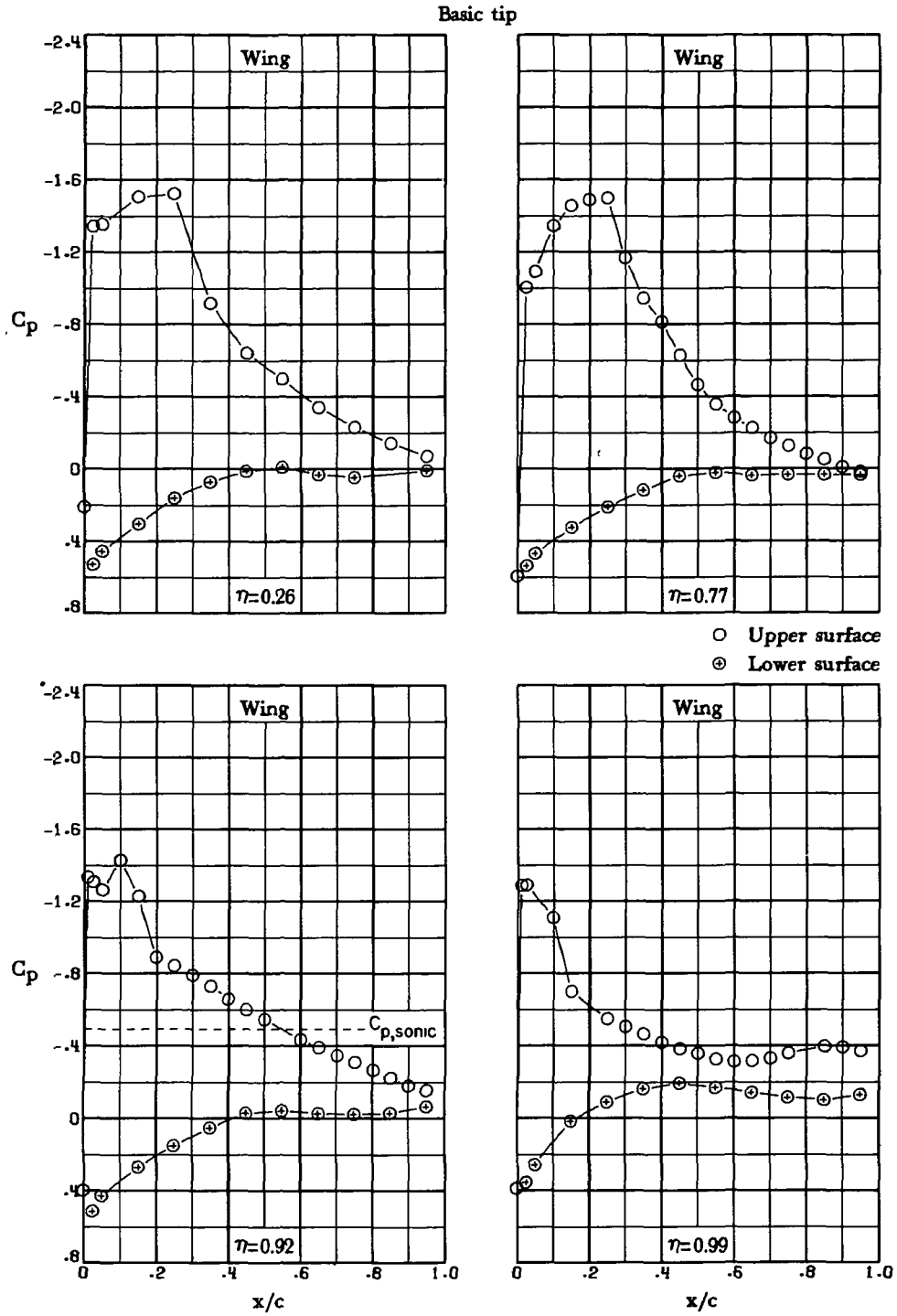

(r) $M_\infty = 0.78$; $\alpha = 7.2^\circ$.

Figure 8.- Continued.

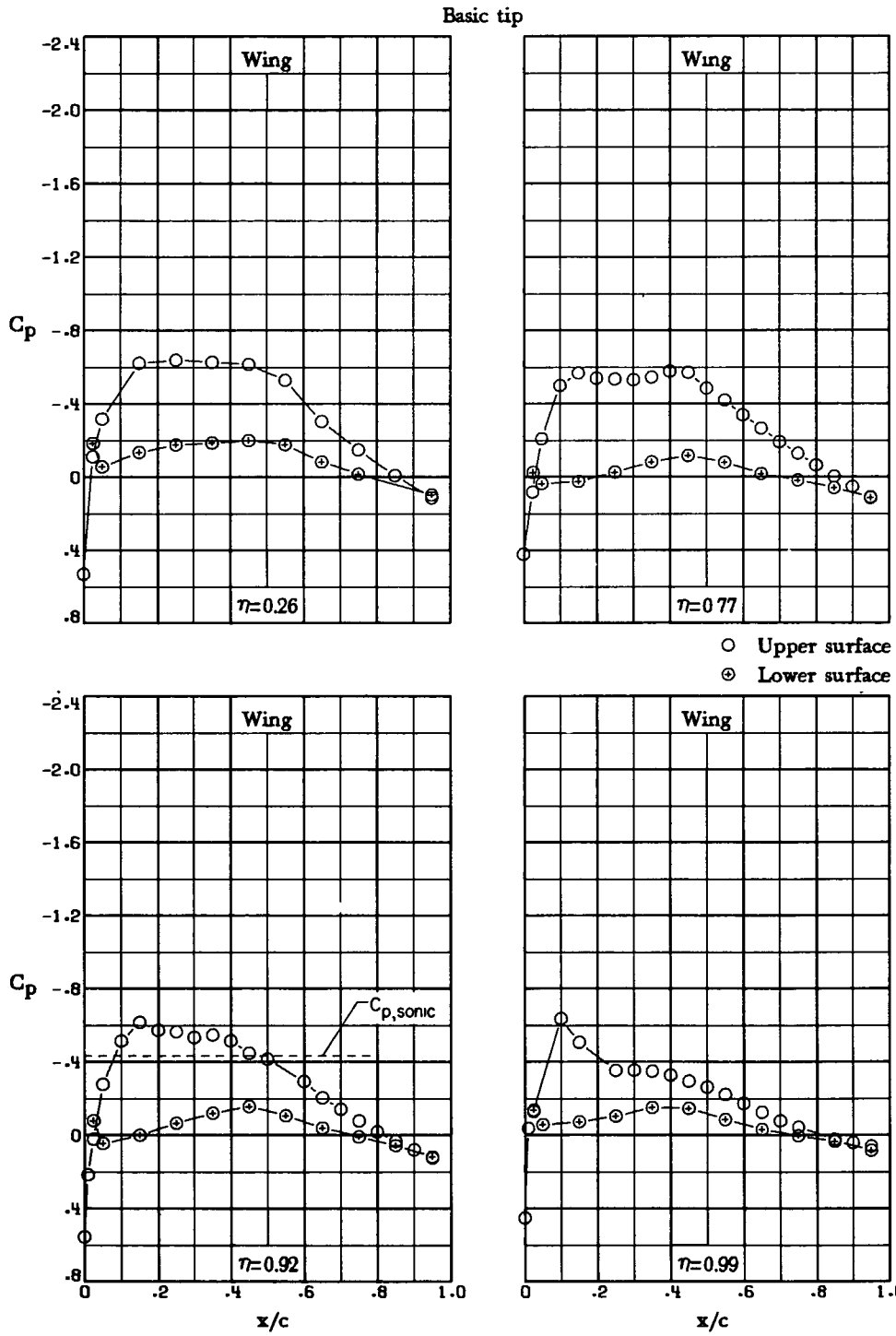

(s) $M_\infty = 0.80$; $\alpha = 0^\circ$.

Figure 8.- Continued.

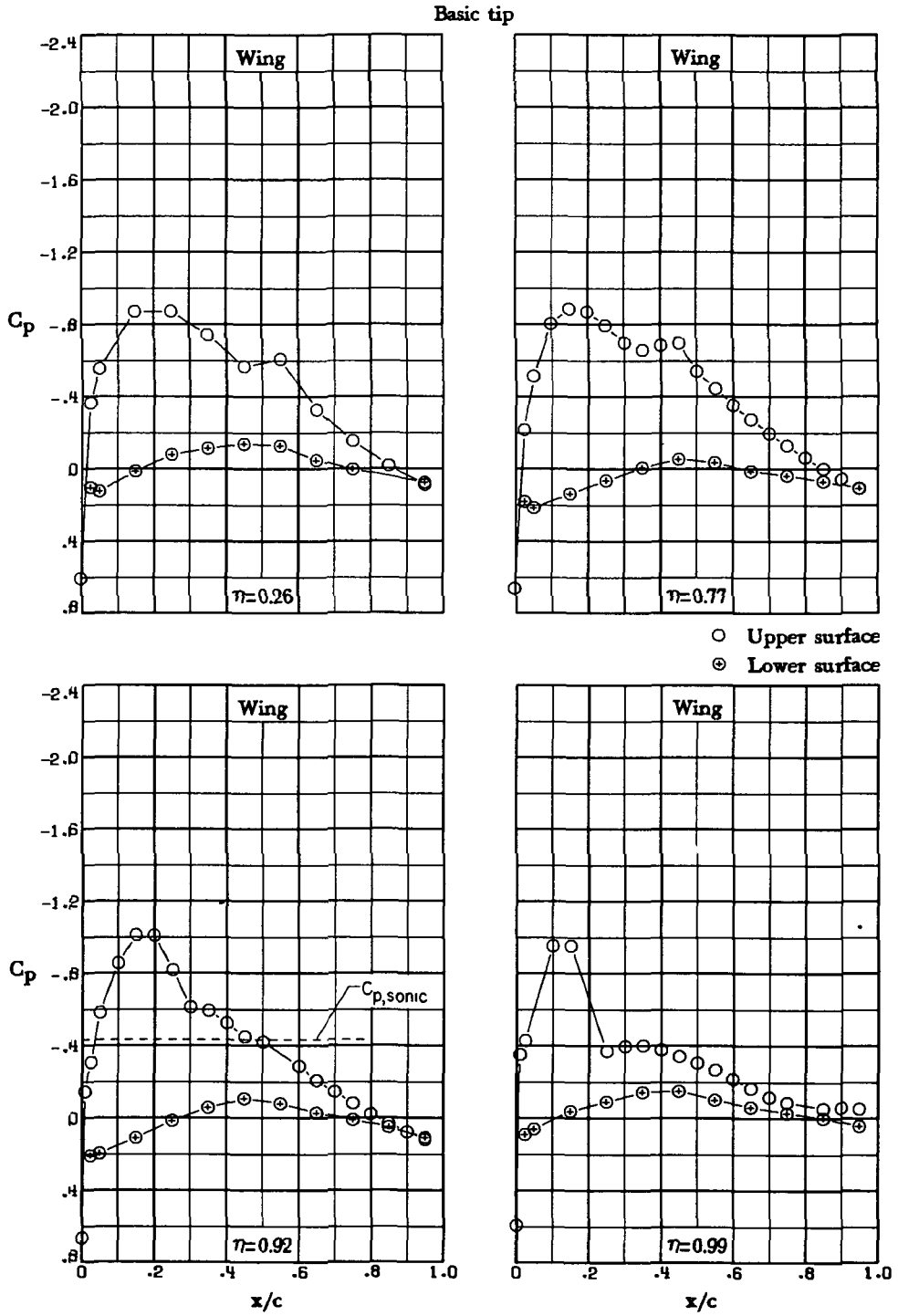

(t) M_∞ = 0.80; α = 2.0°.

Figure 8.- Continued.

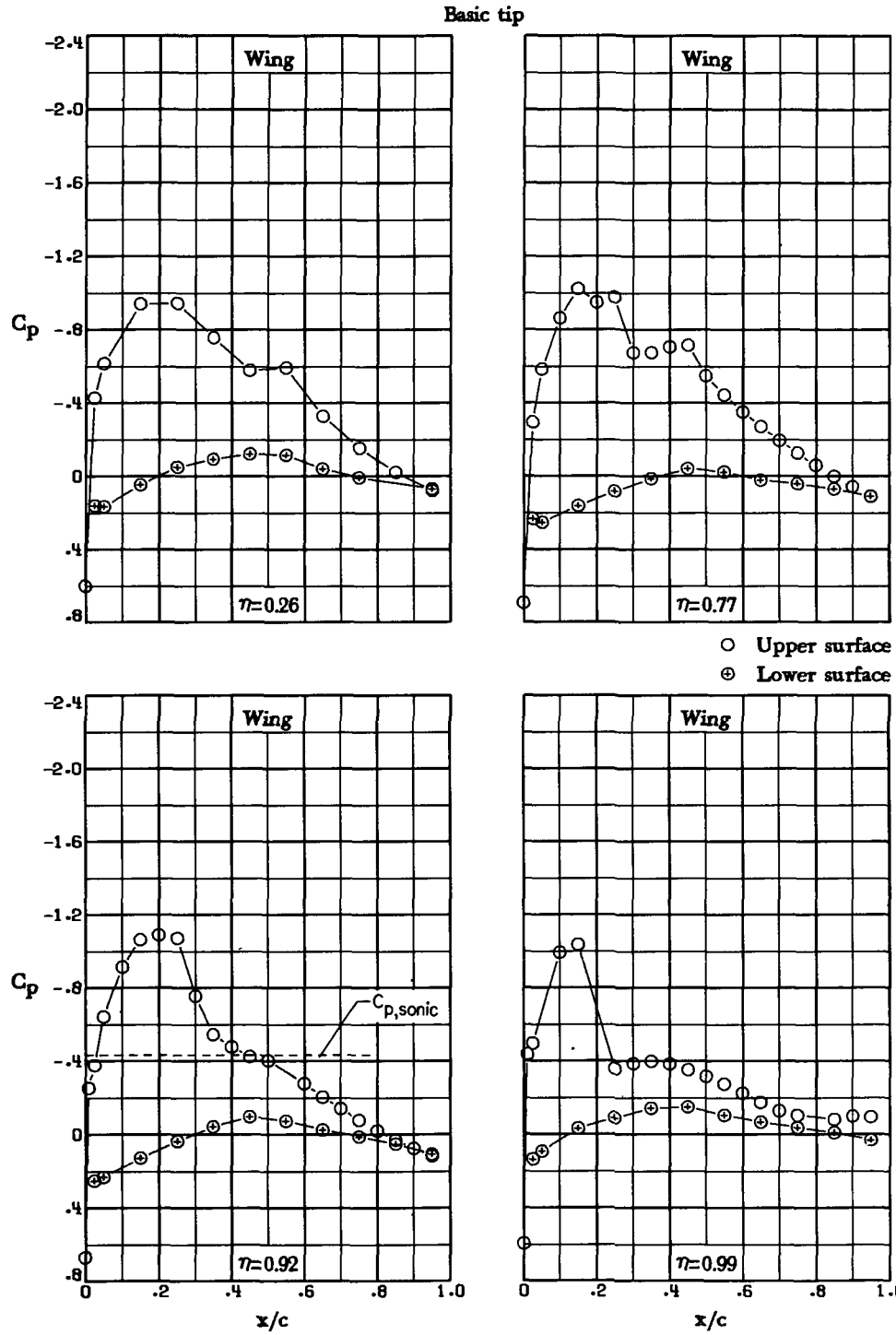

(u) $M_\infty = 0.80$; $\alpha = 2.5^\circ$.

Figure 8.- Continued.

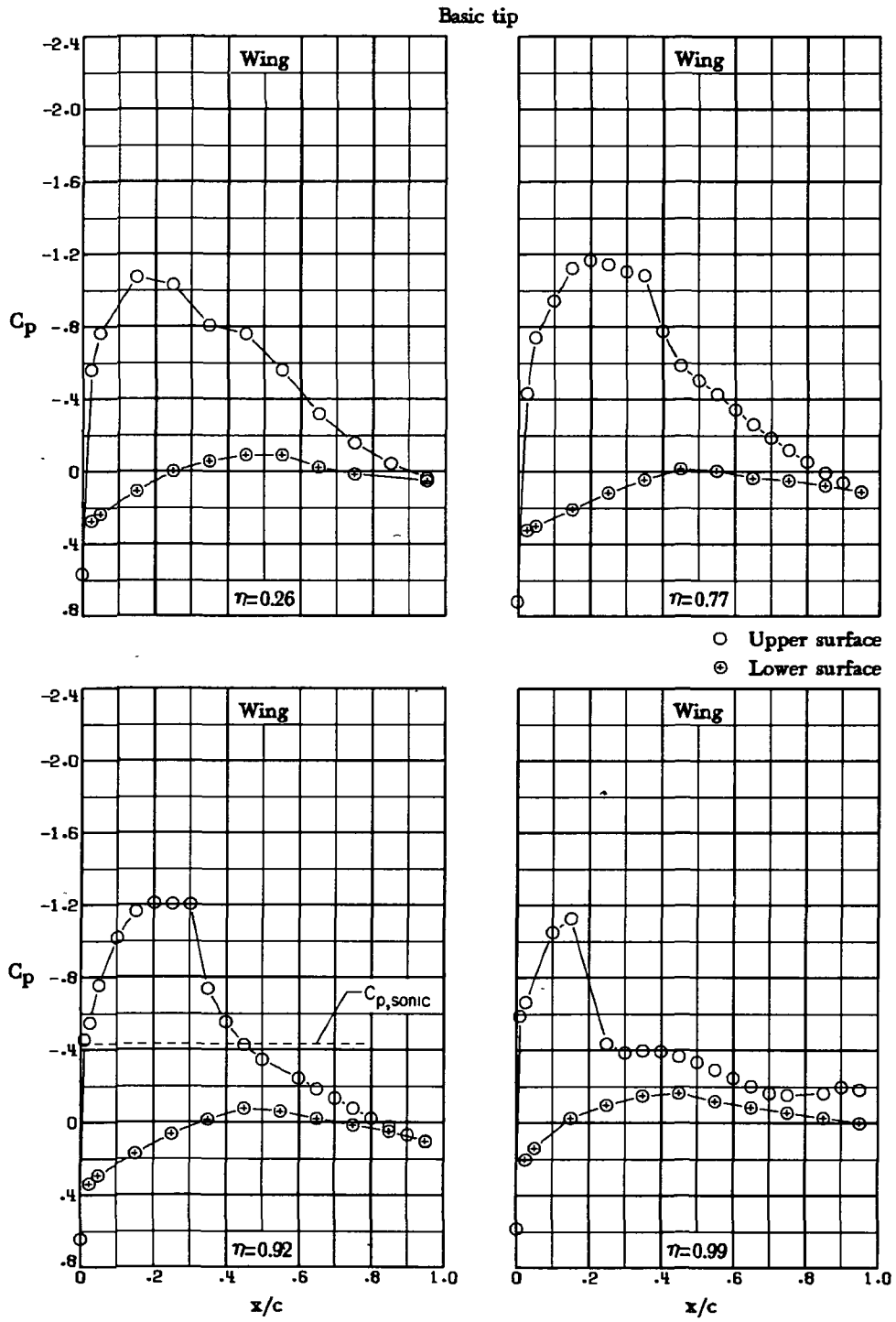

(v) $M_\infty = 0.80$; $\alpha = 3.5^\circ$.

Figure 8.- Continued.

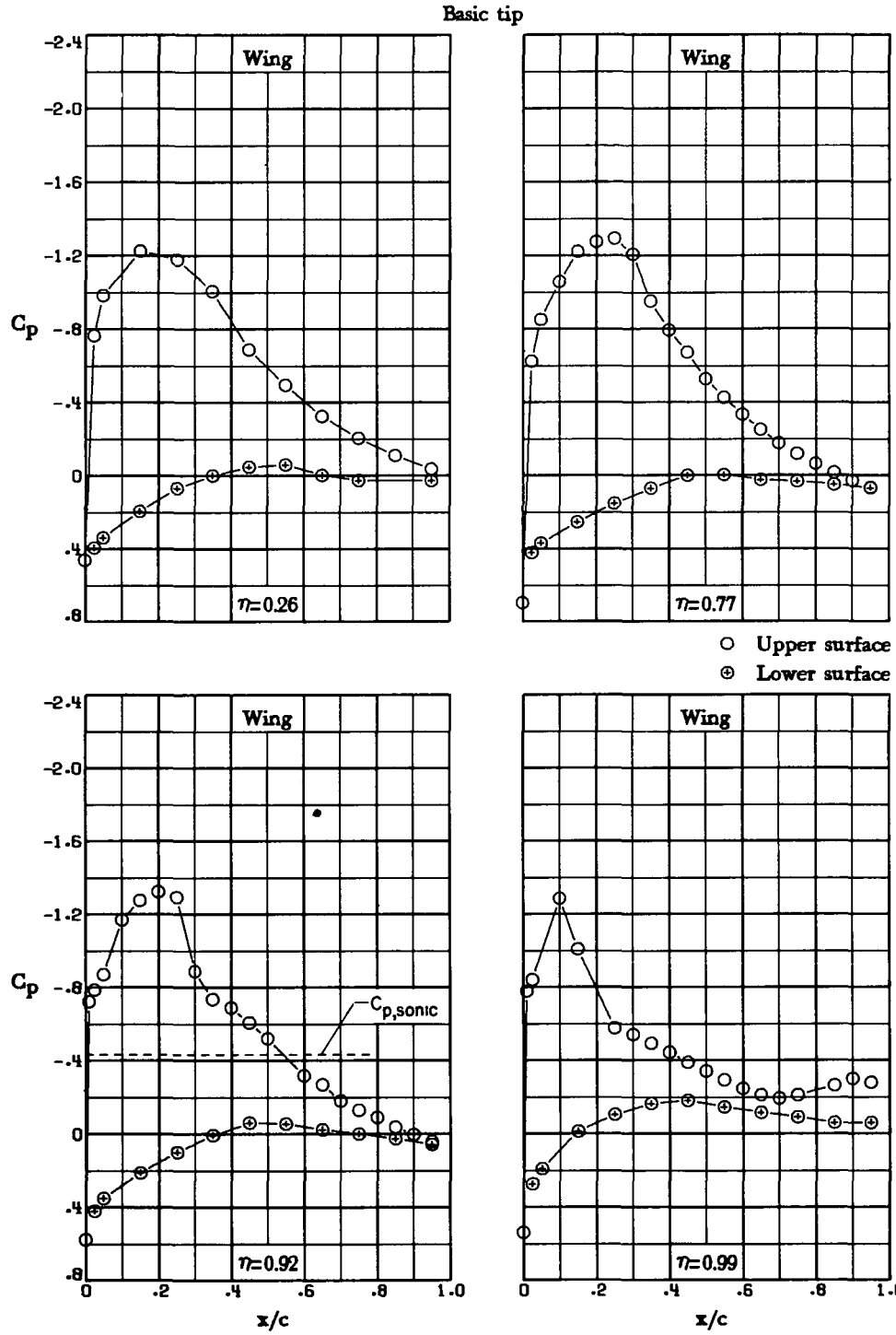

(w) $M_\infty = 0.80$; $\alpha = 5.0^\circ$.

Figure 8.- Continued.

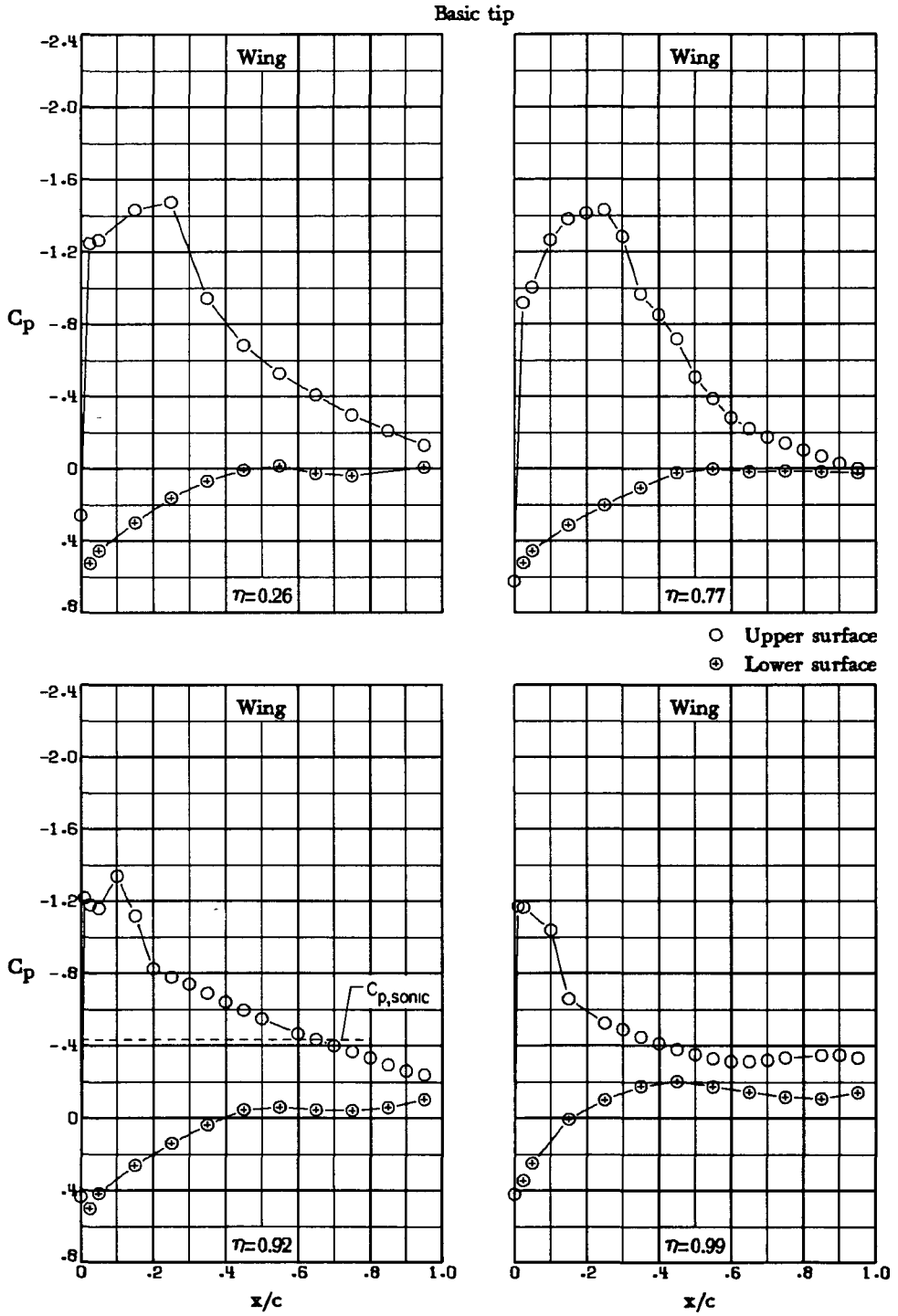

(x) $M_\infty = 0.80$; $\alpha = 7.2^\circ$.

Figure 8.- Concluded.

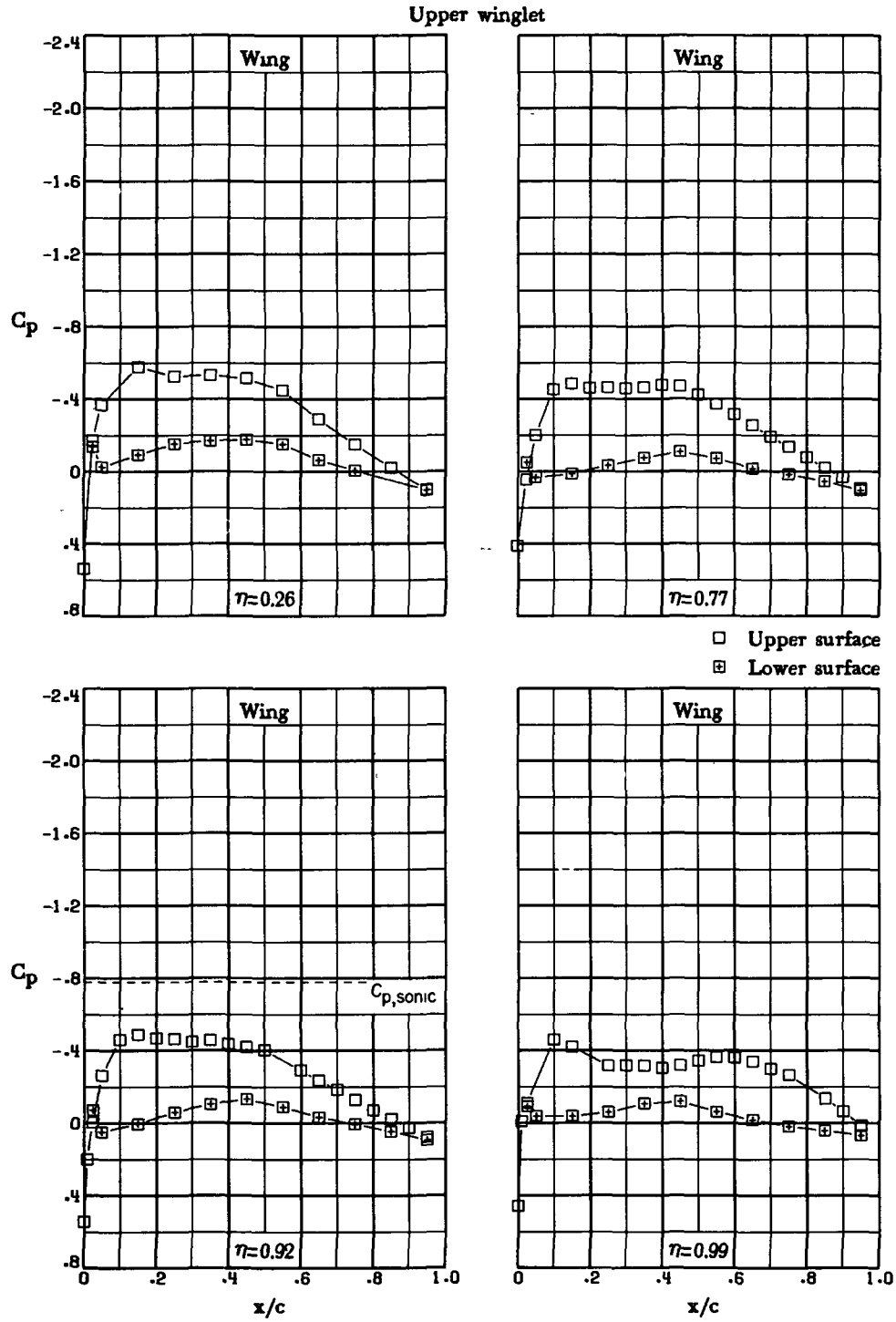

(a) $M_\infty = 0.70$; $\alpha = 0^o$.

Figure 9.- Pressure distributions for upper-winglet configuration.

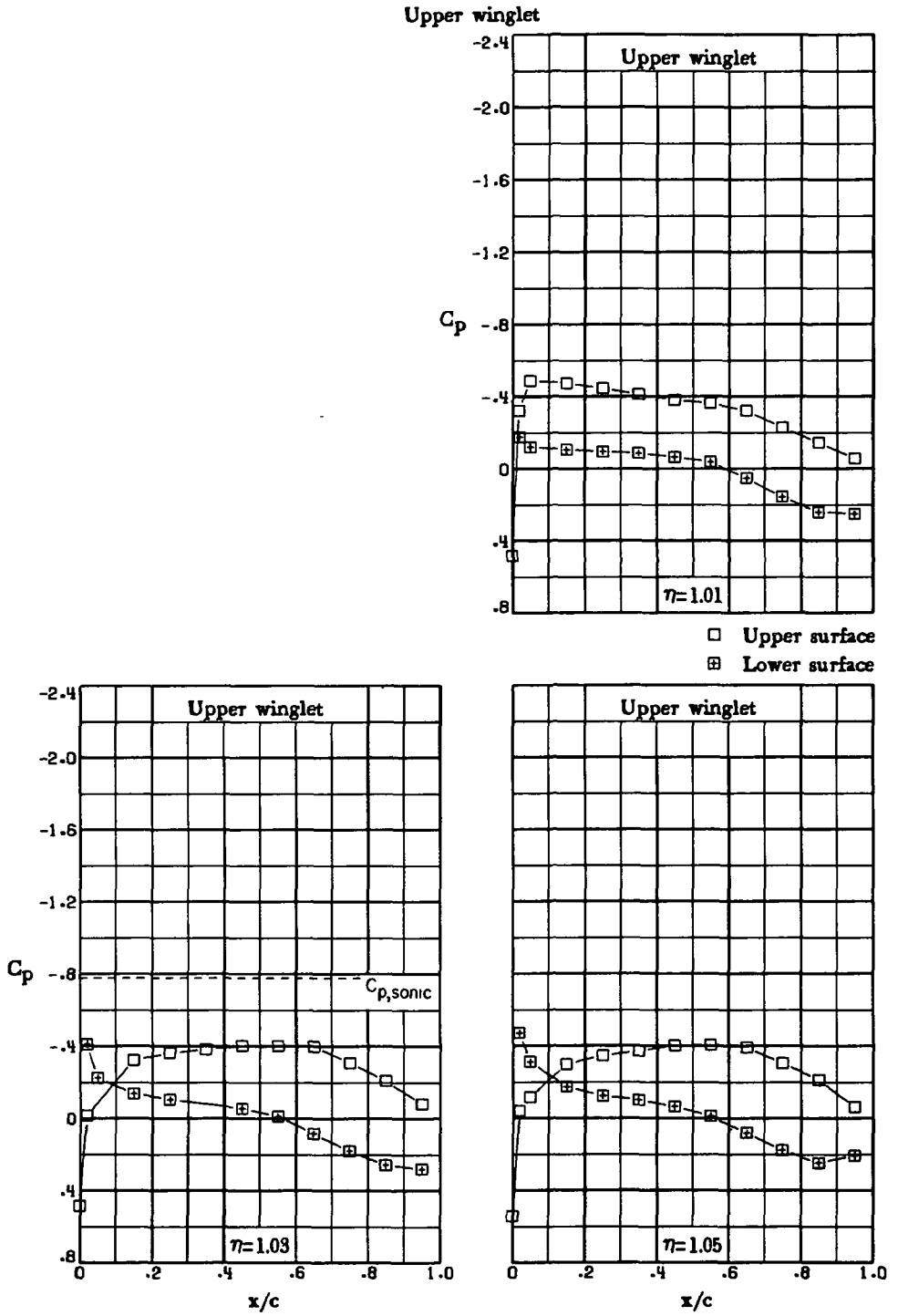

(a) M_∞ = 0.70; α = 0°. Concluded.

Figure 9.- Continued.

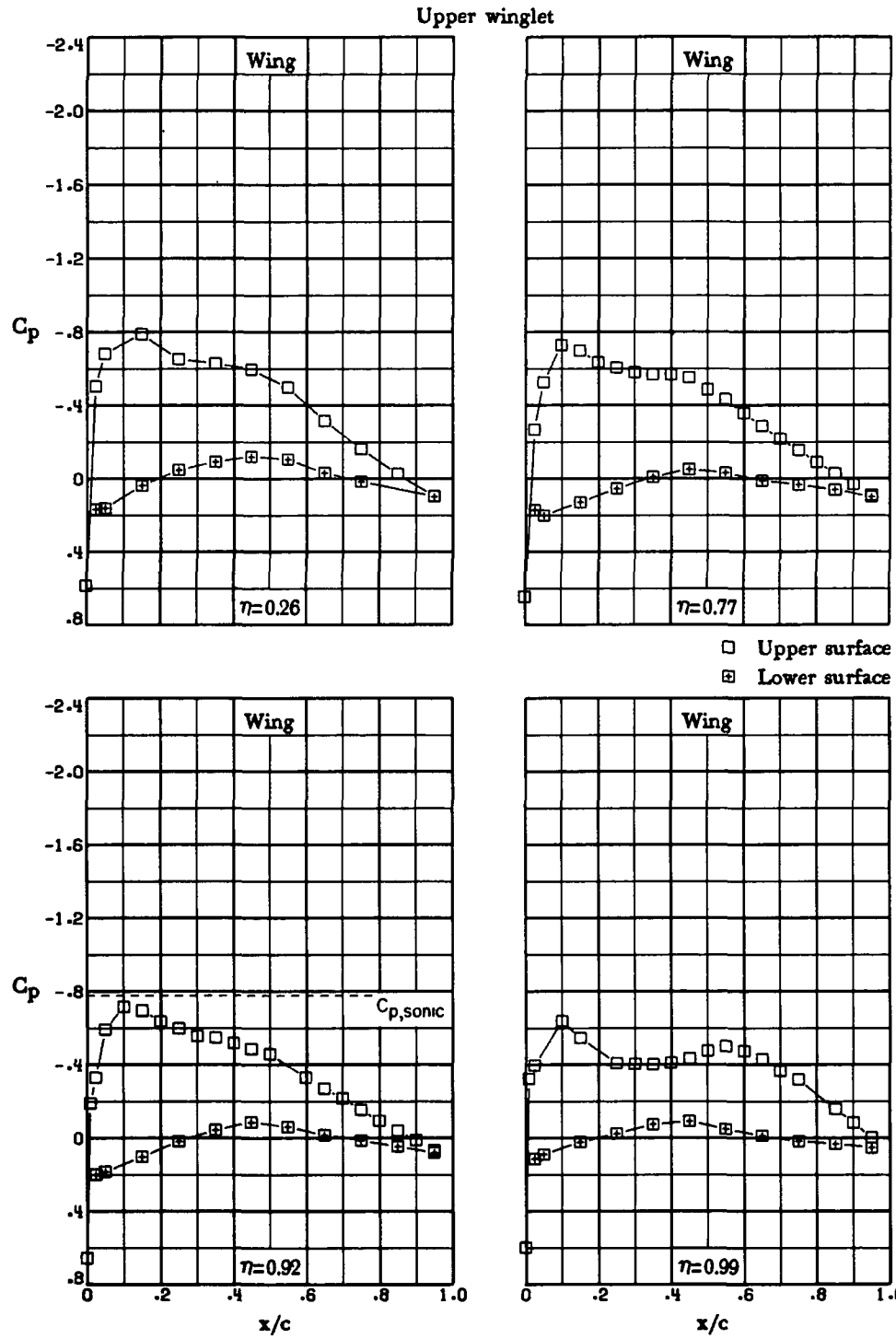

(b) M_∞ = 0.70; α = 2.0°.

Figure 9.- Continued.

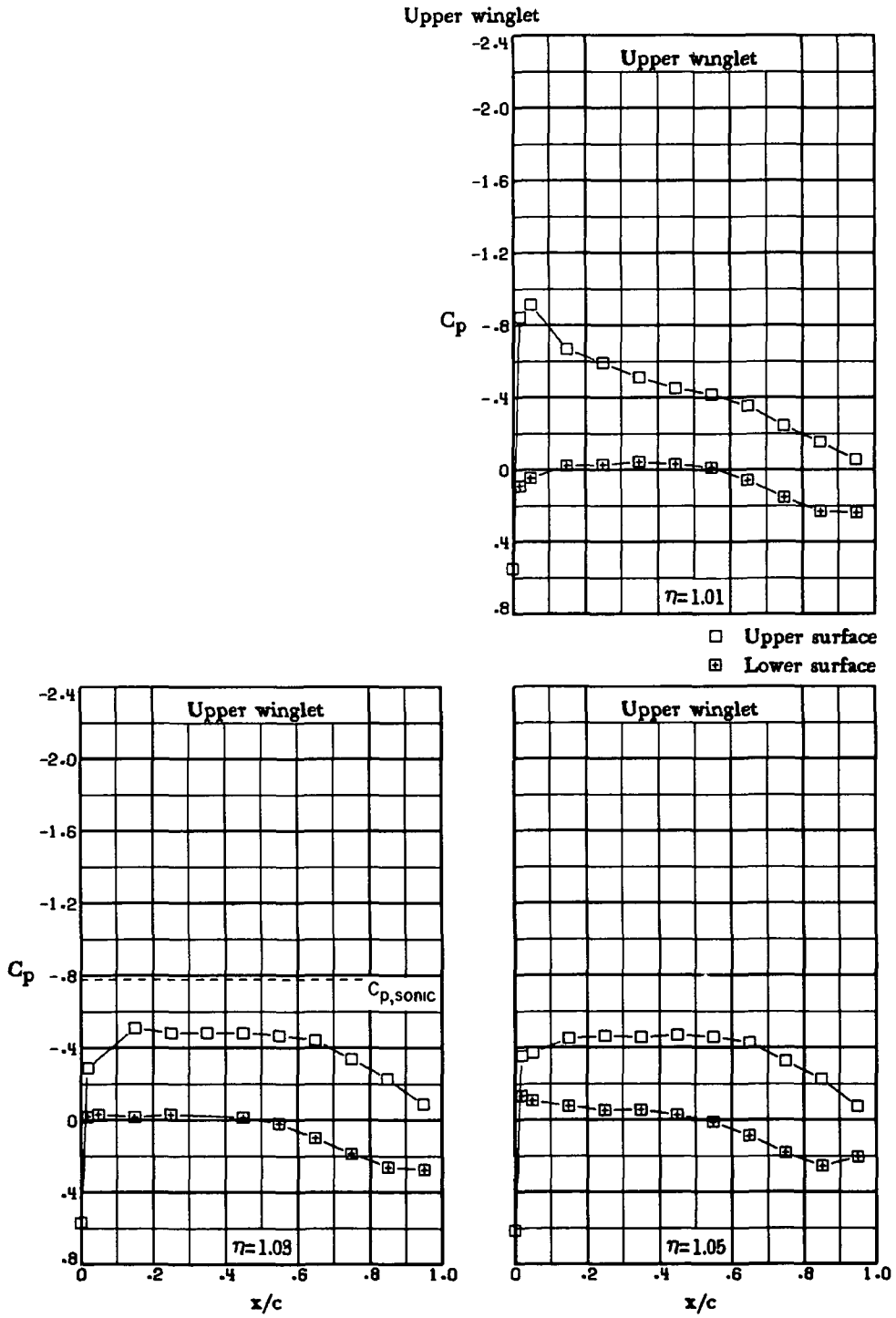

(b) M_∞ = 0.70; α = 2.0°. Concluded.

Figure 9.- Continued.

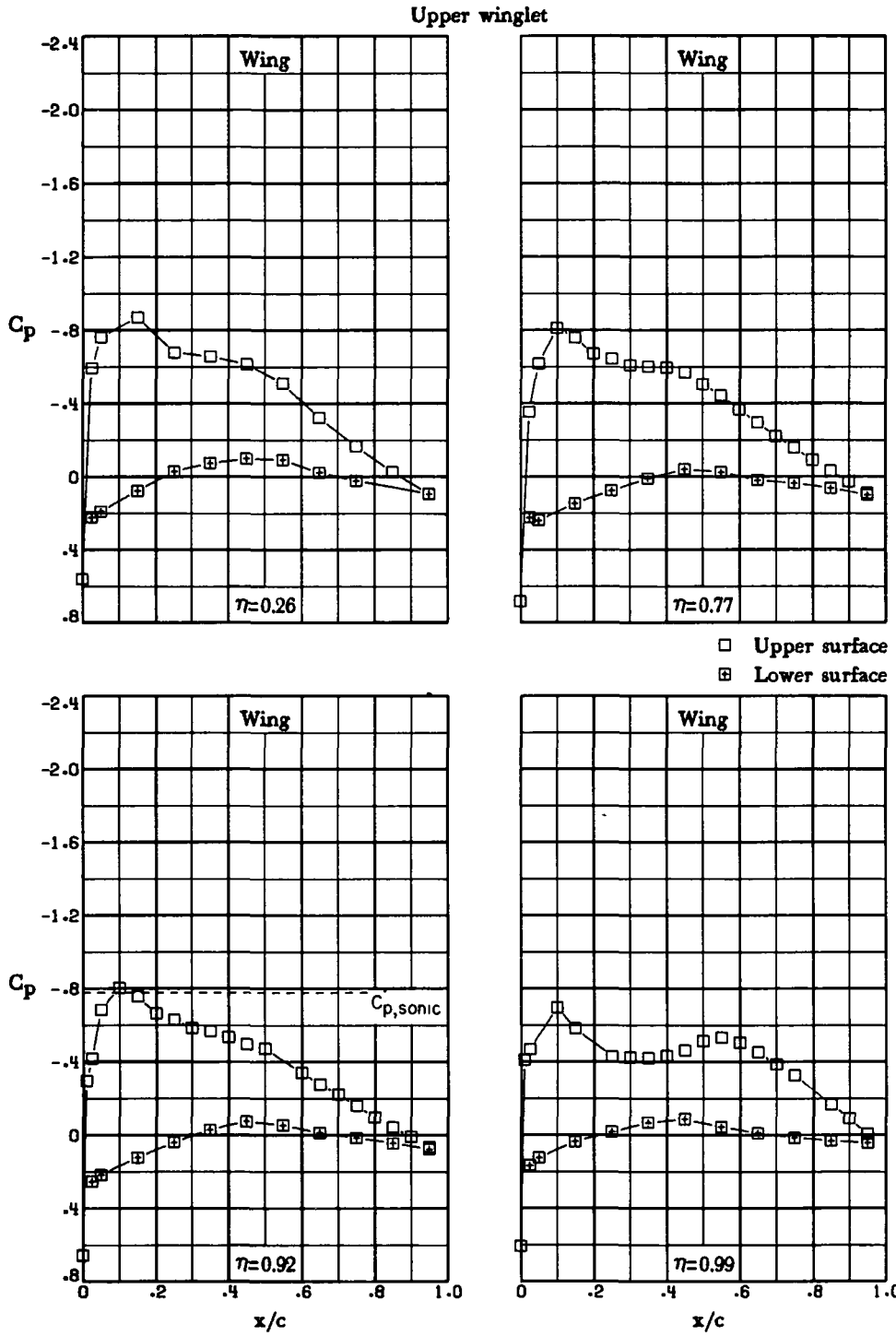

(c) M_∞ = 0.70; α = 2.5°.

Figure 9.- Continued.

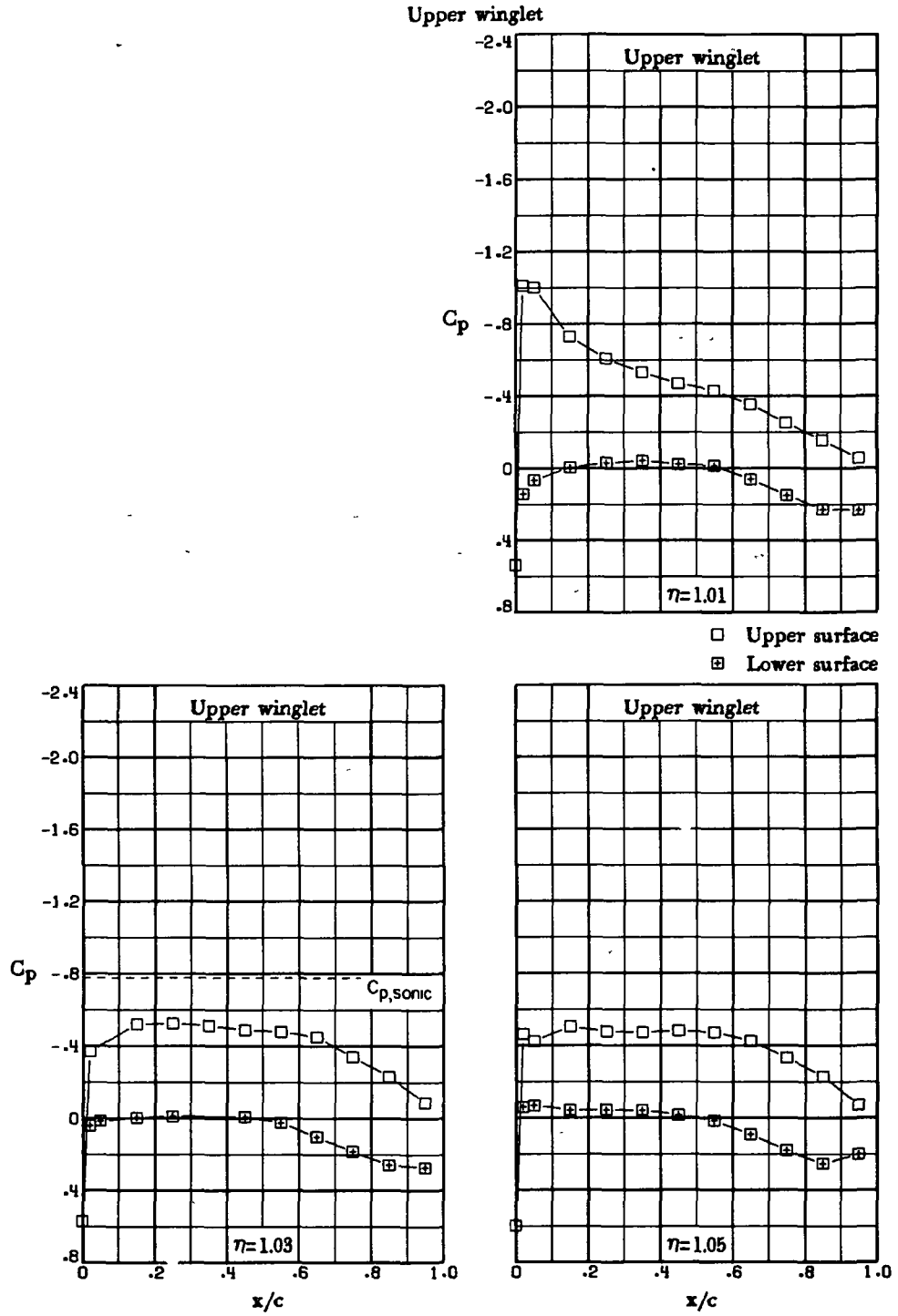

(c) $M_\infty = 0.70$; $\alpha = 2.5^o$. Concluded.

Figure 9.- Continued.

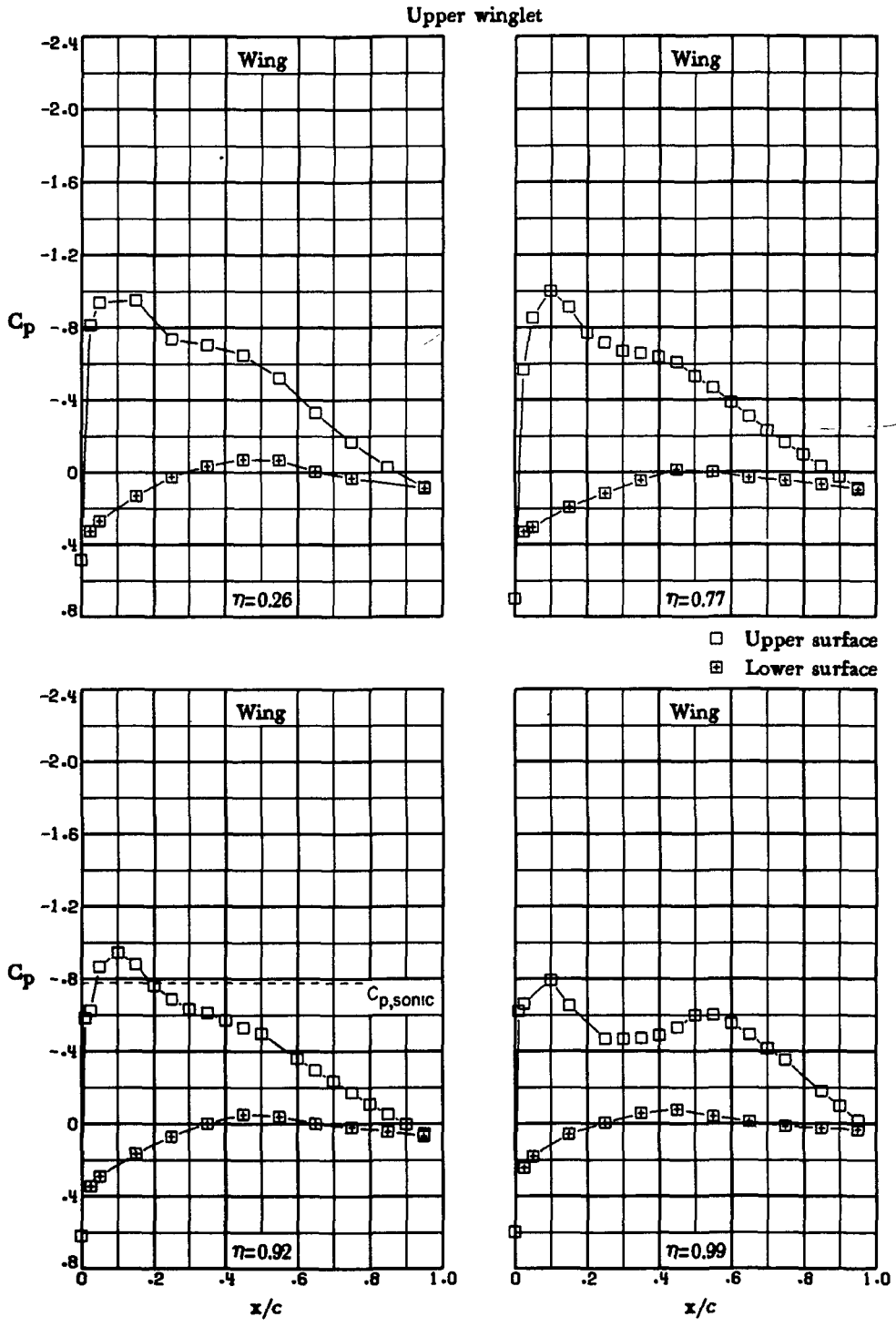

(d) $M_\infty = 0.70$; $\alpha = 3.5^\circ$.

Figure 9.- Continued.

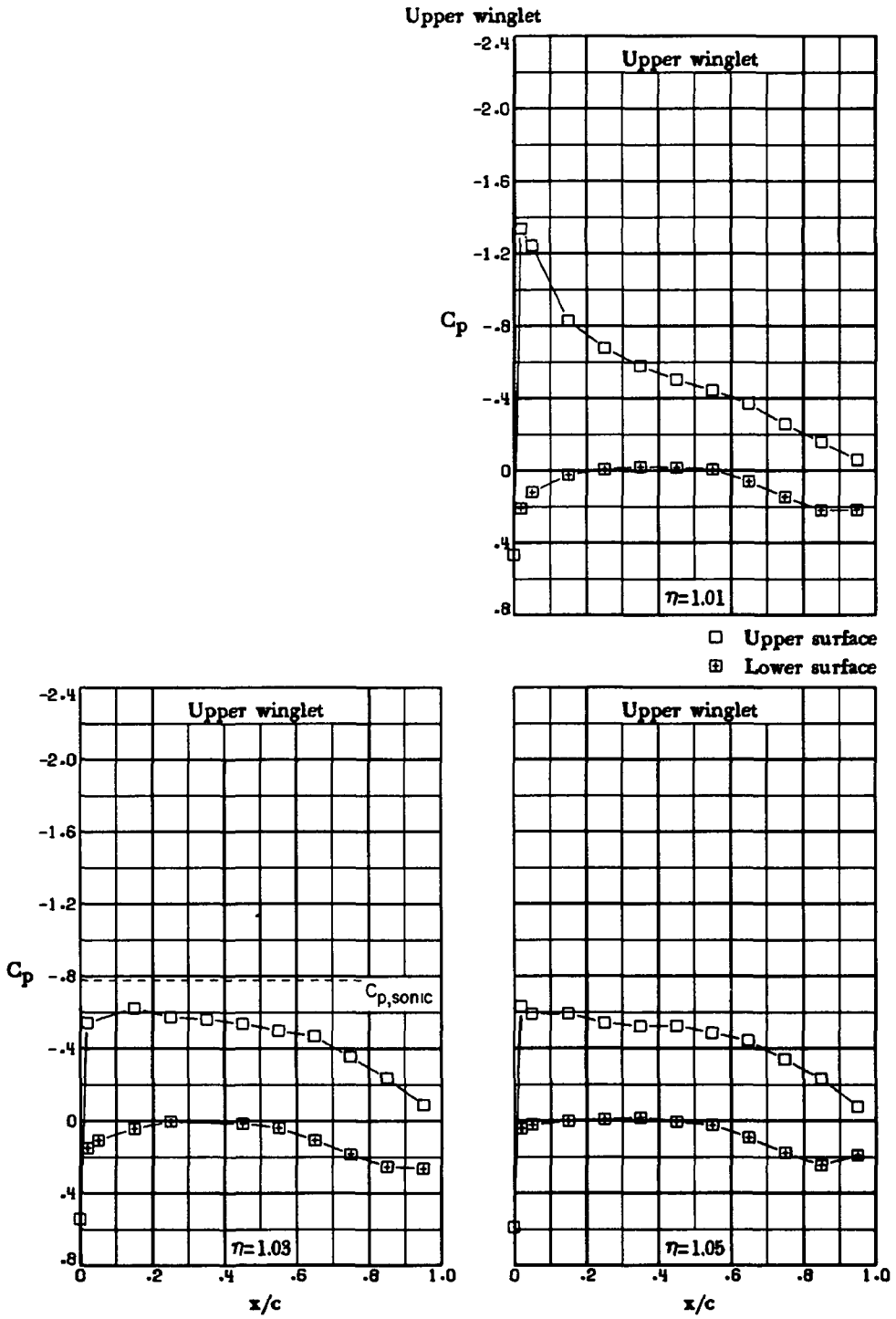

(d) M_∞ = 0.70; α = 3.5°. Concluded.

Figure 9.- Continued.

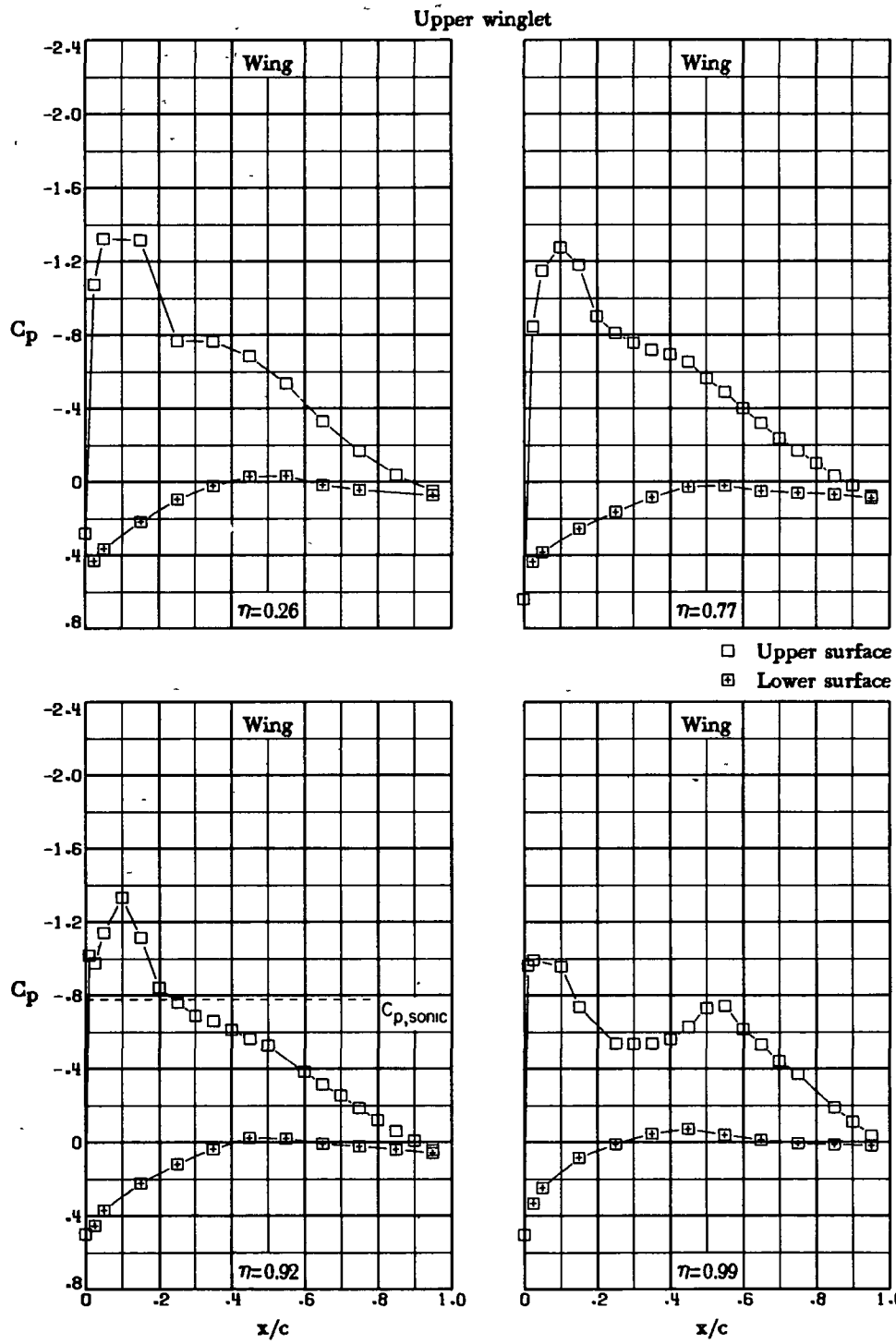

(e) M_∞ = 0.70; α = 5.0°.

Figure 9.- Continued.

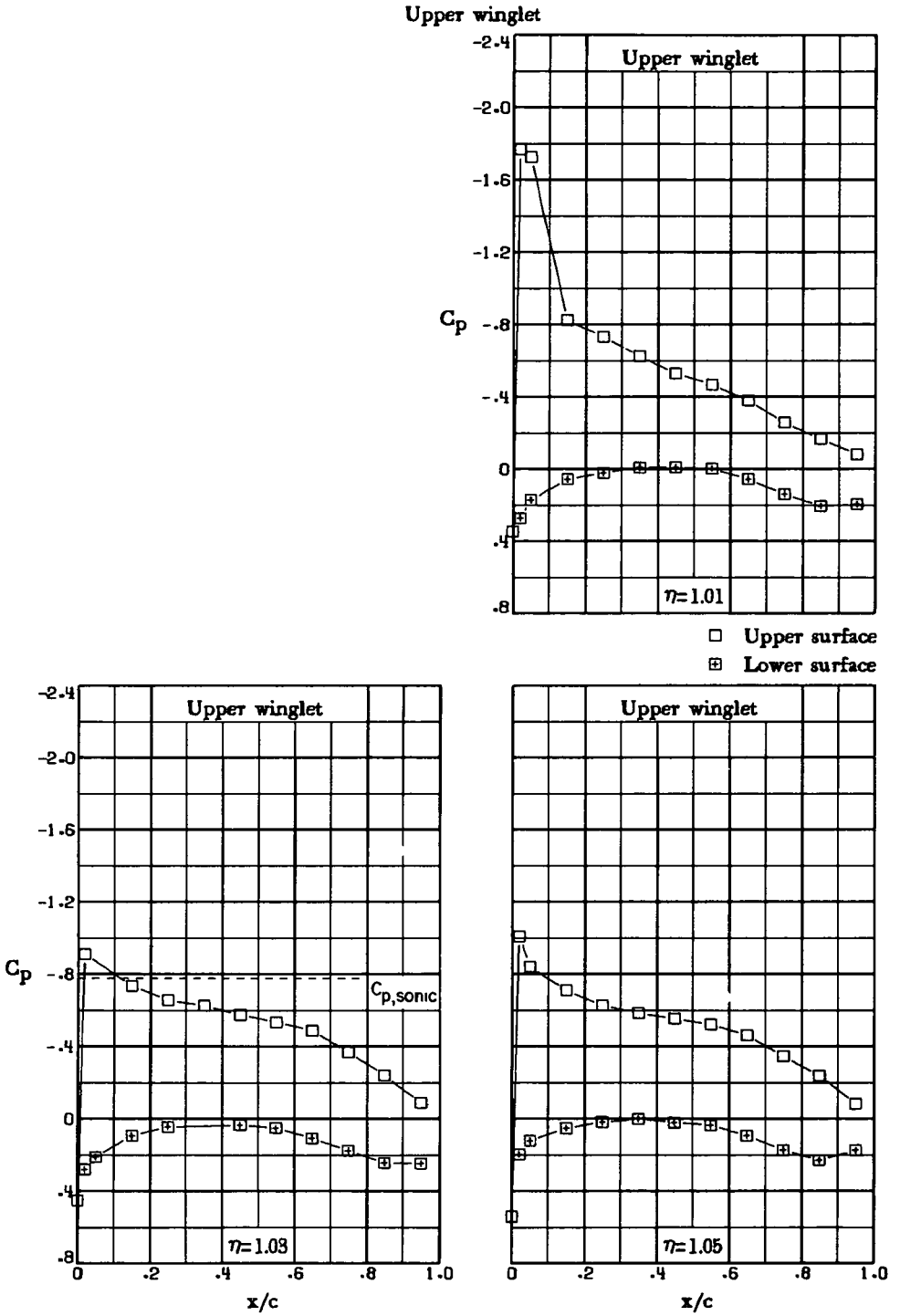

(e) M_∞ = 0.70; α = 5.0°. Concluded.

Figure 9.- Continued.

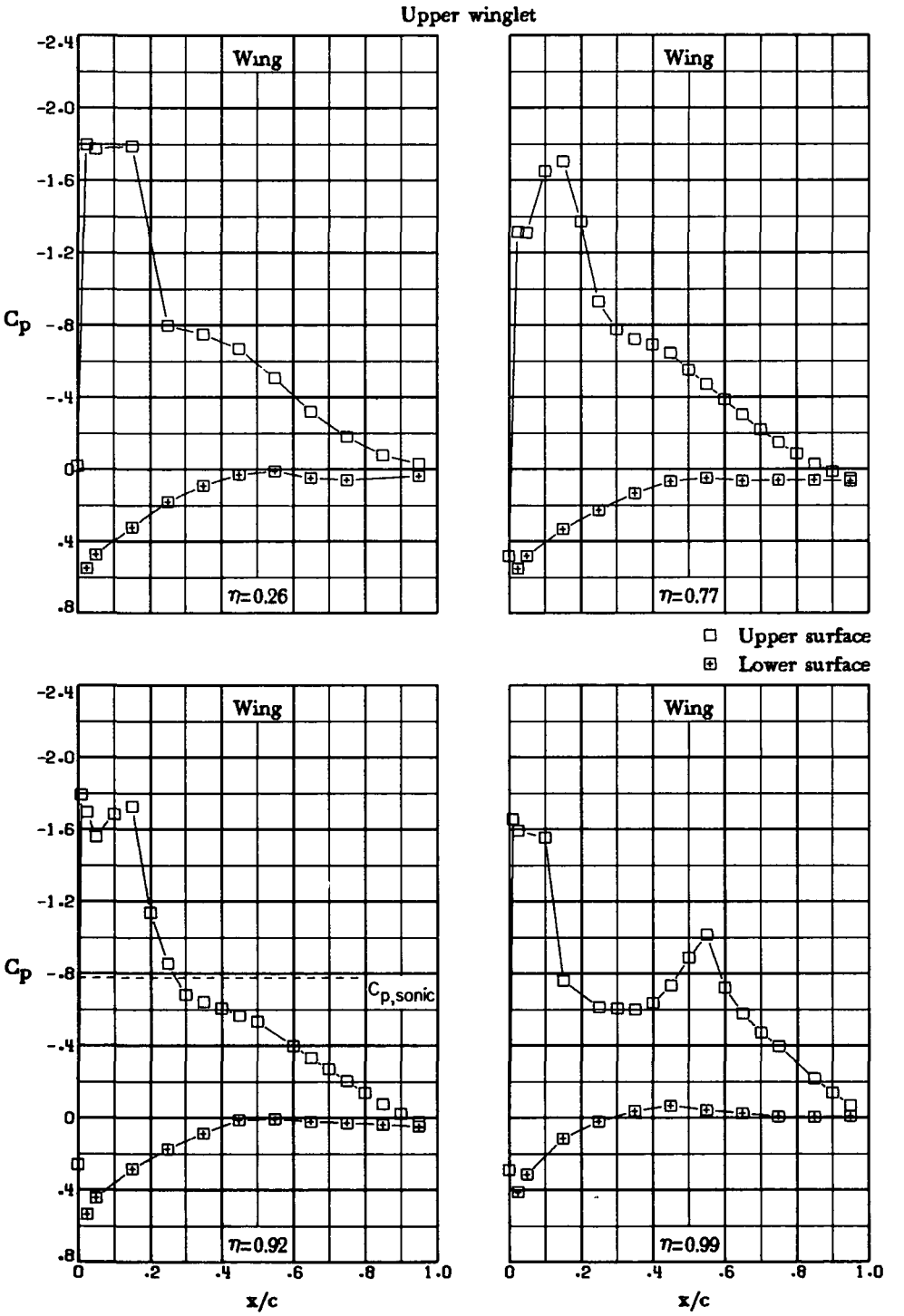

(f) $M_\infty = 0.70$; $\alpha = 7.2^\circ$.

Figure 9.- Continued.

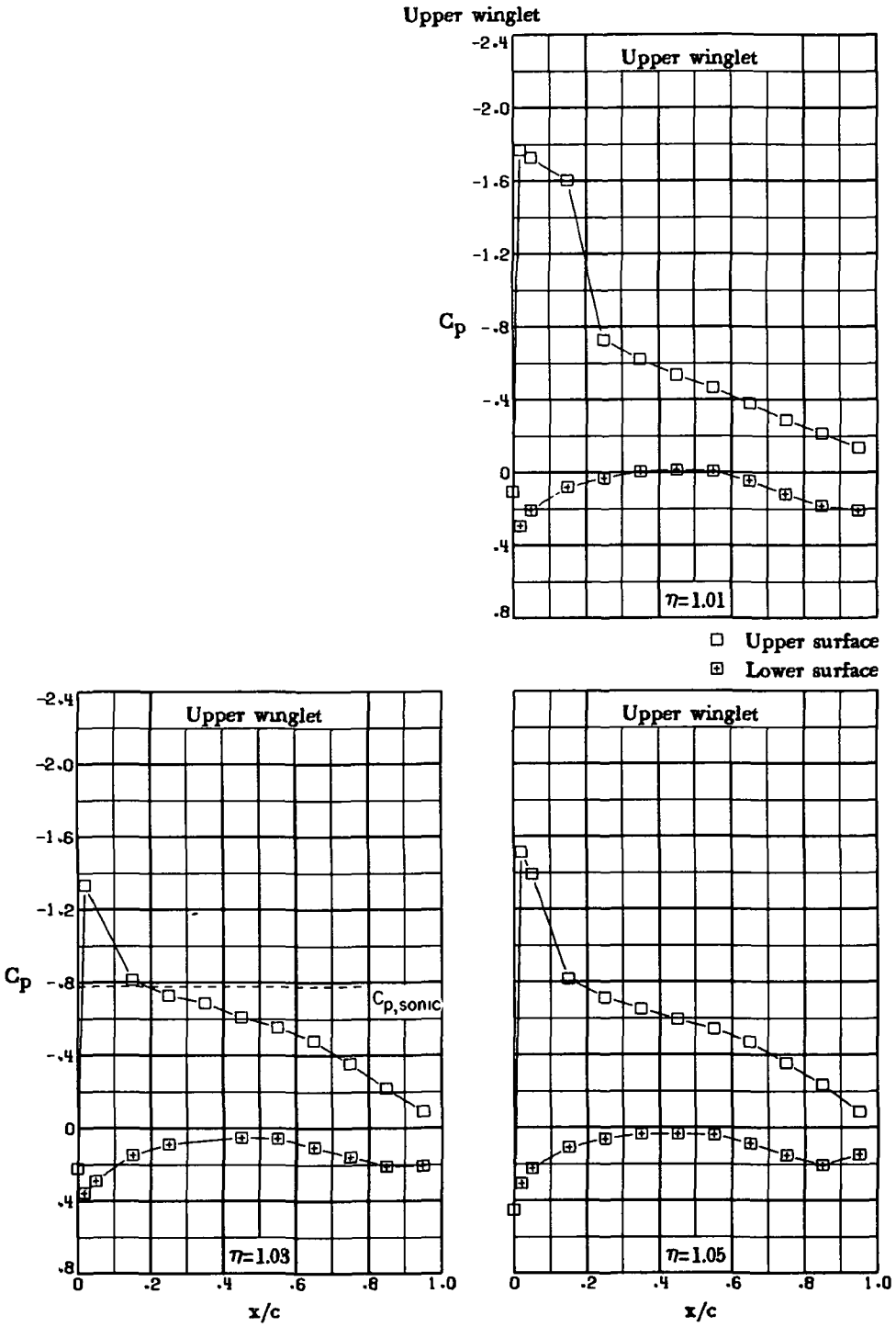

(f) $M_\infty = 0.70$; $\alpha = 7.2^o$. Concluded.

Figure 9.- Continued.

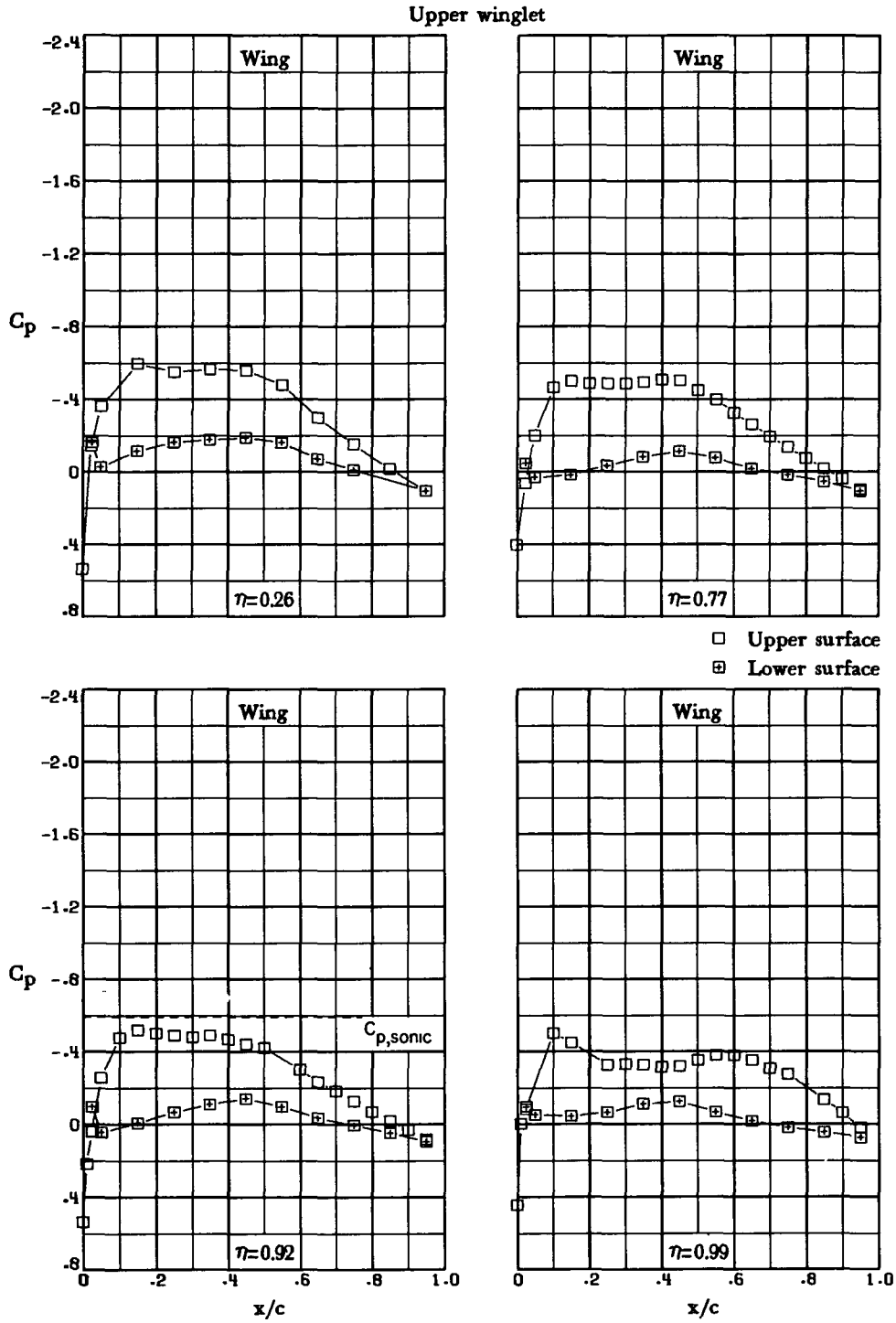

(g) $M_\infty = 0.75$; $\alpha = 0^o$.

Figure 9.- Continued.

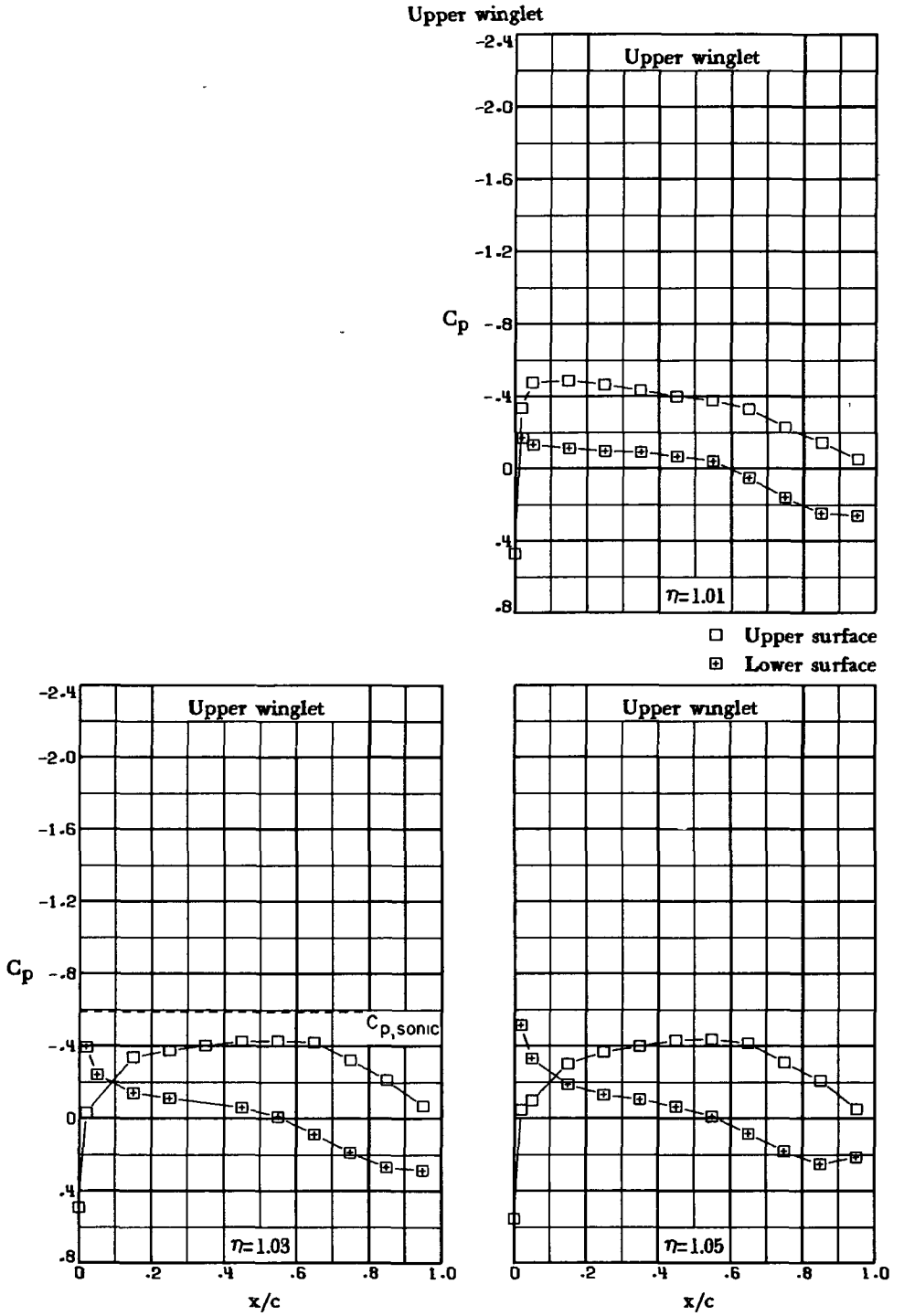

(g) $M_\infty = 0.75$; $\alpha = 0^\circ$. Concluded.

Figure 9.- Continued.

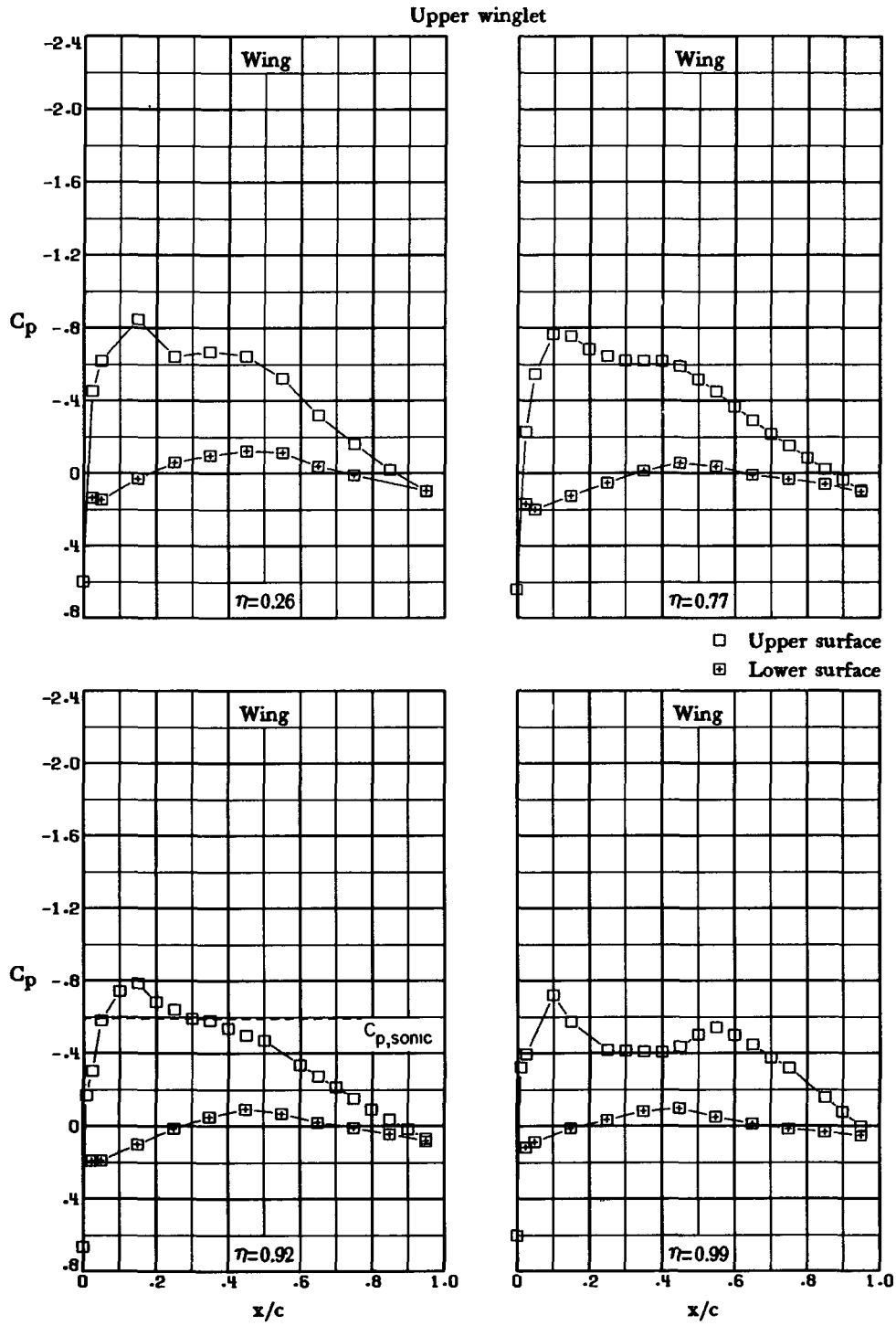

(h) $M_\infty = 0.75$; $\alpha = 2.0^\circ$.

Figure 9.- Continued.

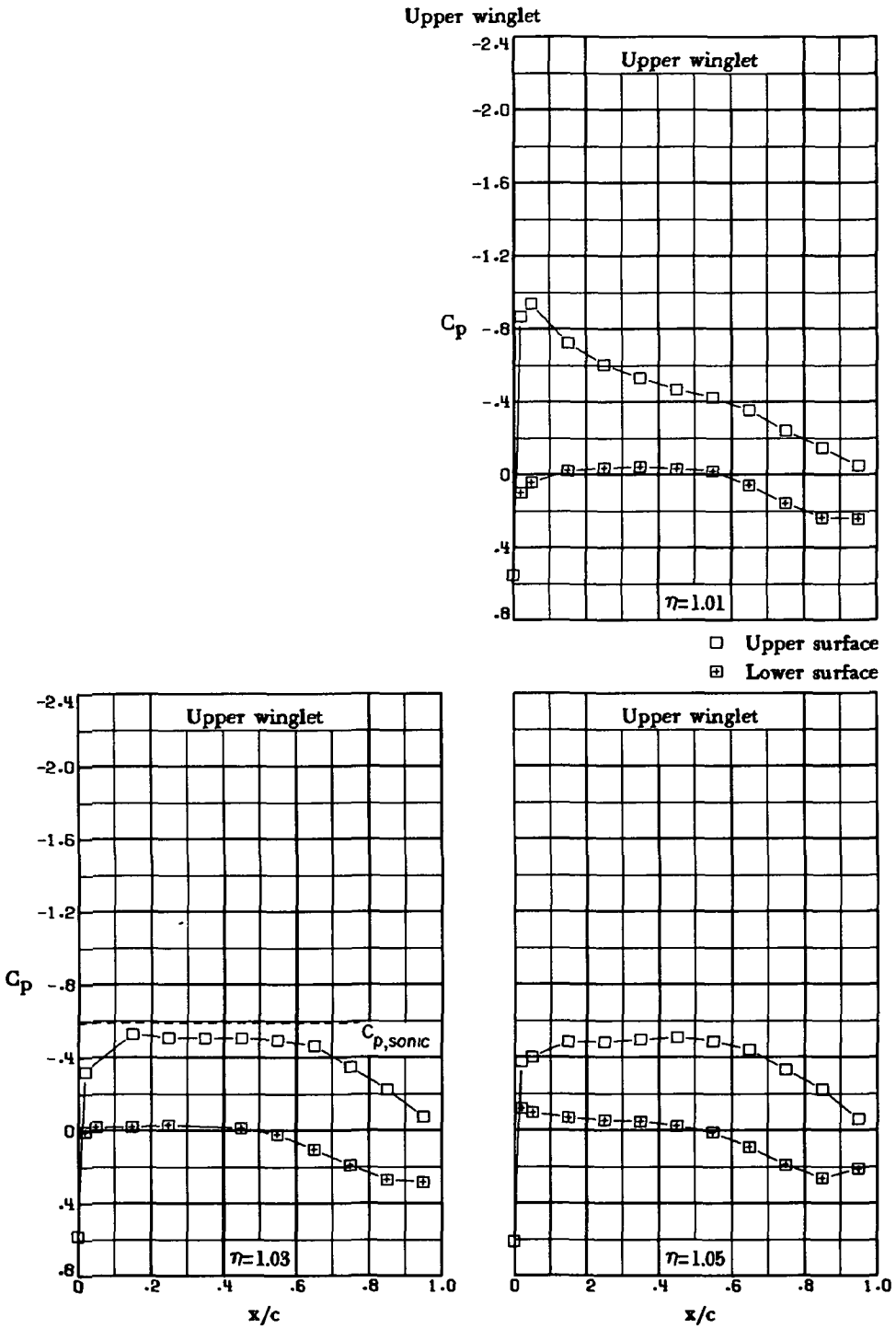

(h) $M_\infty = 0.75$; $\alpha = 2.0^\circ$. Concluded.

Figure 9.- Continued.

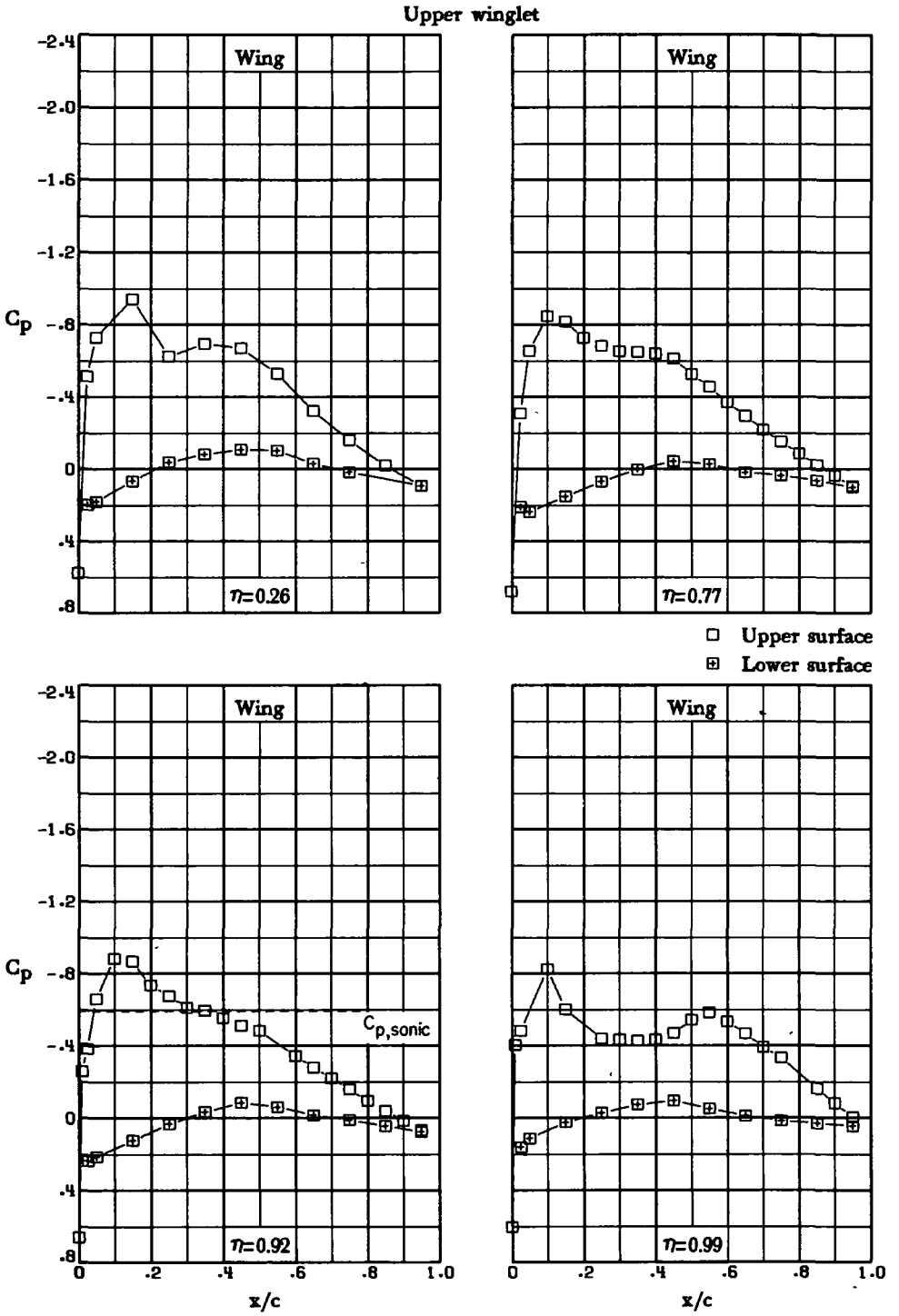

(i) $M_\infty = 0.75$; $\alpha = 2.5^\circ$.

Figure 9.- Continued.

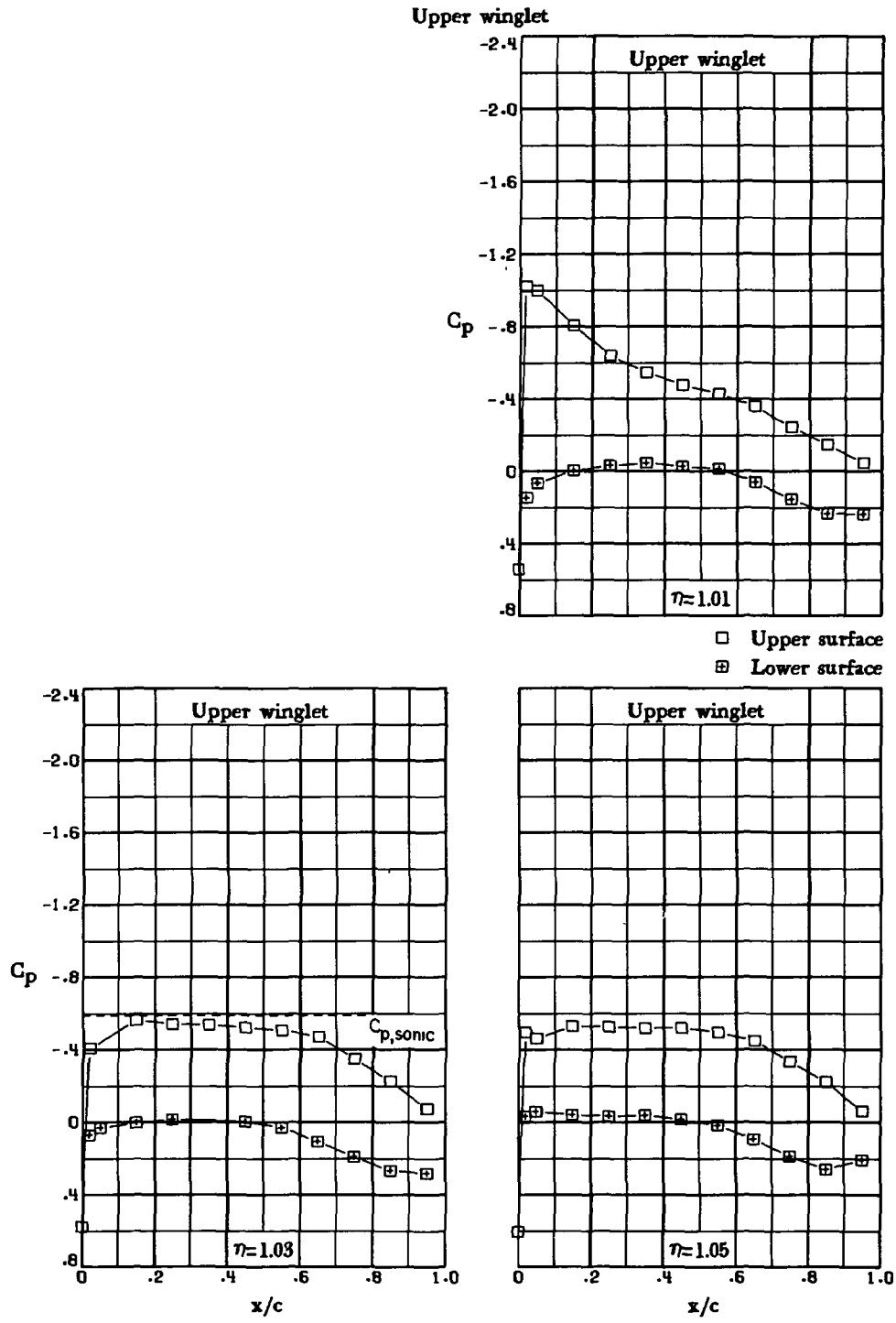

(i) $M_\infty = 0.75$; $\alpha = 2.5^o$. Concluded.

Figure 9.- Continued.

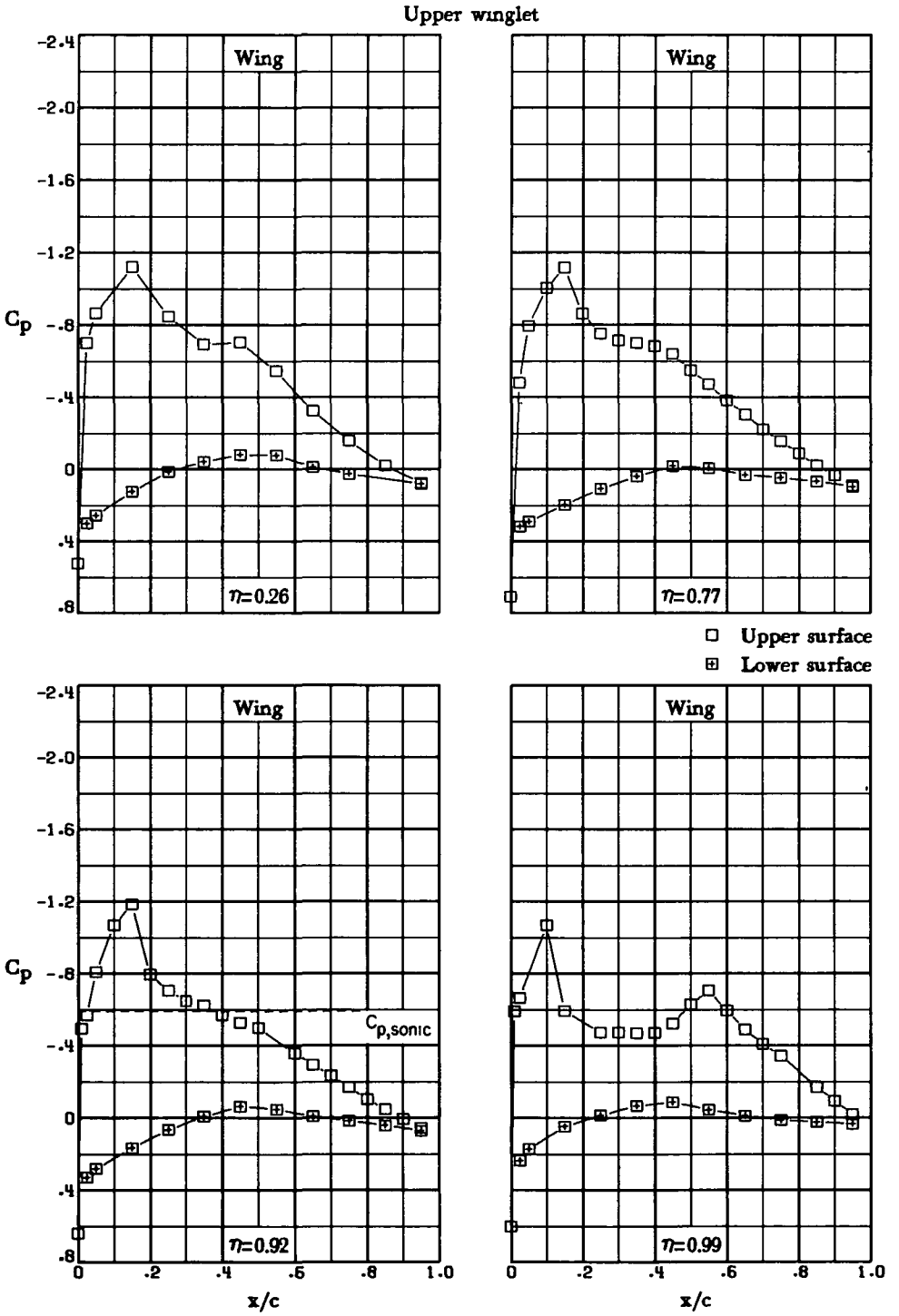

(j) $M_\infty = 0.75$; $\alpha = 3.5^\circ$.

Figure 9.- Continued.

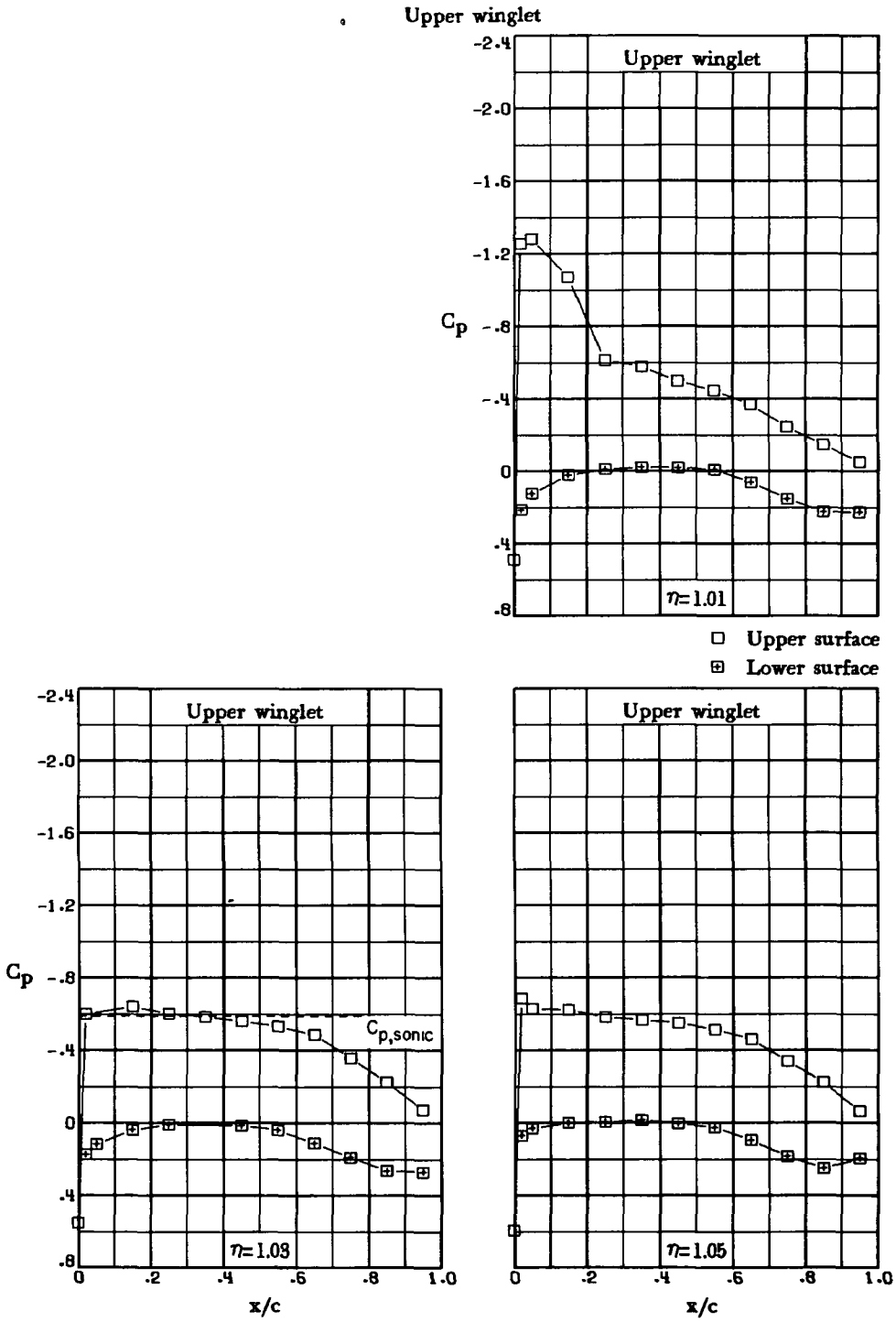

(j) M_∞ = 0.75; α = 3.5°. Concluded.

Figure 9.- Continued.

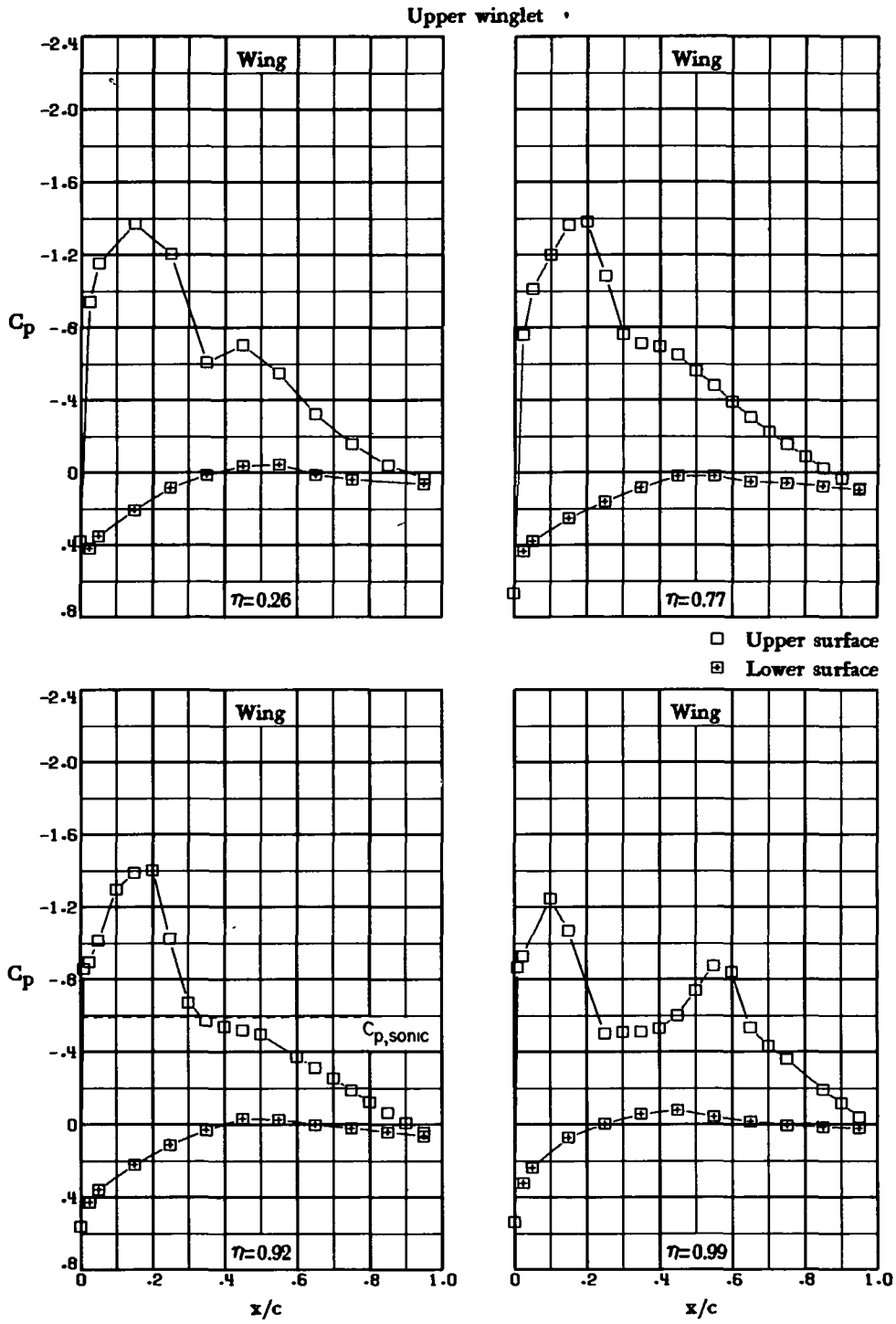

(k) $M_\infty = 0.75$; $\alpha = 5.0^\circ$.

Figure 9.- Continued.

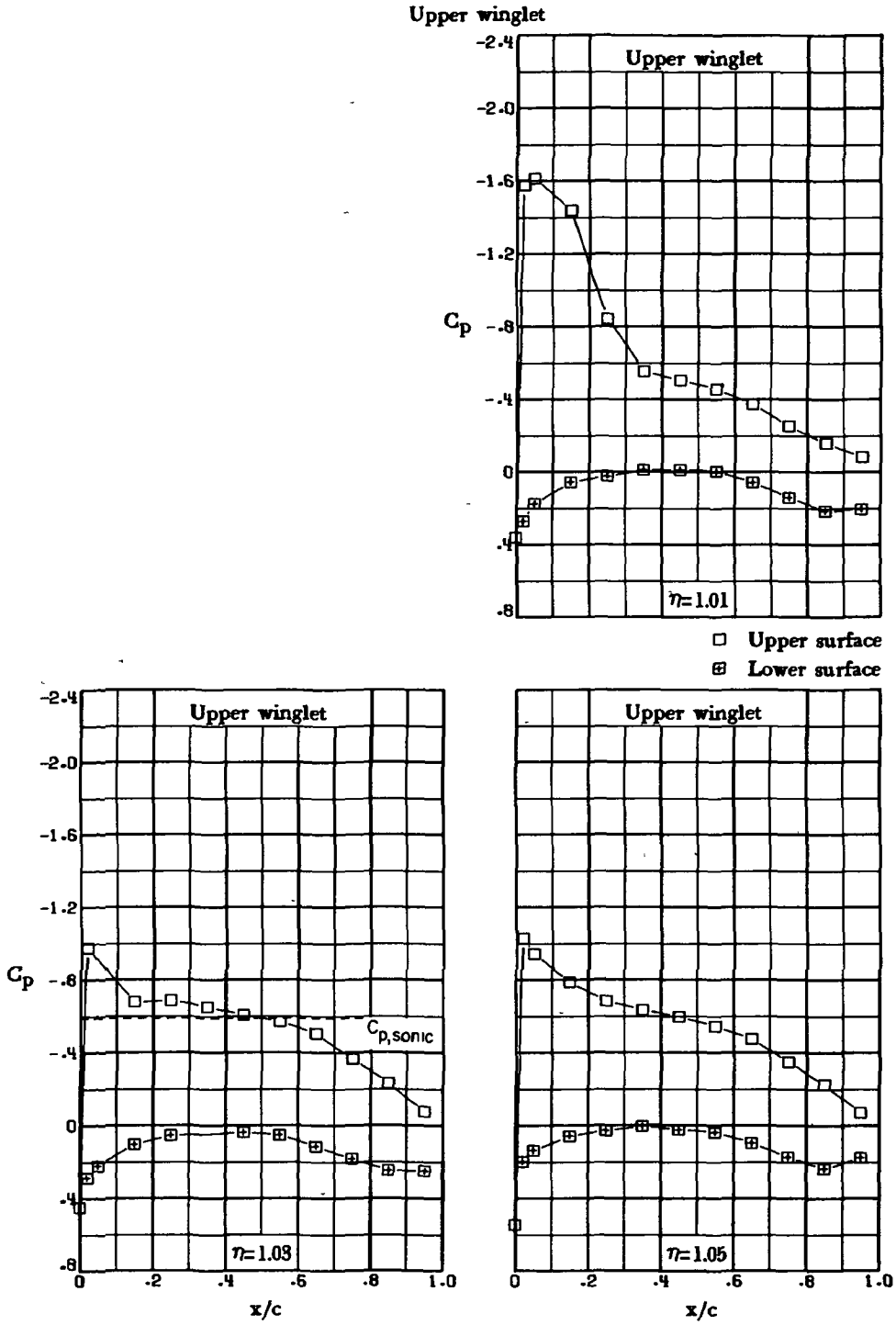

(k) M_∞ = 0.75; α = 5.0°. Concluded.

Figure 9.- Continued.

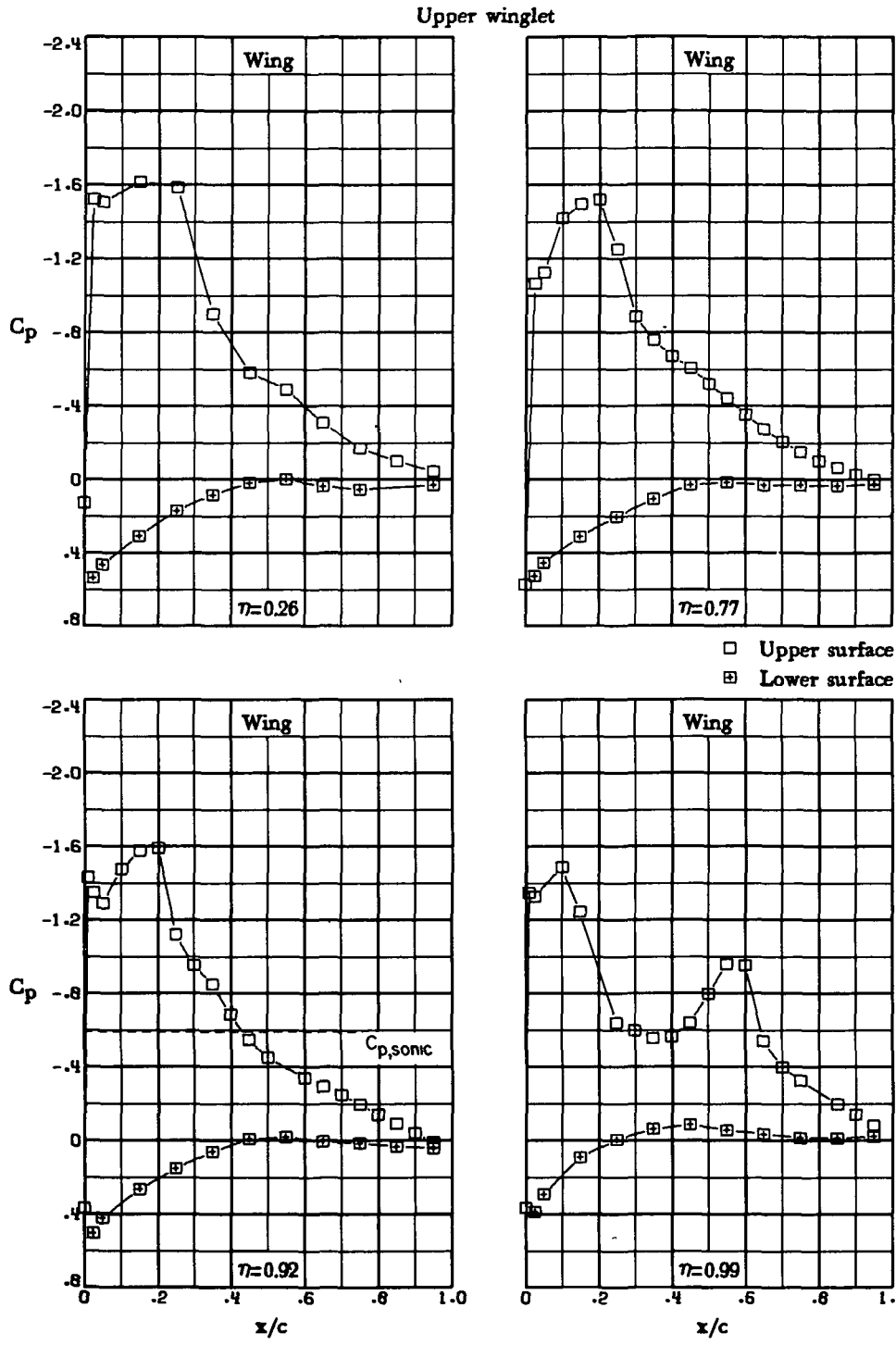

(1) $M_\infty = 0.75$; $\alpha = 7.2^\circ$.

Figure 9.- Continued.

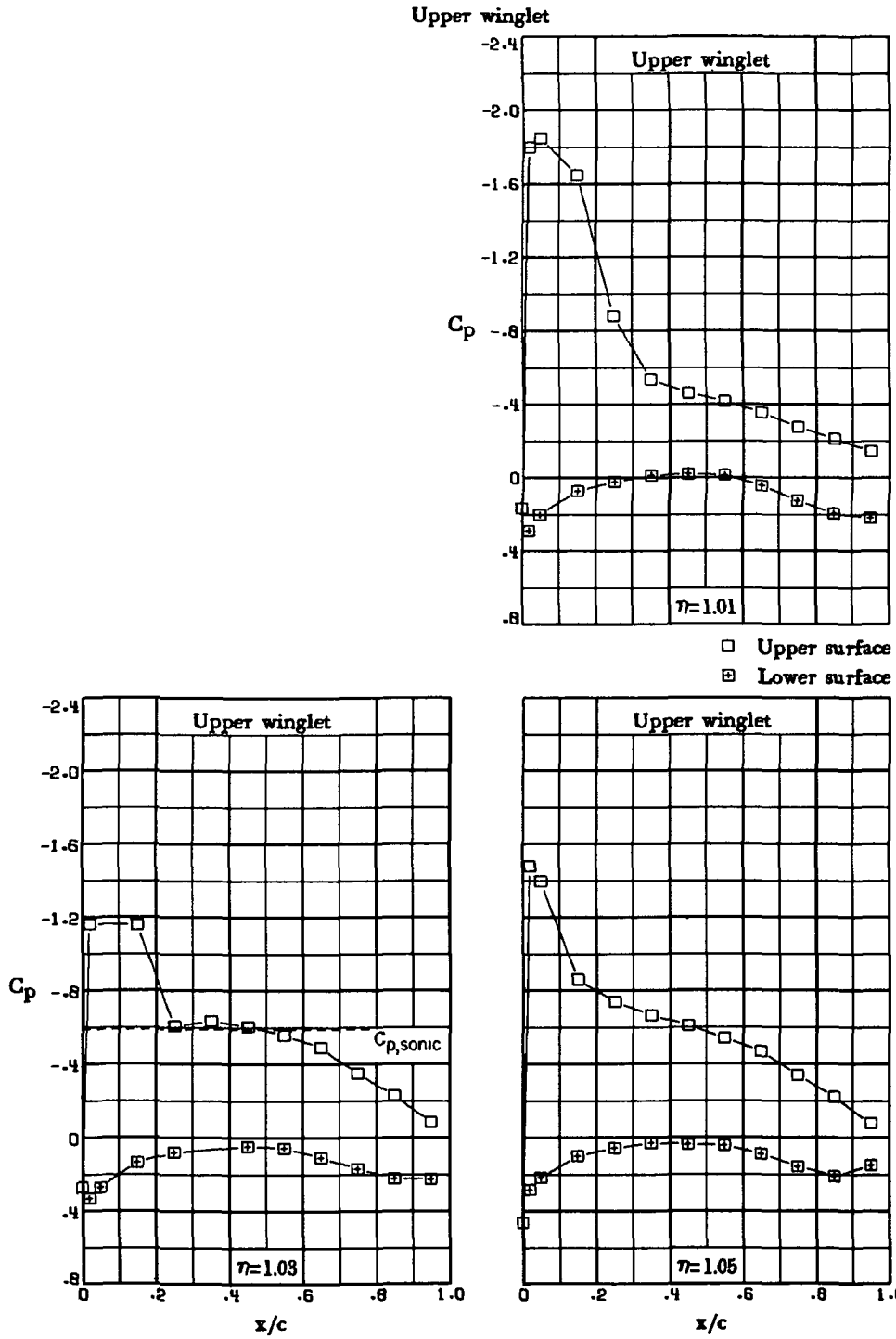

(l) $M_\infty = 0.75$; $\alpha = 7.2^\circ$. Concluded.

Figure 9.- Continued.

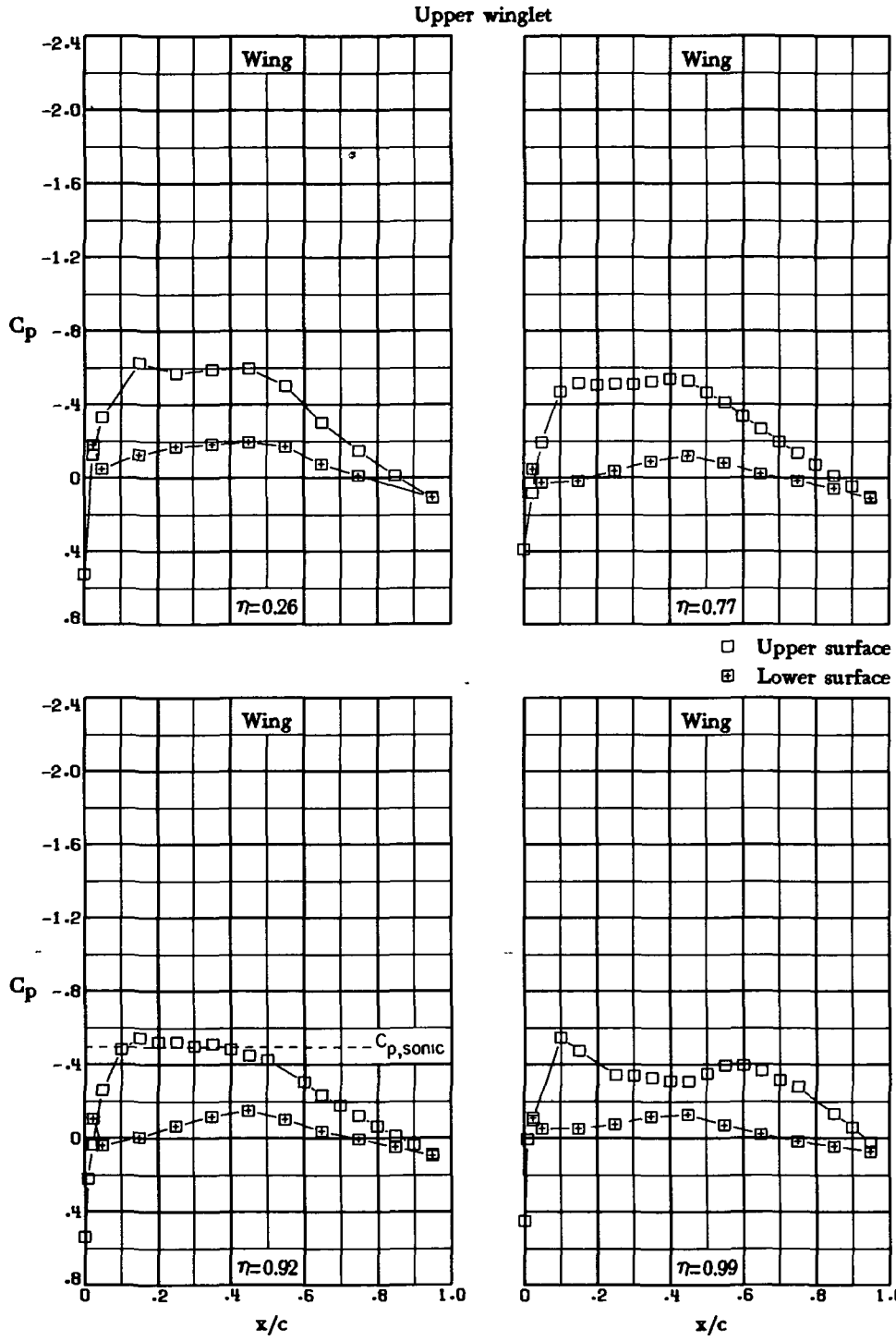

(m) $M_\infty = 0.78$; $\alpha = 0^o$.

Figure 9.- Continued.

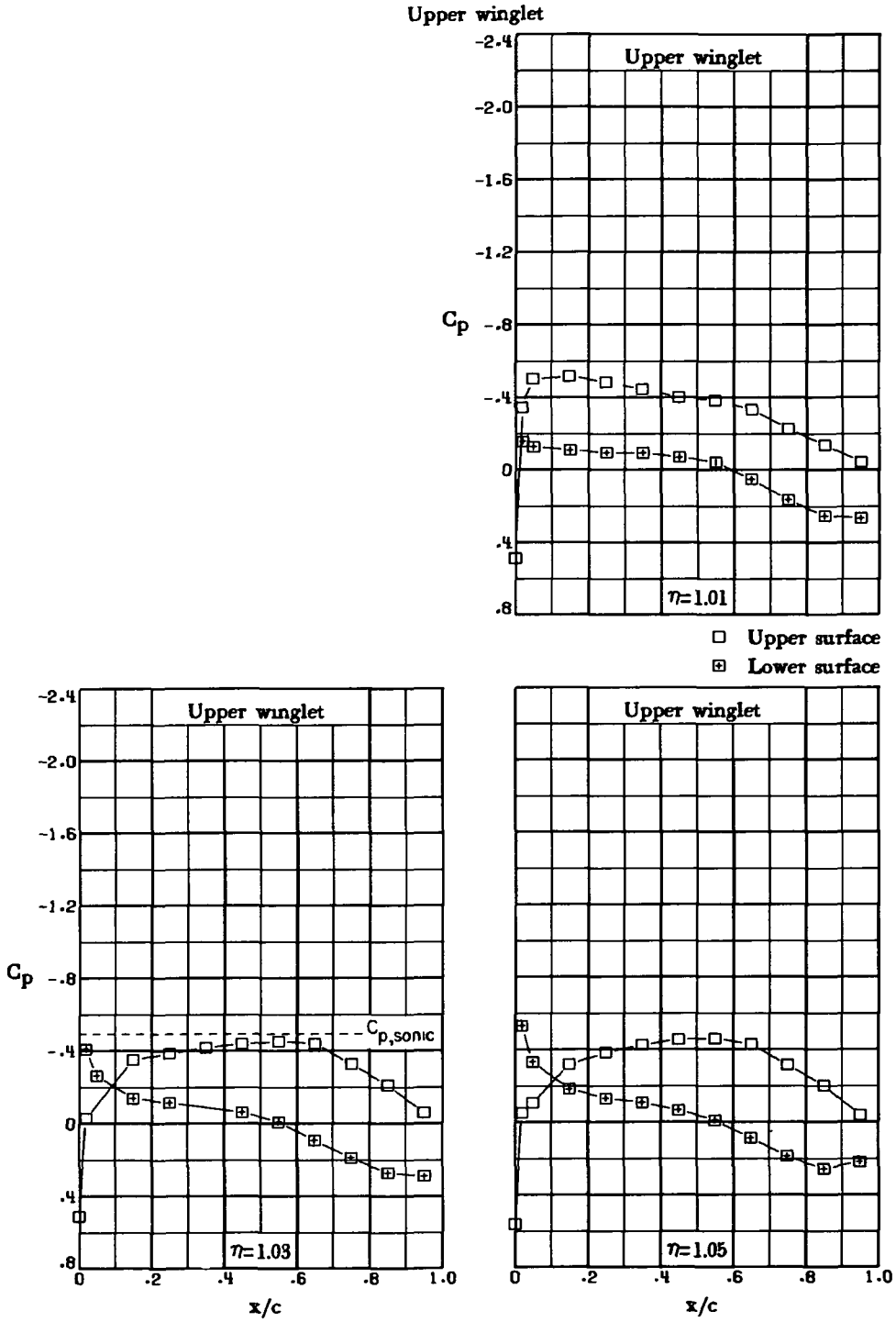

(m) $M_\infty = 0.78$; $\alpha = 0^\circ$. Concluded.

Figure 9.- Continued.

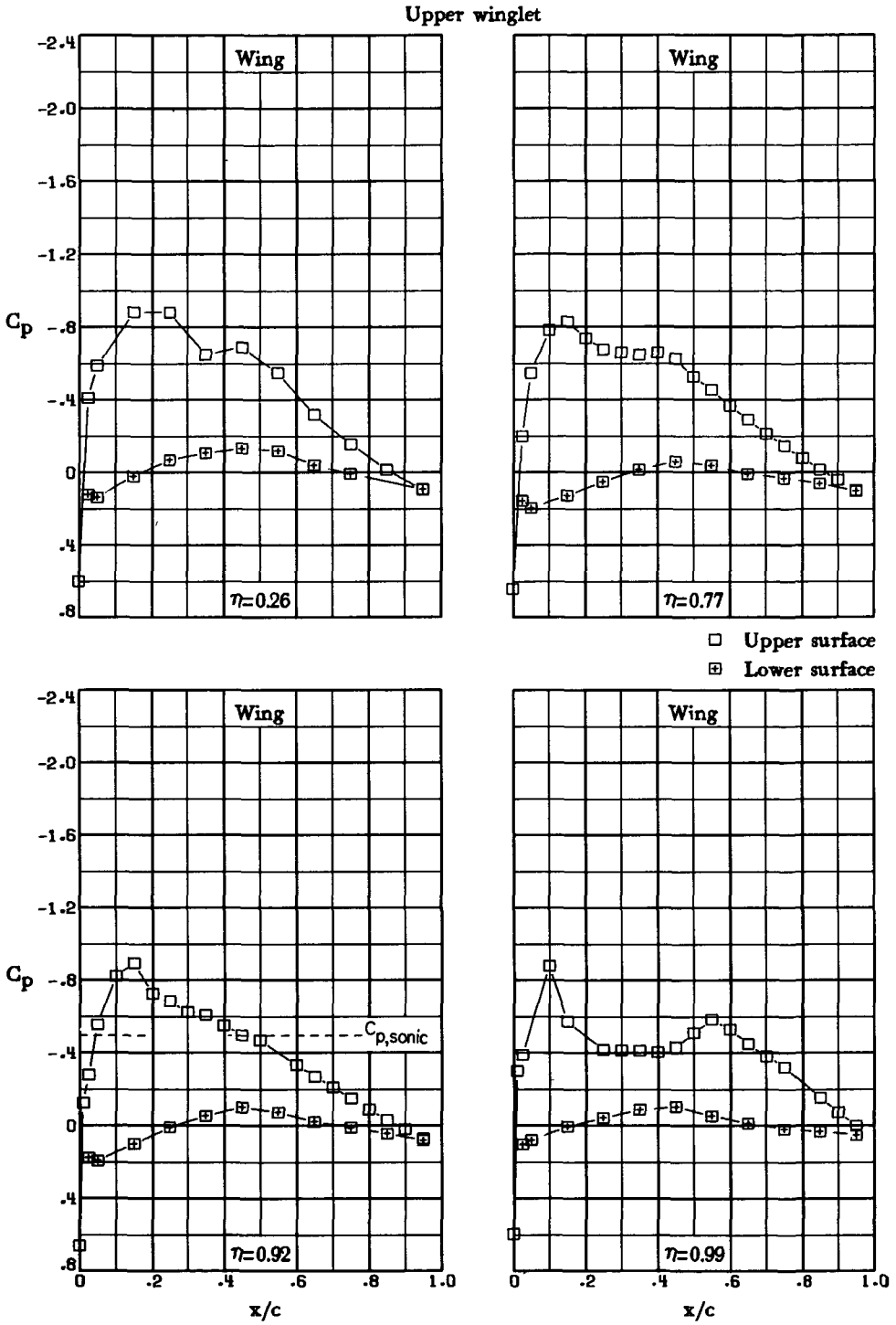

(n) $M_\infty = 0.78$; $\alpha = 2.0^\circ$.

Figure 9.- Continued.

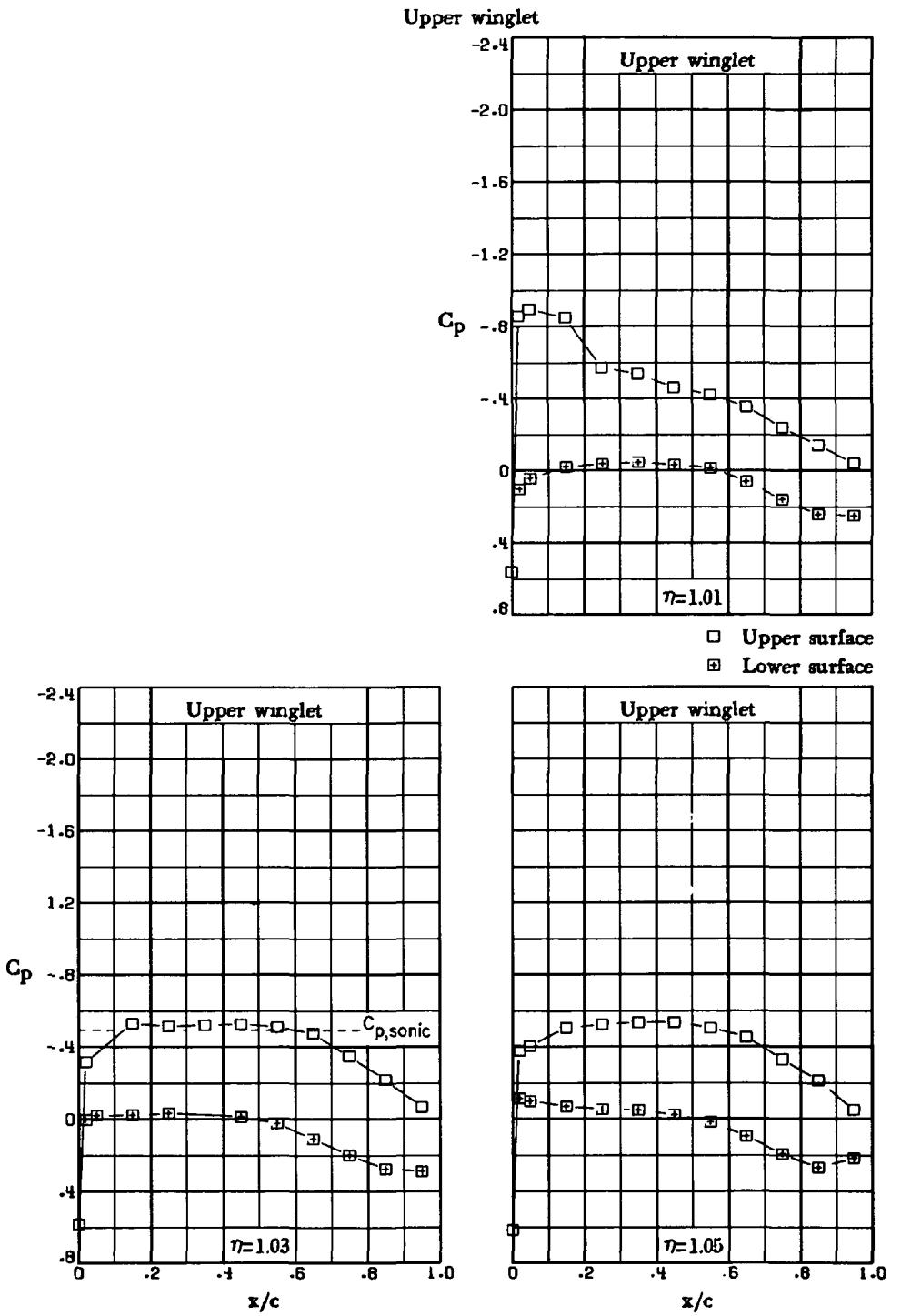

(n) $M_\infty = 0.78$; $\alpha = 2.0^\circ$. Concluded.

Figure 9.- Continued.

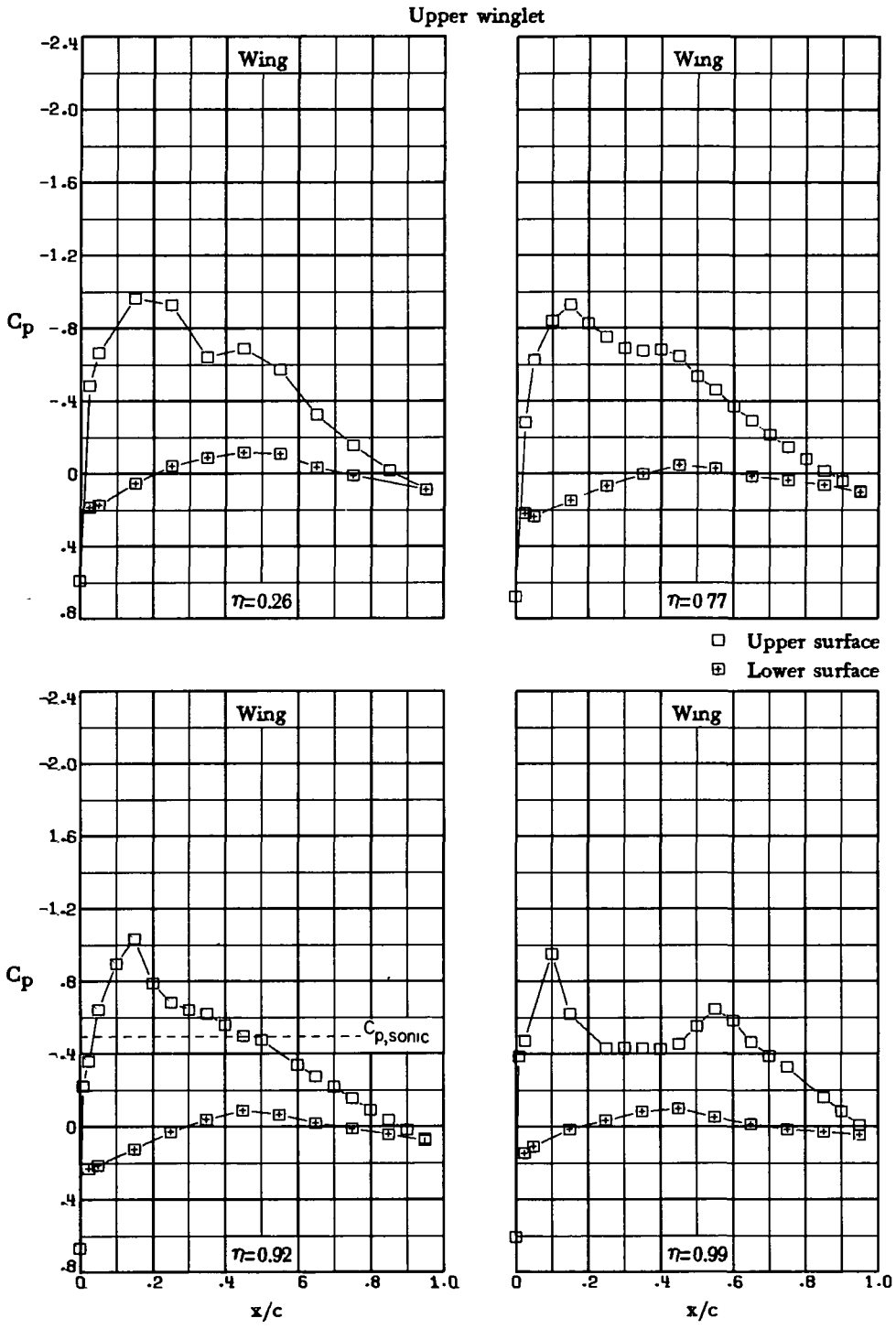

(o) M_∞ = 0.78; α = 2.5°.

Figure 9.- Continued.

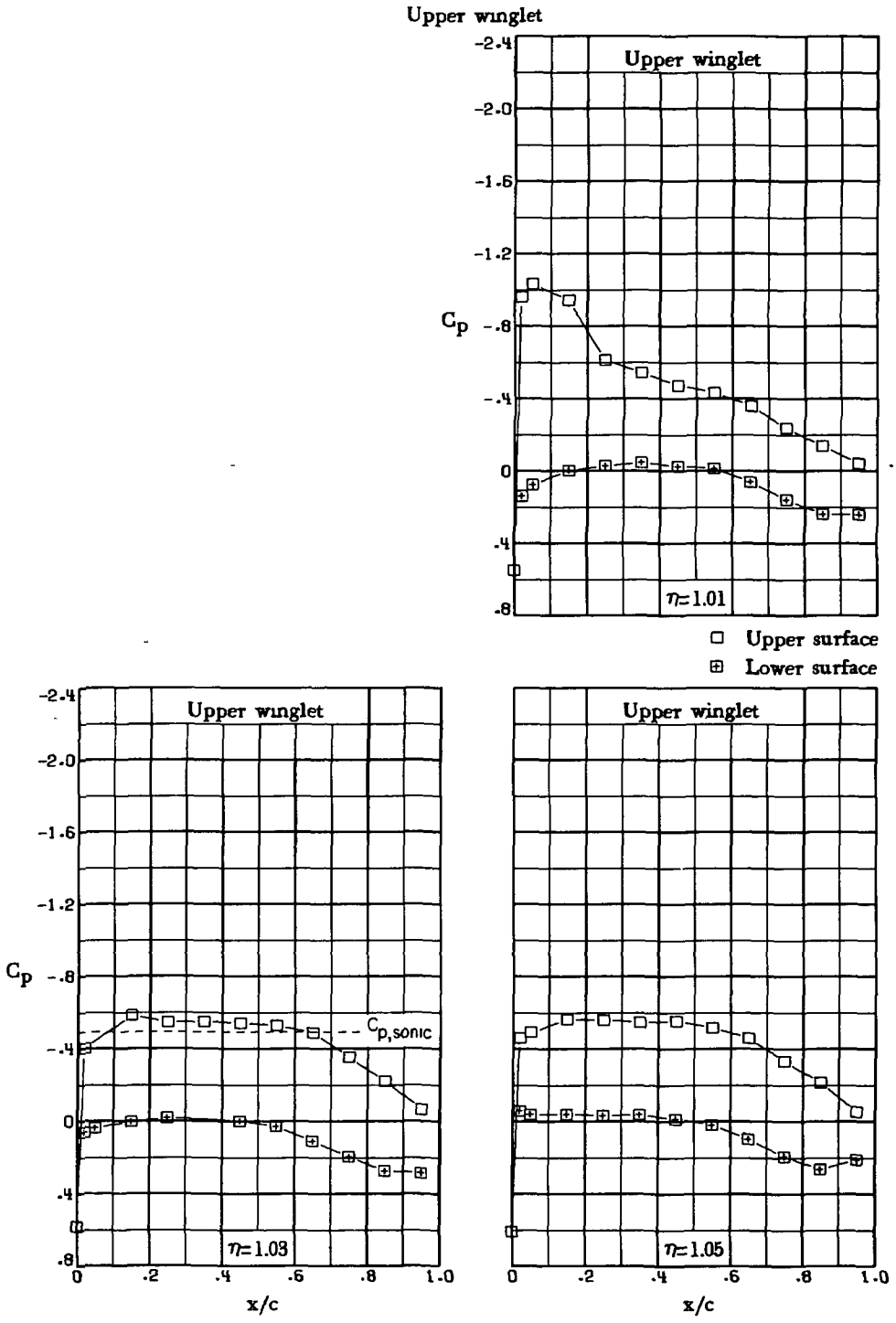

(o) M_∞ = 0.78; α = 2.5°. Concluded.

Figure 9.- Continued.

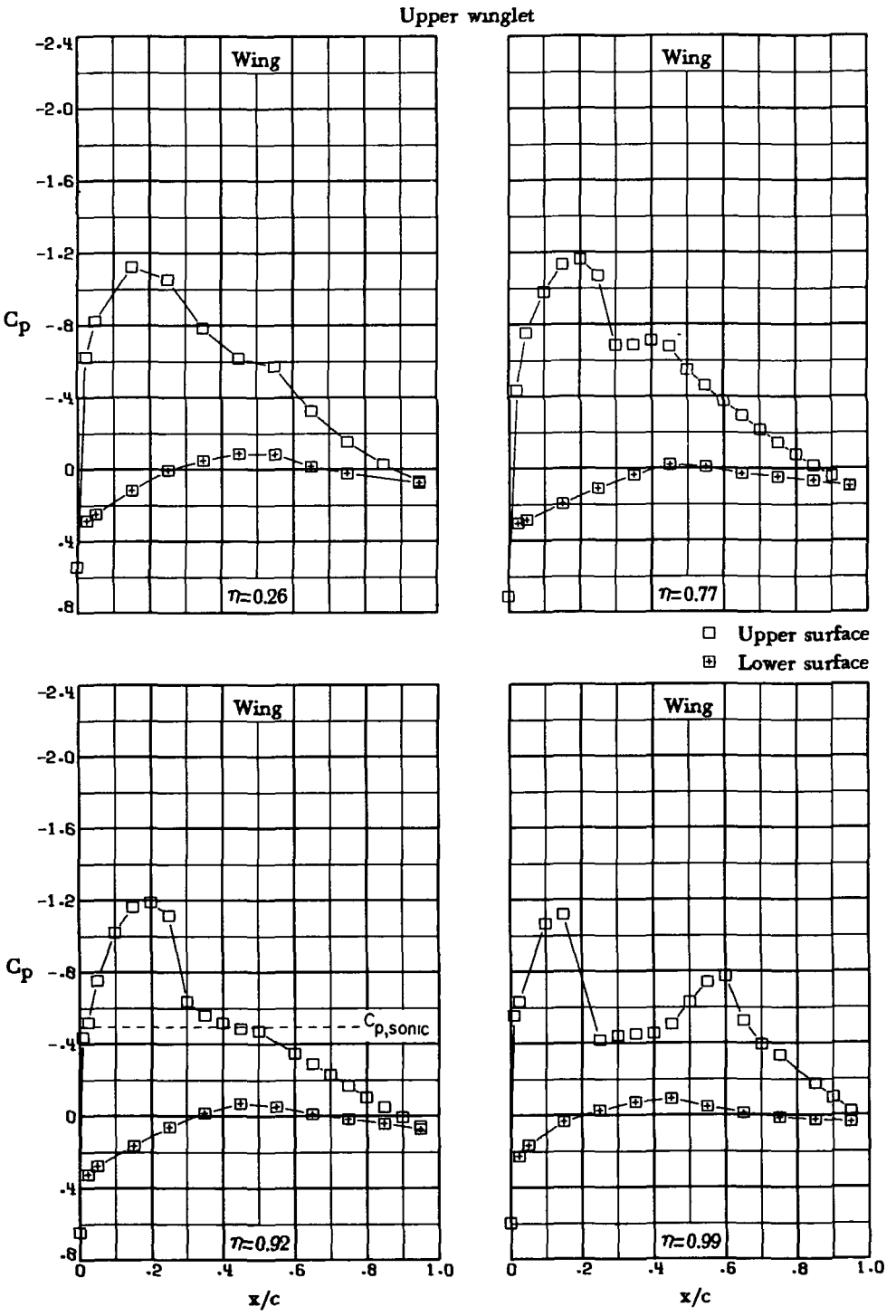

(p) $M_\infty = 0.78$; $\alpha = 3.5^\circ$.

Figure 9.- Continued.

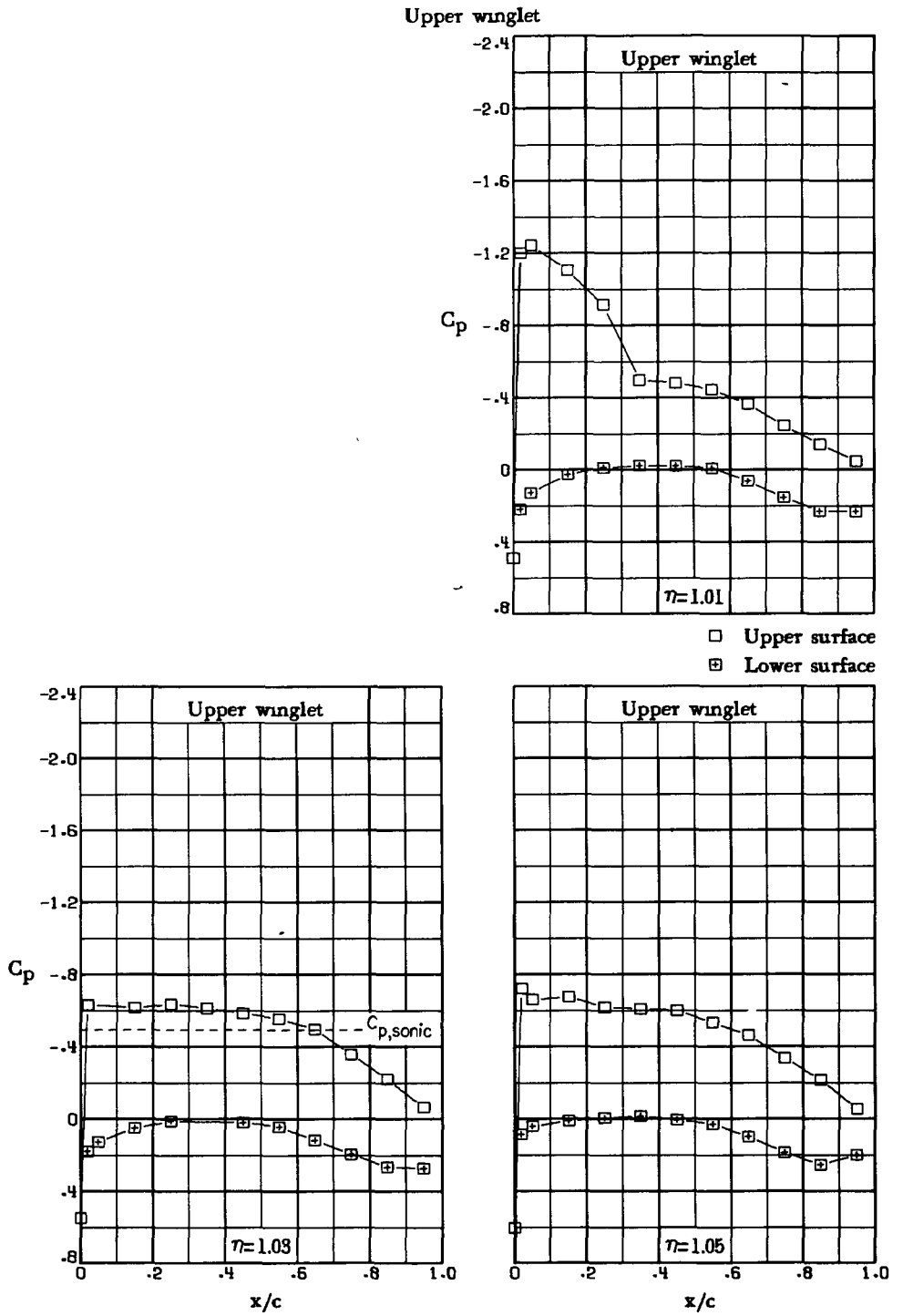

(p) M_∞ = 0.78; α = 3.5°. Concluded.

Figure 9.- Continued.

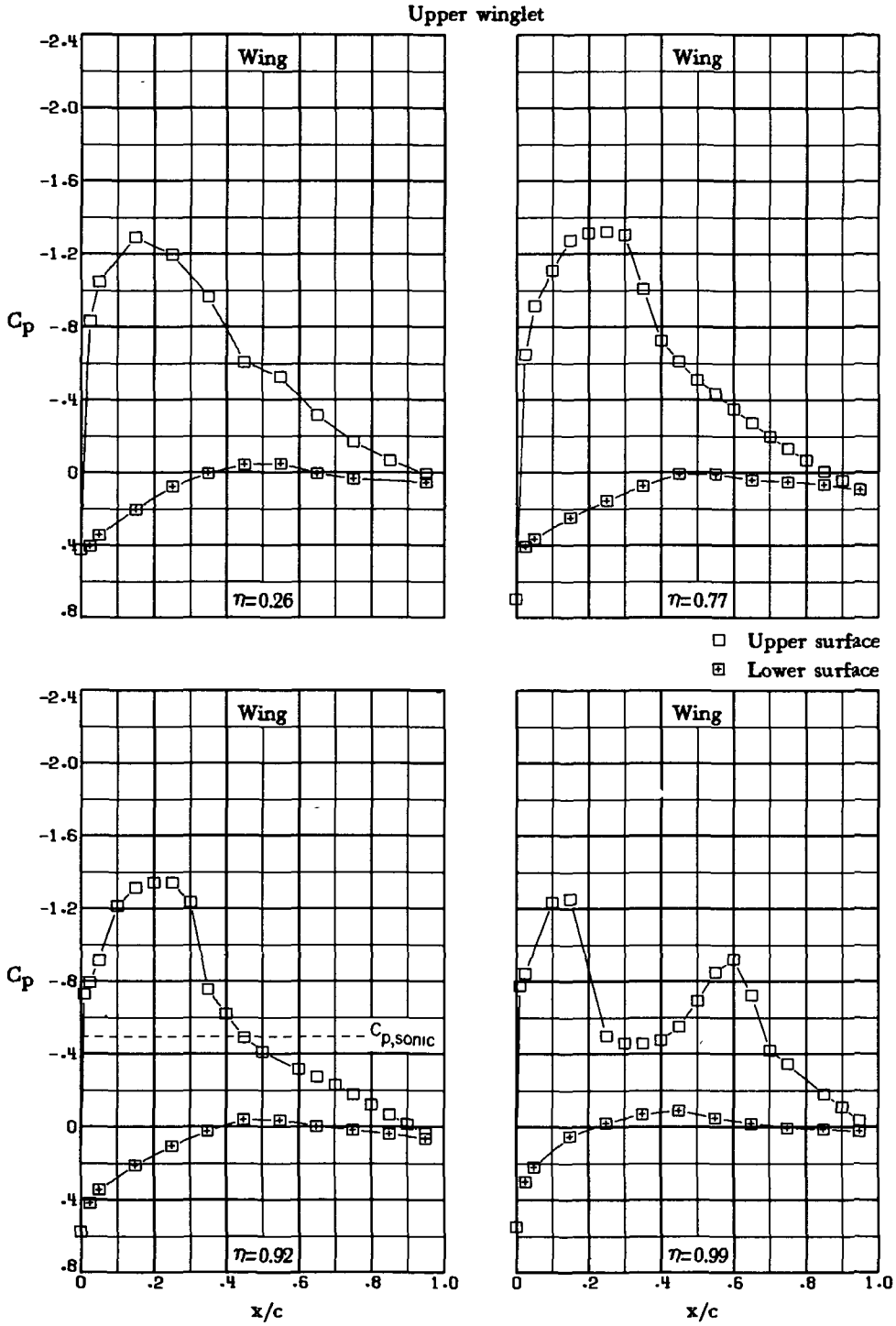

(q) $M_\infty = 0.78$; $\alpha = 5.0^\circ$.

Figure 9.- Continued.

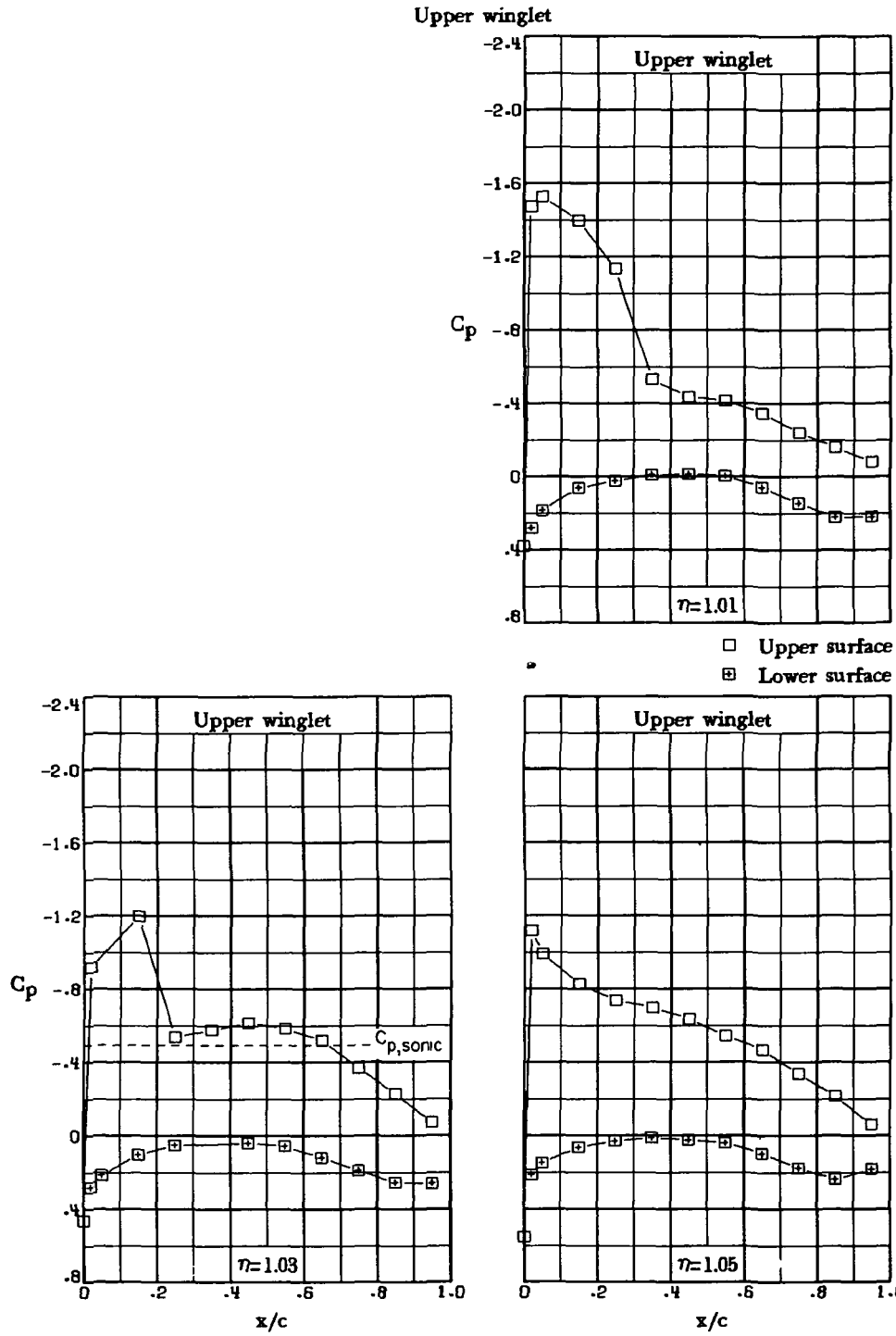

(q) $M_\infty = 0.78$; $\alpha = 5.0^\circ$. Concluded.

Figure 9.- Continued.

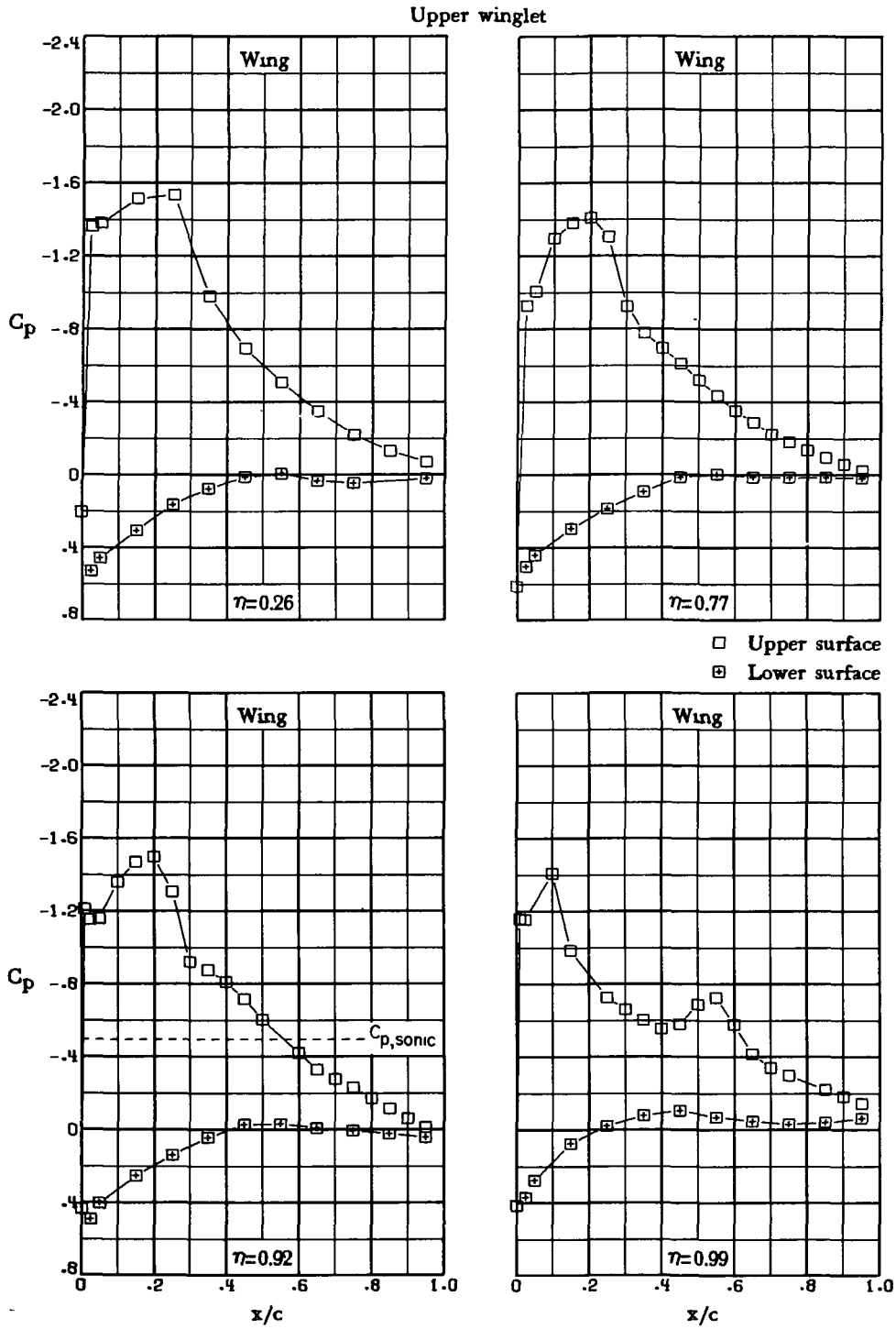

(r) $M_\infty = 0.78$; $\alpha = 7.2^\circ$.

Figure 9.- Continued.

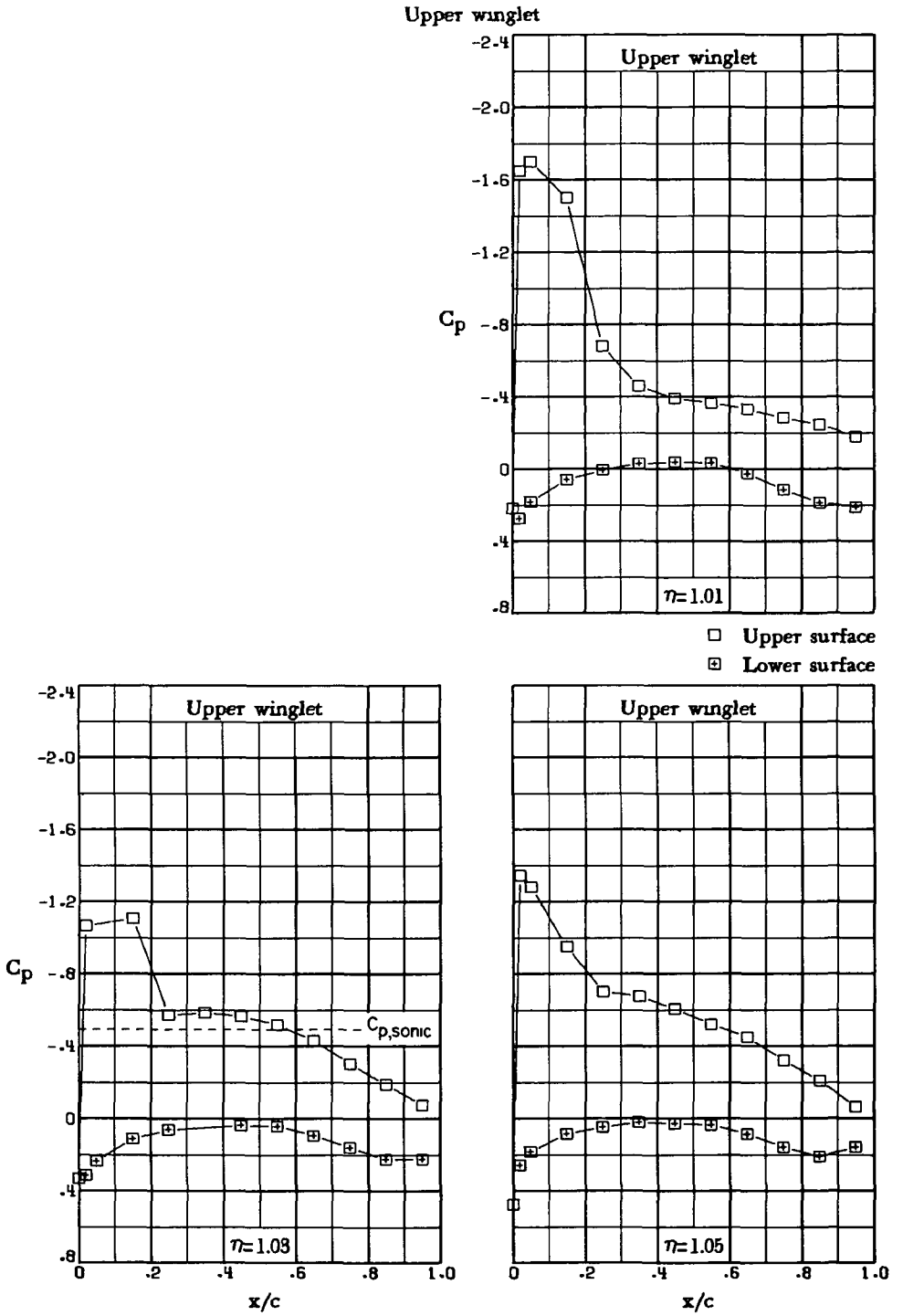

(r) M_∞ = 0.78; α = 7.2°. Concluded.

Figure 9.- Continued.

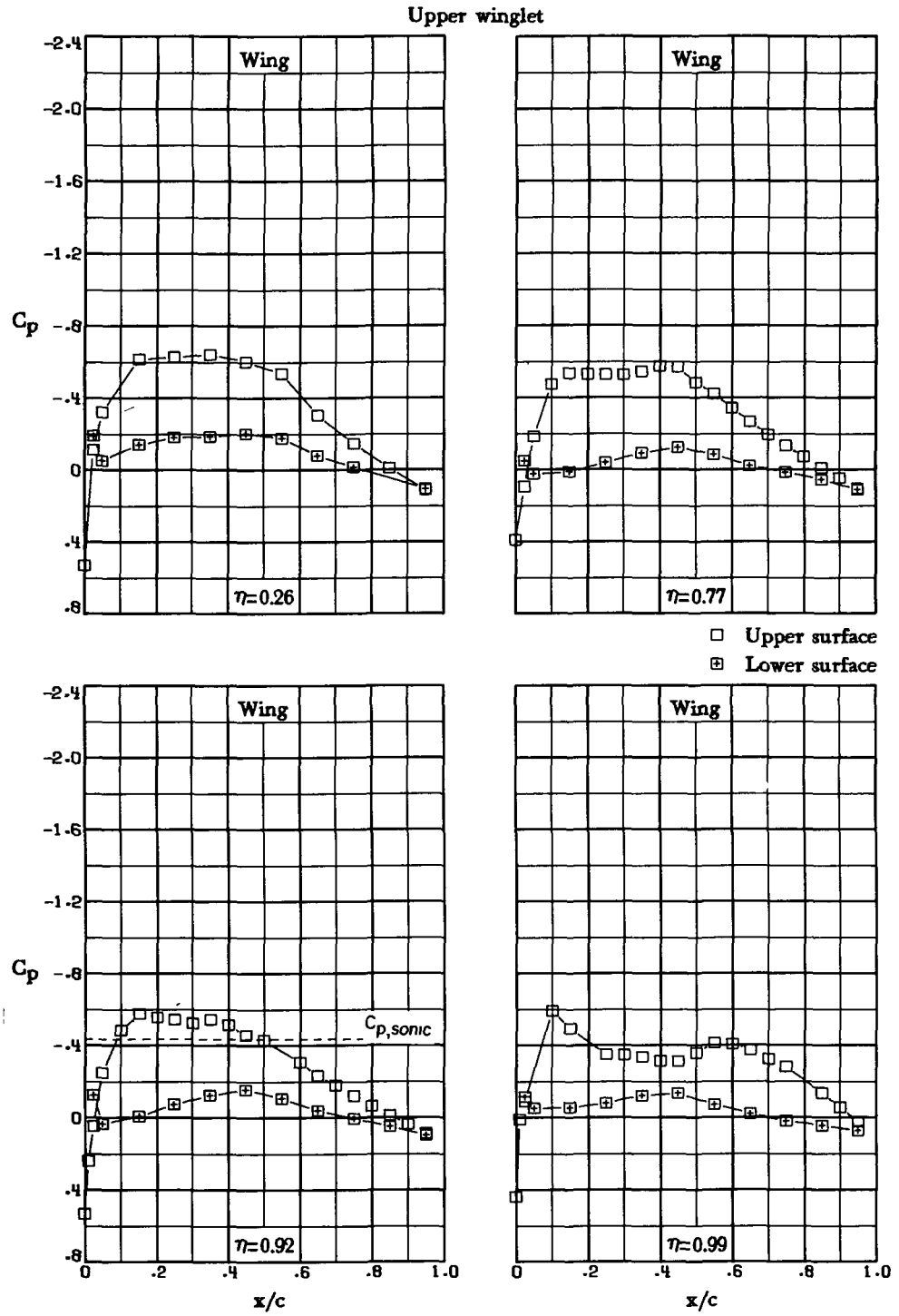

(s) $M_\infty = 0.80$; $\alpha = 0^\circ$.

Figure 9.- Continued.

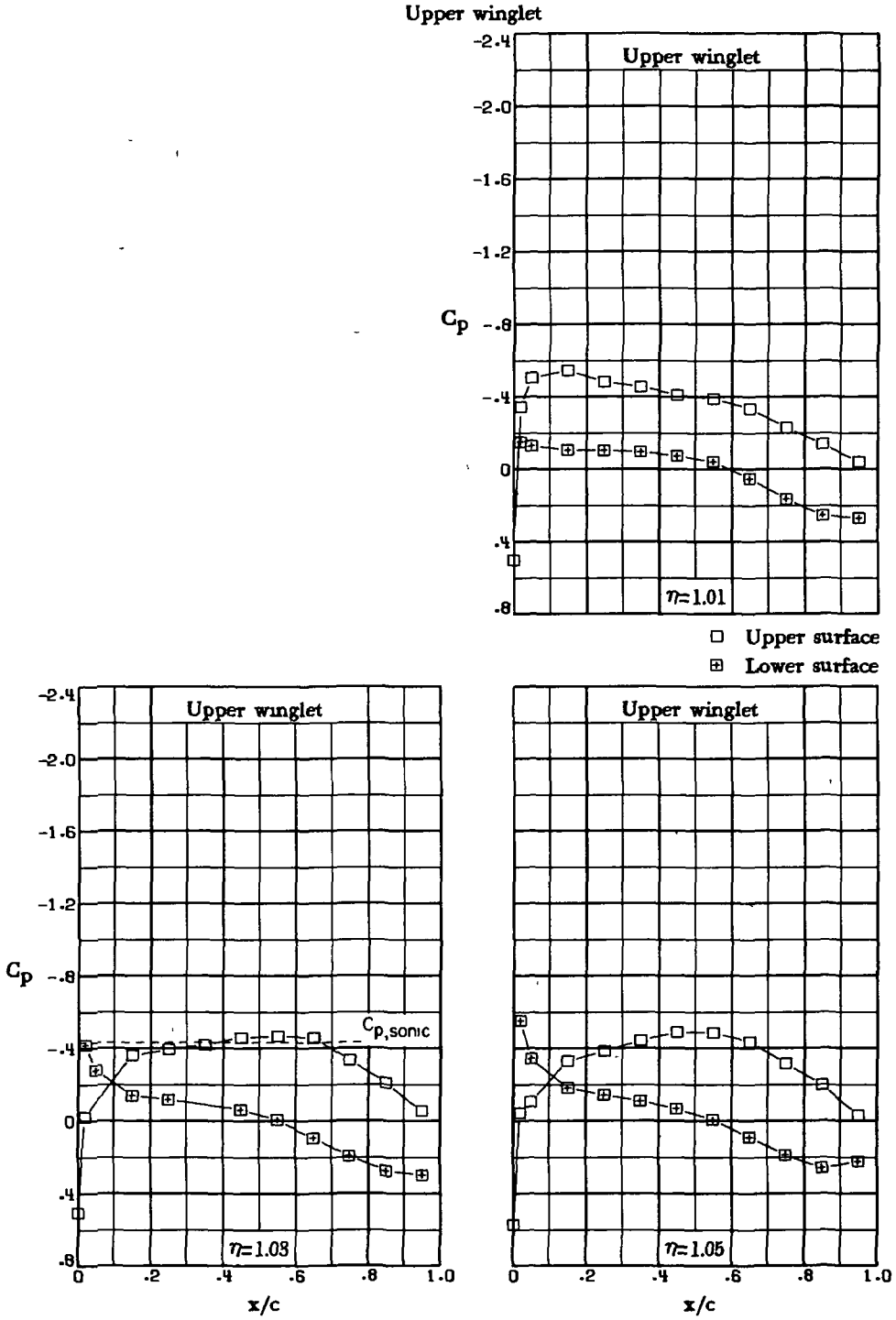

(s) $M_\infty = 0.80$; $\alpha = 0^\circ$. Concluded.

Figure 9.- Continued.

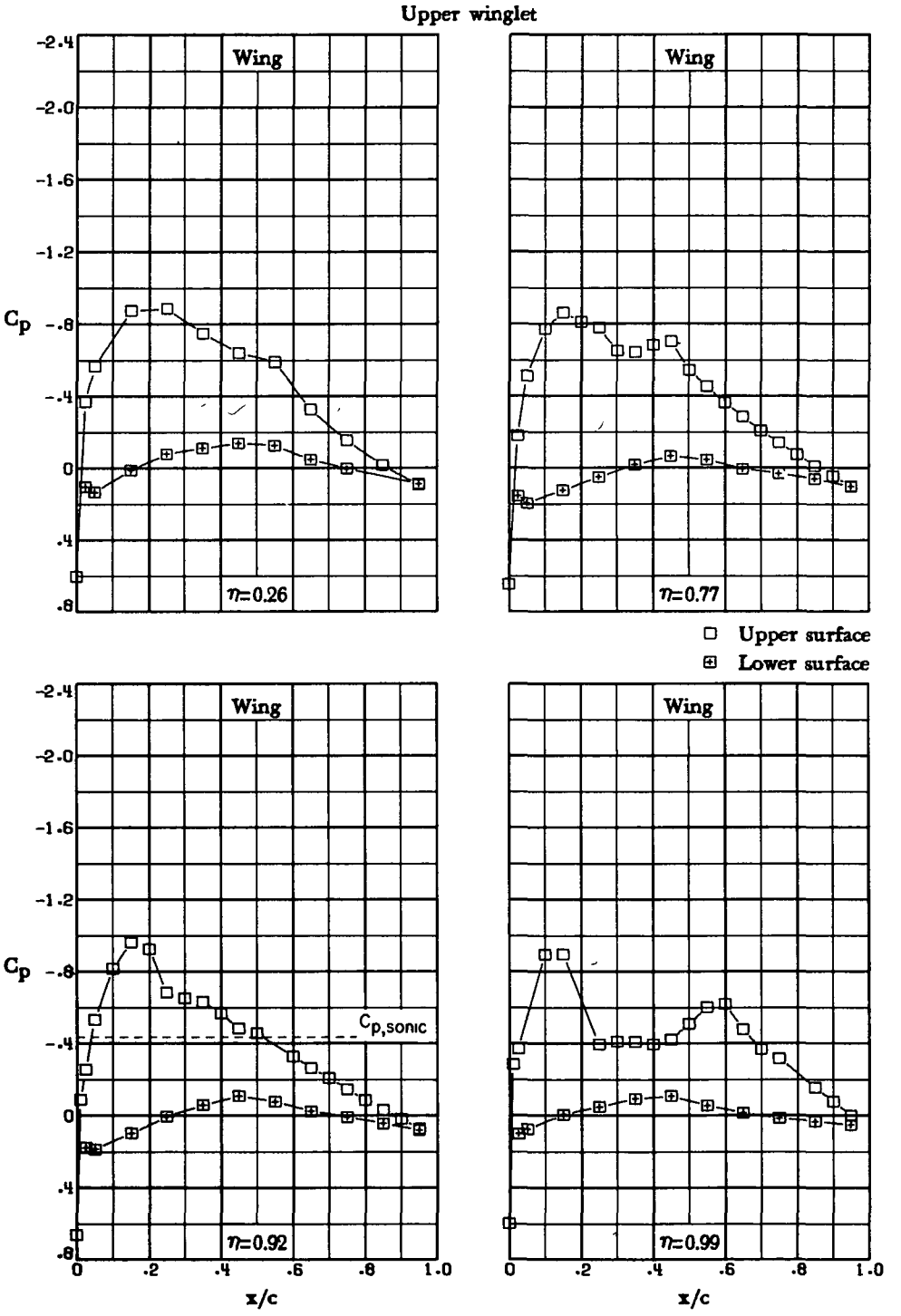

(t) M_∞ = 0.80; α = 2.1°.

Figure 9.- Continued.

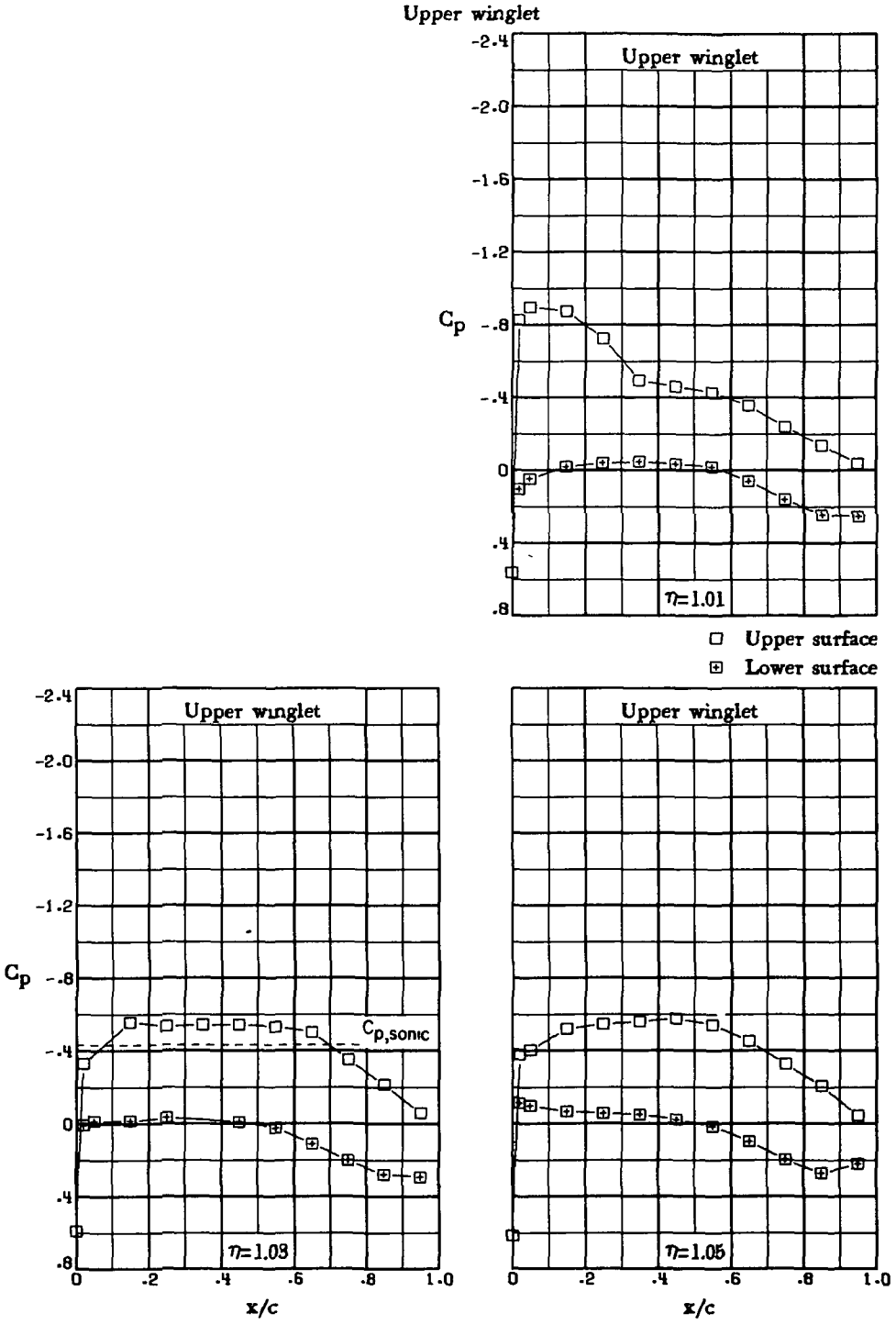

(t) $M_\infty = 0.80$; $\alpha = 2.1^\circ$. Concluded.

Figure 9.- Continued.

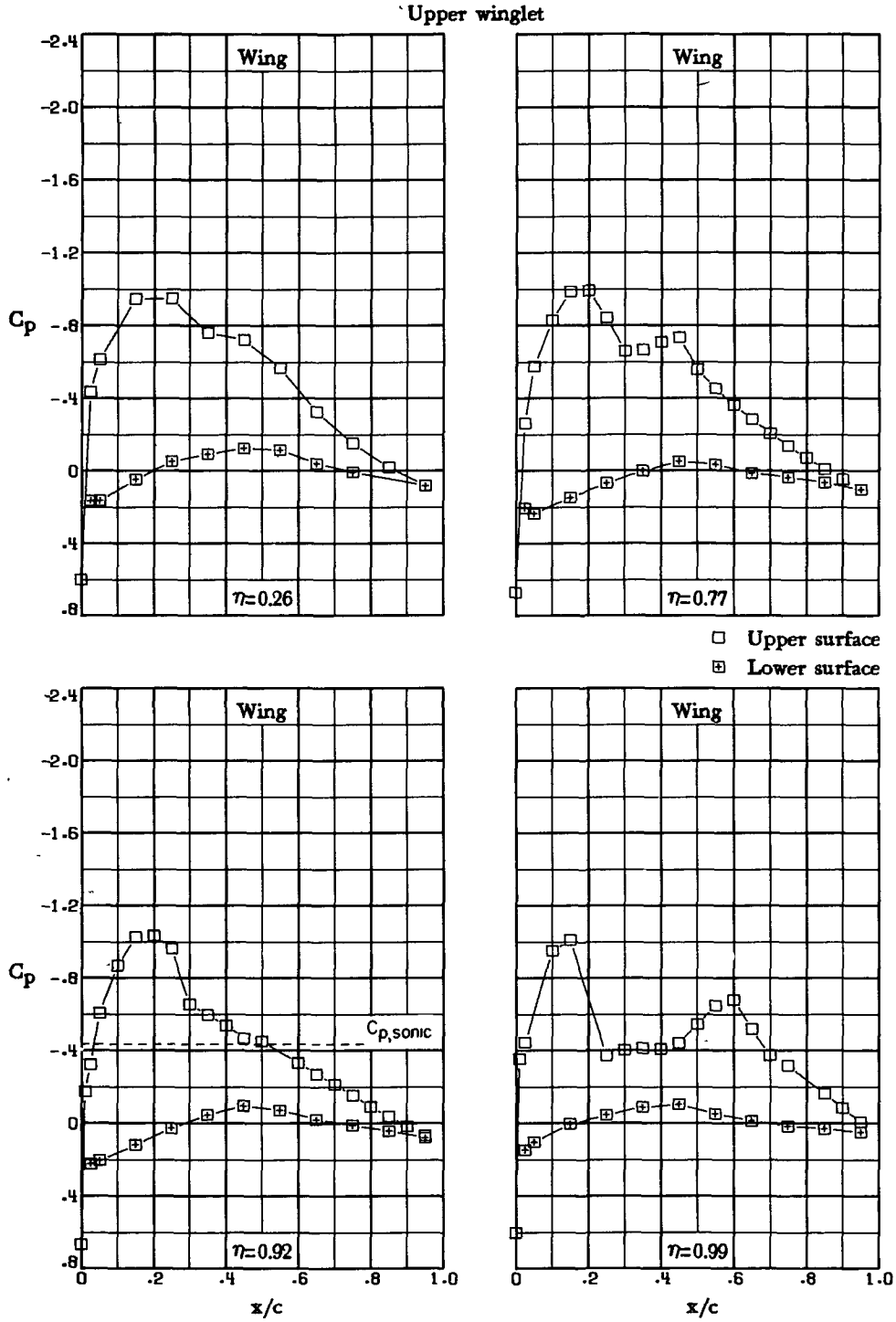

(u) $M_\infty = 0.80$; $\alpha = 2.5^\circ$.

Figure 9.- Continued.

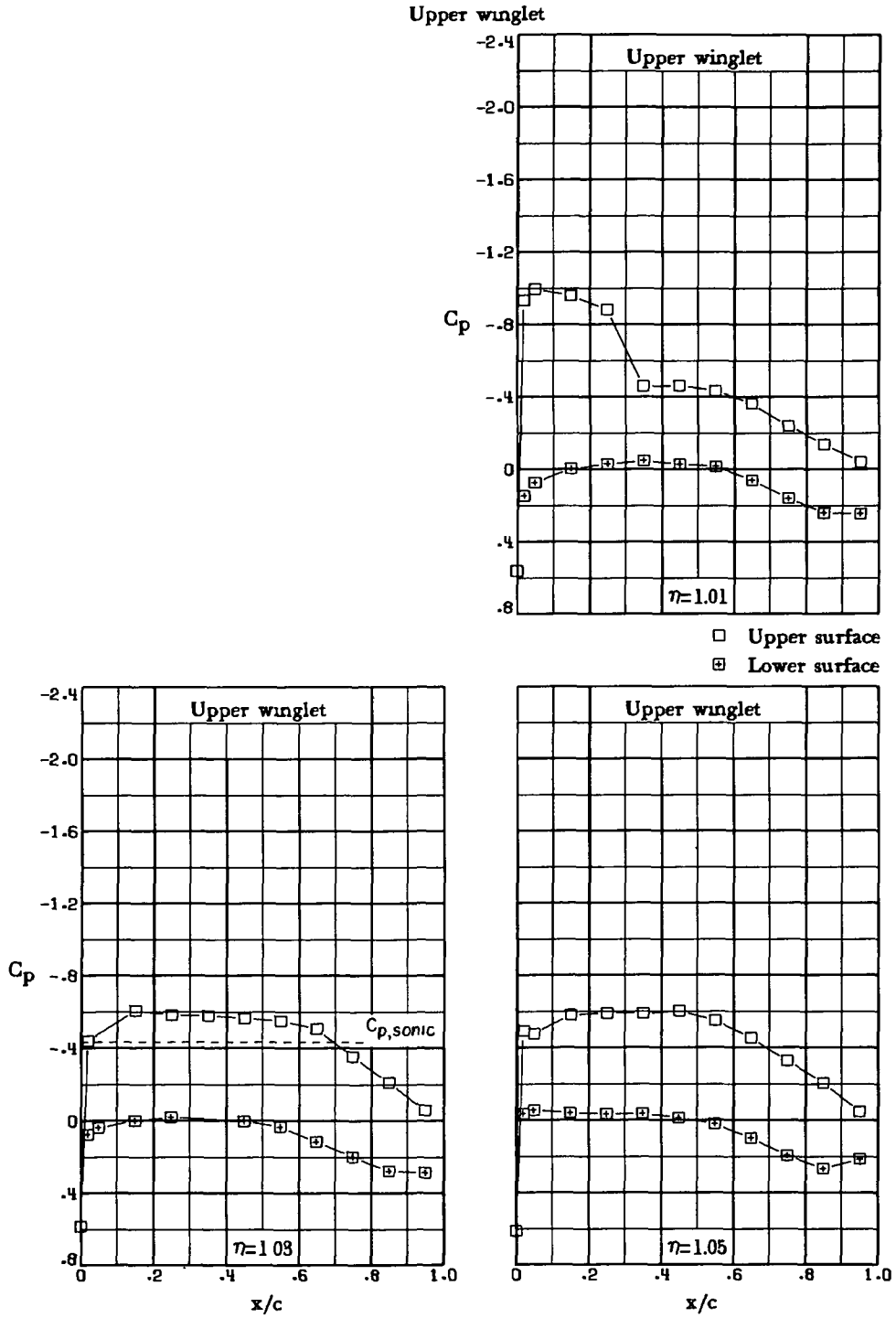

(u) M_∞ = 0.80; α = 2.5°. Concluded.

Figure 9.- Continued.

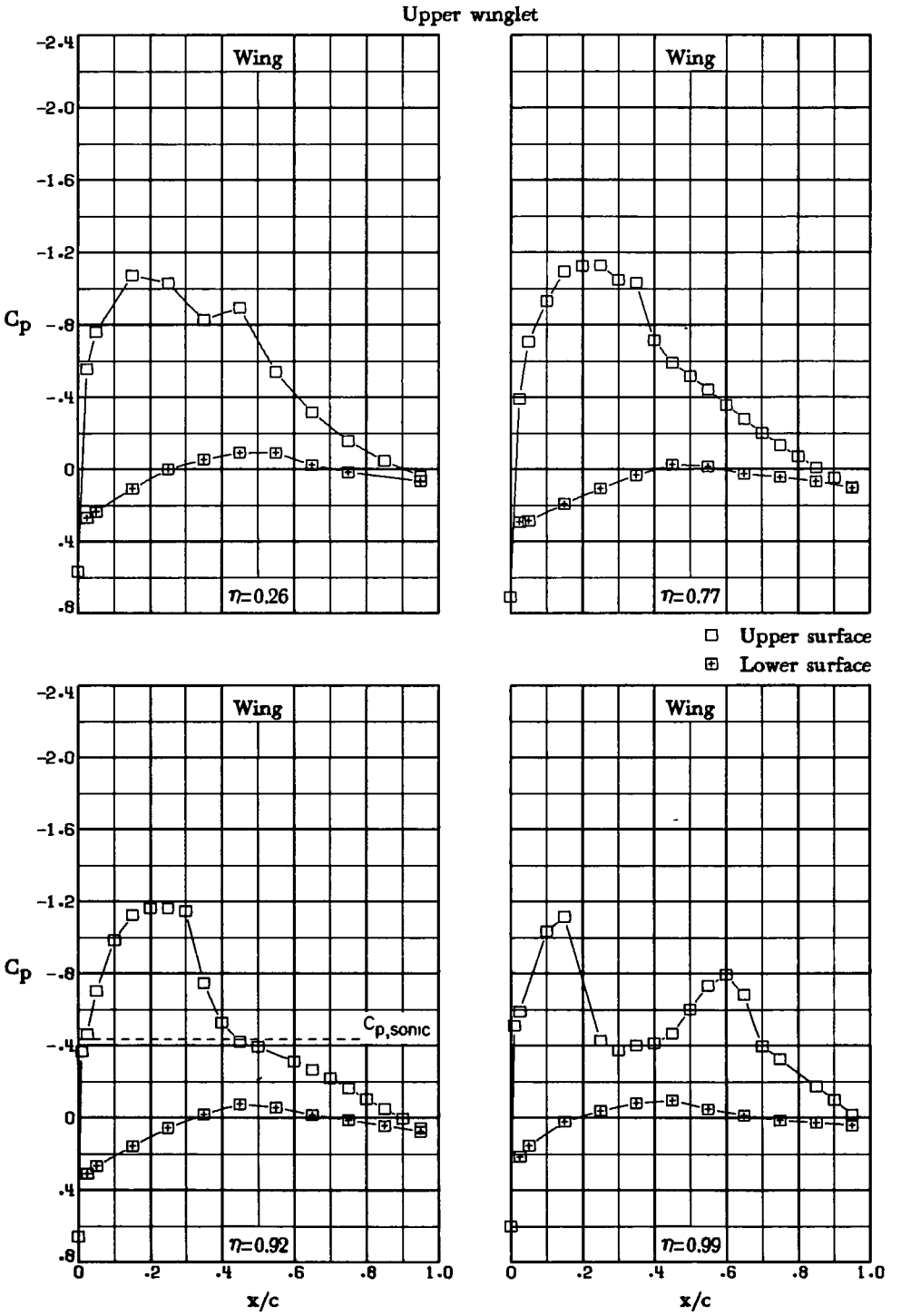

(v) $M_\infty = 0.80$; $\alpha = 3.5^\circ$.

Figure 9.- Continued.

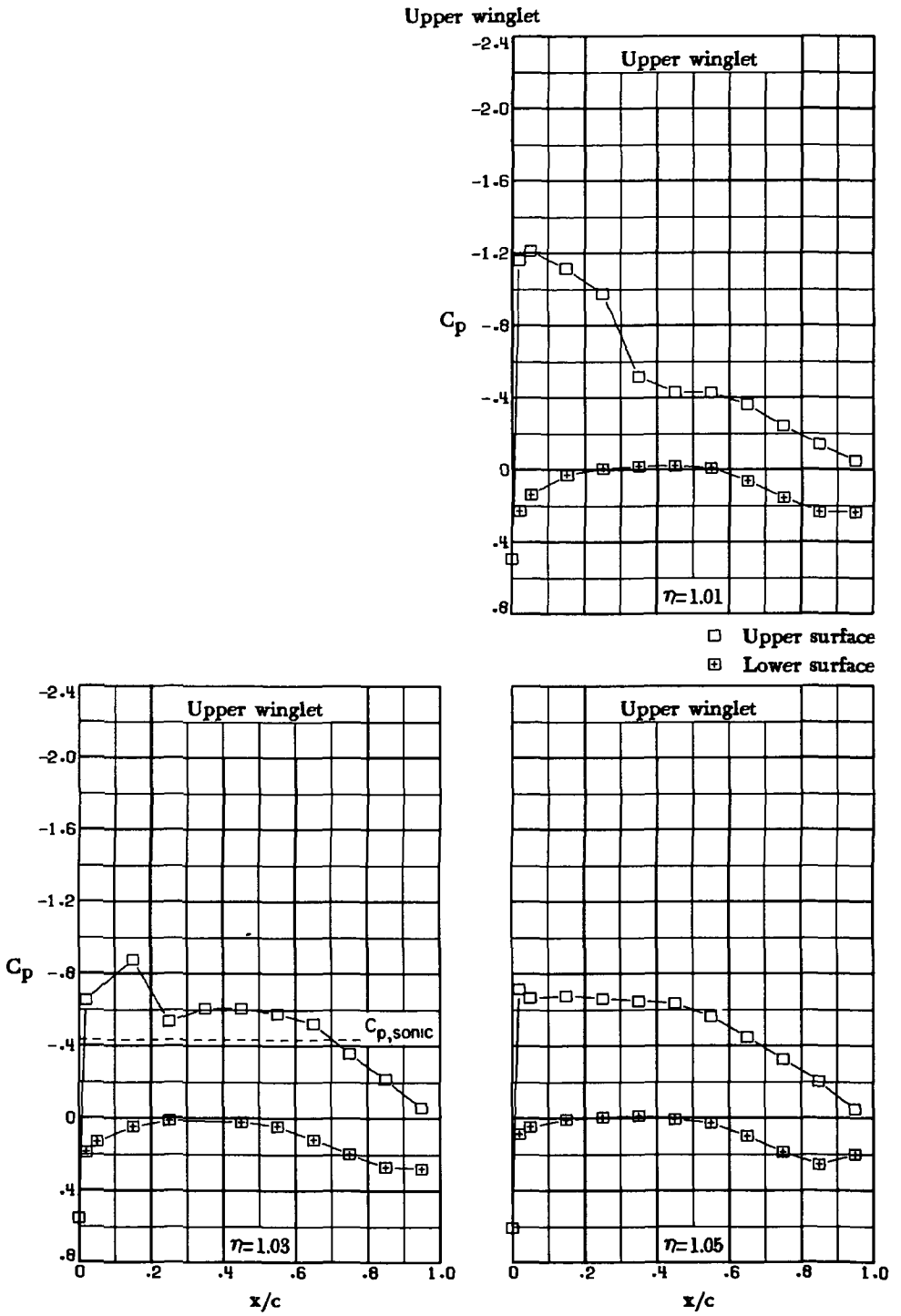

(v) M_∞ = 0.80; α = 3.5°. Concluded.

Figure 9.- Continued.

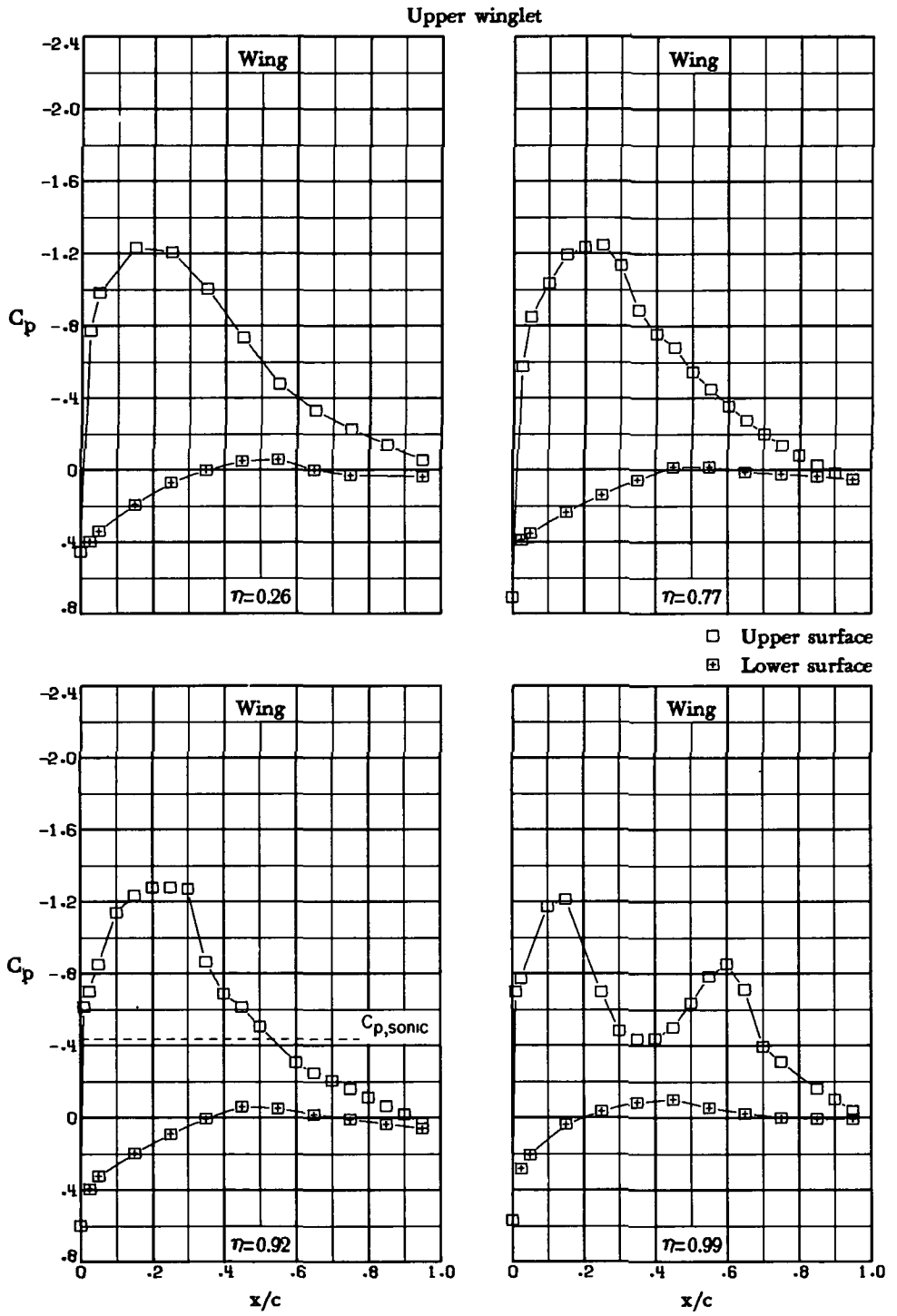

(w) $M_\infty = 0.80$; $\alpha = 5.1^\circ$.

Figure 9.- Continued.

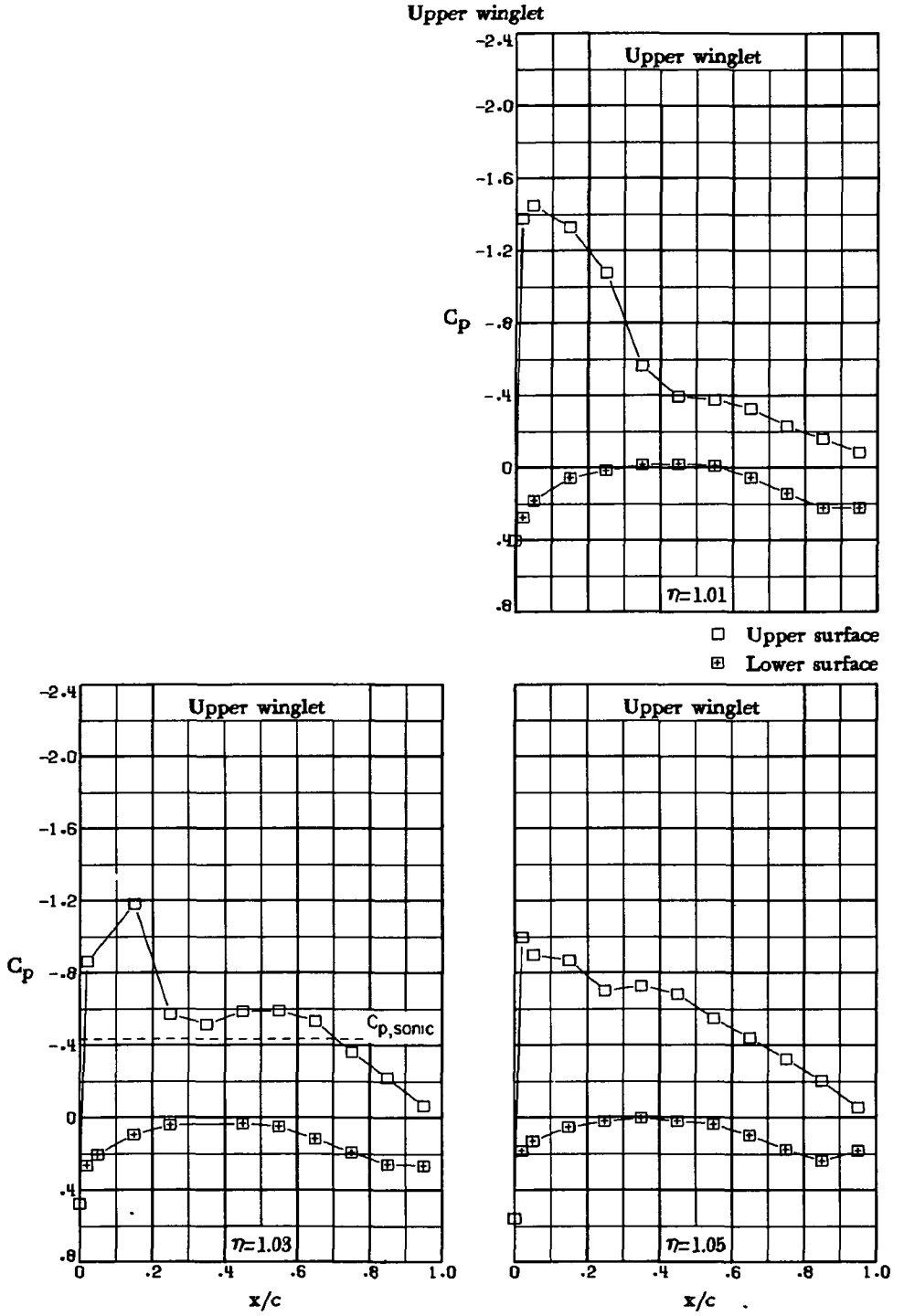

(w) M_∞ = 0.80; α = 5.1°. Concluded.

Figure 9.- Continued.

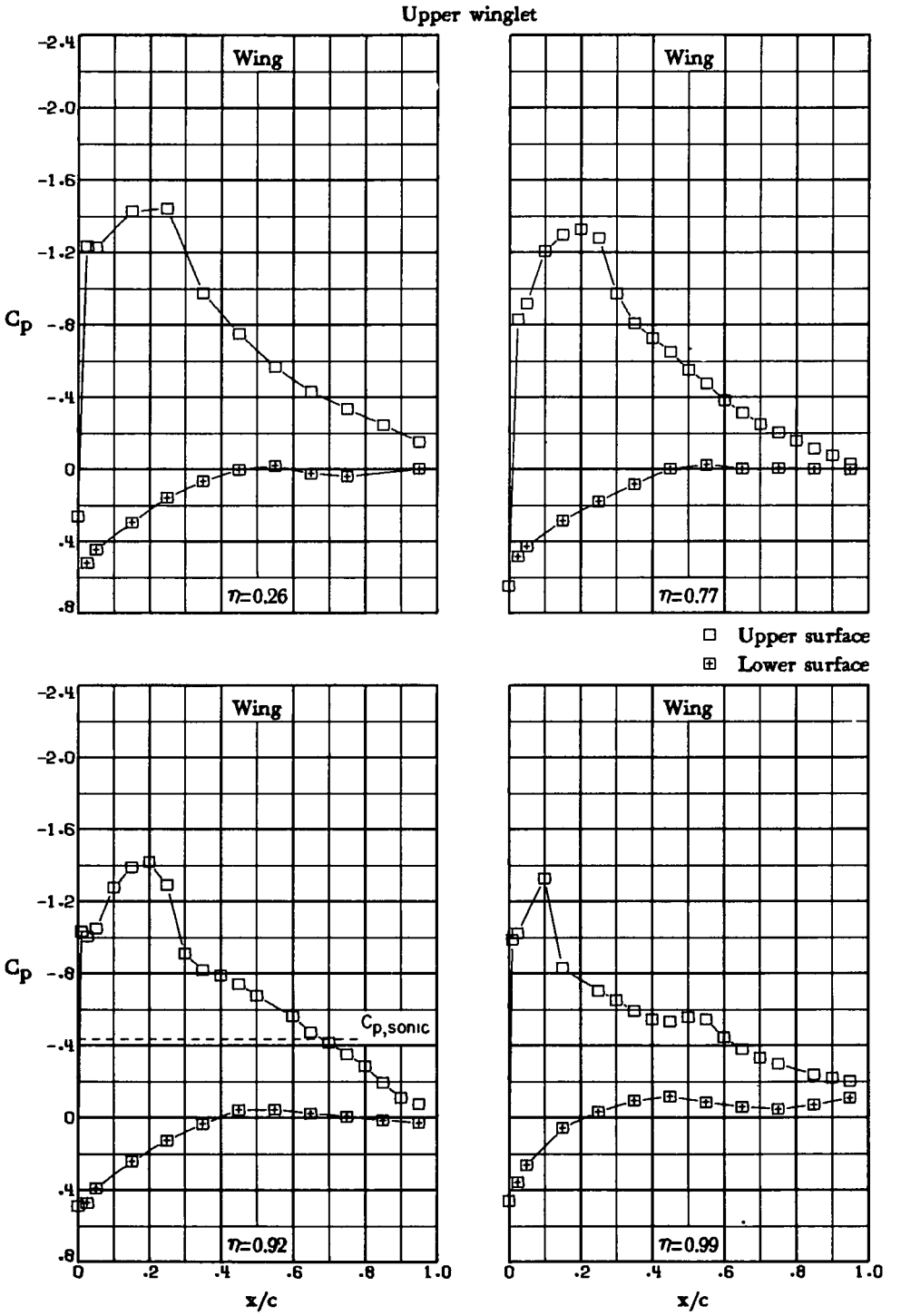

(x) $M_\infty = 0.80$; $\alpha = 7.1^\circ$.

Figure 9.- Continued.

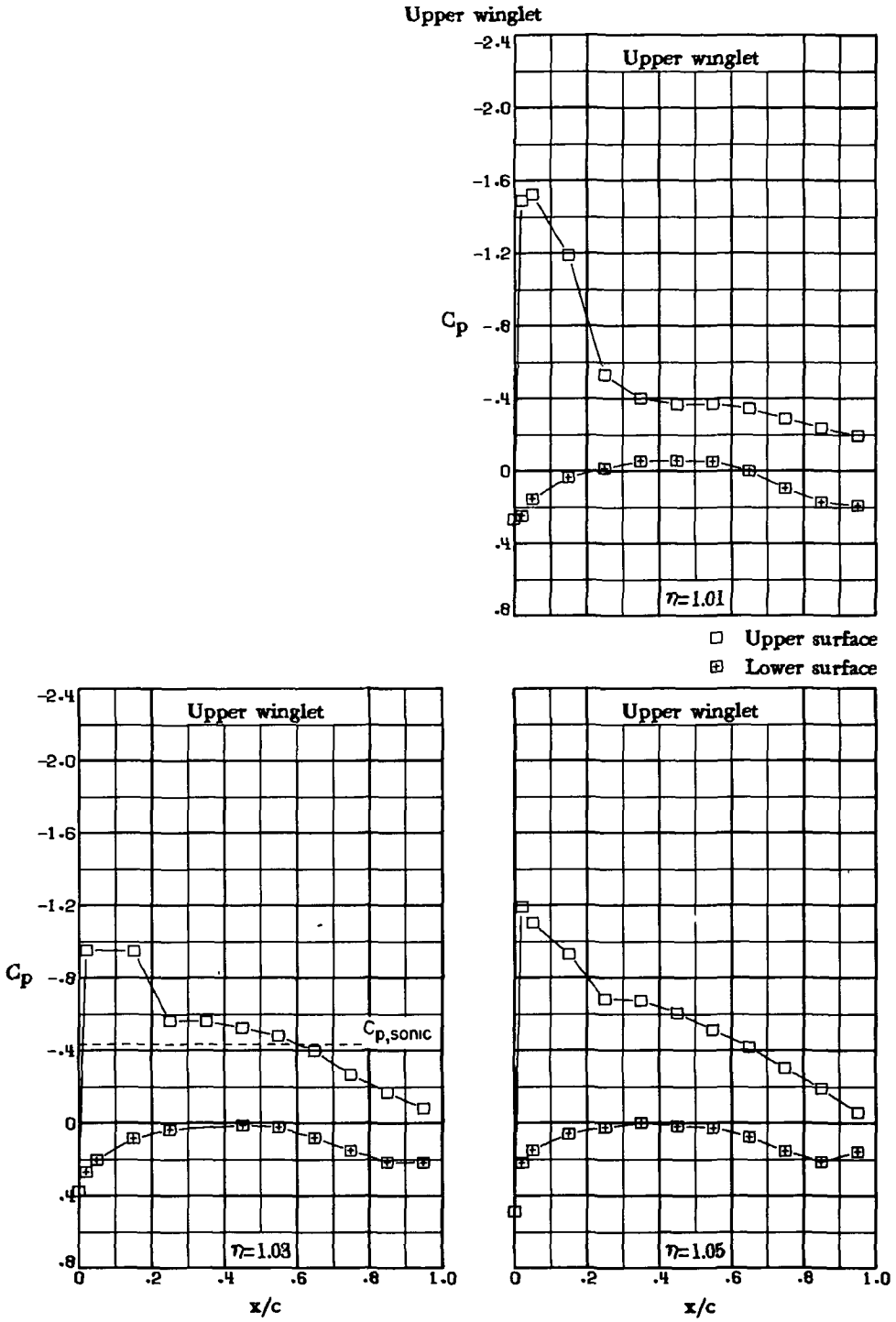

(x) M_∞ = 0.80; α = 7.1°. Concluded.

Figure 9.- Concluded.

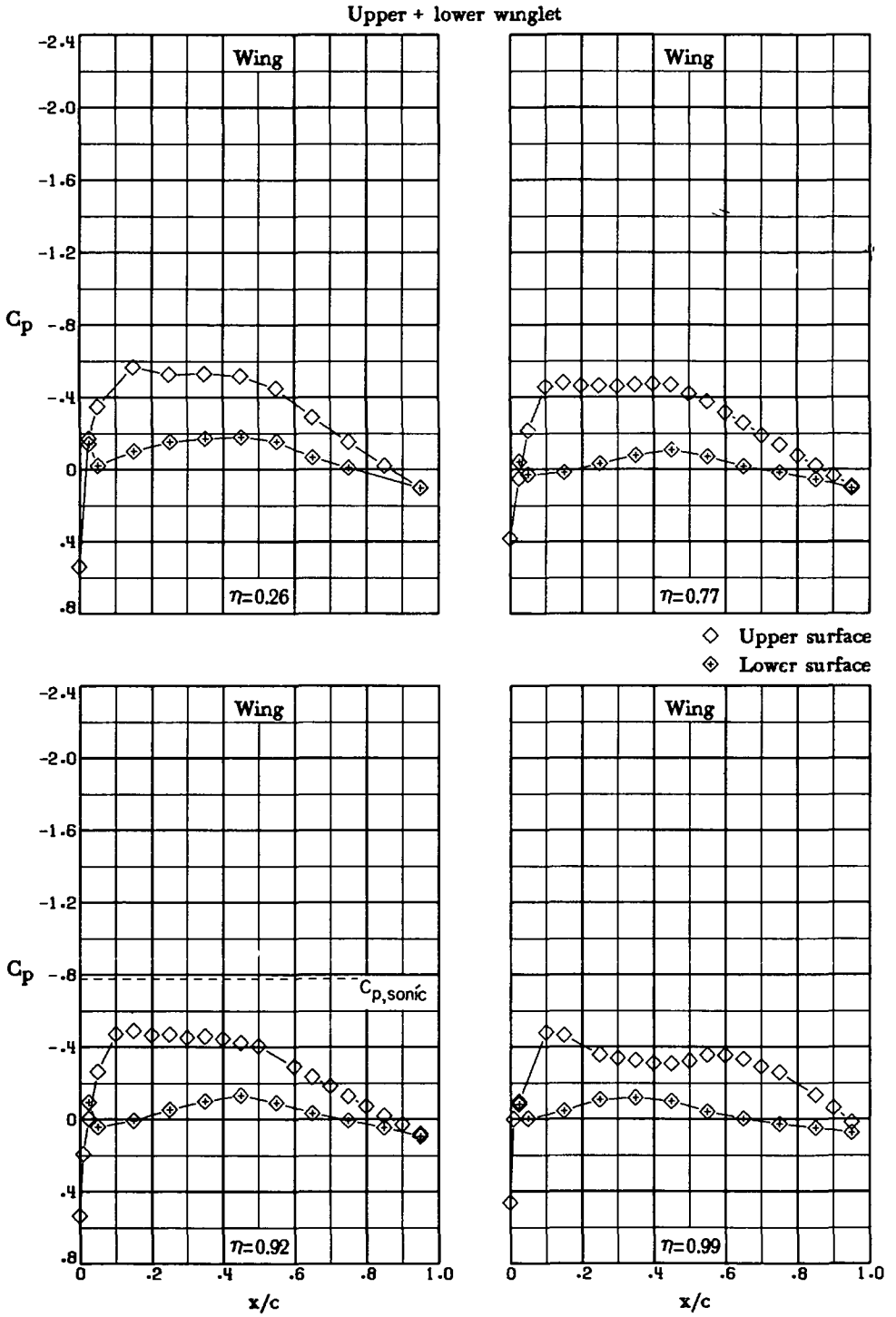

(a) $M_\infty = 0.70$; $\alpha = 0^o$.

Figure 10.- Pressure distributions for upper-and-lower-winglet configuration.

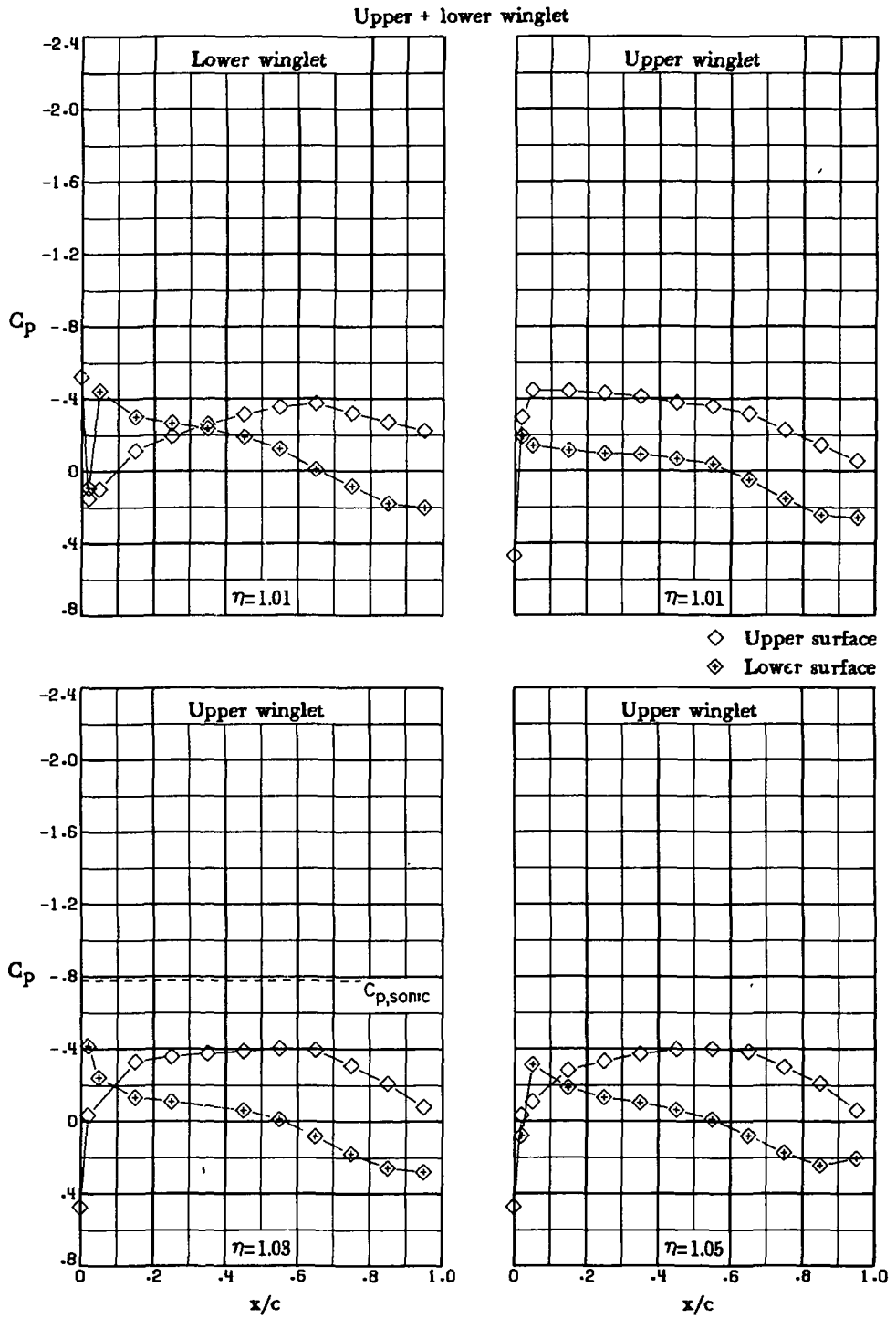

(a) $M_\infty = 0.70$; $\alpha = 0^o$. Concluded.

Figure 10.- Continued.

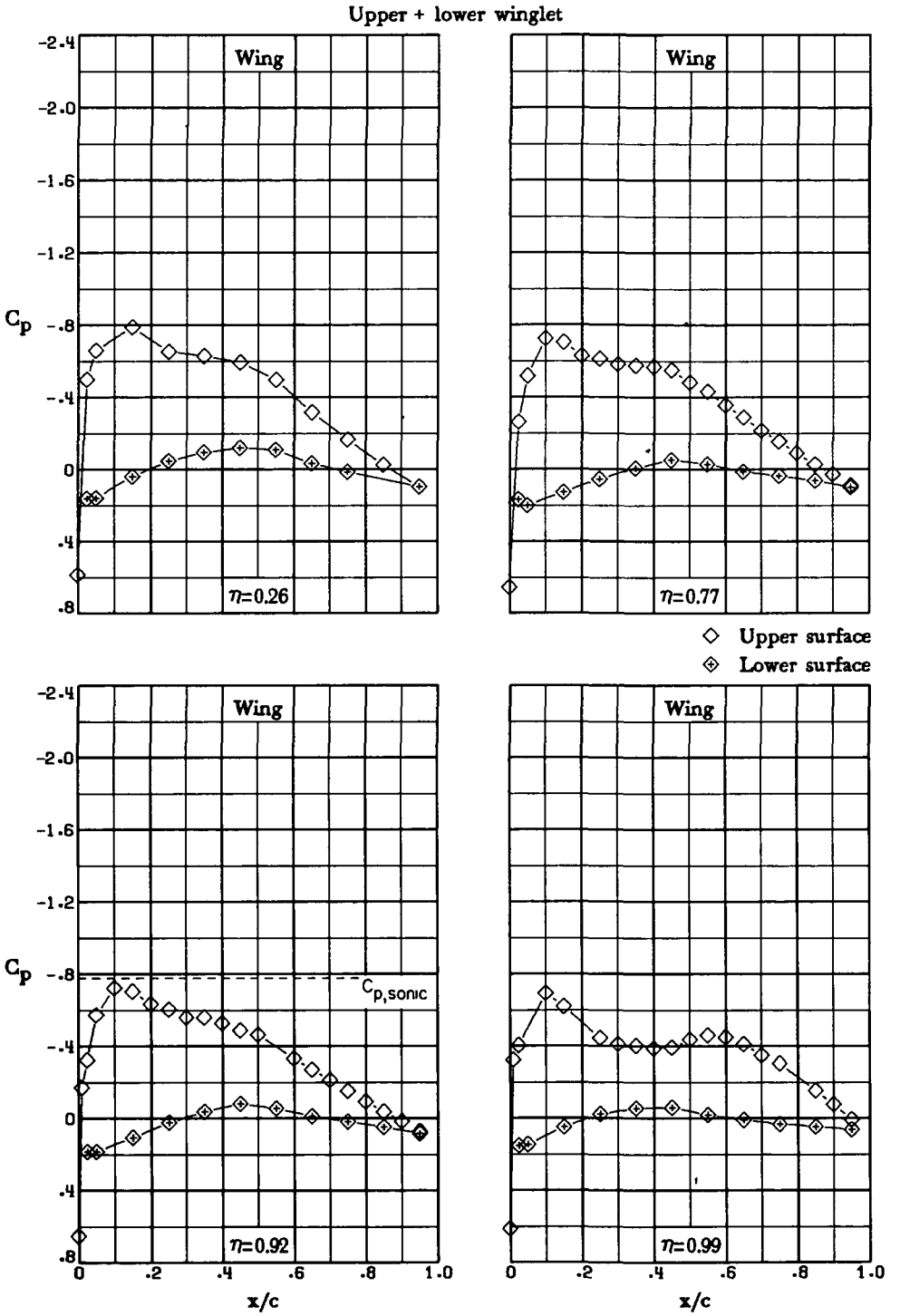

(b) $M_\infty = 0.70$; $\alpha = 2.0^o$.

Figure 10.- Continued.

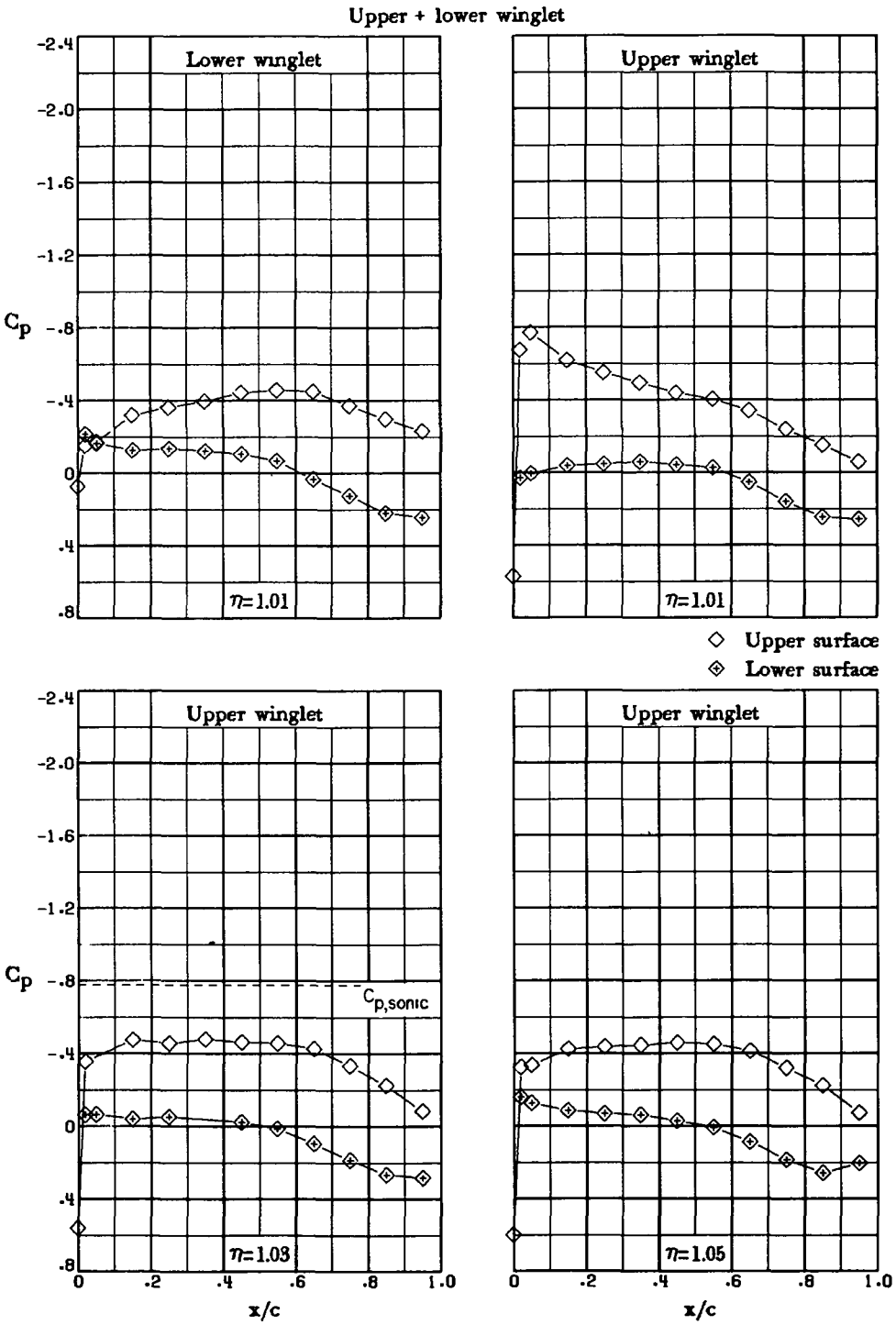

(b) $M_\infty = 0.70$; $\alpha = 2.0^\circ$. Concluded.

Figure 10.- Continued.

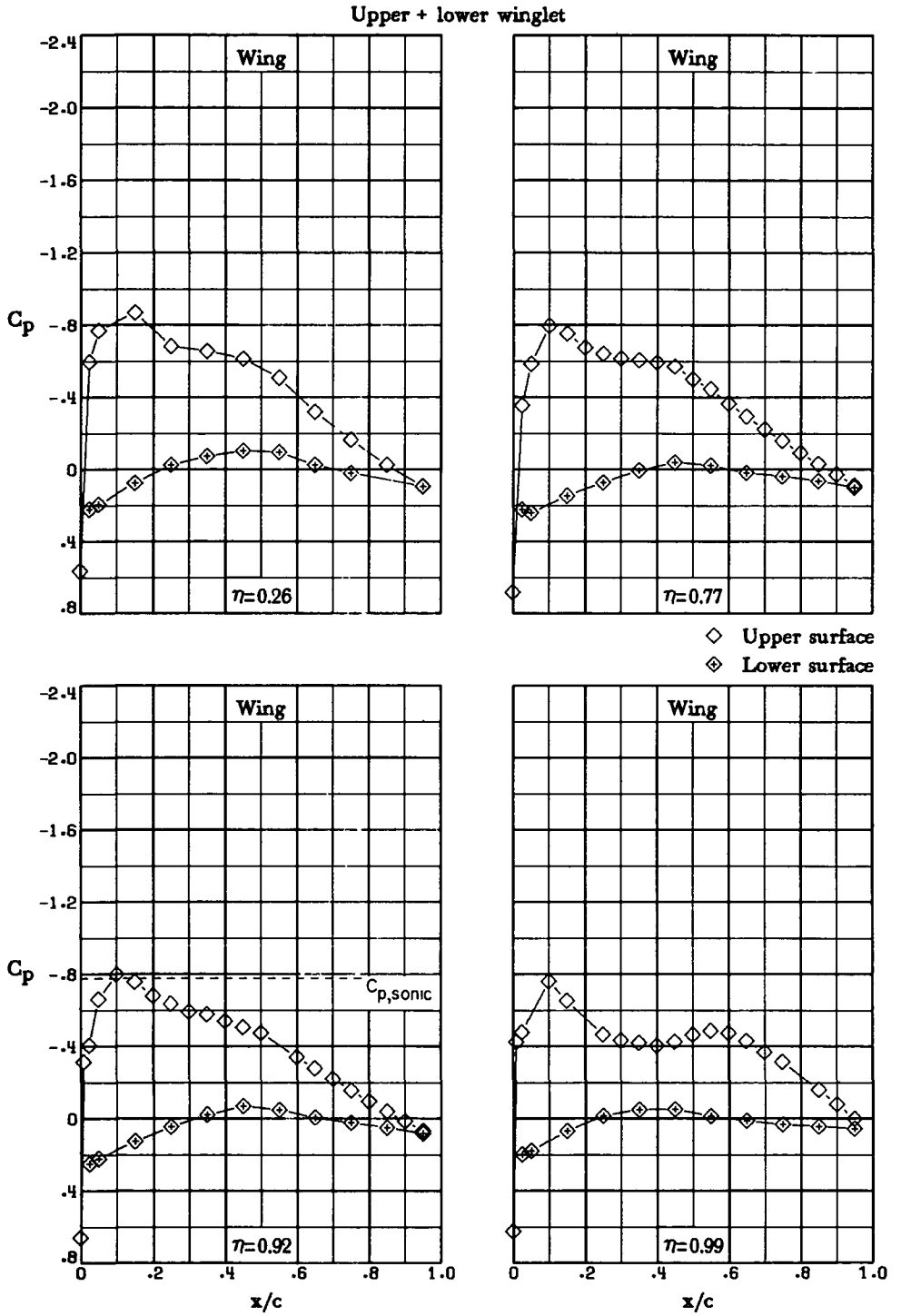

(c) $M_\infty = 0.70$; $\alpha = 2.5^\circ$.

Figure 10.- Continued.

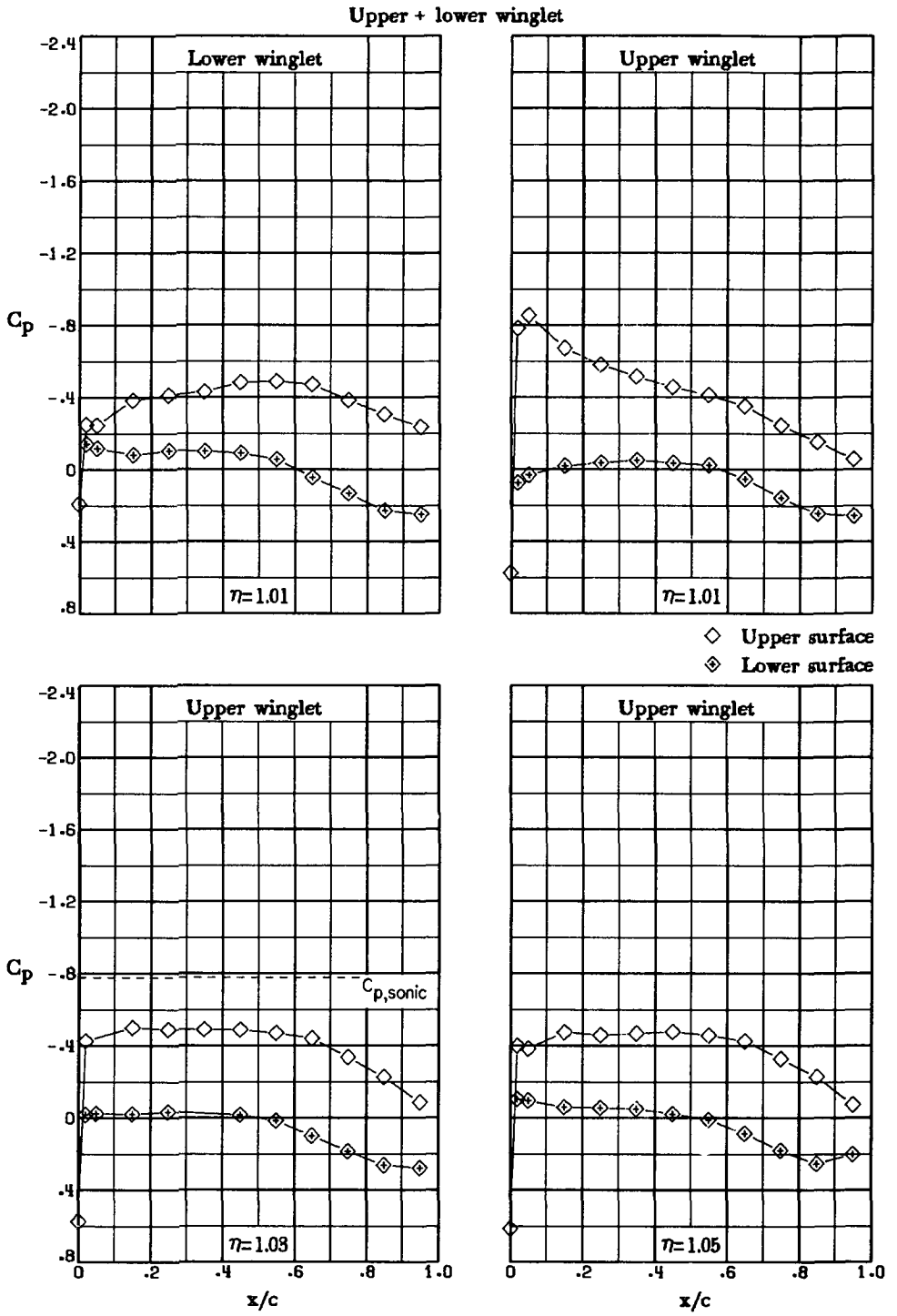

(c) $M_\infty = 0.70$; $\alpha = 2.5^\circ$. Concluded.

Figure 10.- Continued.

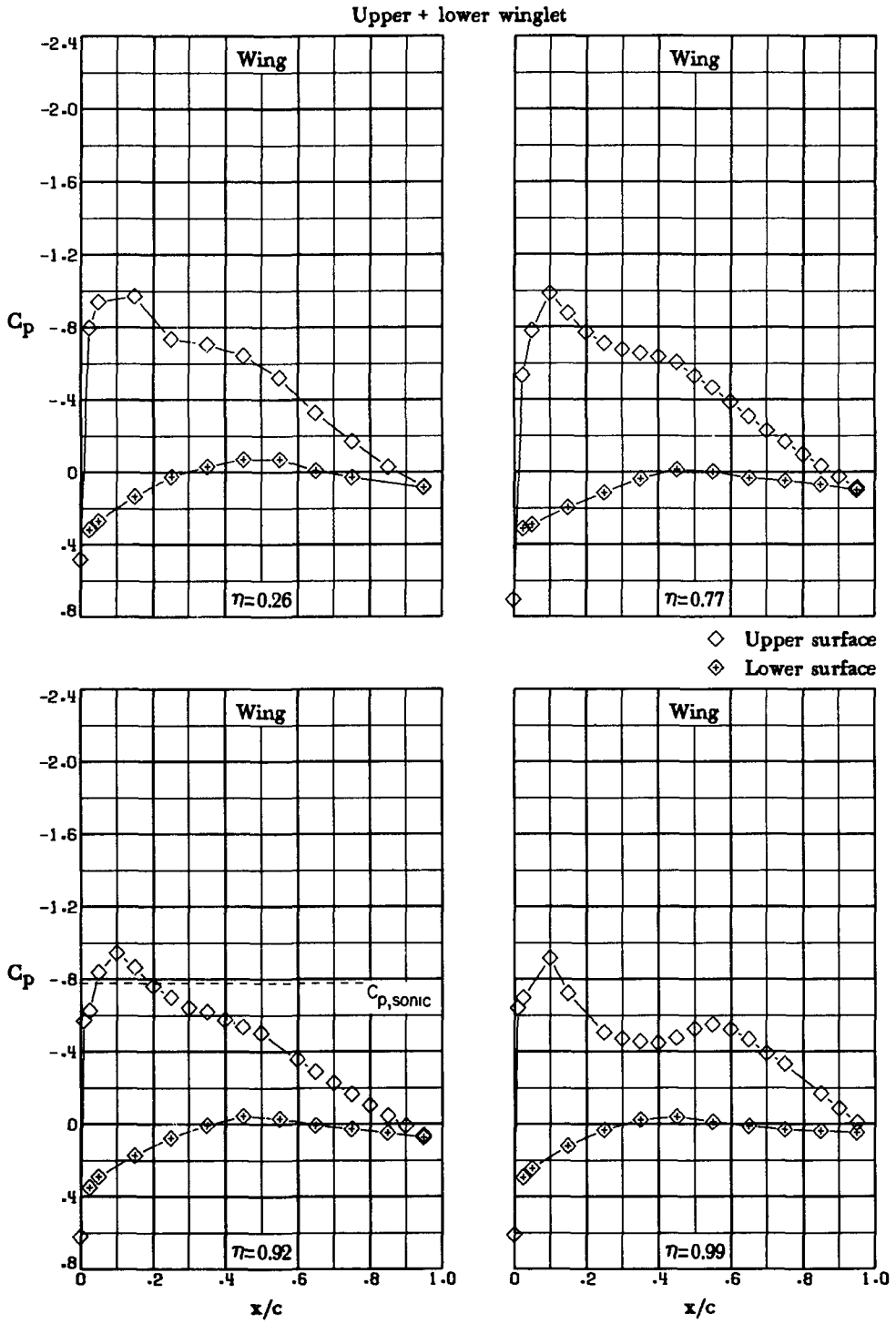

(d) $M_\infty = 0.70$; $\alpha = 3.5^\circ$.

Figure 10.- Continued.

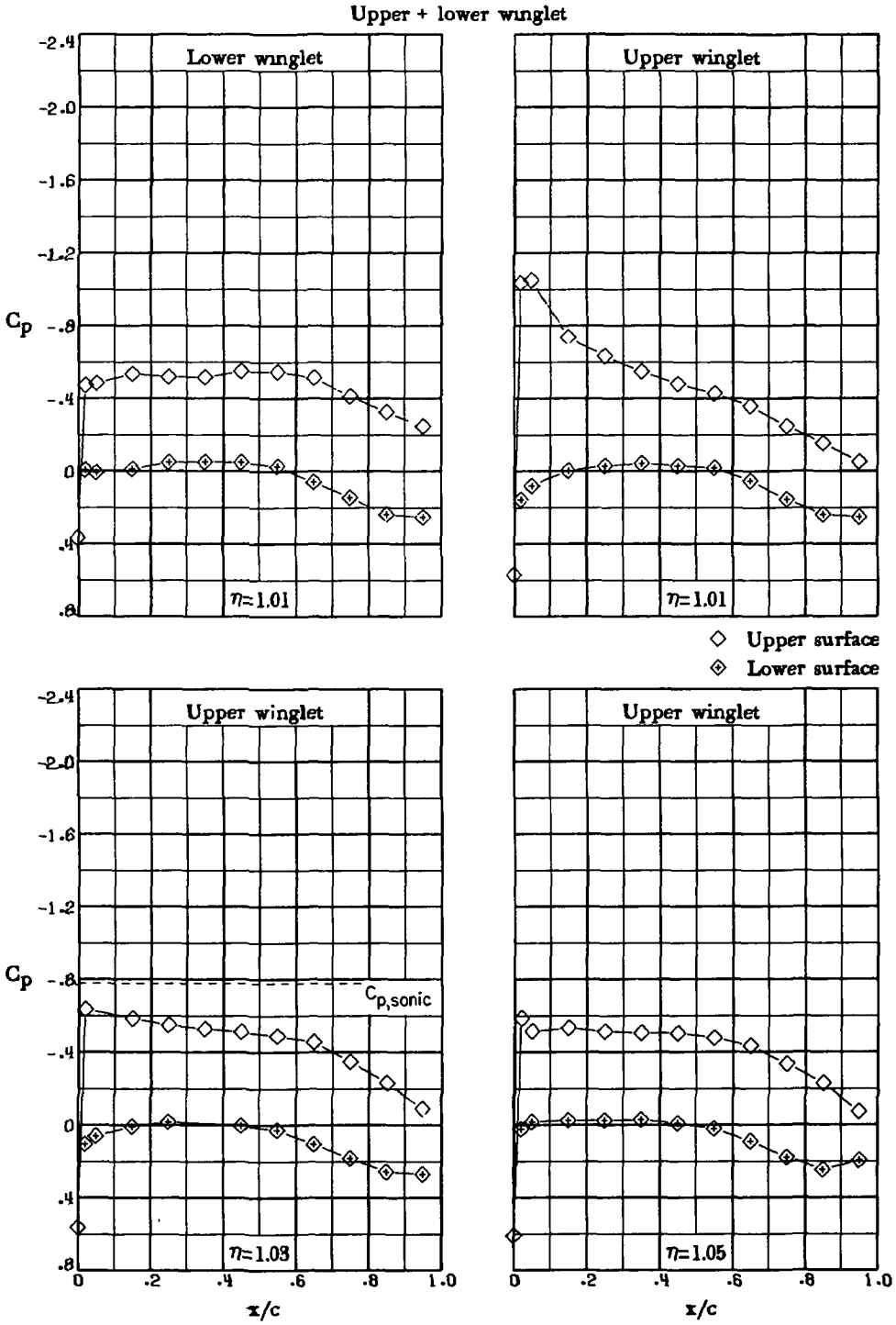

(d) M_∞ = 0.70; α = 3.5°. Concluded.

Figure 10.- Continued.

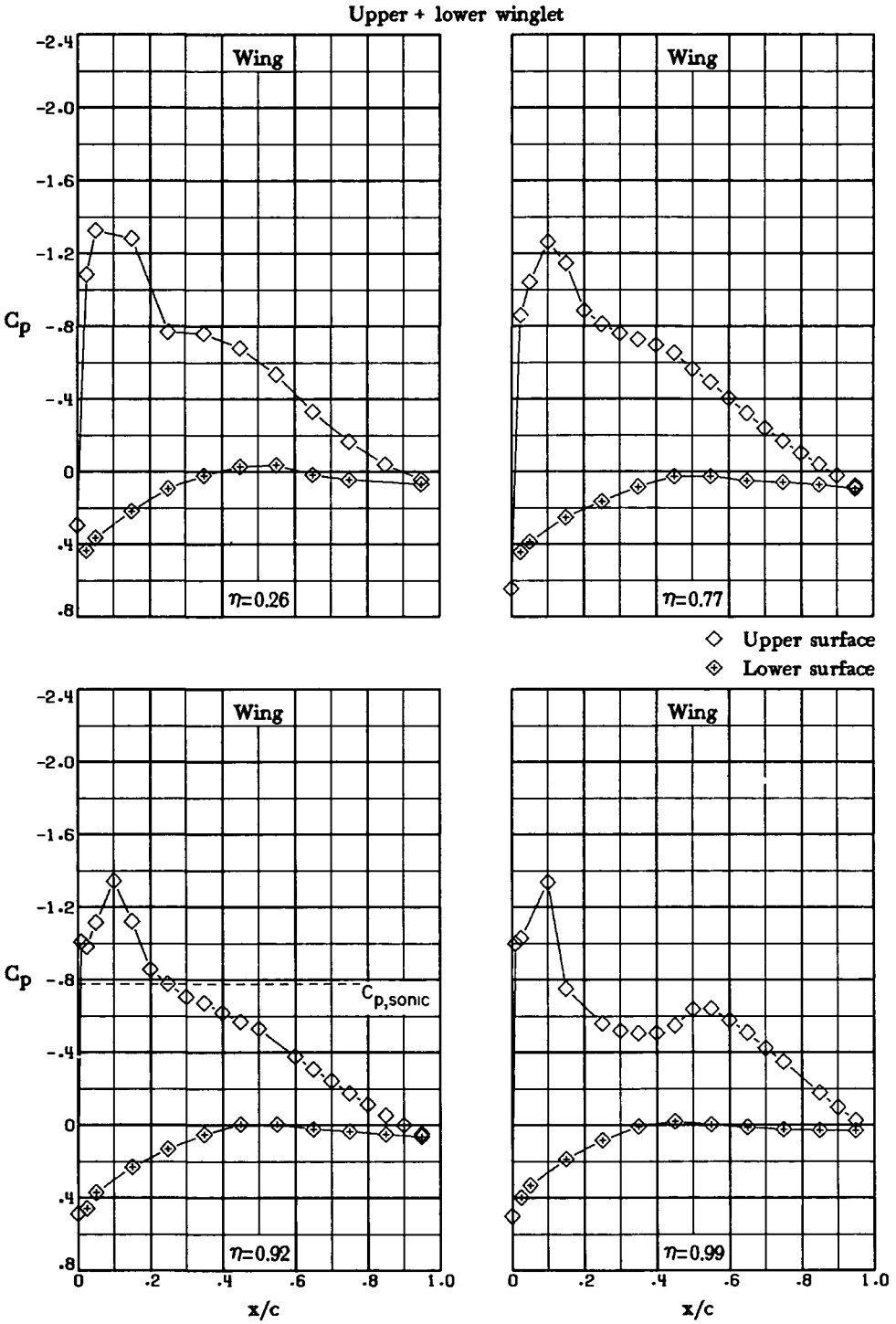

(e) M_∞ = 0.70; α = 5.0°.

Figure 10.- Continued.

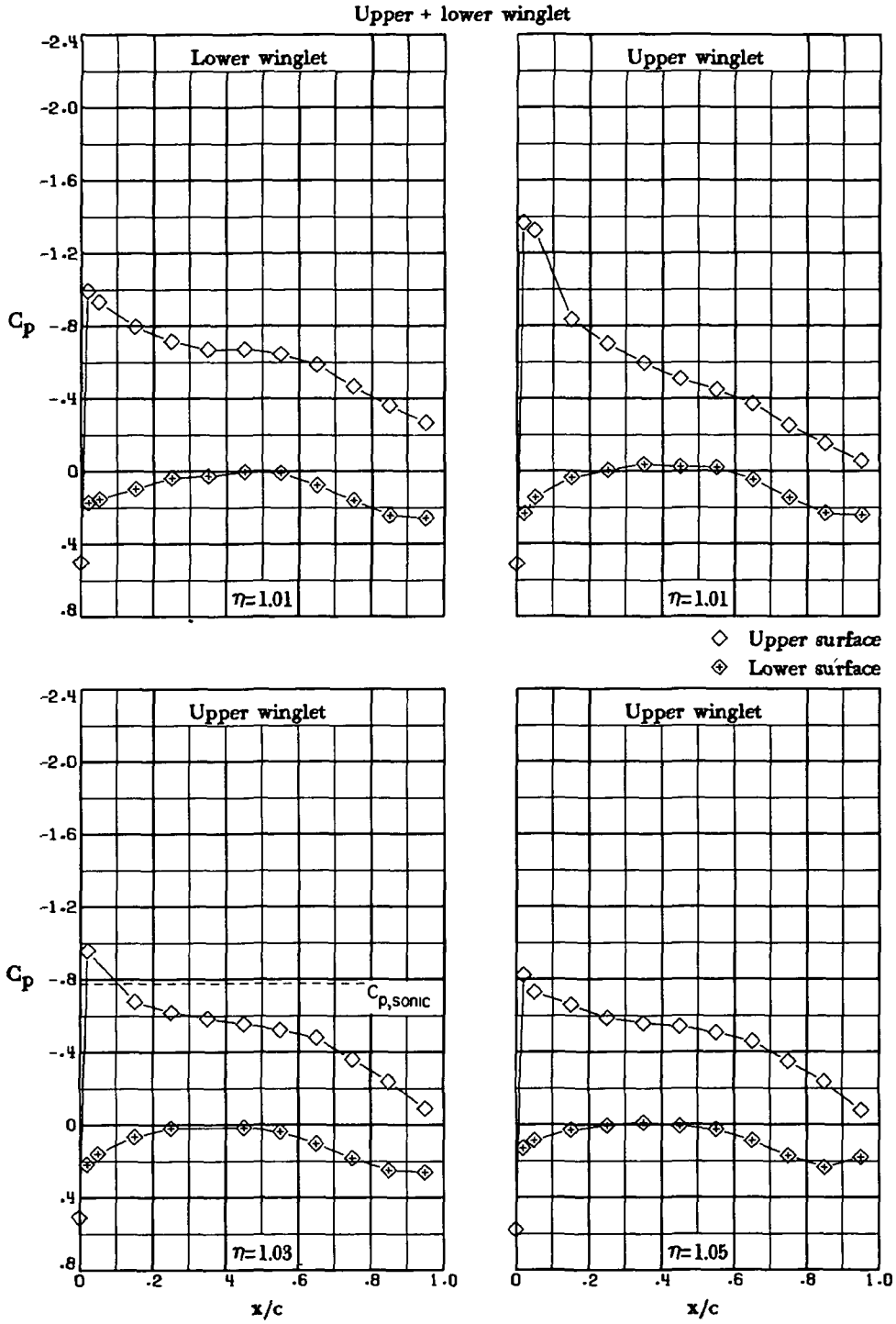

(e) $M_\infty = 0.70$; $\alpha = 5.0^\circ$. Concluded.

Figure 10.- Continued.

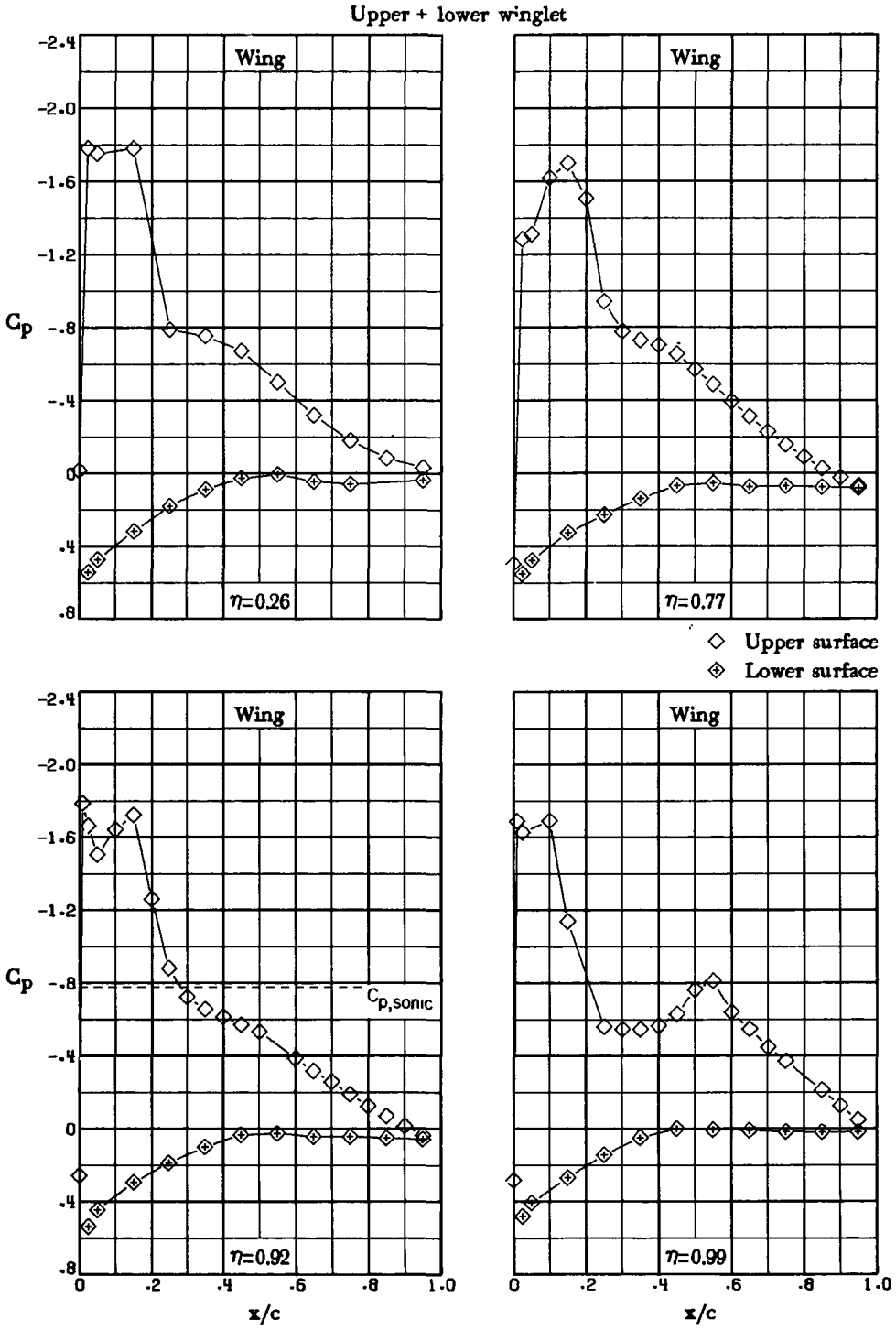

(f) $M_\infty = 0.70$; $\alpha = 7.1^\circ$.

Figure 10.- Continued.

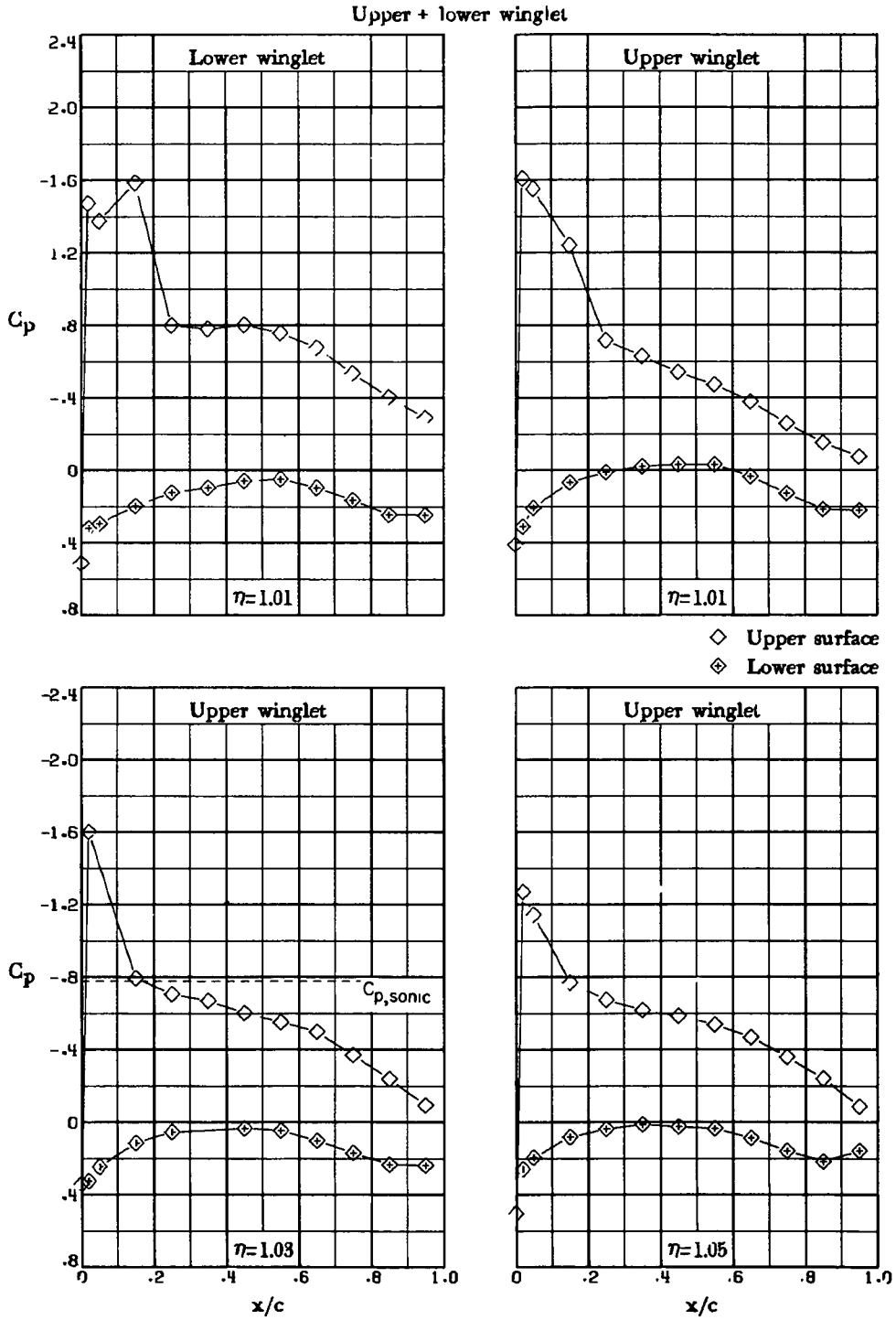

(f) $M_\infty = 0.70$; $\alpha = 7.1^\circ$. Concluded.

Figure 10.- Continued.

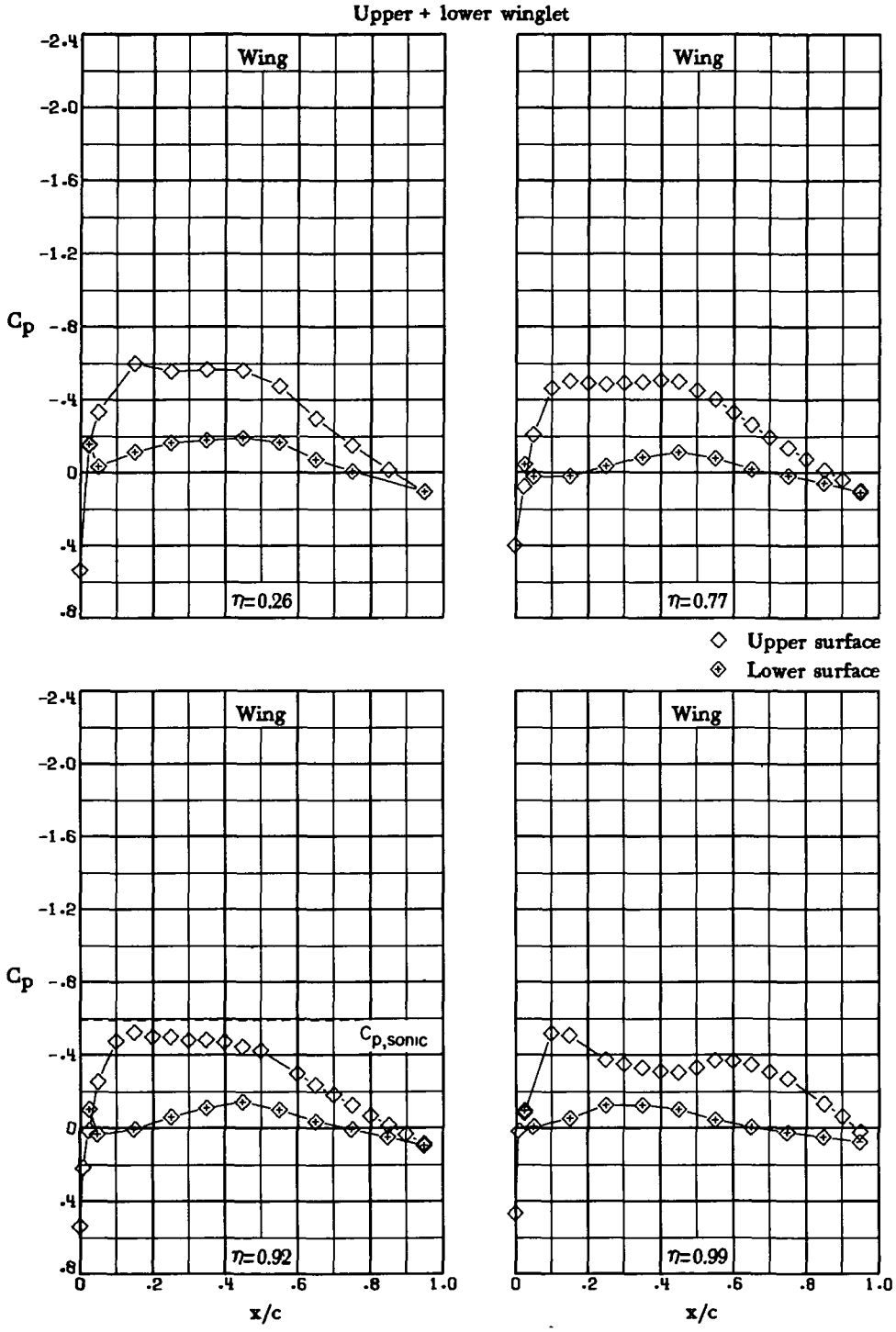

(g) $M_\infty = 0.75$; $\alpha = 0^\circ$.

Figure 10.- Continued.

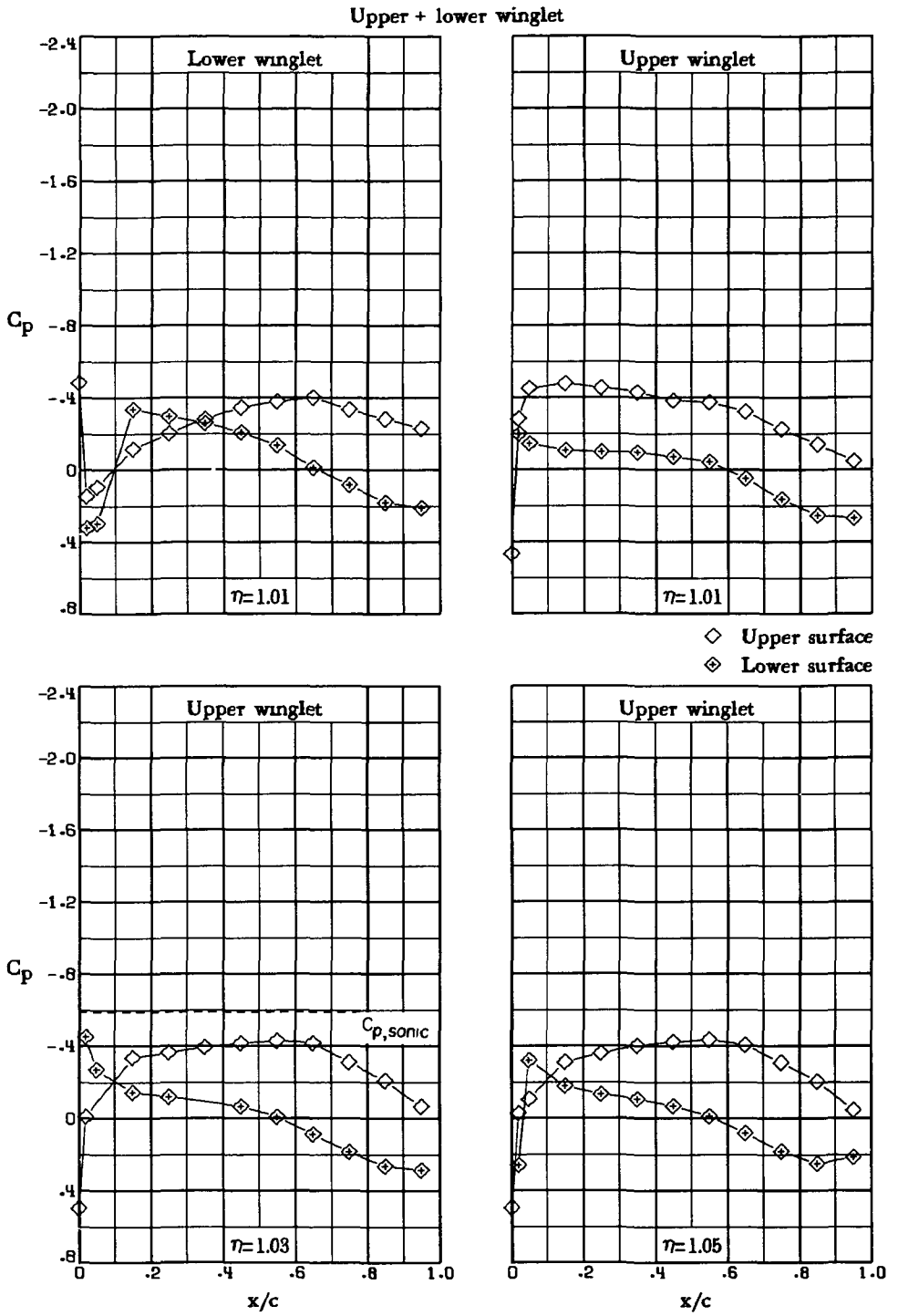

(g) M_∞ = 0.75; α = 0°. Concluded.

Figure 10.- Continued.

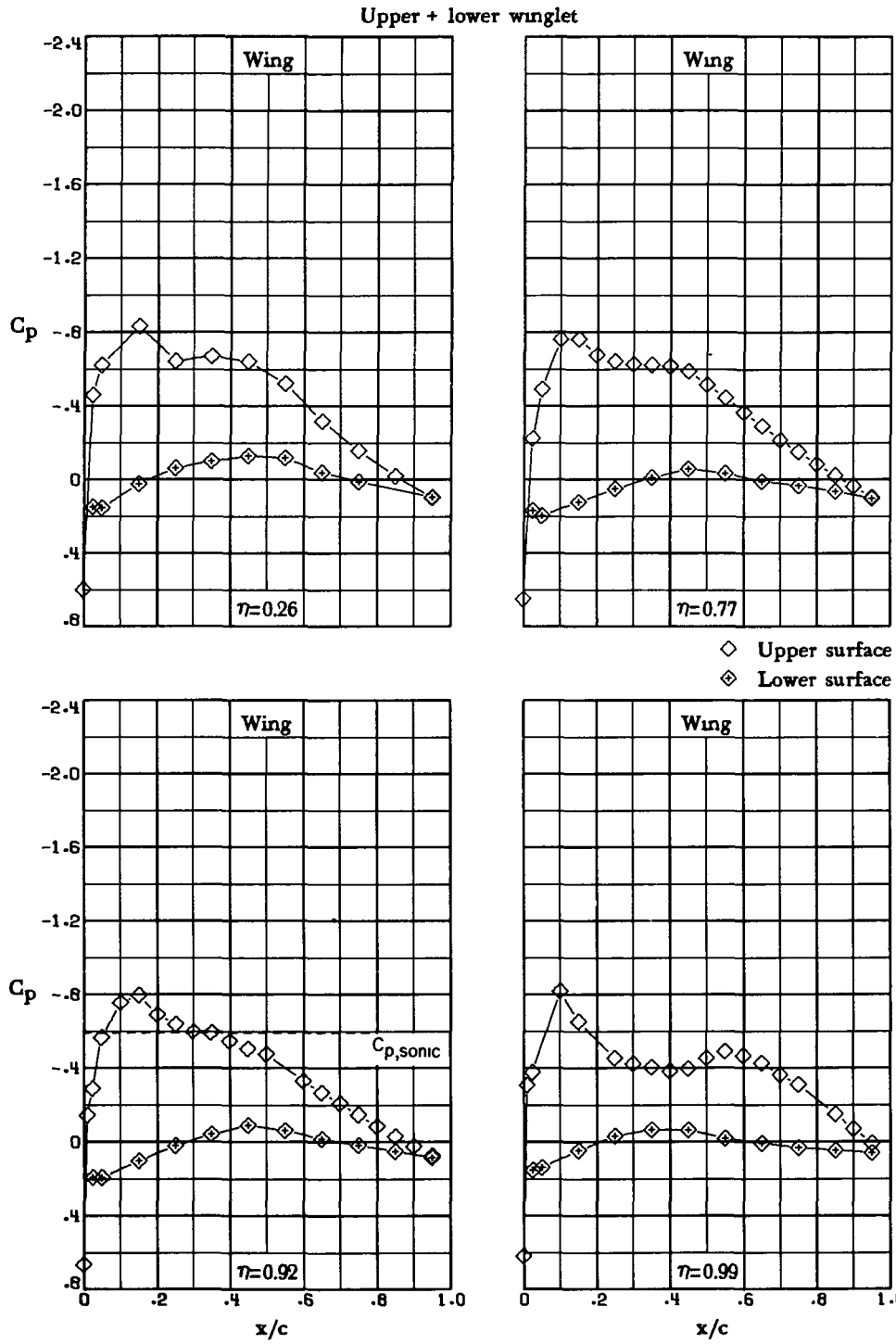

(h) $M_\infty = 0.75$; $\alpha = 2.0^\circ$.

Figure 10.- Continued.

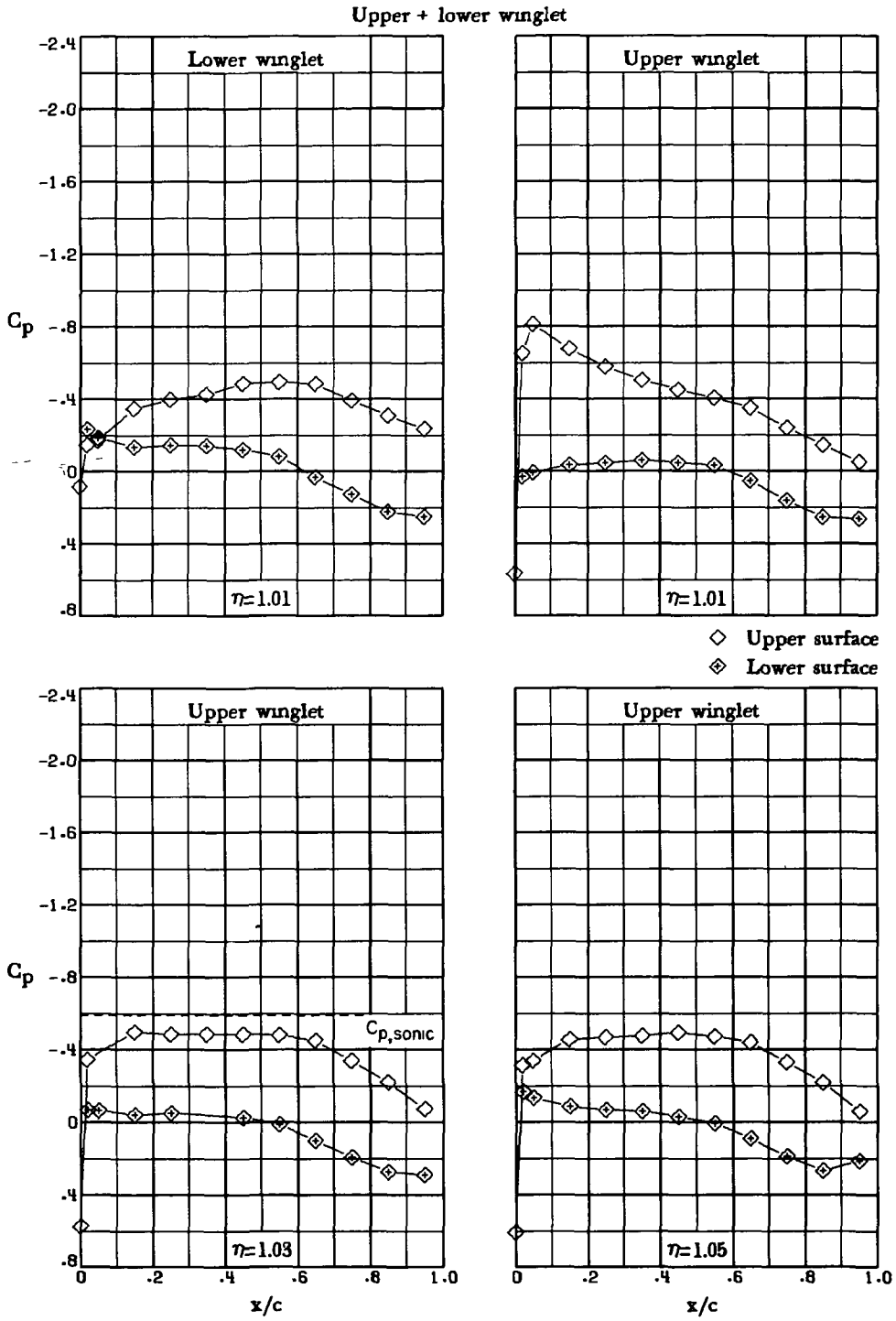

(h) $M_\infty = 0.75$; $\alpha = 2.0^\circ$. Concluded.

Figure 10.- Continued.

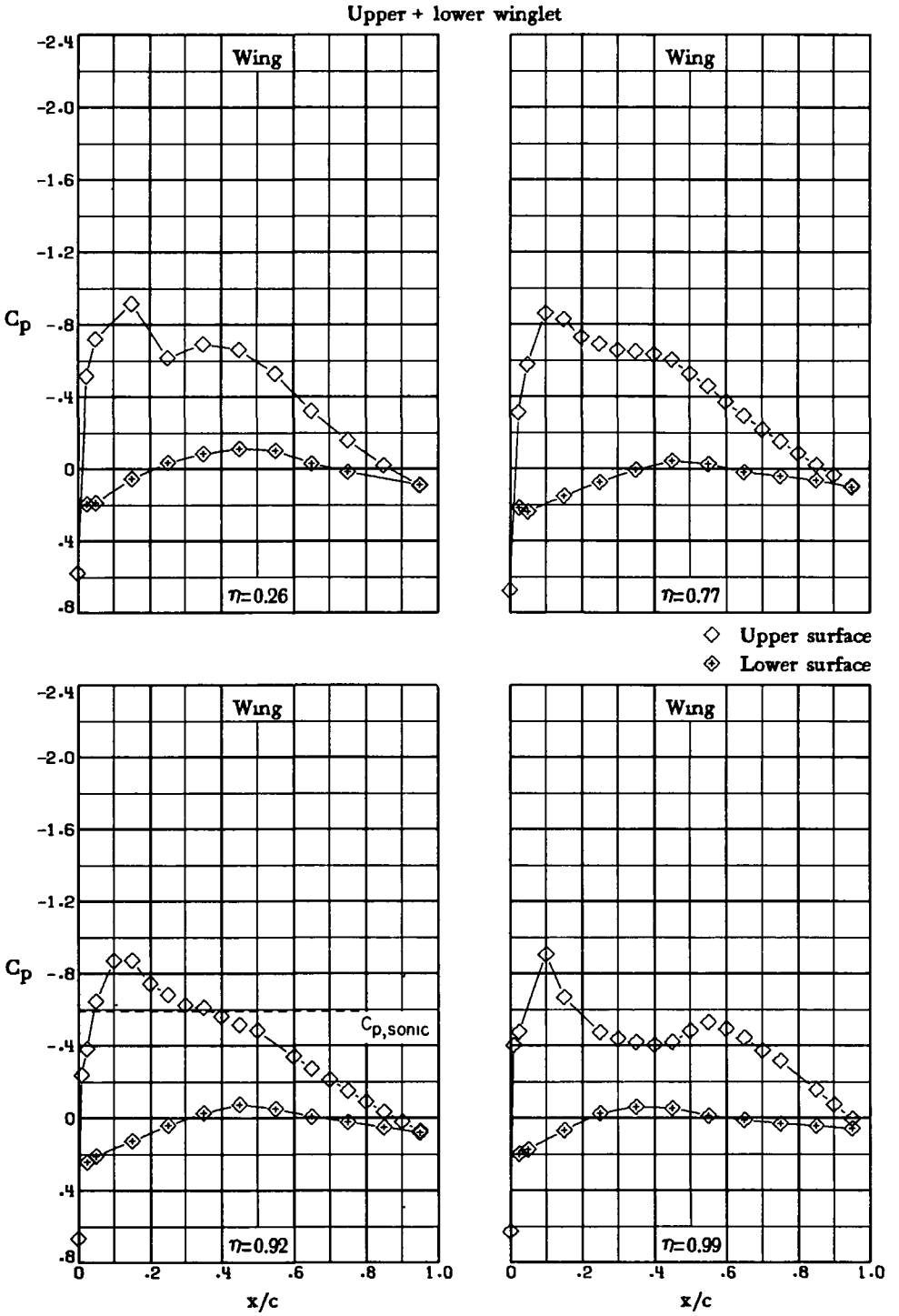

(i) $M_\infty = 0.75$; $\alpha = 2.5^\circ$.

Figure 10.- Continued.

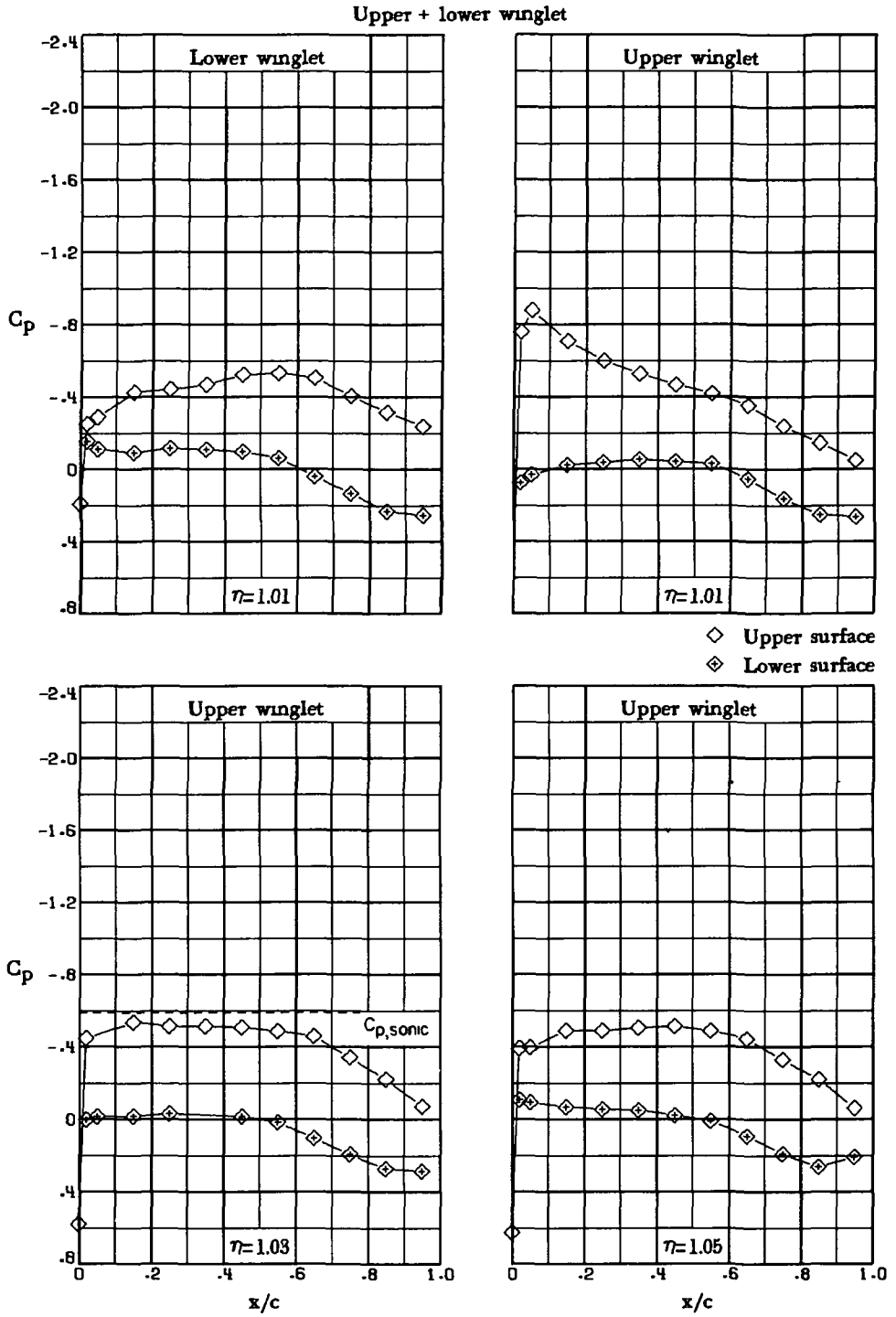

(i) $M_\infty = 0.75$; $\alpha = 2.5^\circ$. Concluded.

Figure 10.- Continued.

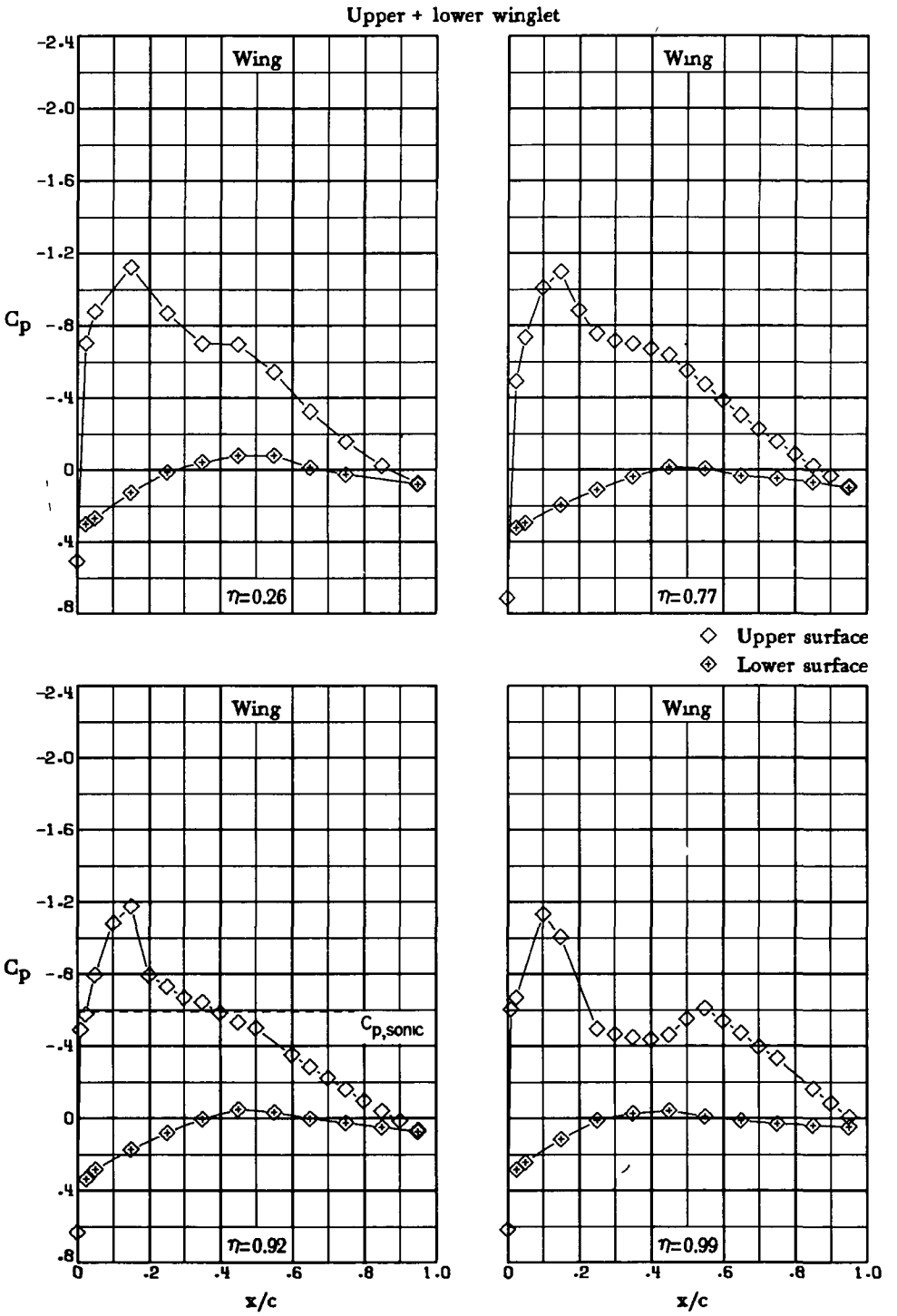

(j) $M_\infty = 0.75$; $\alpha = 3.5^o$.

Figure 10.- Continued.

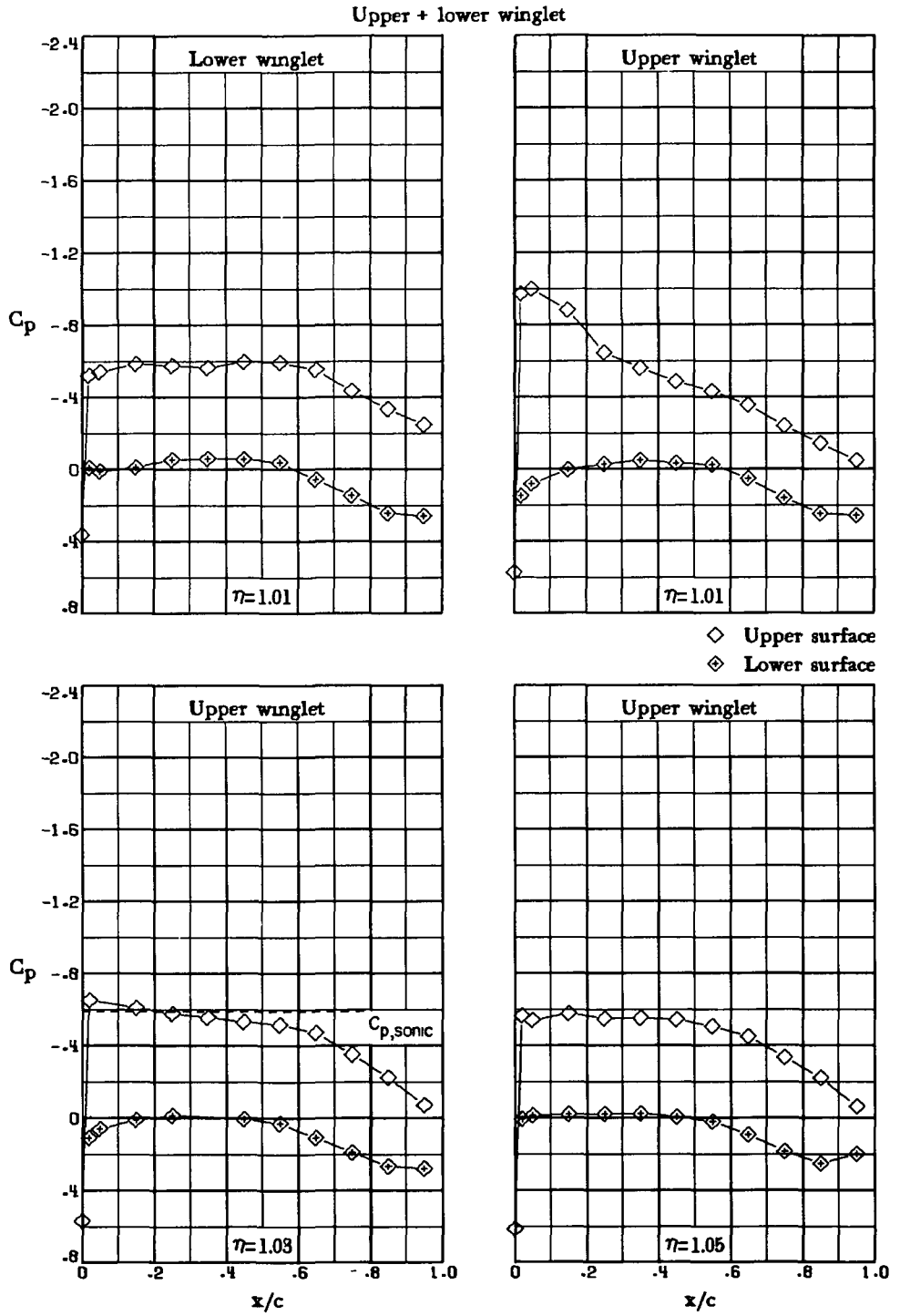

(j) M_∞ = 0.75; α = 3.5°. Concluded.

Figure 10.- Continued.

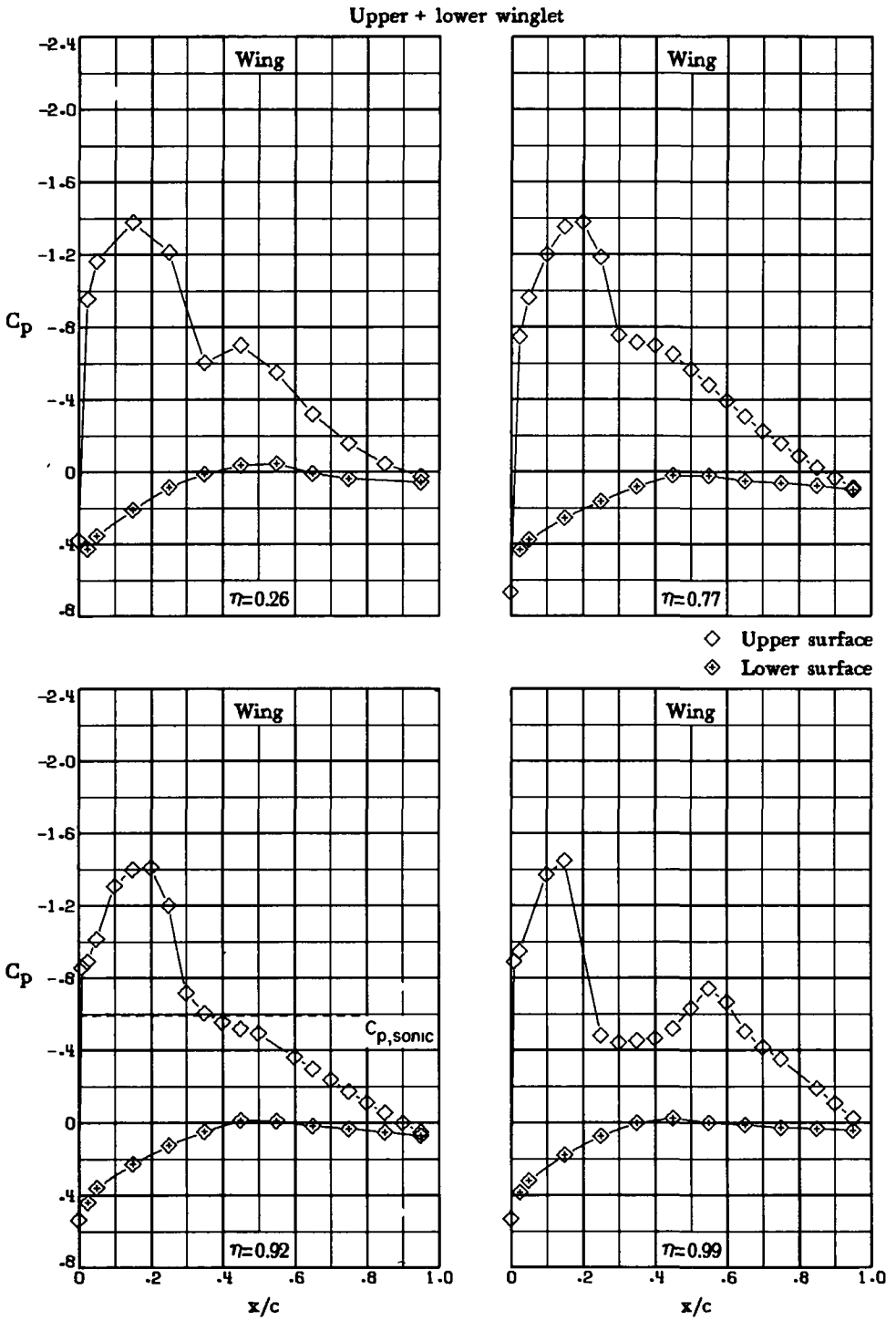

(k) $M_\infty = 0.75$; $\alpha = 5.0^o$.

Figure 10.- Continued.

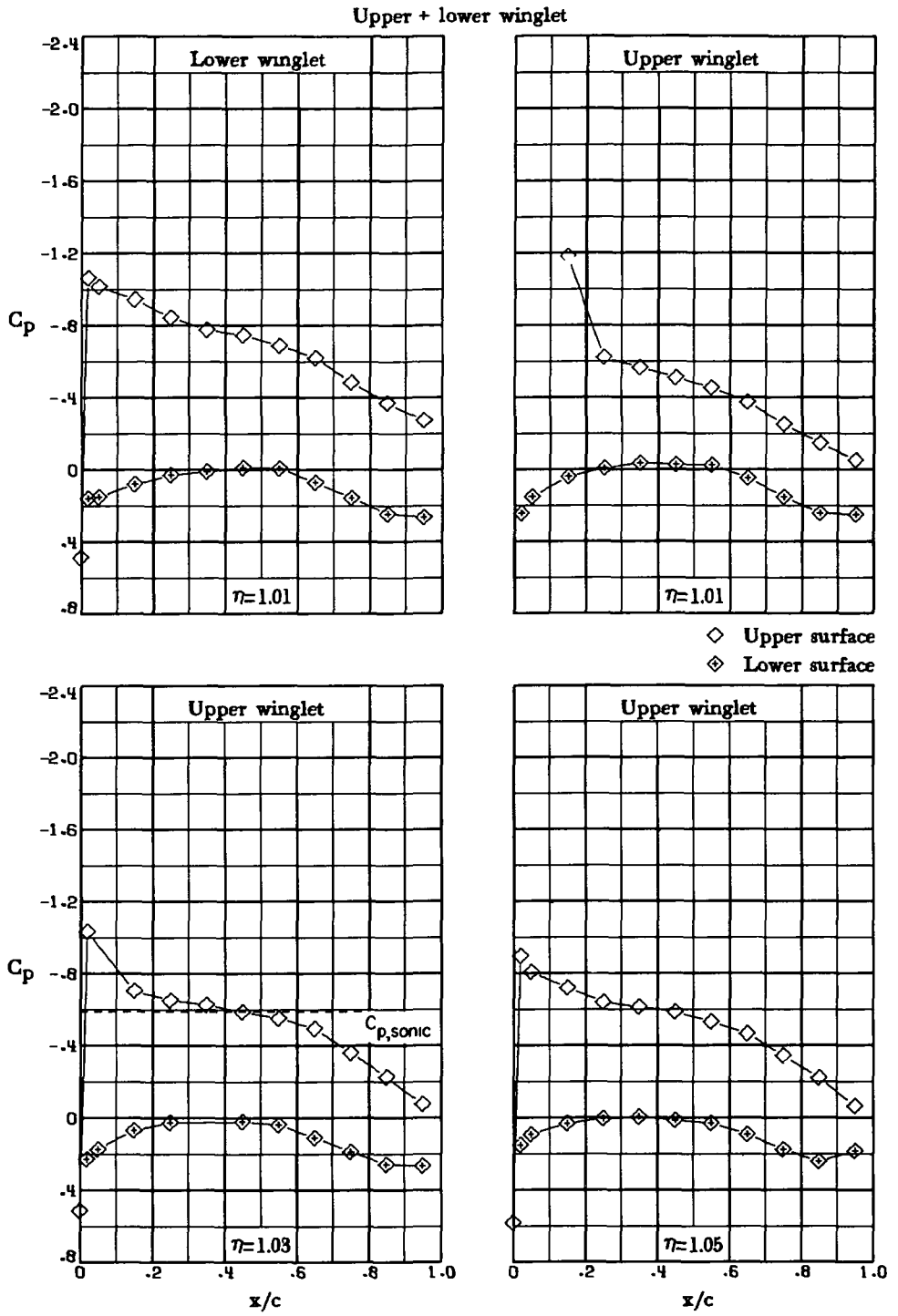

(k) M_∞ = 0.75; α = 5.0°. Concluded.

Figure 10.- Continued.

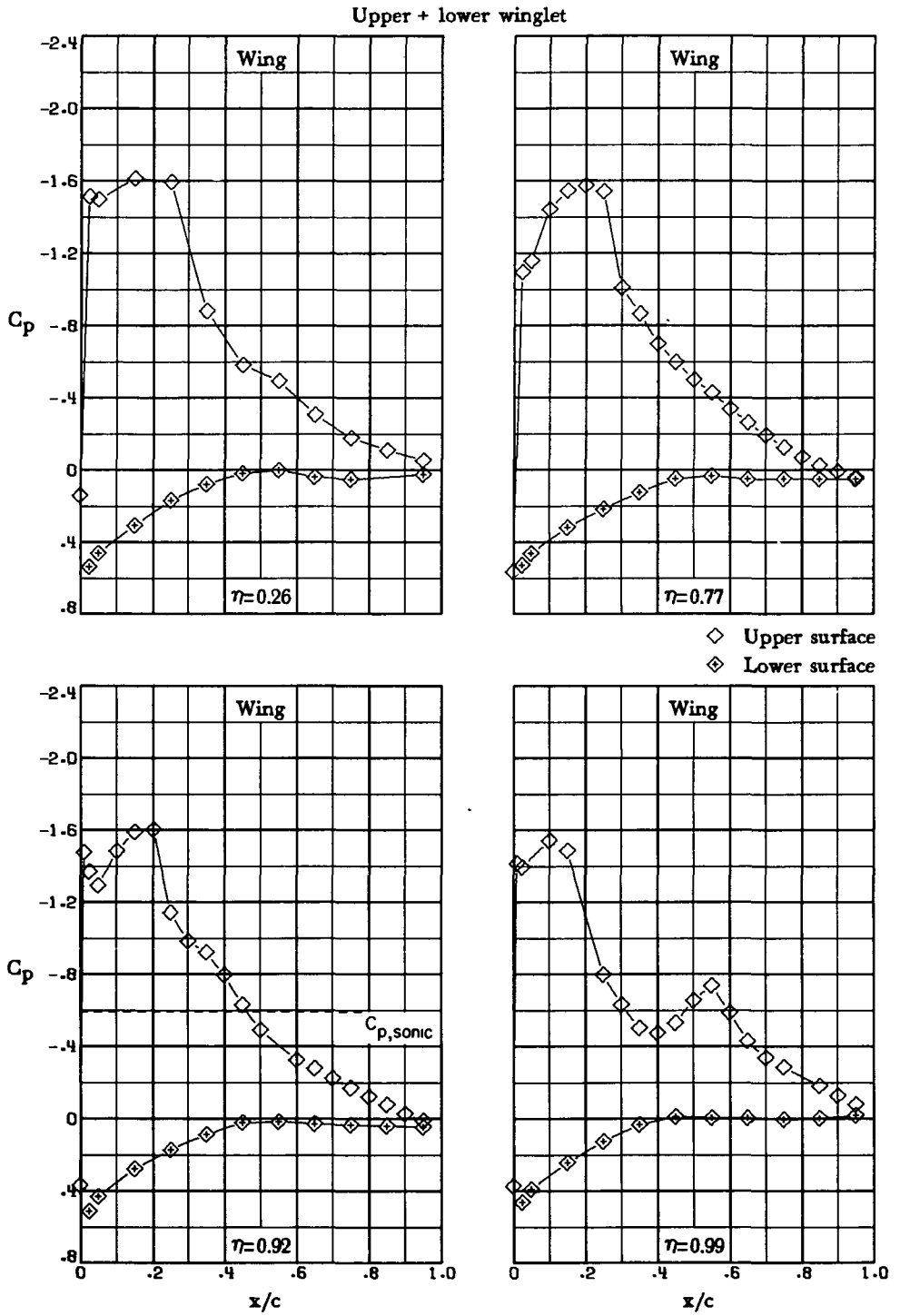

(l) $M_\infty = 0.75$; $\alpha = 7.1^\circ$.

Figure 10.- Continued.

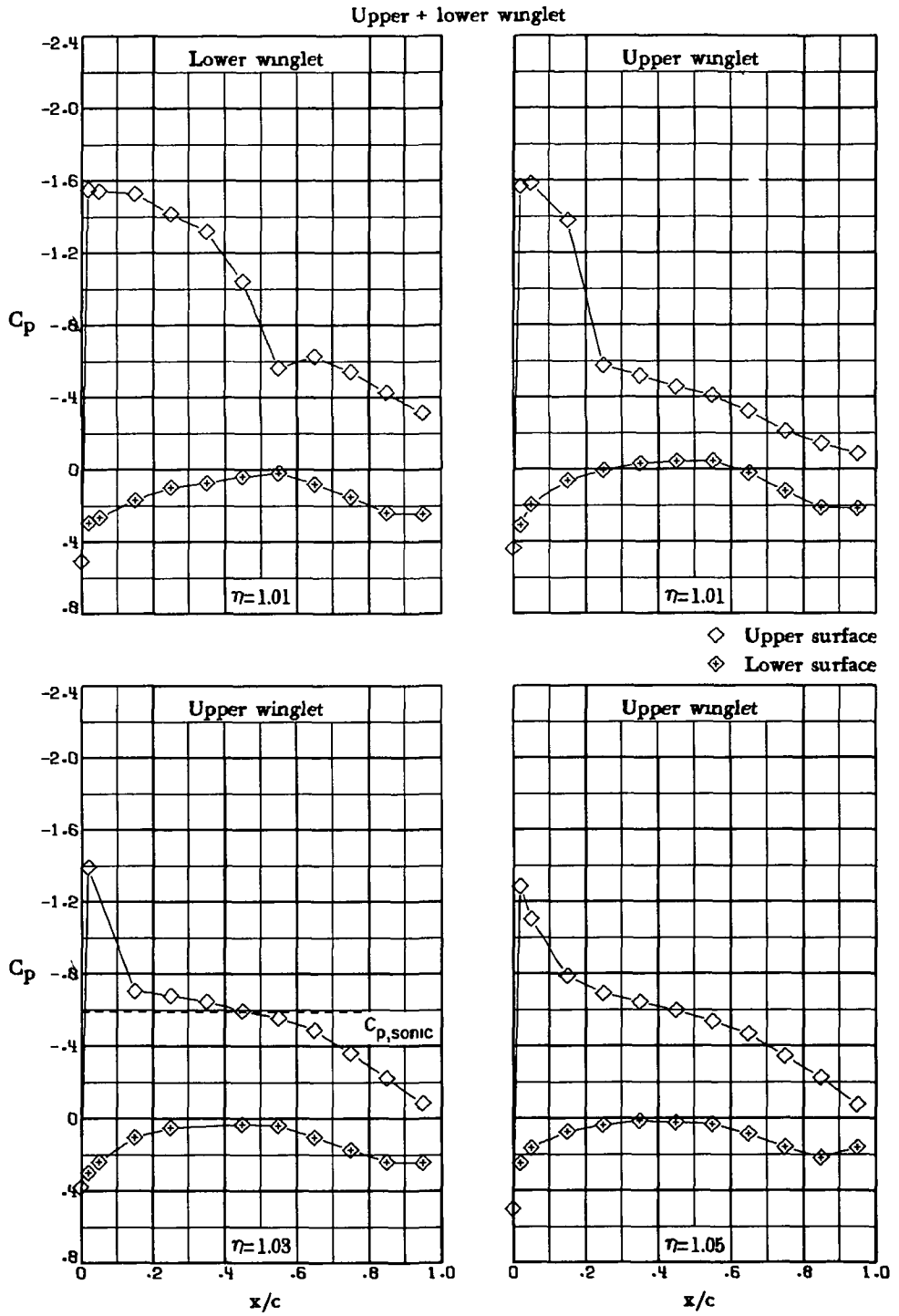

(l) M_∞ = 0.75; α = 7.1°. Concluded.

Figure 10.- Continued.

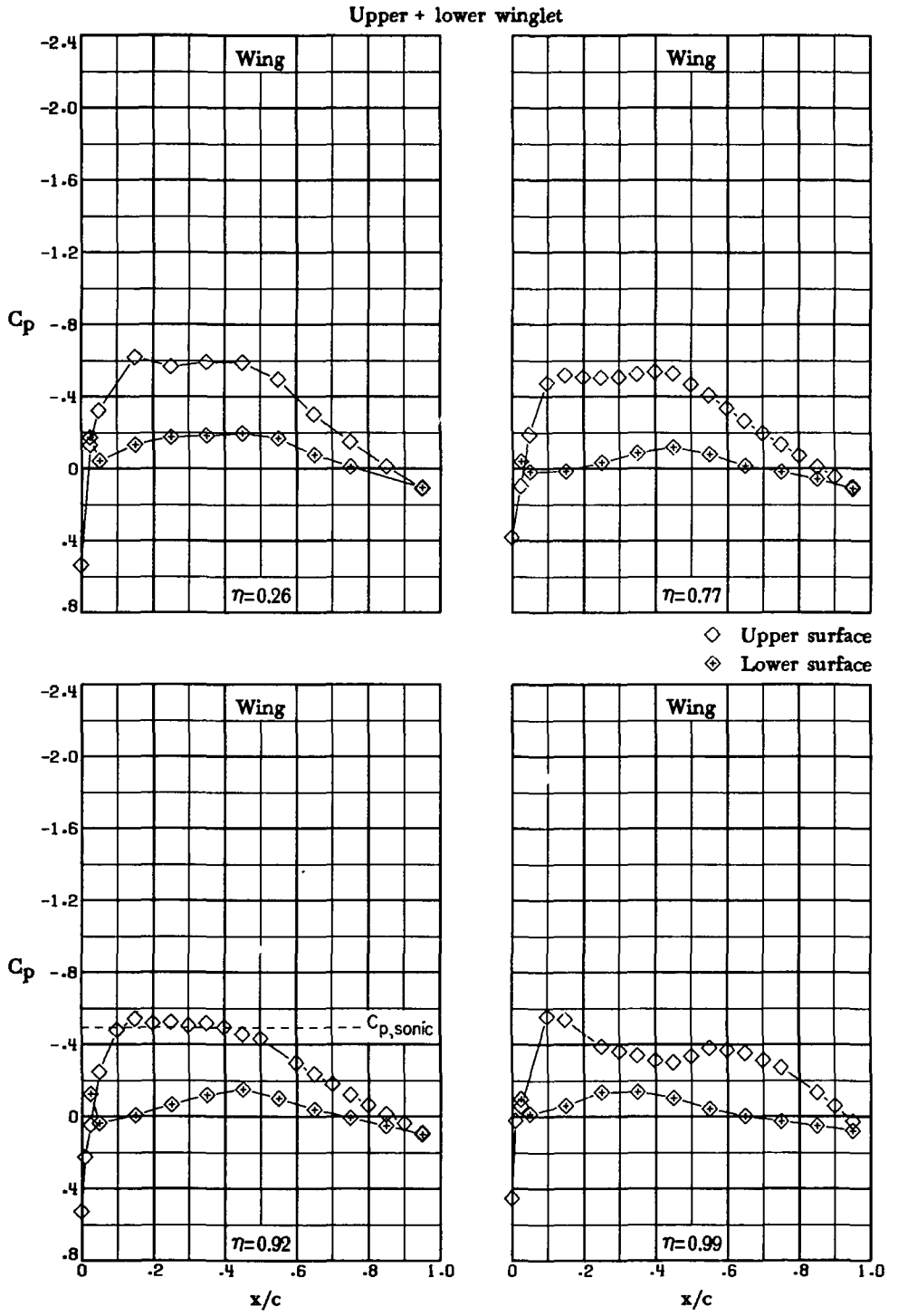

(m) $M_\infty = 0.78$; $\alpha = 0^o$.

Figure 10.- Continued.

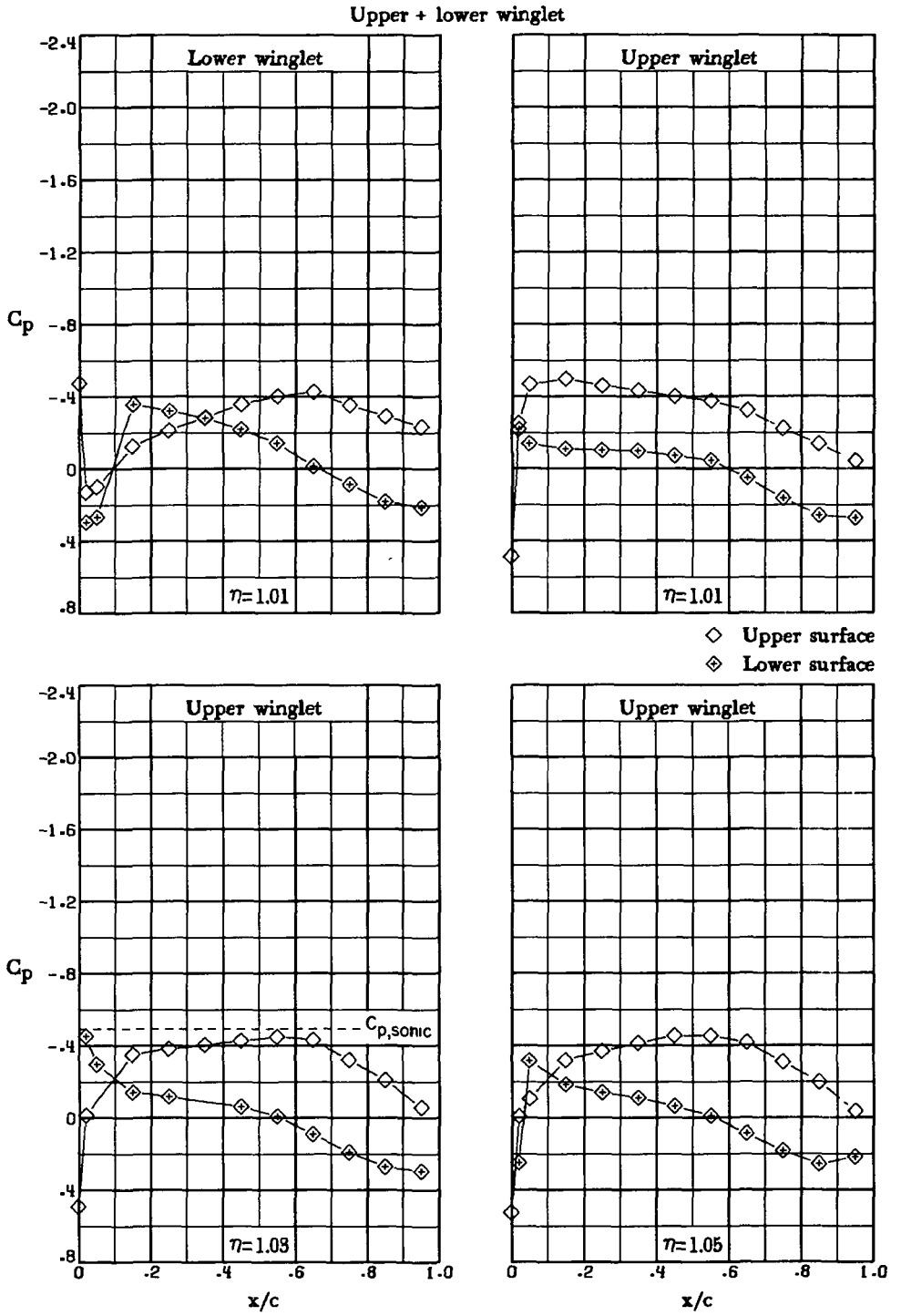

(m) $M_\infty = 0.78$; $\alpha = 0^o$. Concluded.

Figure 10.- Continued.

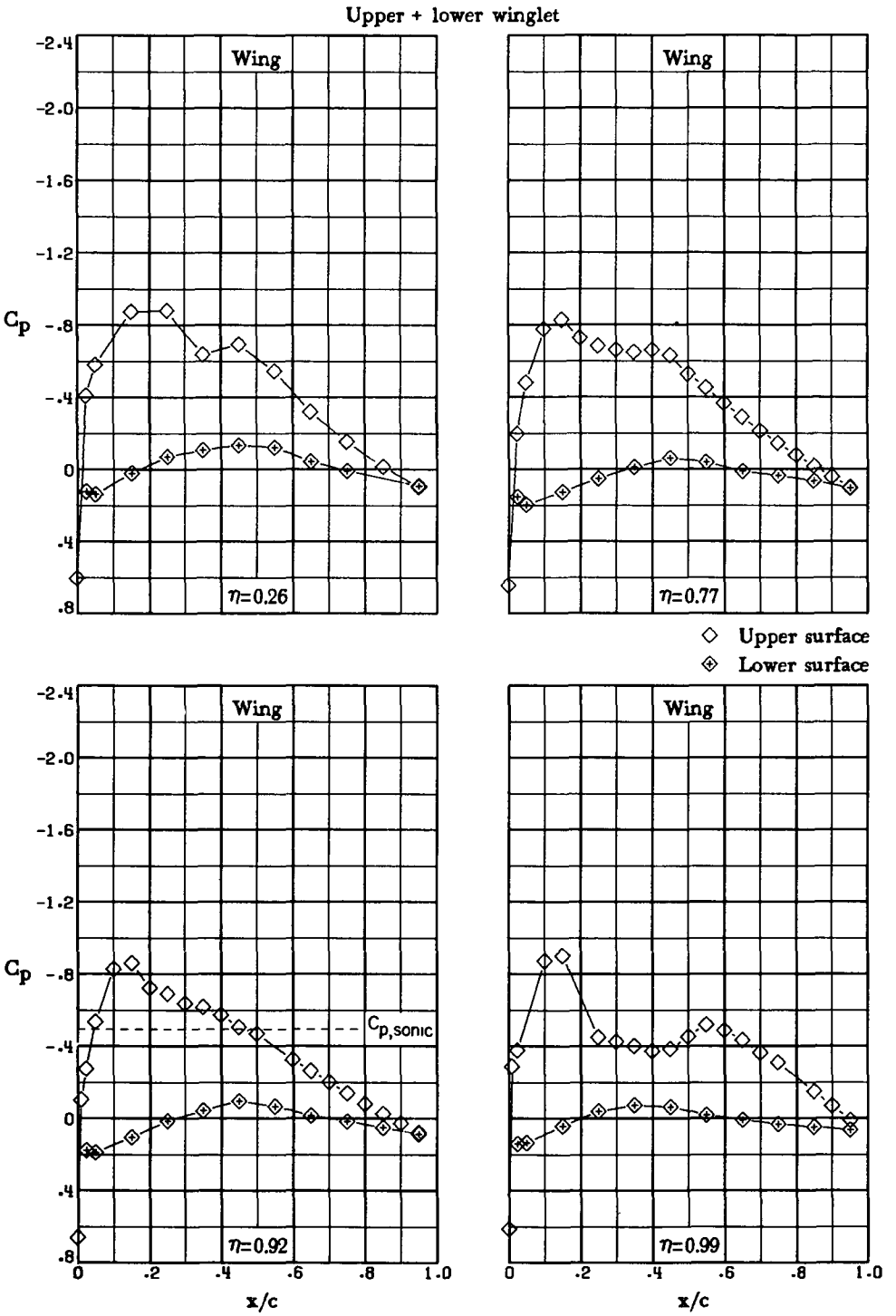

(n) $M_\infty = 0.78$; $\alpha = 2.0^\circ$.

Figure 10.- Continued.

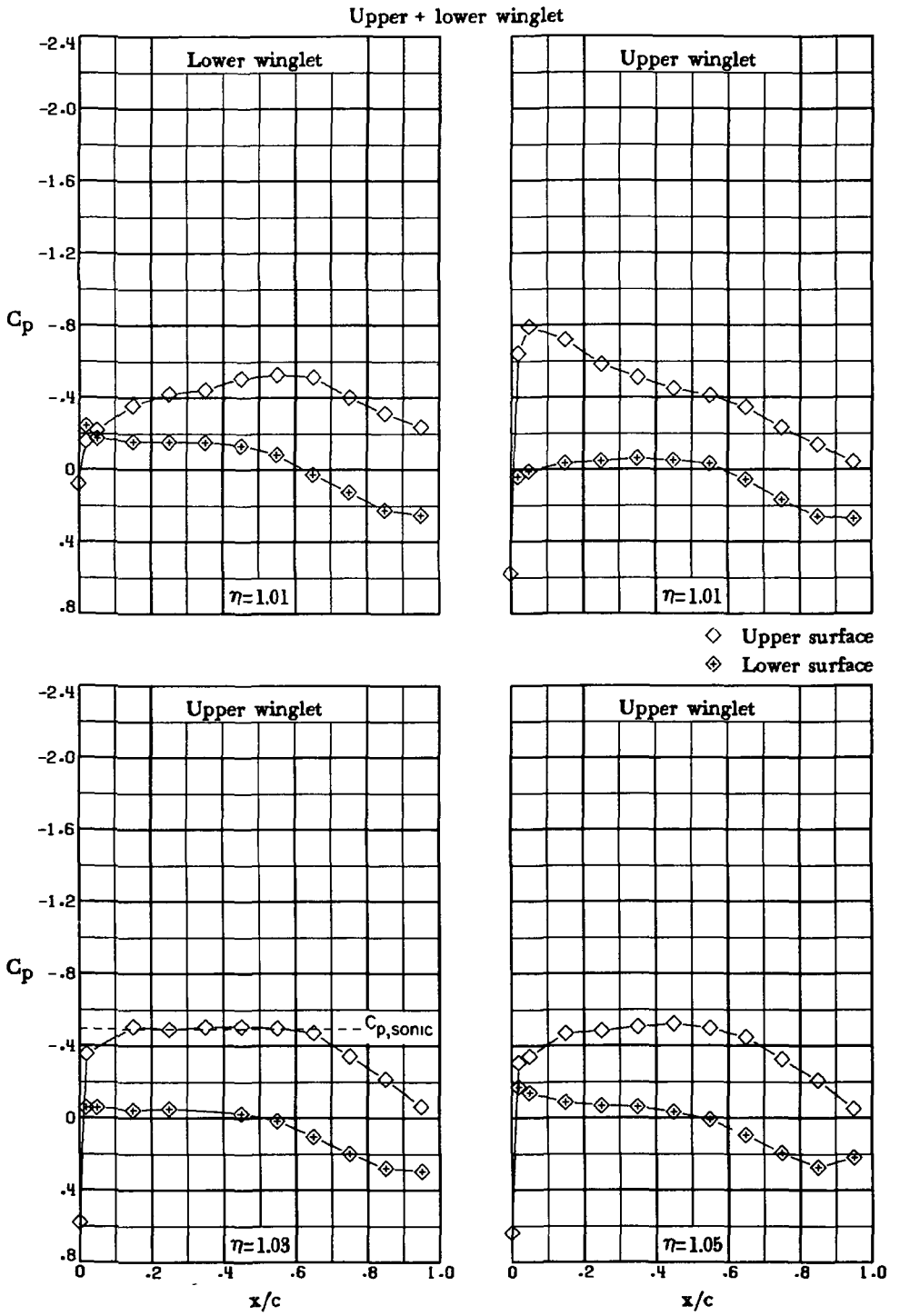

(n) $M_\infty = 0.78$; $\alpha = 2.0^\circ$. Concluded.

Figure 10.- Continued.

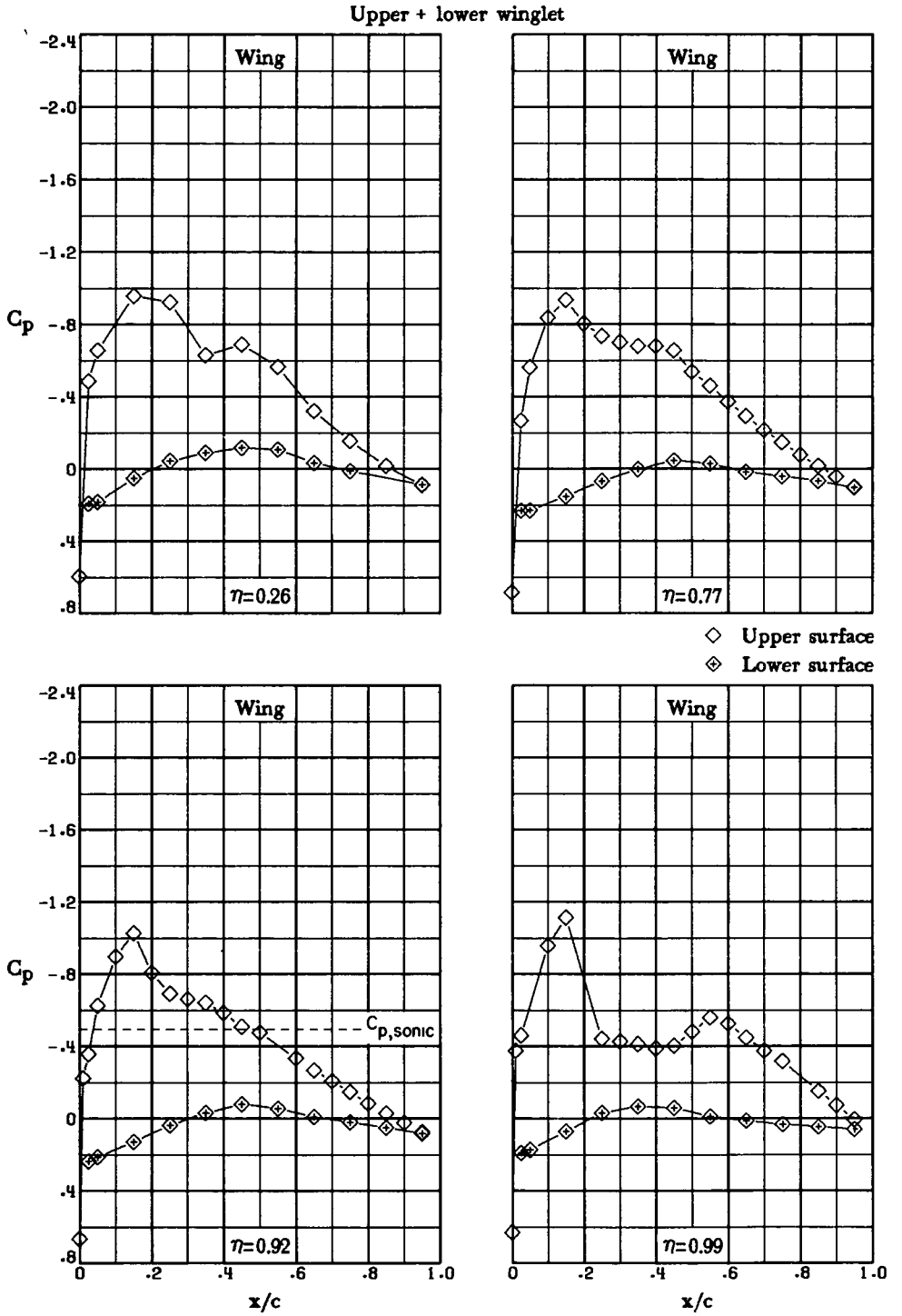

(o) $M_\infty = 0.78$; $\alpha = 2.5^\circ$.

Figure 10.- Continued.

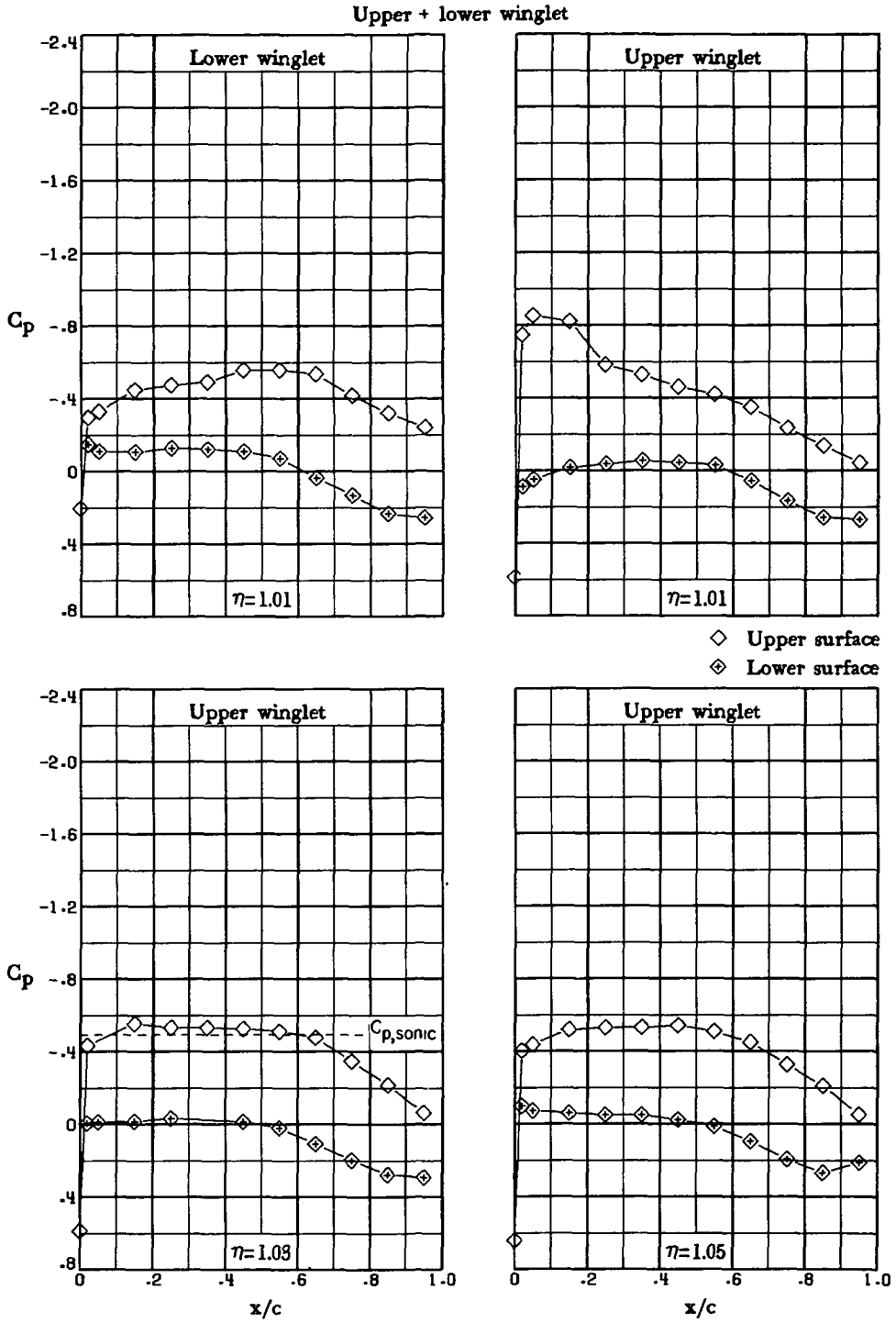

(o) $M_\infty = 0.78$; $\alpha = 2.5^\circ$. Concluded.

Figure 10.- Continued.

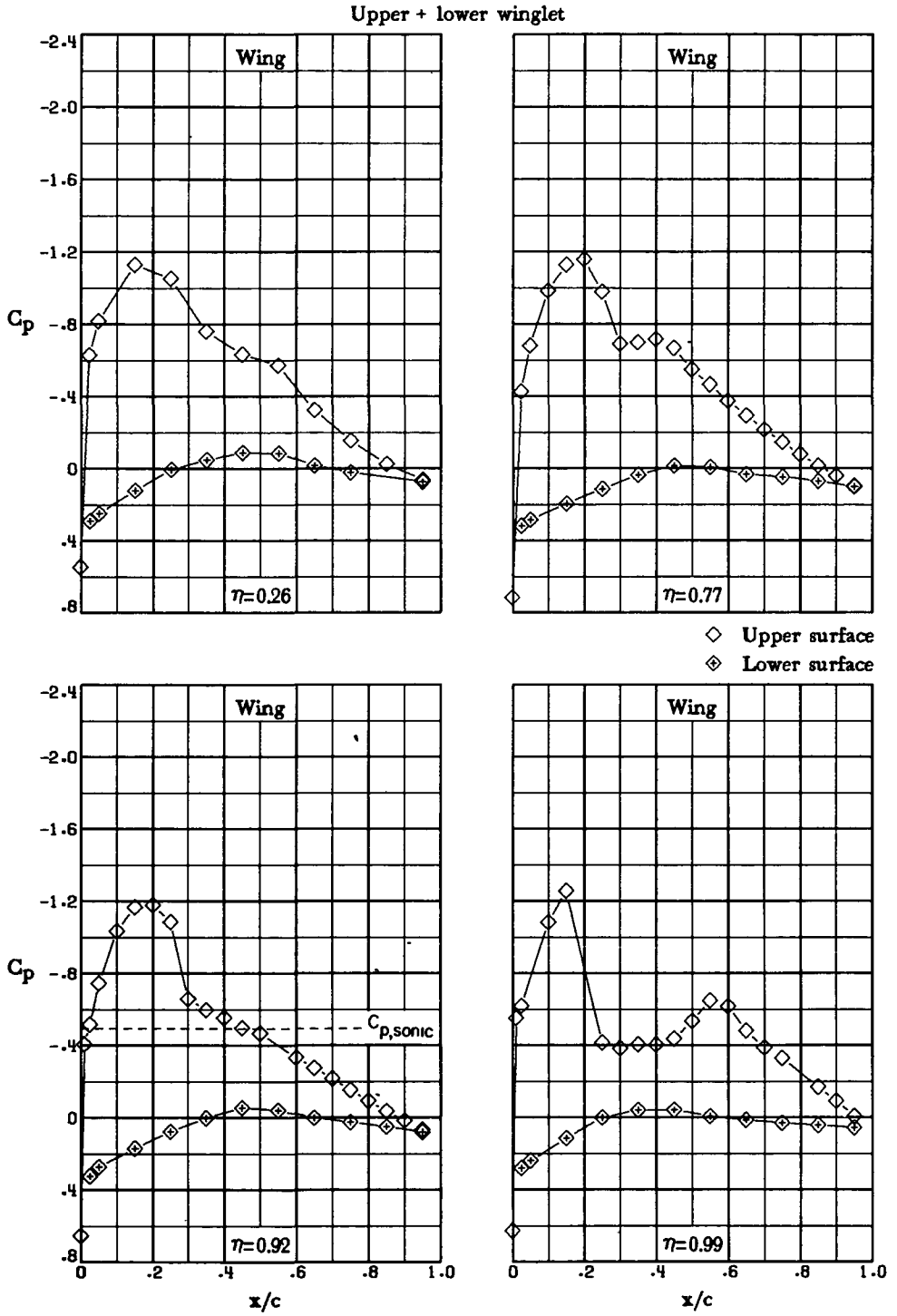

(p) $M_\infty = 0.78$; $\alpha = 3.5^\circ$.

Figure 10.- Continued.

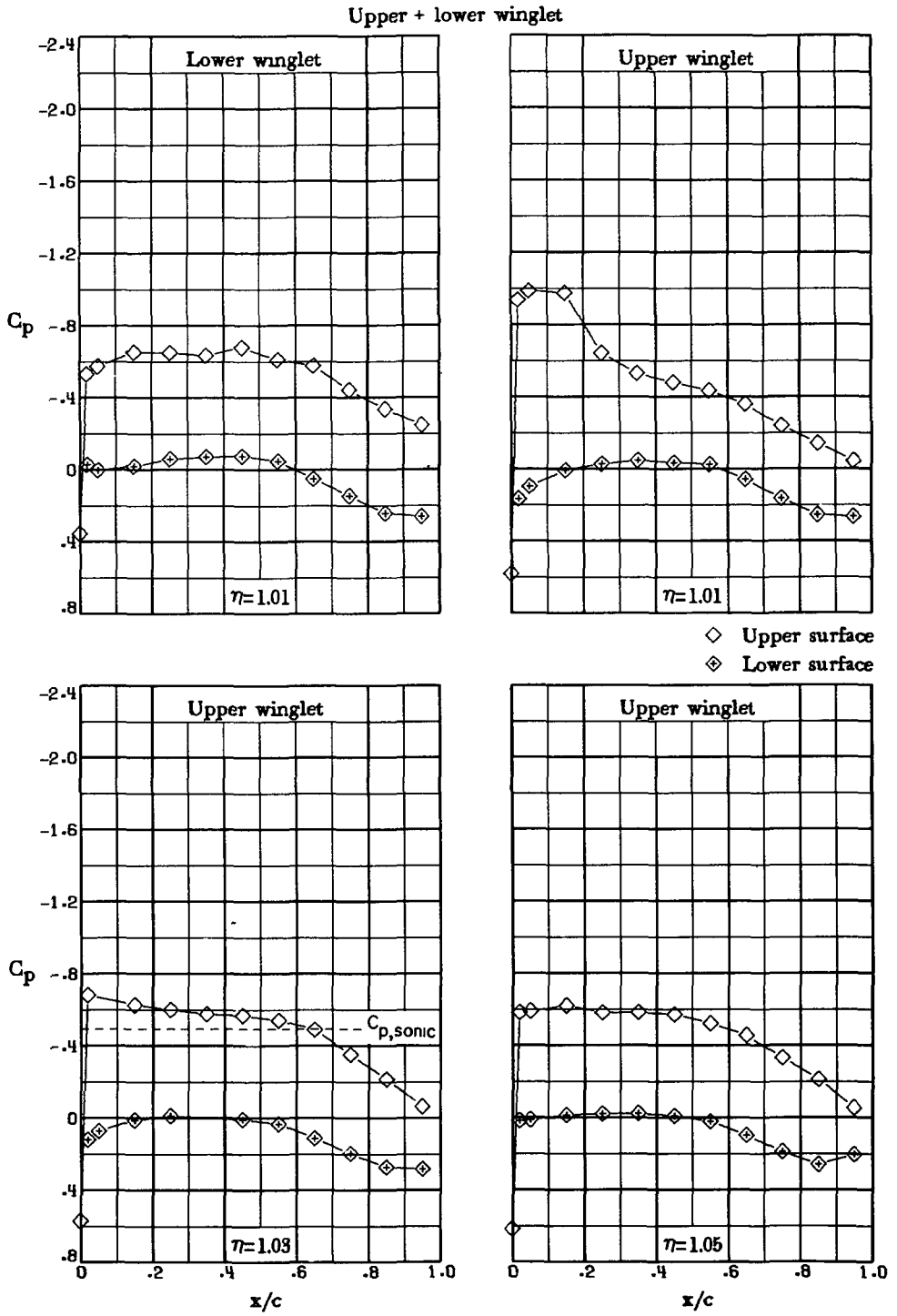

(p) $M_\infty = 0.78$; $\alpha = 3.5^\circ$. Concluded.

Figure 10.- Continued.

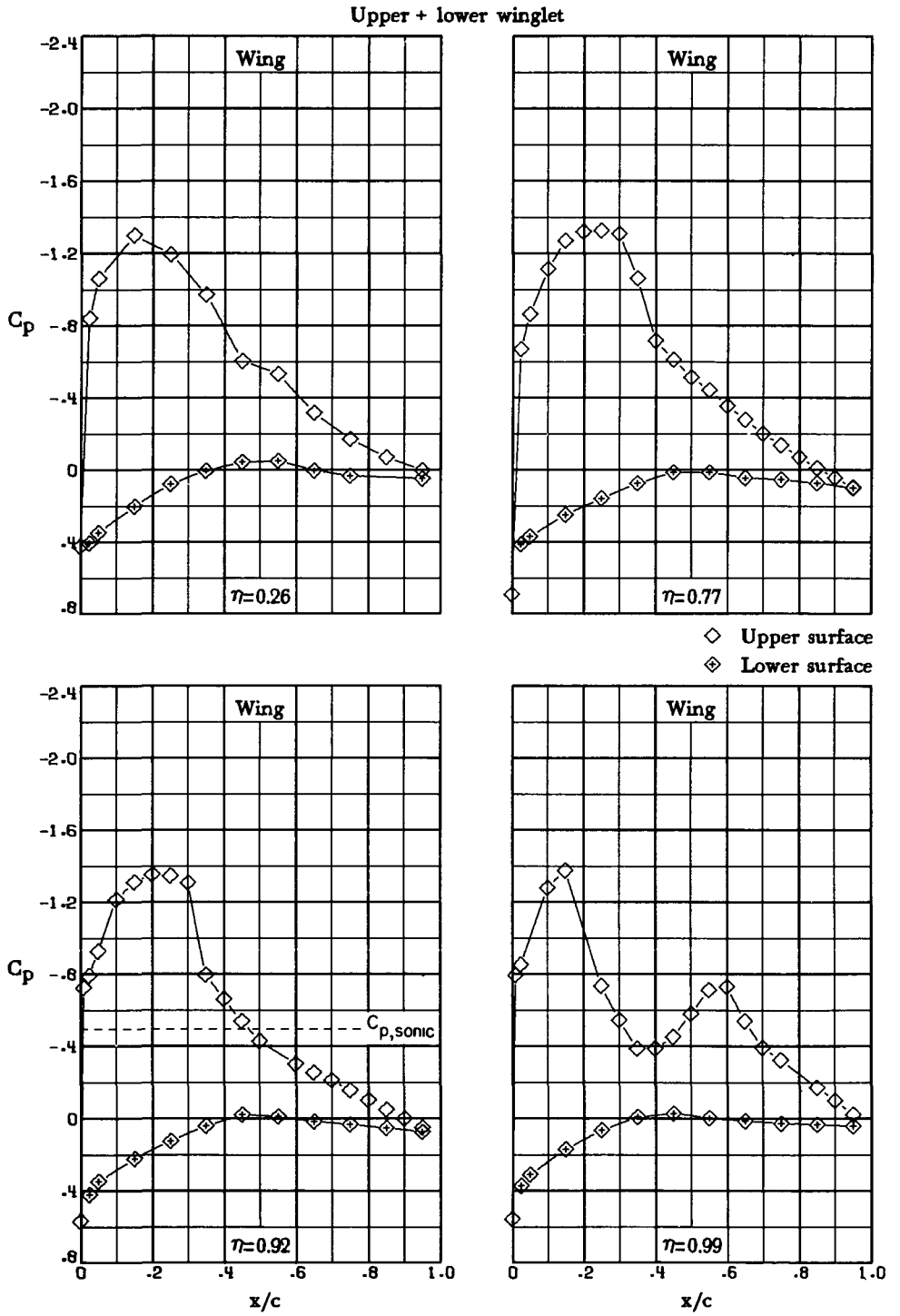

(q) $M_\infty = 0.78$; $\alpha = 5.0^\circ$.

Figure 10.- Continued.

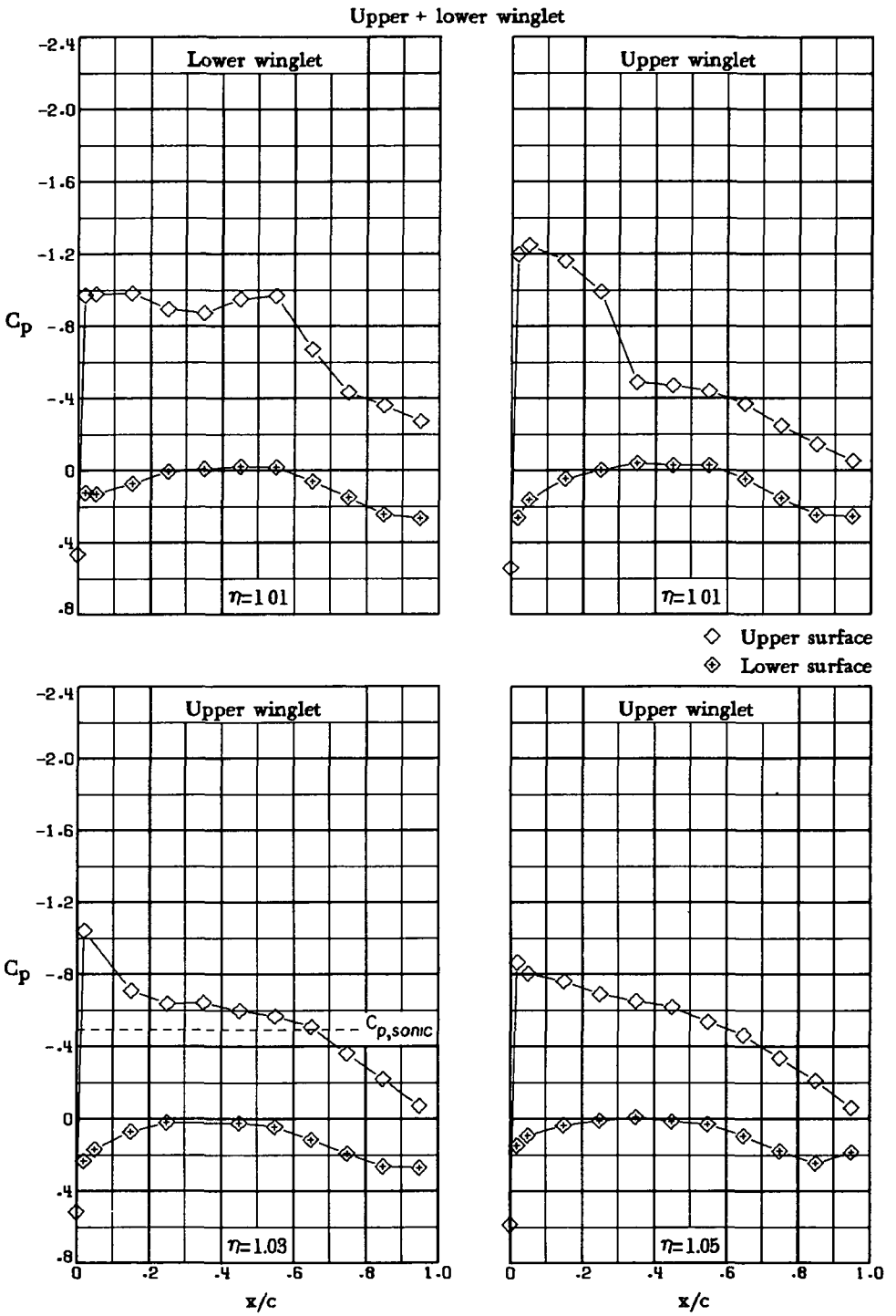

(q) M_∞ = 0.78; α = 5.0°. Concluded.

Figure 10.- Continued.

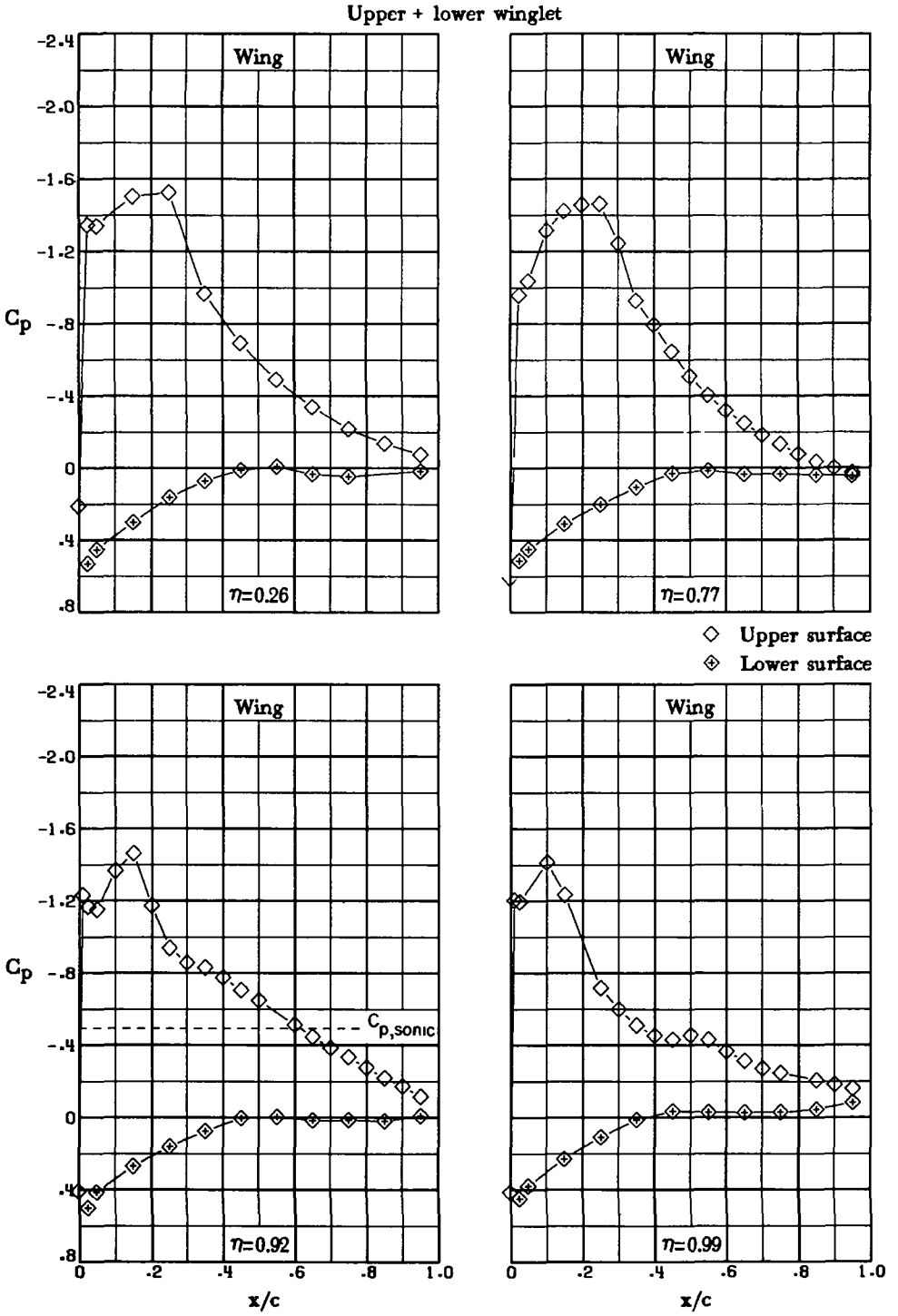

(r) $M_\infty = 0.78$; $\alpha = 7.1^\circ$.

Figure 10.- Continued.

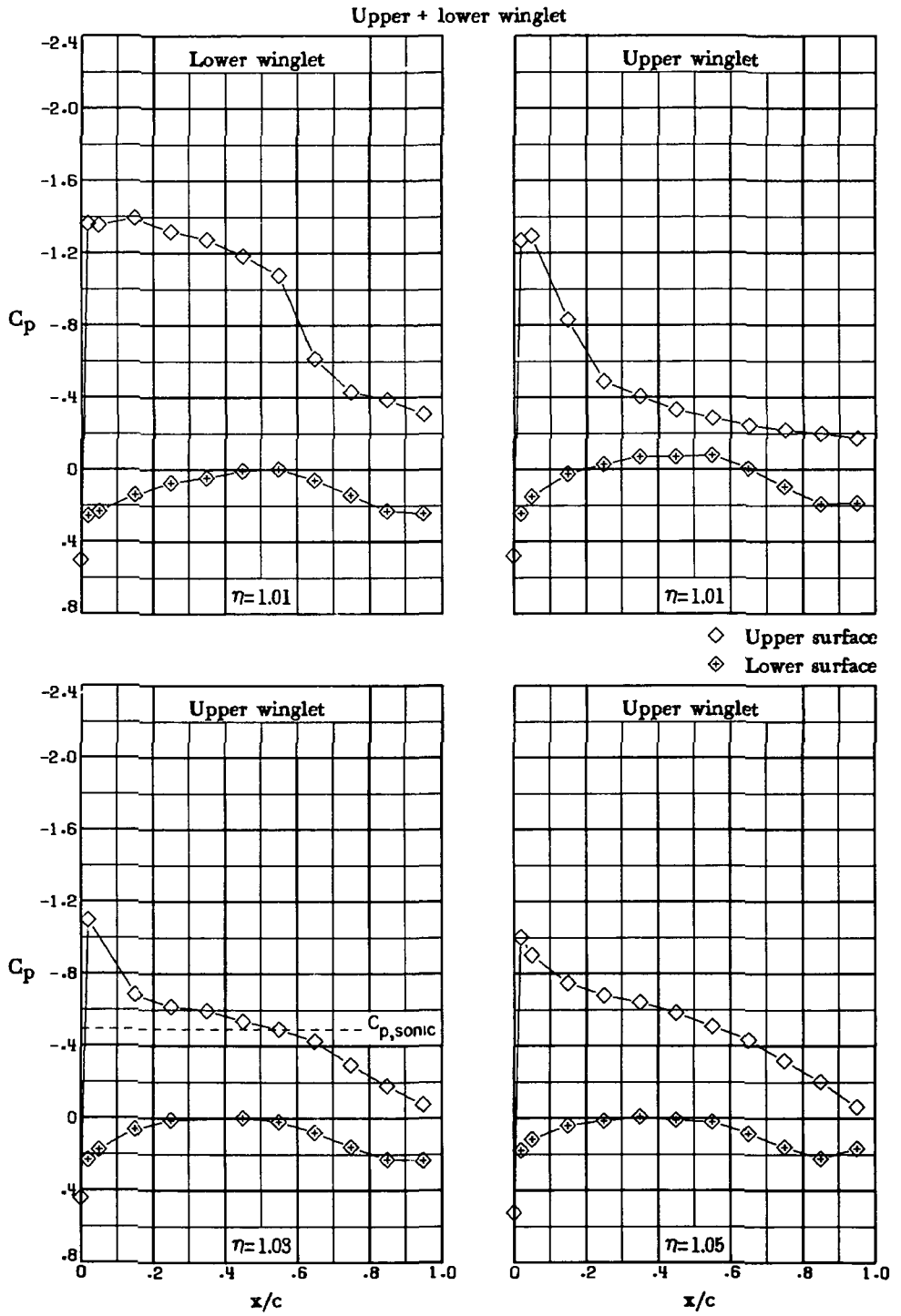

(r) M_∞ = 0.78; α = 7.1°. Concluded.

Figure 10.- Continued.

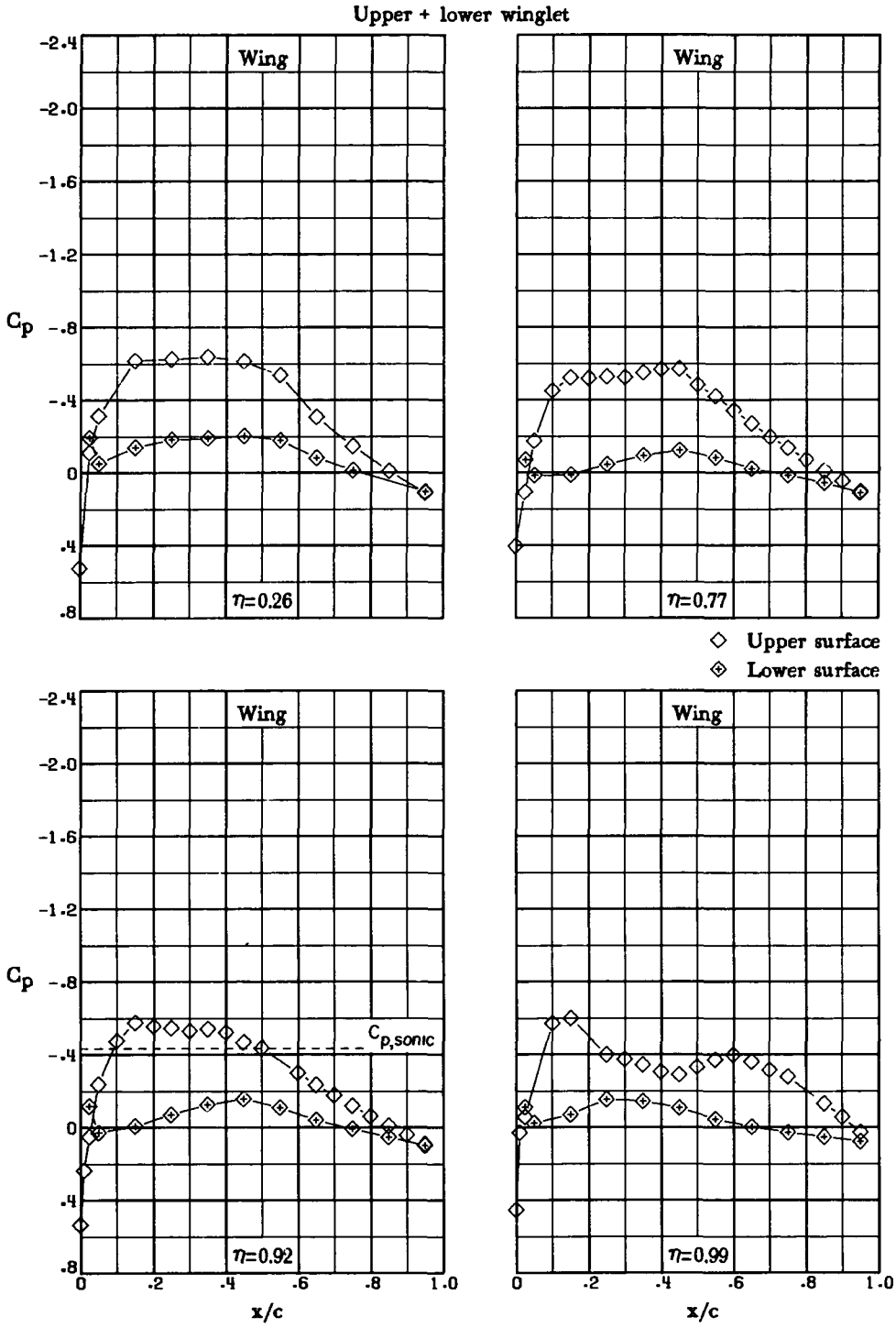

(s) $M_\infty = 0.80$; $\alpha = 0^o$.

Figure 10.- Continued.

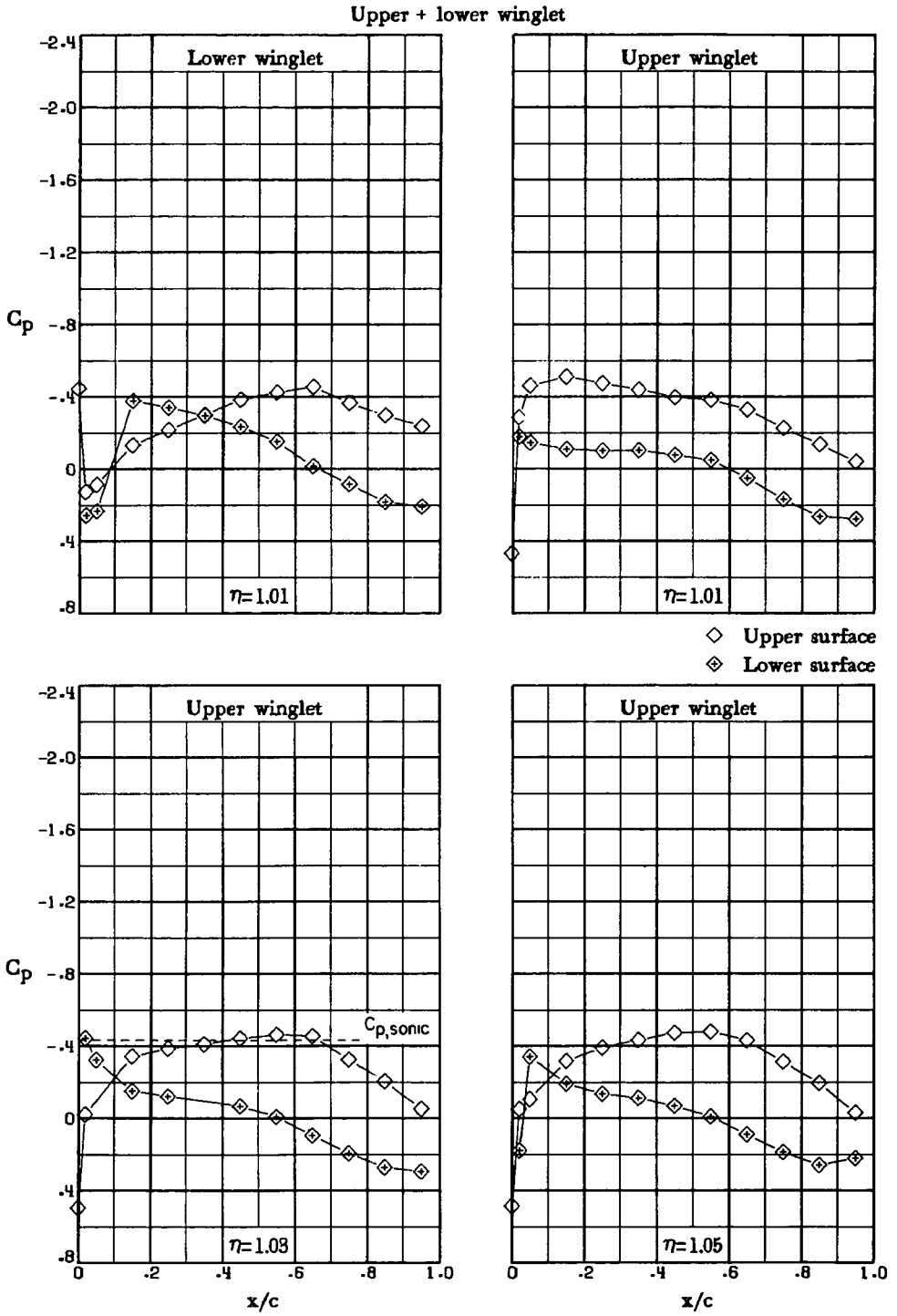

(s) M_∞ = 0.80; α = 0°. Concluded.

Figure 10.- Continued.

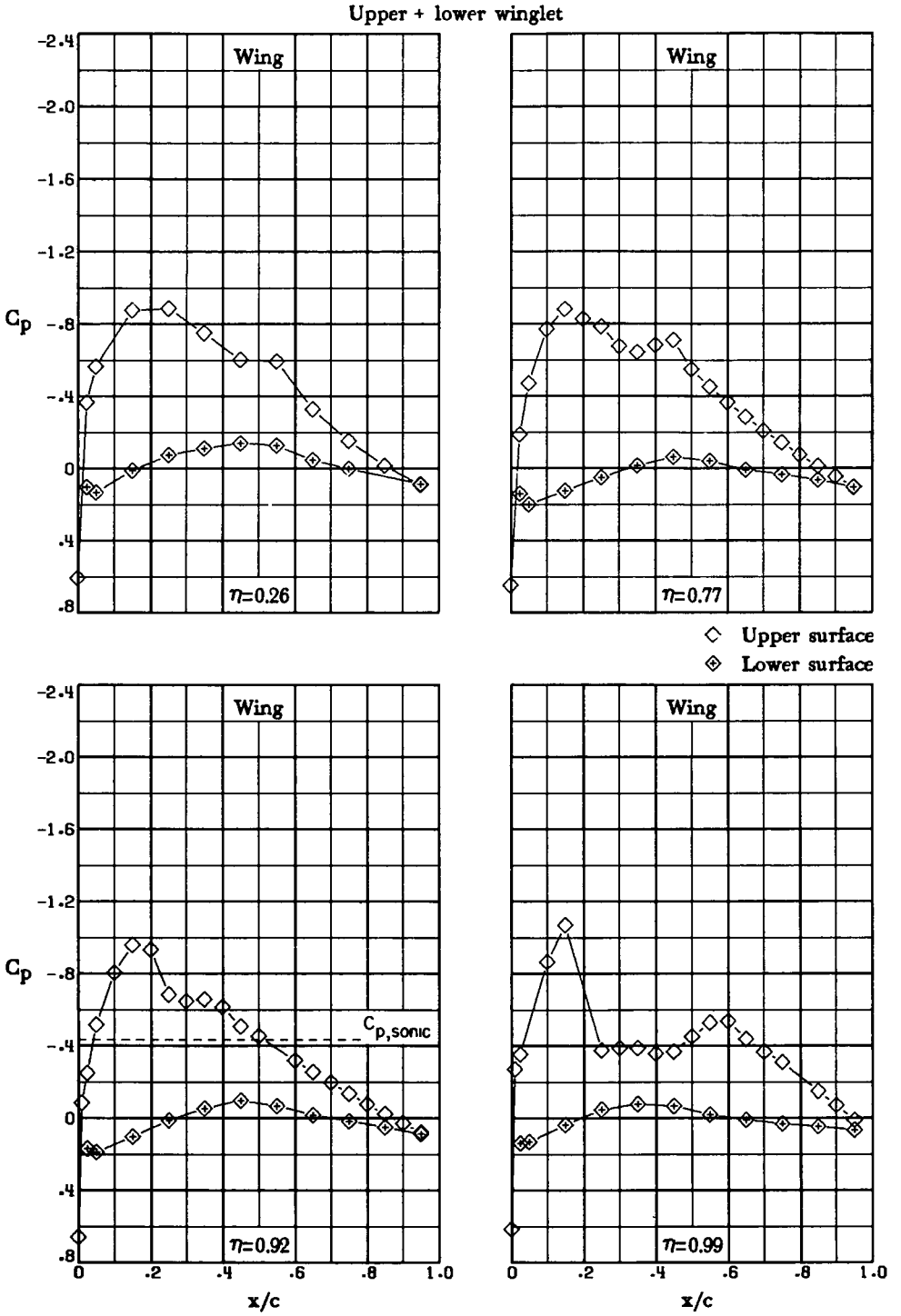

(t) $M_\infty = 0.80$; $\alpha = 2.0^\circ$.

Figure 10.- Continued.

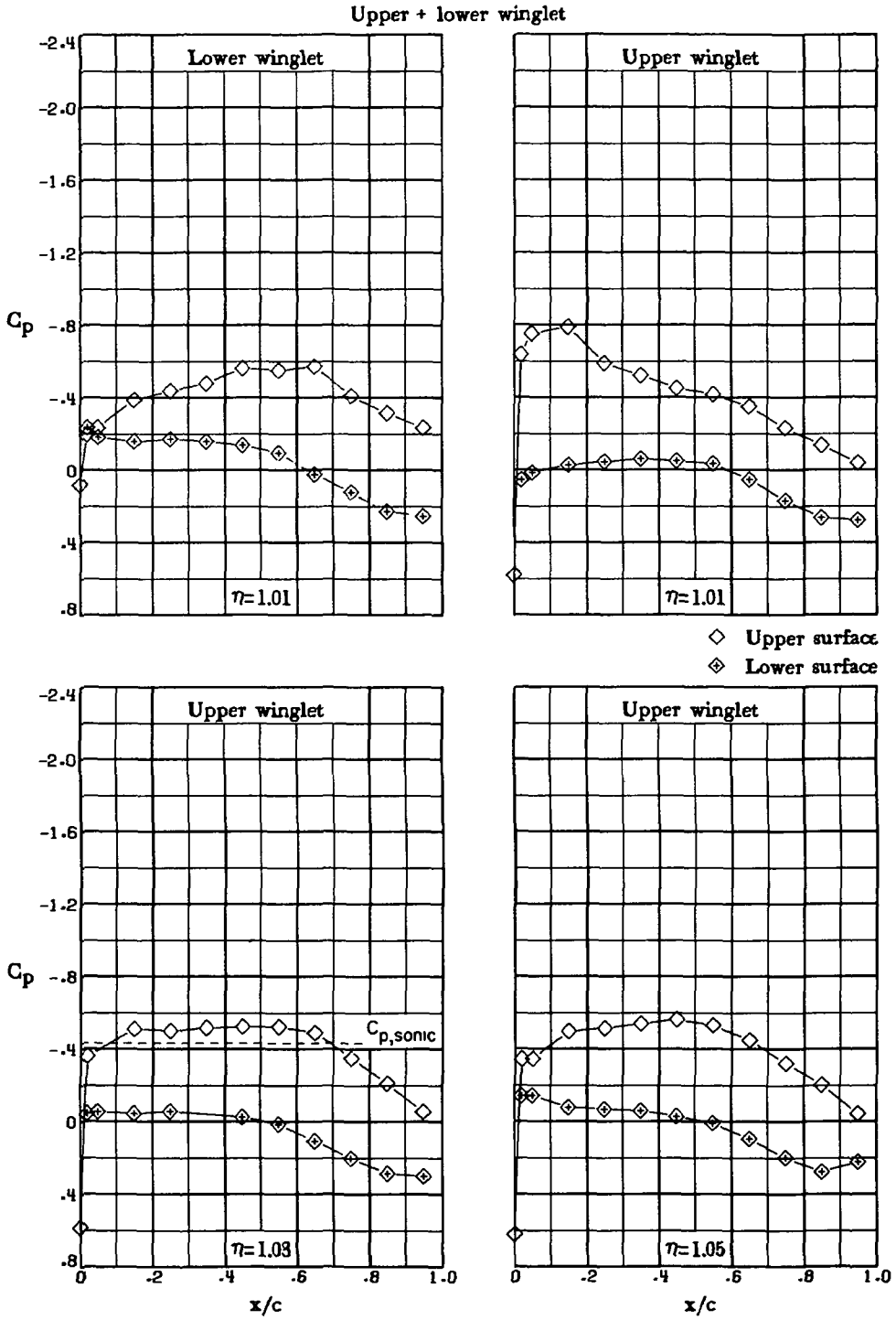

(t) $M_\infty = 0.80$; $\alpha = 2.0^\circ$. Concluded.

Figure 10.- Continued.

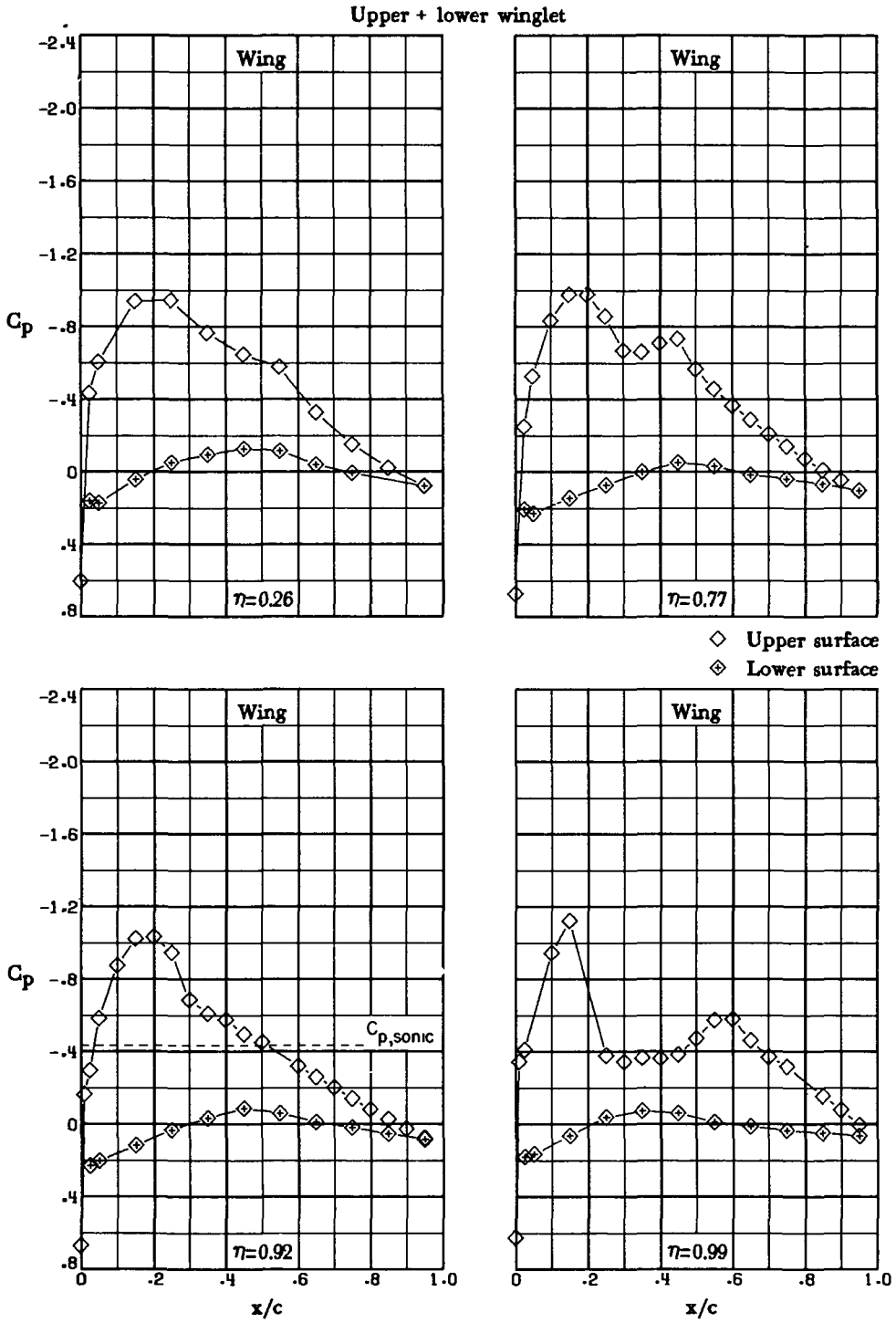

(u) $M_\infty = 0.80$; $\alpha = 2.5^\circ$.

Figure 10.- Continued.

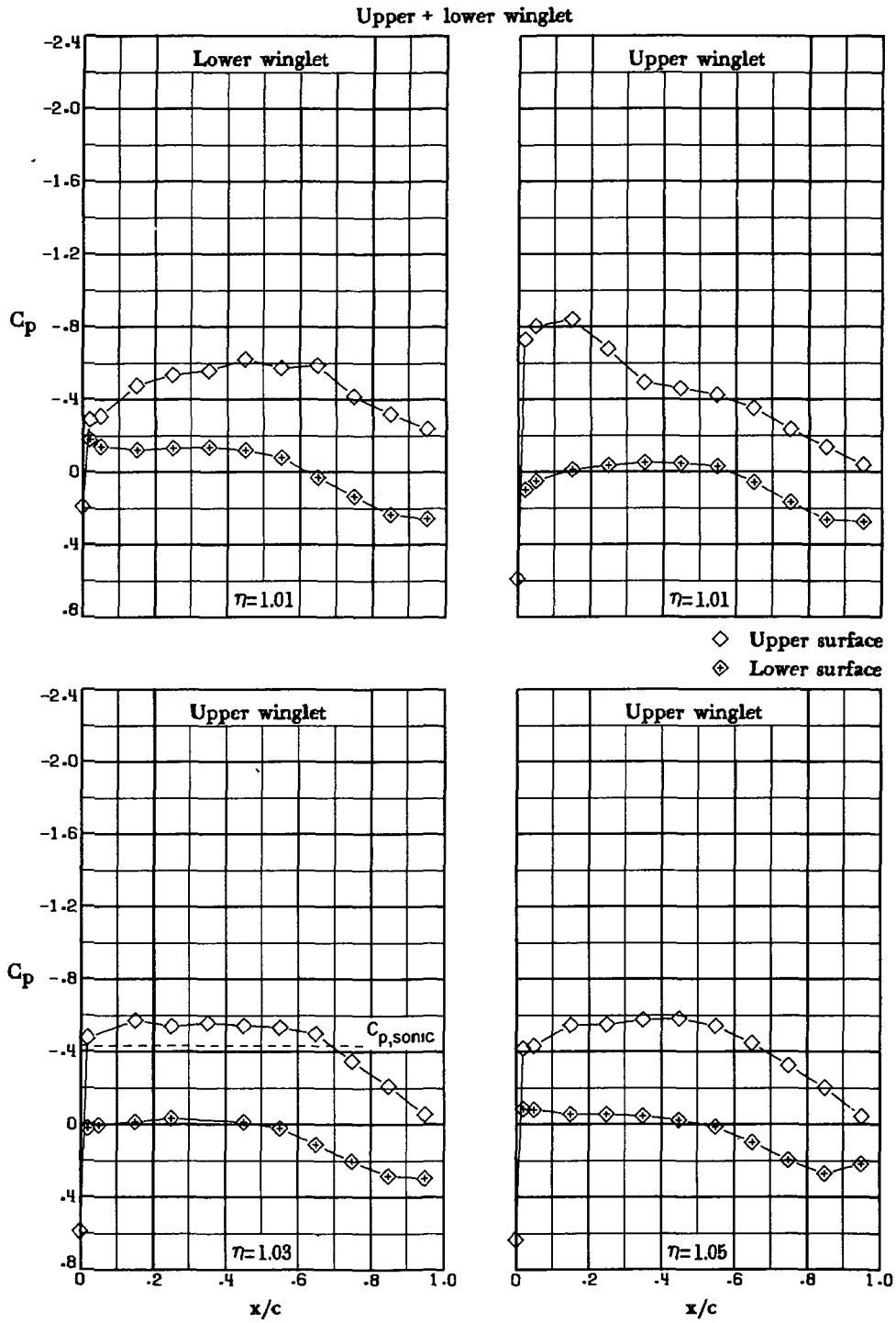

(u) M_∞ = 0.80; α = 2.5°. Concluded.

Figure 10.- Continued.

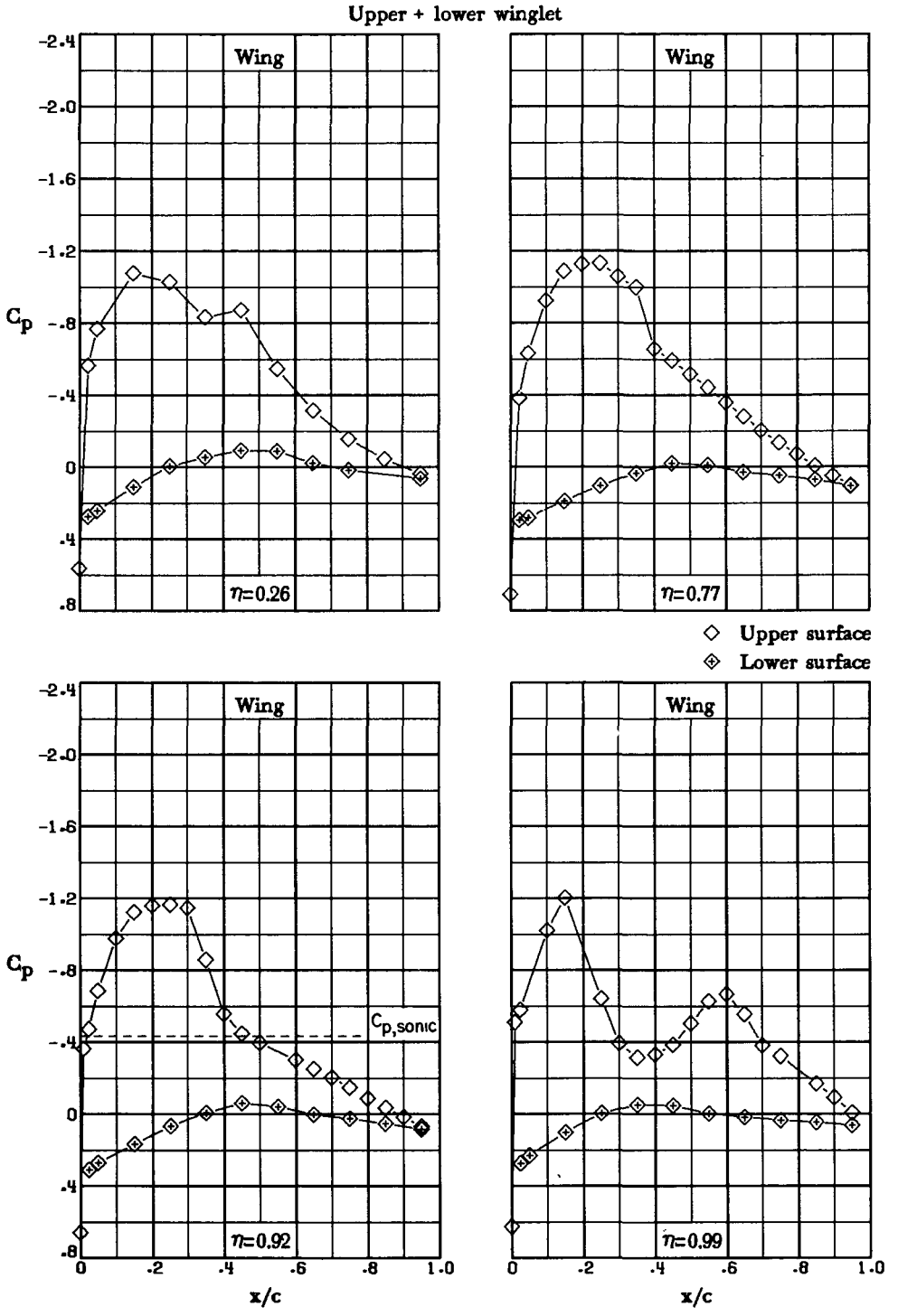

(v) $M_\infty = 0.80$; $\alpha = 3.5^\circ$.

Figure 10.- Continued.

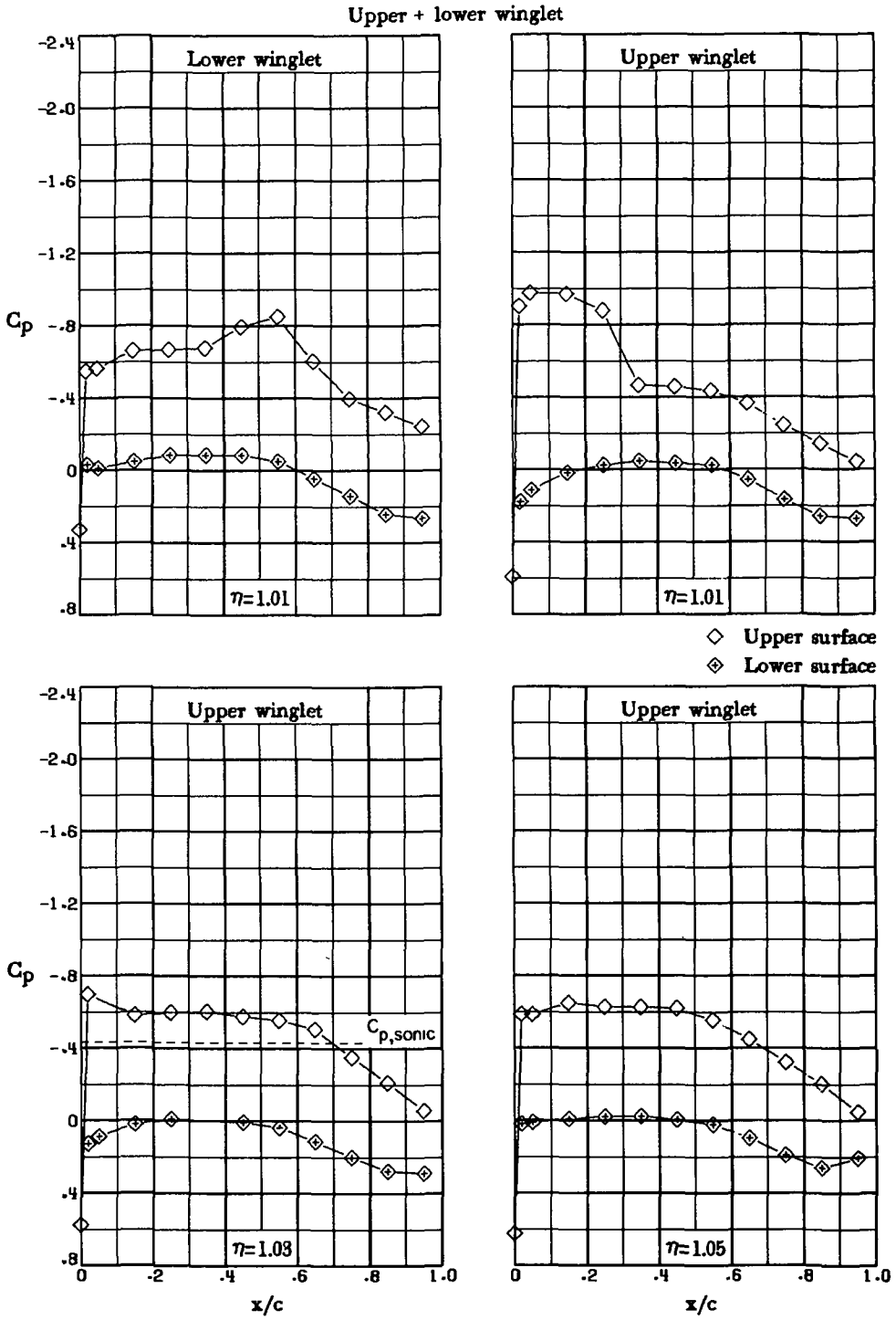

(v) $M_\infty = 0.80$; $\alpha = 3.5^\circ$. Concluded.

Figure 10.- Continued.

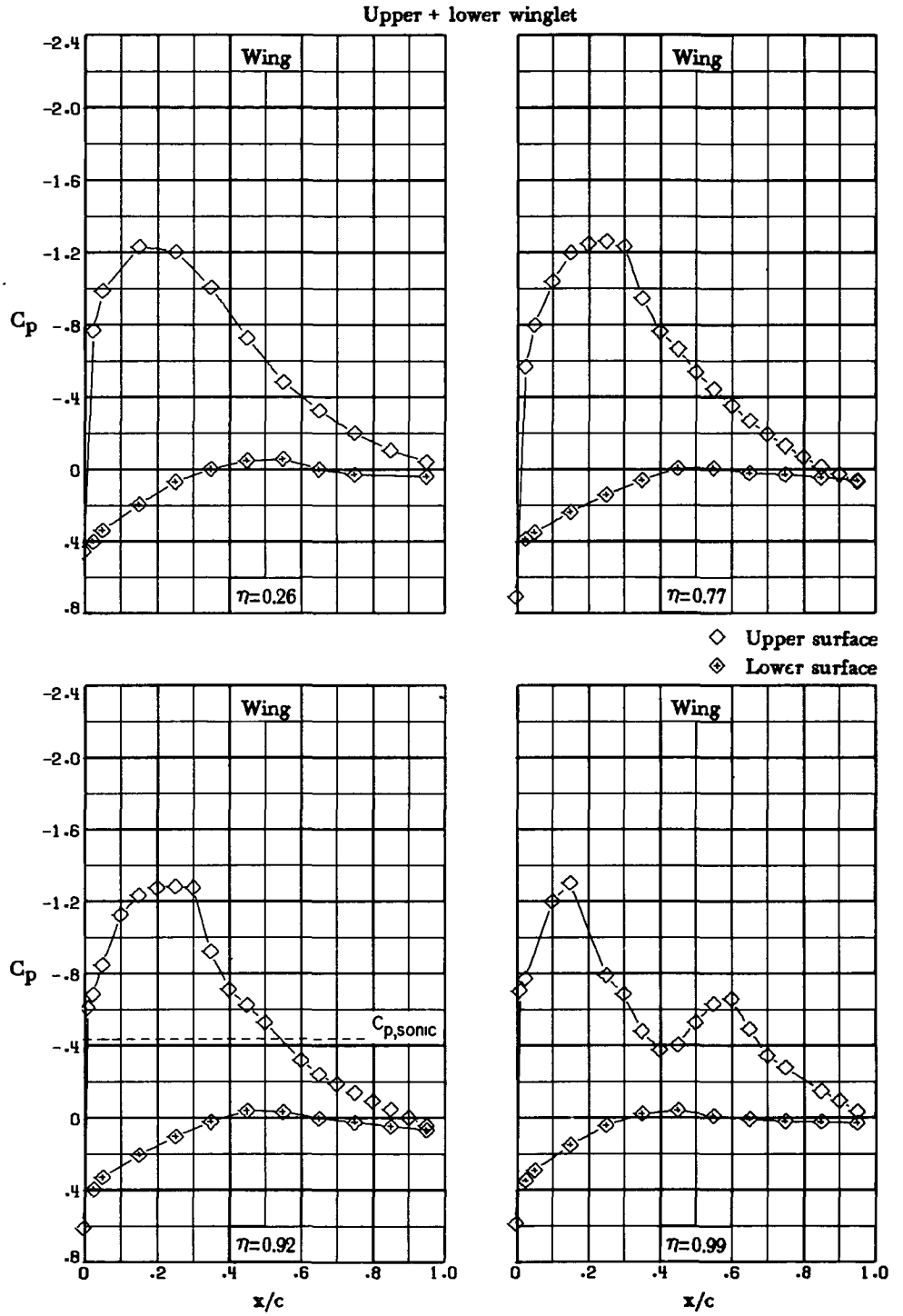

(w) M_∞ = 0.80; α = 5.0°.

Figure 10.- Continued.

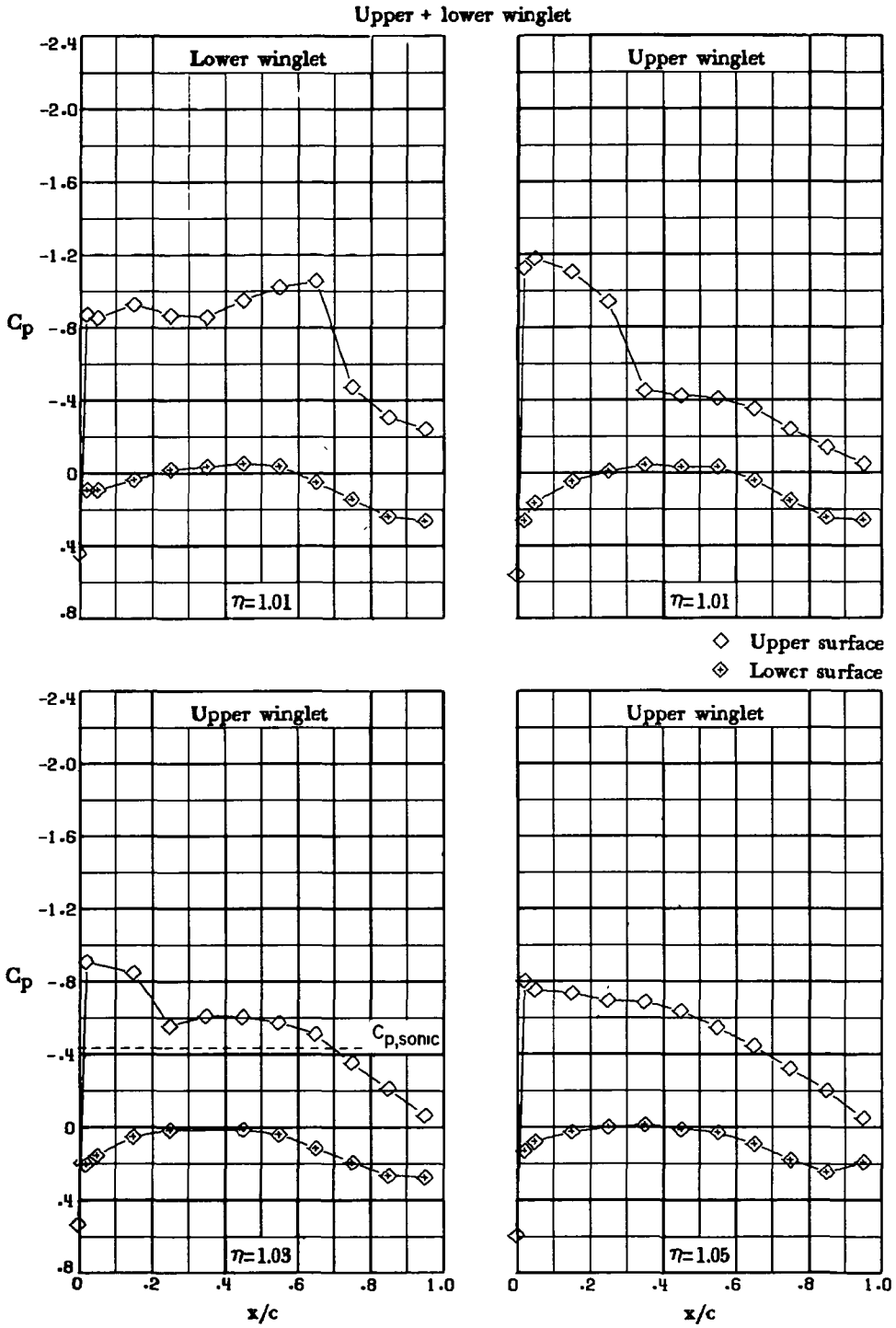

(w) $M_\infty = 0.80$; $\alpha = 5.0^\circ$. Concluded.

Figure 10.- Continued.

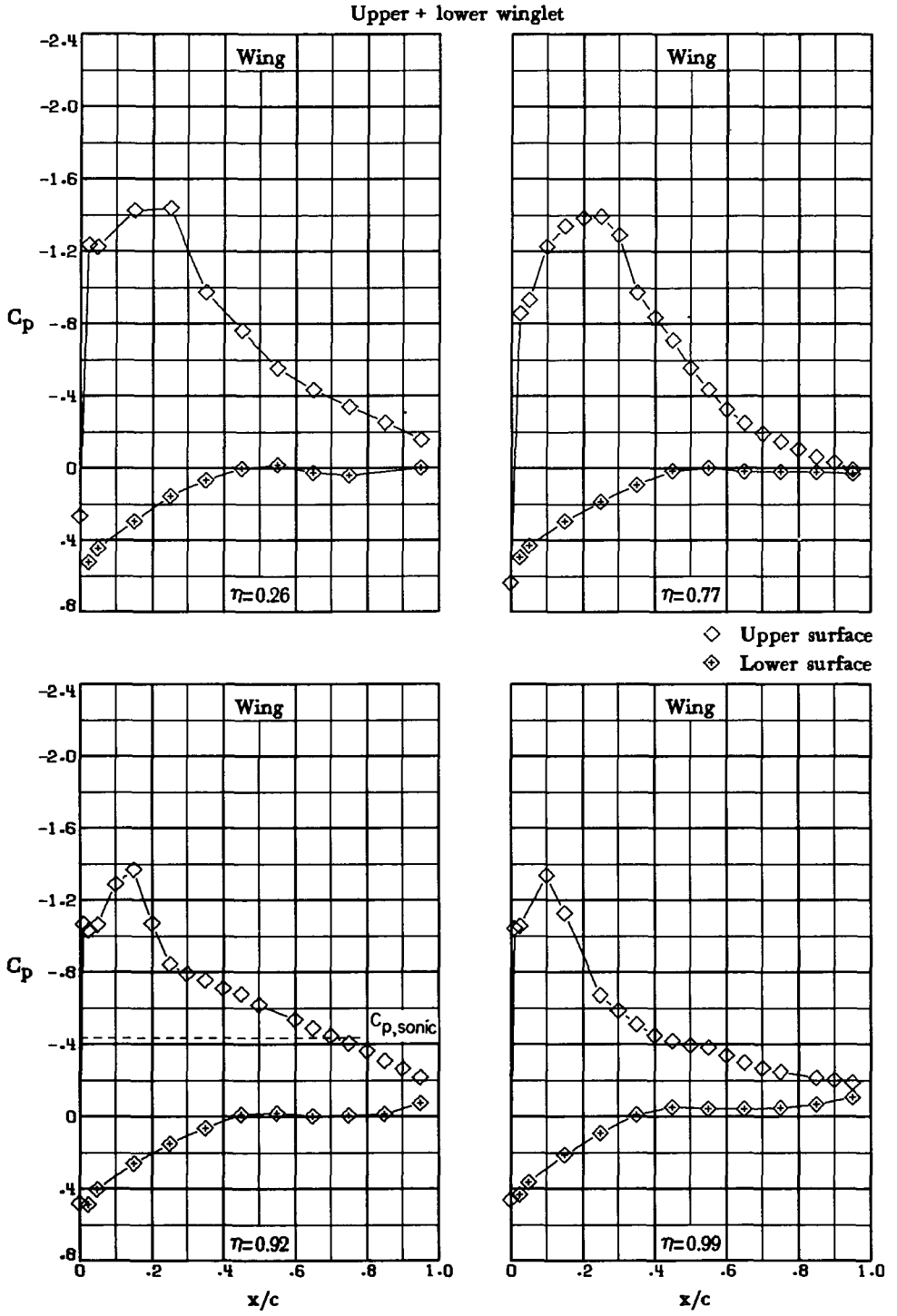

(x) M_∞ = 0.80; α = 7.1°.

Figure 10.- Continued.

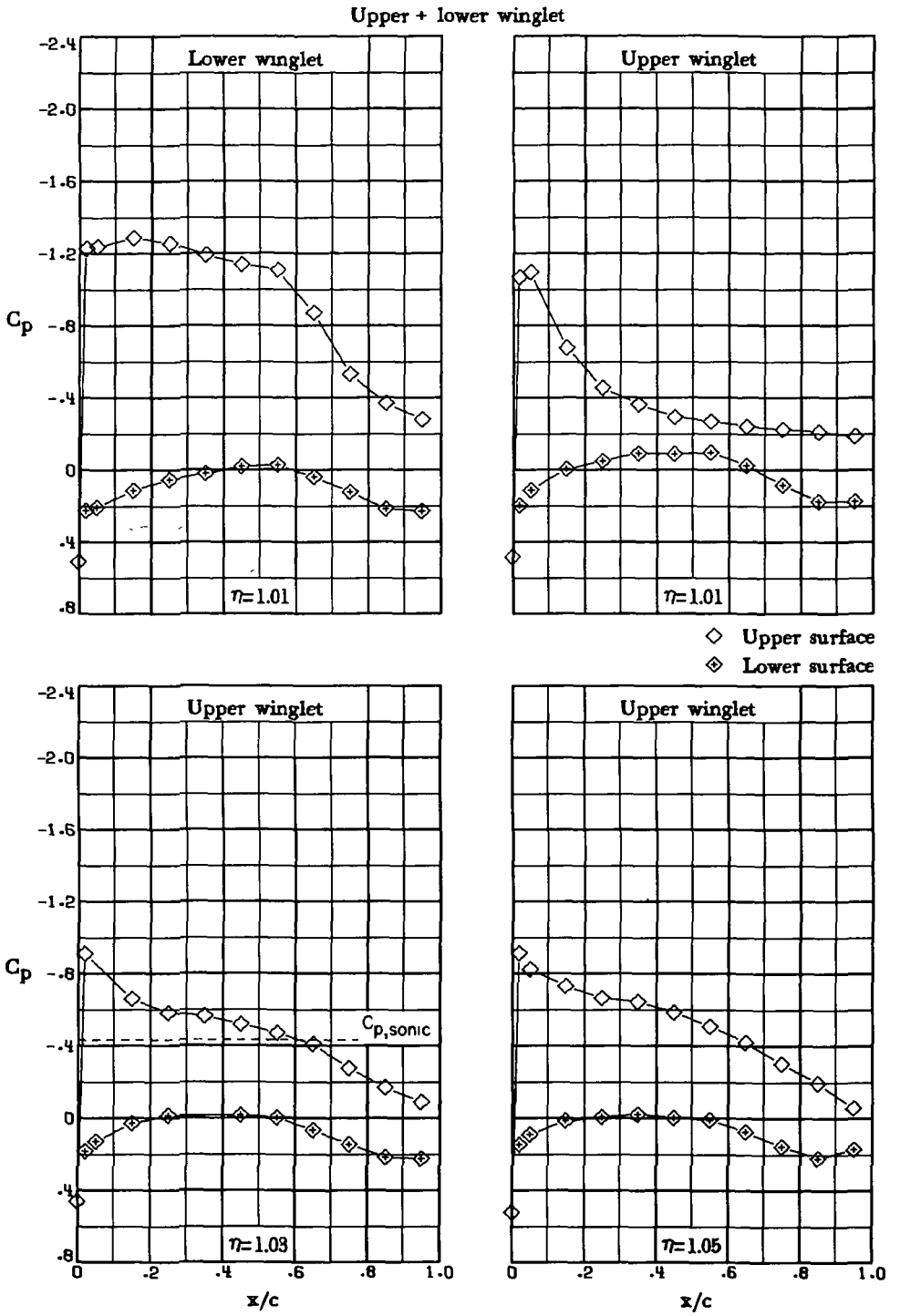

(x) M_∞ = 0.80; α = 7.1°. Concluded.

Figure 10.- Concluded.

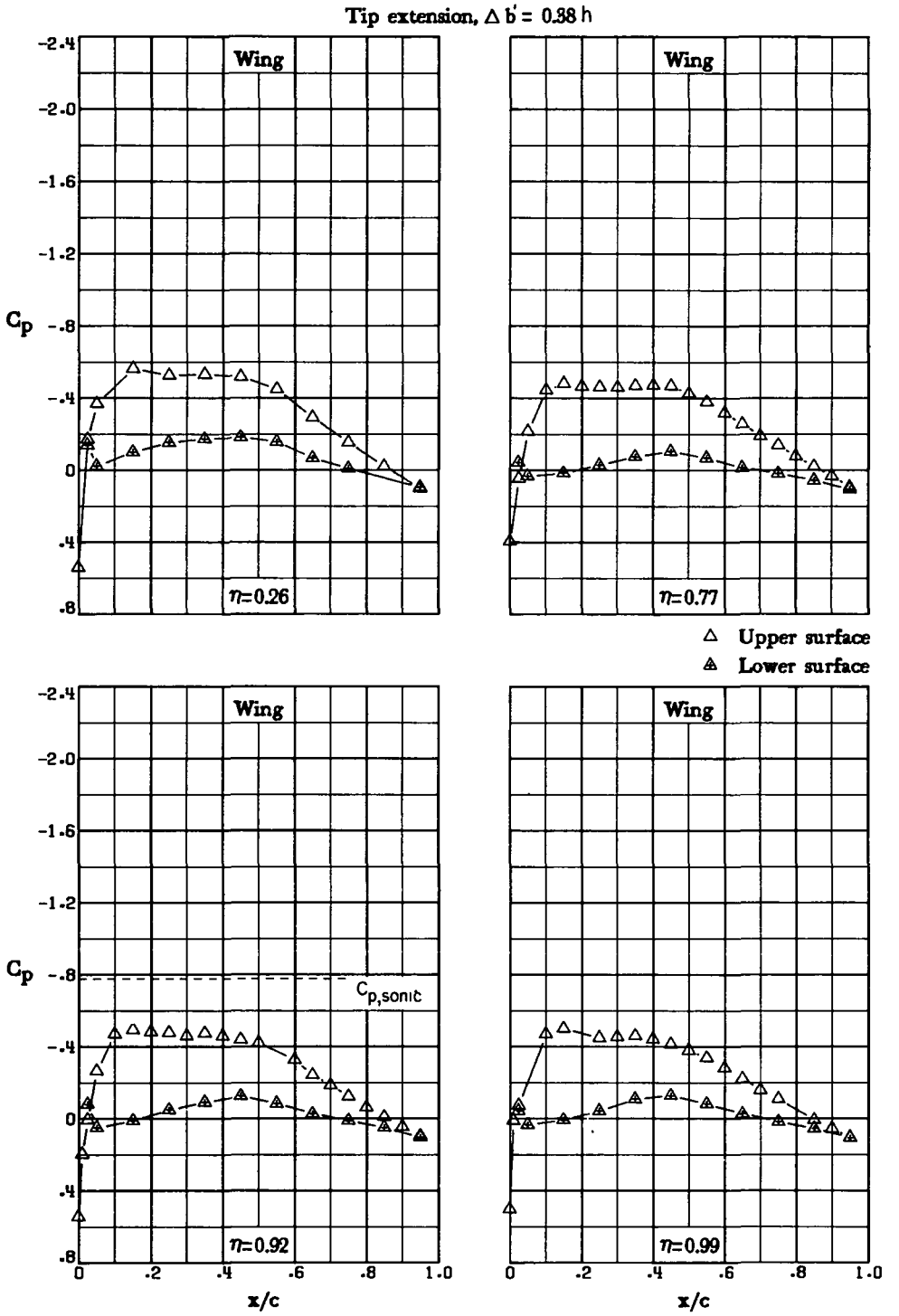

(a) $M_\infty = 0.70$; $\alpha = 0^o$.

Figure 11.- Pressure distributions for tip-extension configuration.

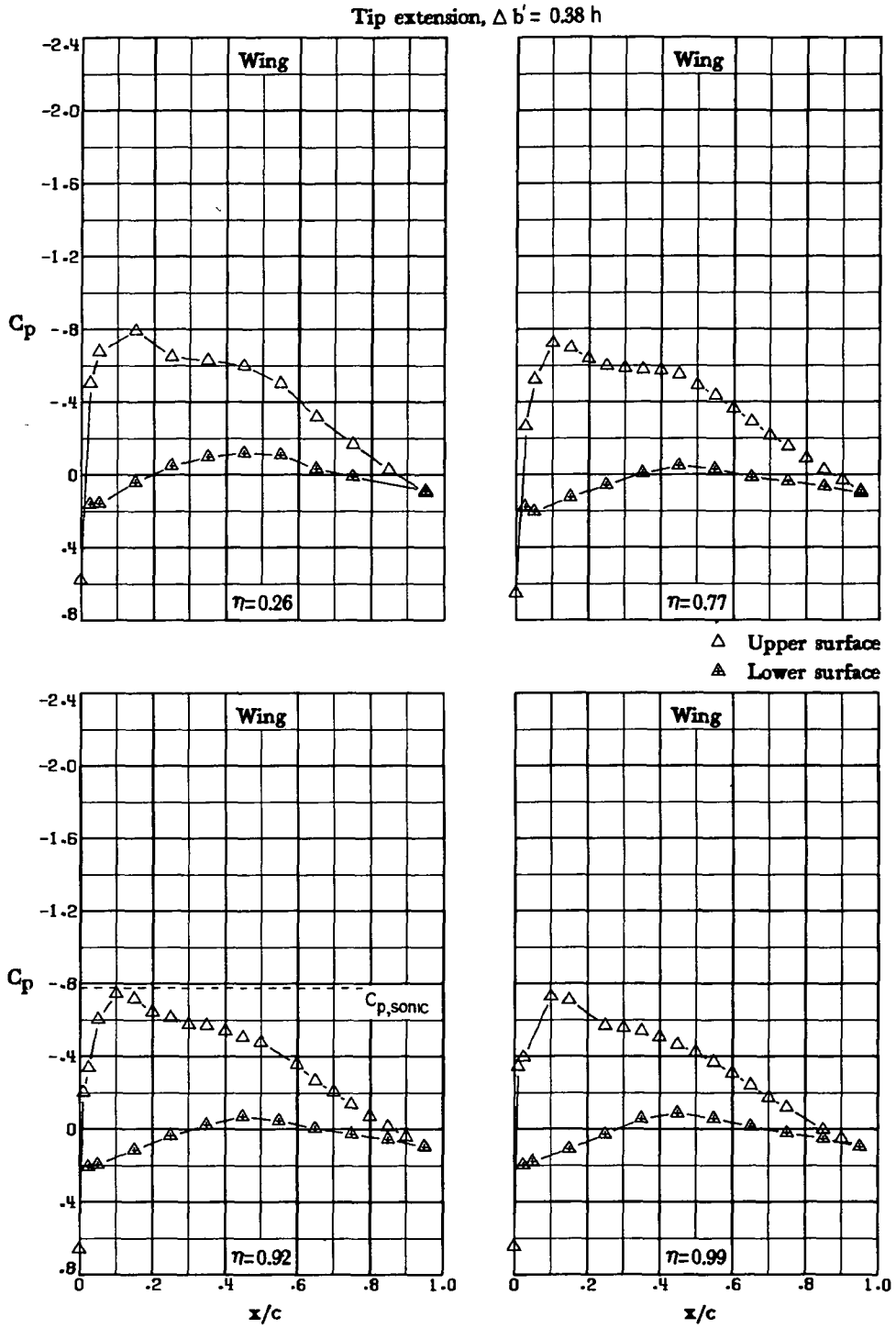

(b) $M_\infty = 0.70$; $\alpha = 2.0^\circ$.

Figure 11.- Continued.

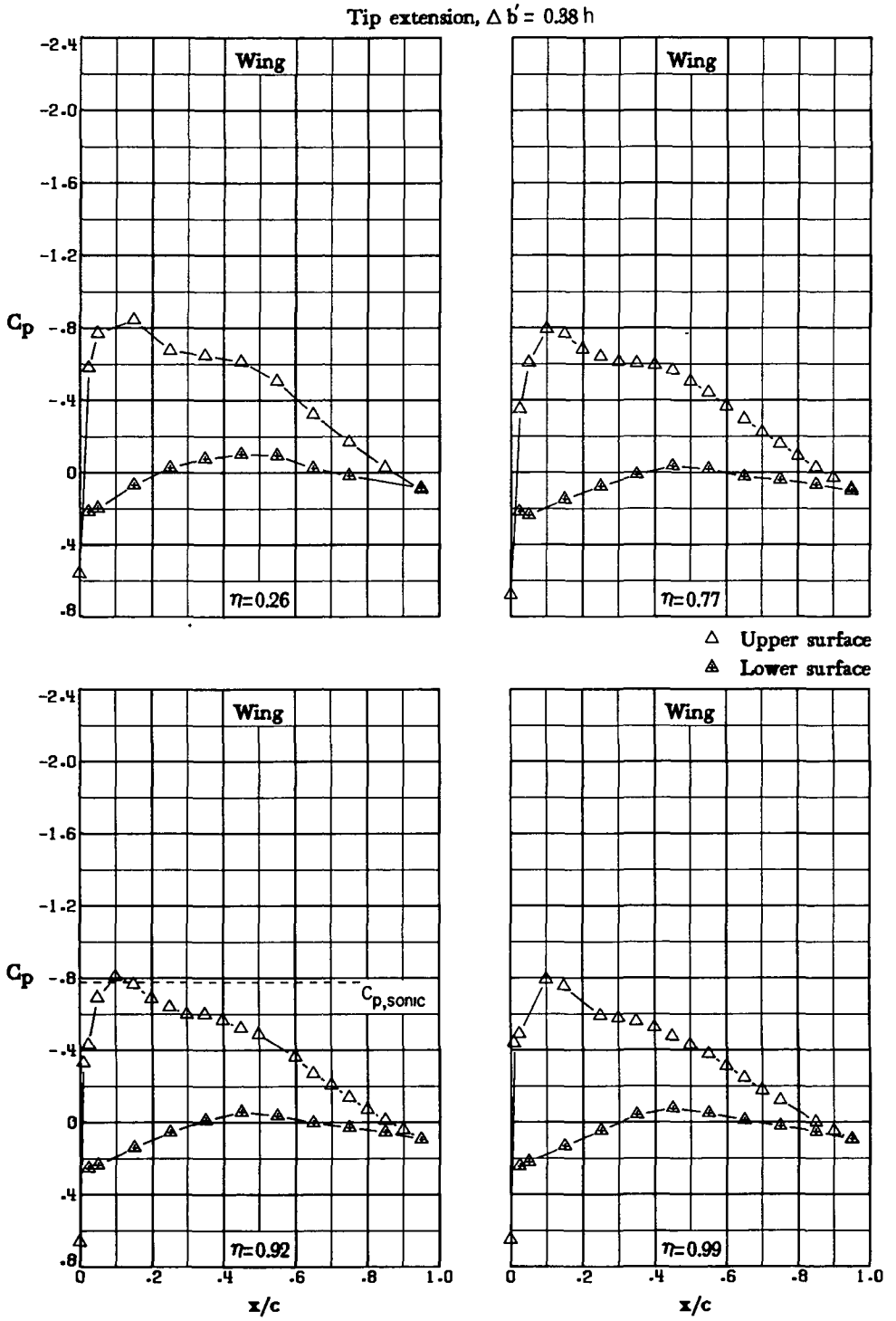

(c) $M_\infty = 0.70$; $\alpha = 2.5^\circ$.

Figure 11.- Continued.

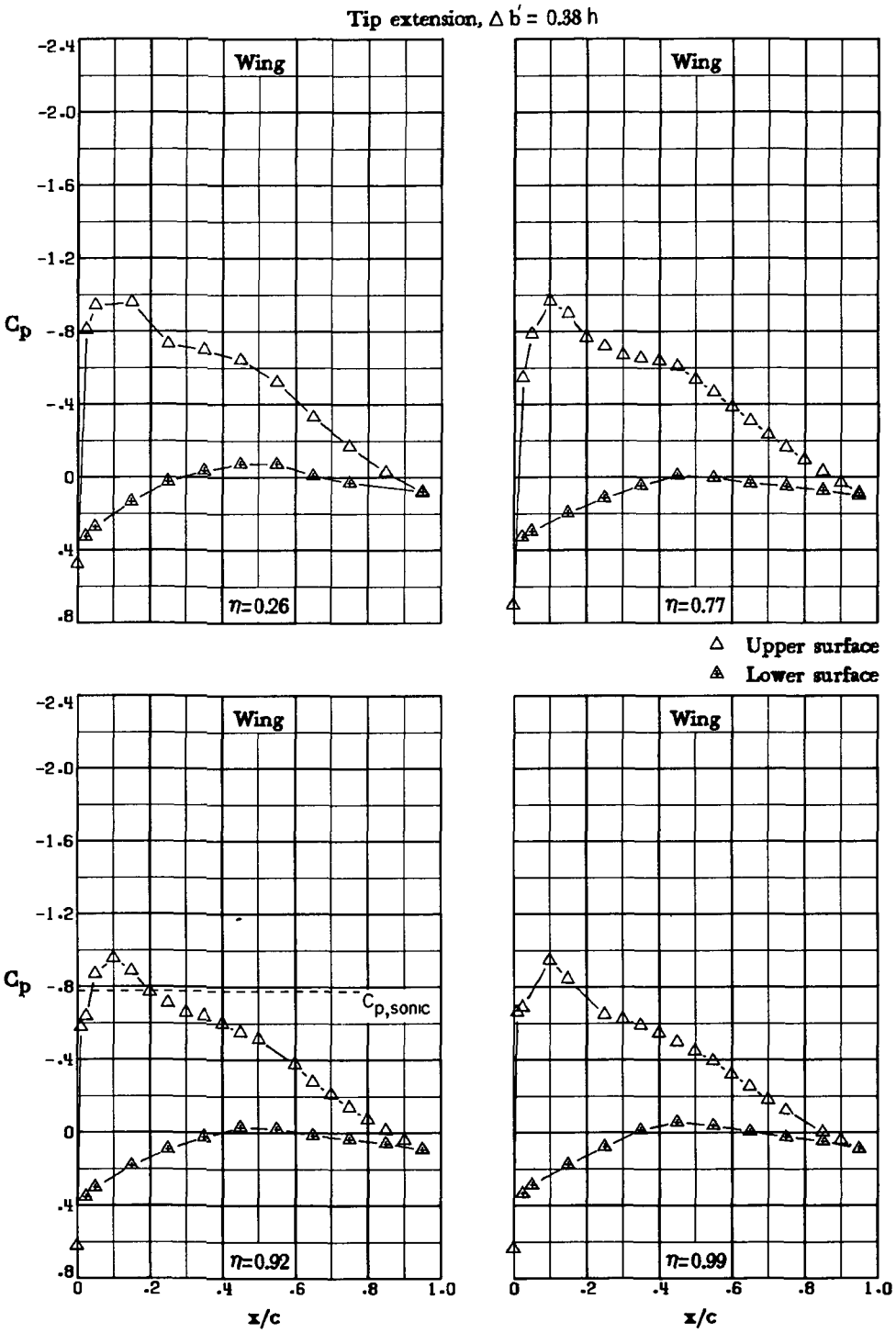

(d) $M_\infty = 0.70$; $\alpha = 3.5^o$.

Figure 11.- Continued.

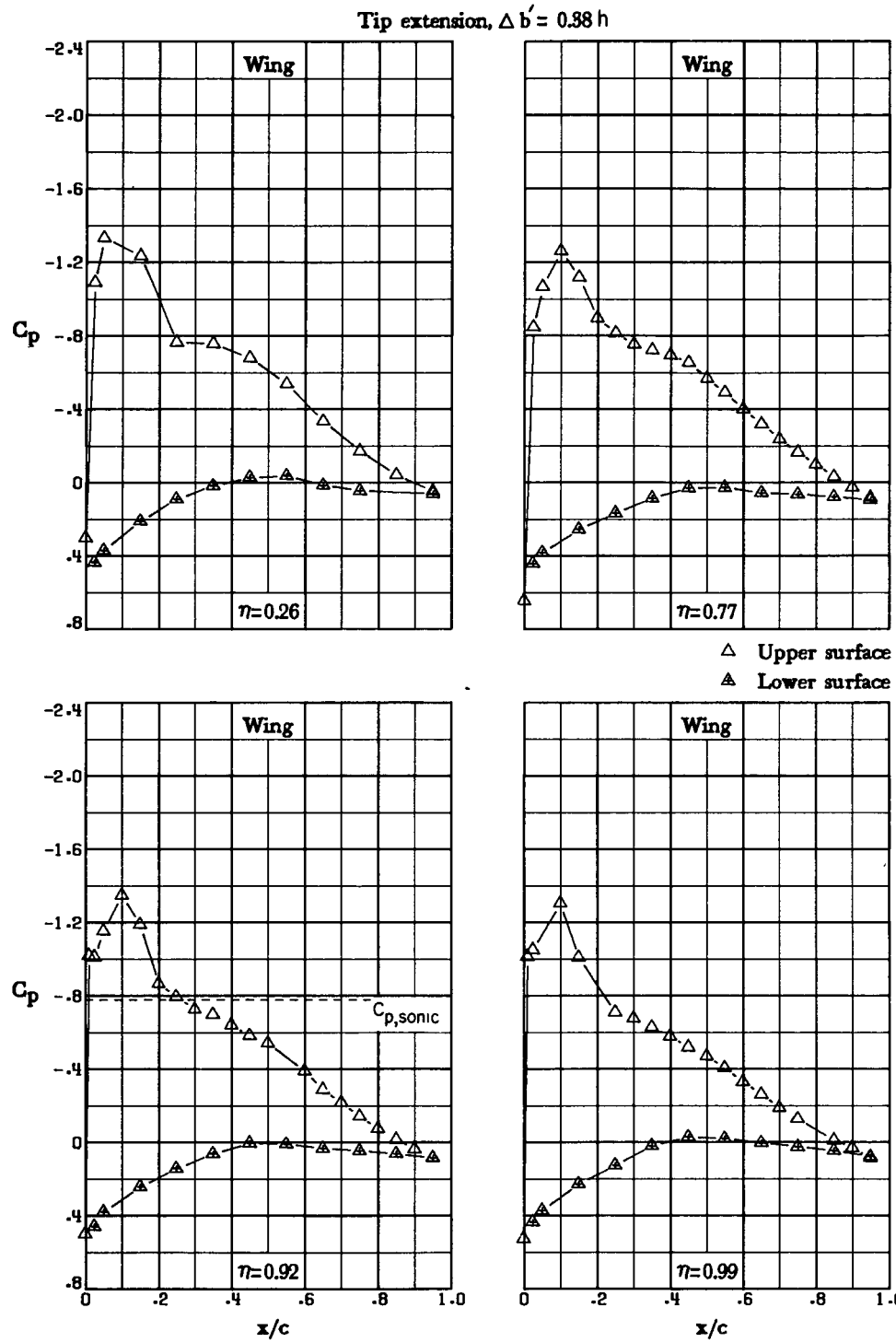

(e) $M_\infty = 0.70$; $\alpha = 5.0^o$.

Figure 11.- Continued.

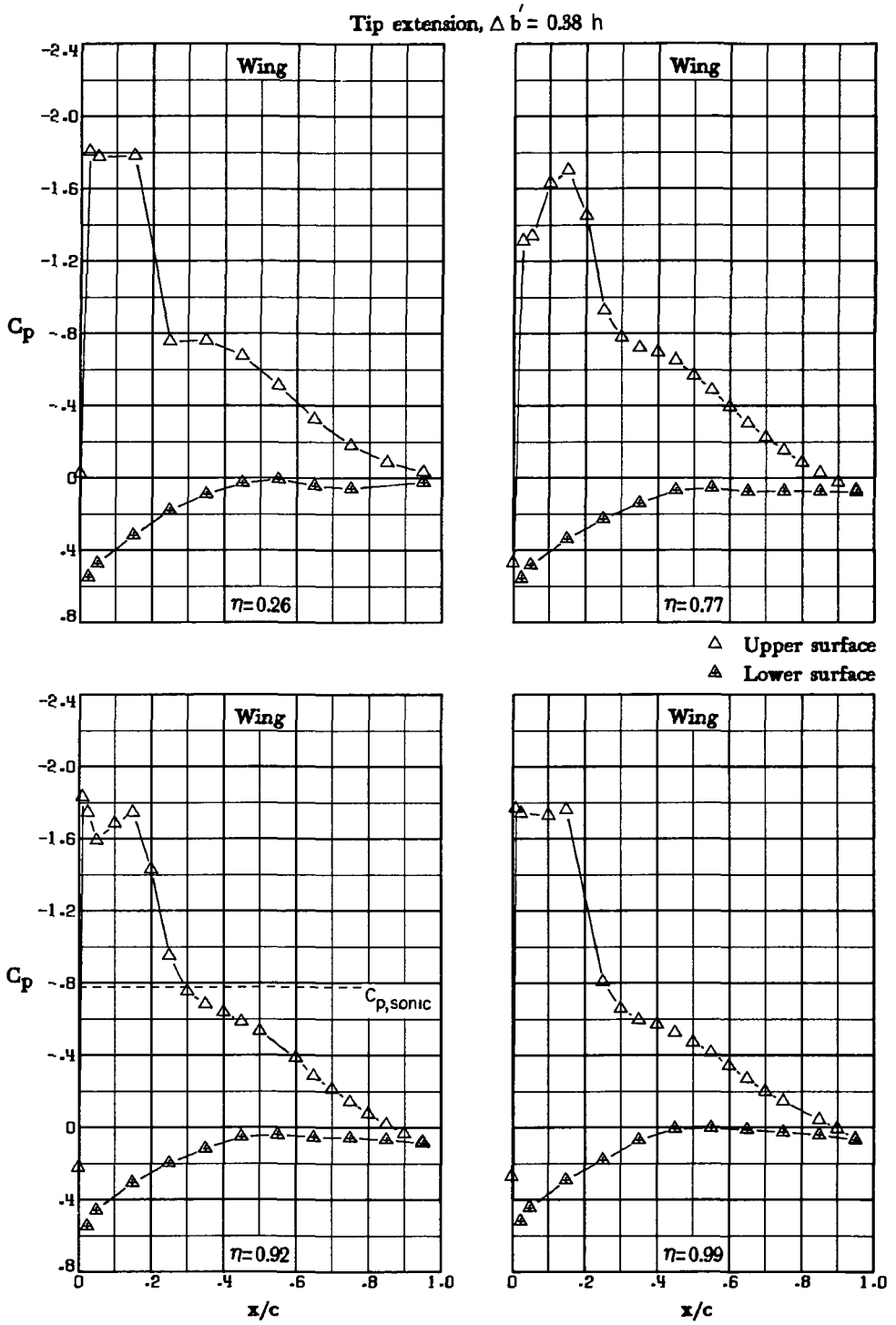

(f) $M_\infty = 0.70$; $\alpha = 7.3^\circ$.

Figure 11.- Continued.

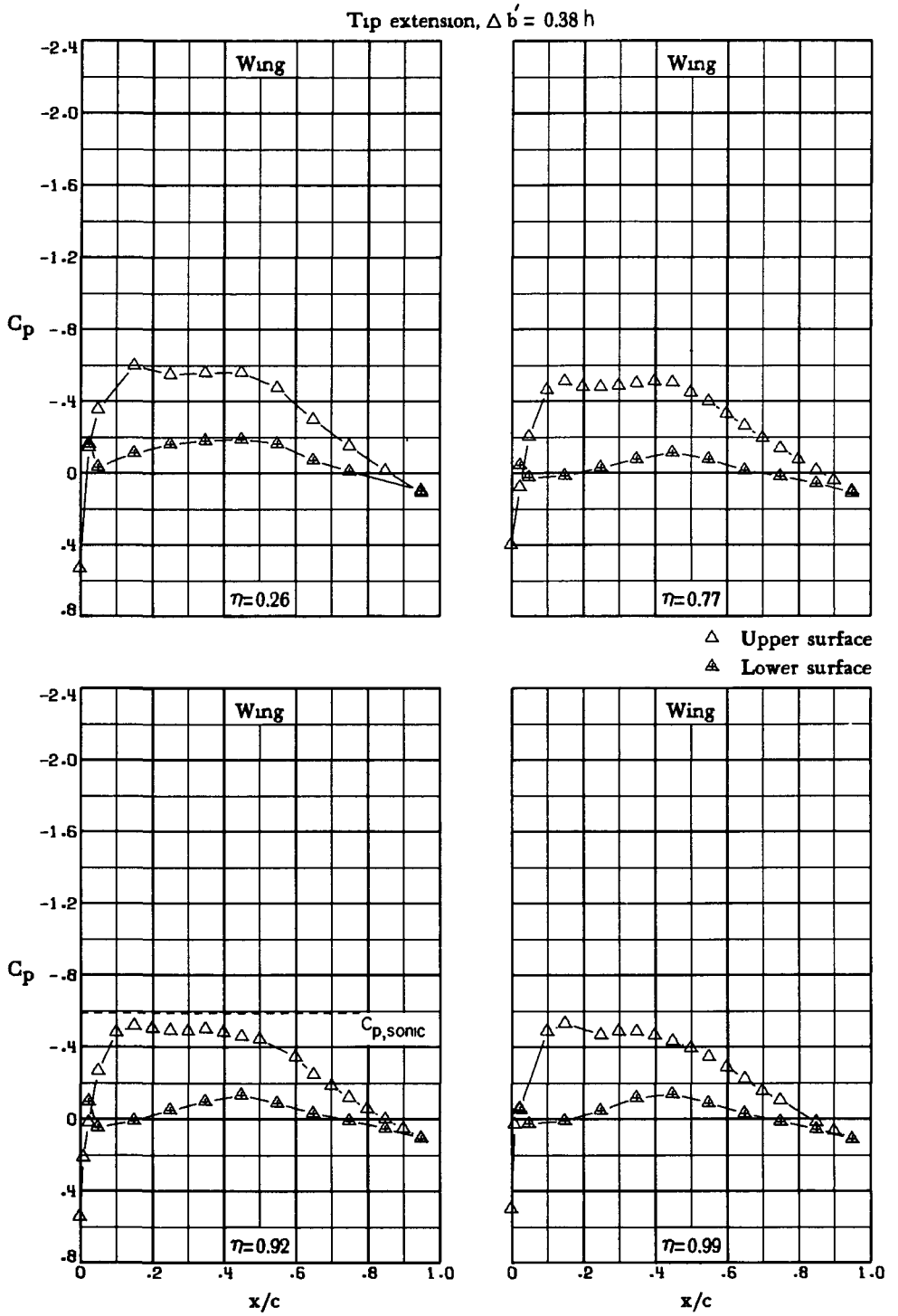

(g) $M_\infty = 0.75$; $\alpha = 0^o$.

Figure 11.- Continued.

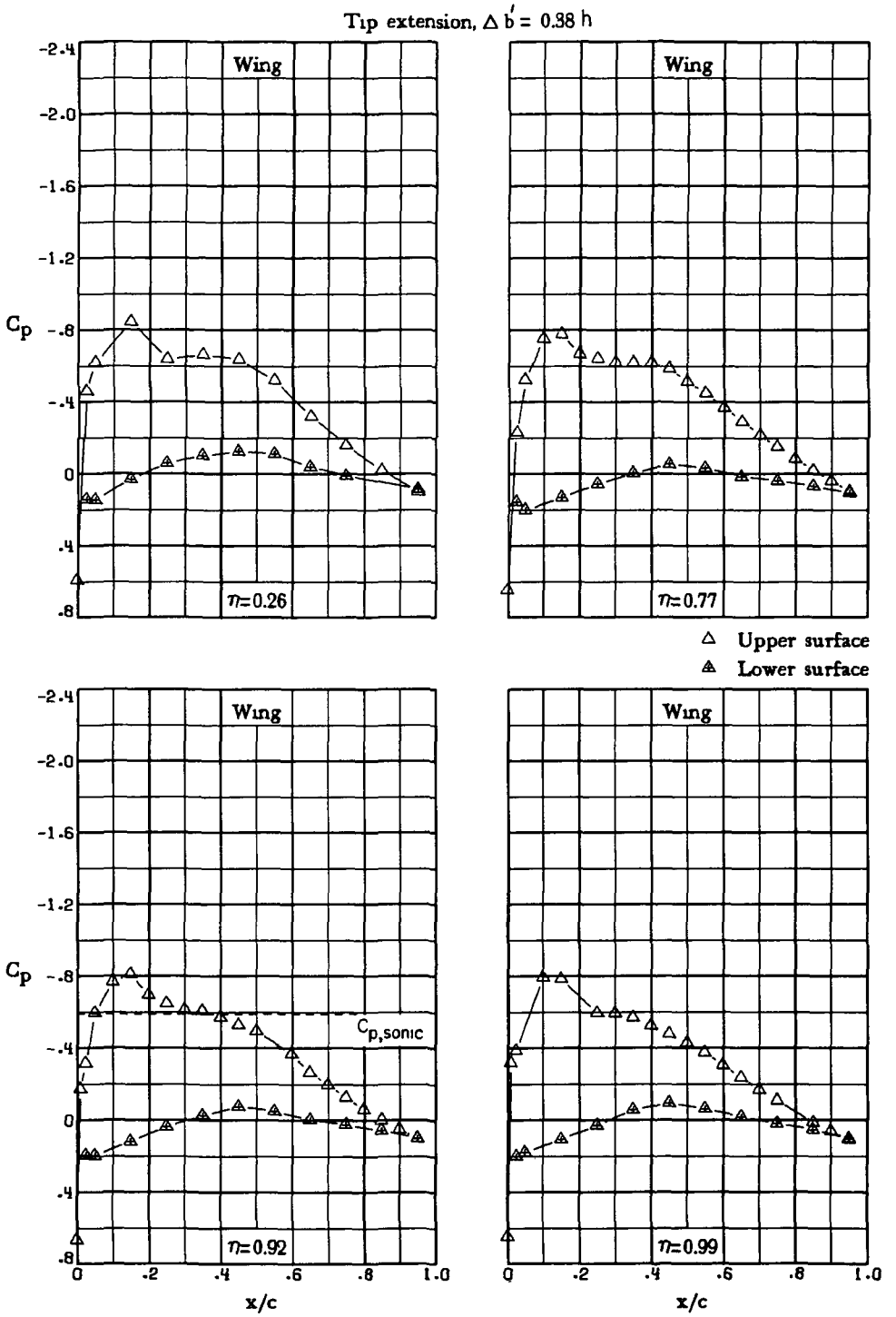

(h) $M_\infty = 0.75$; $\alpha = 2.0^\circ$.

Figure 11.- Continued.

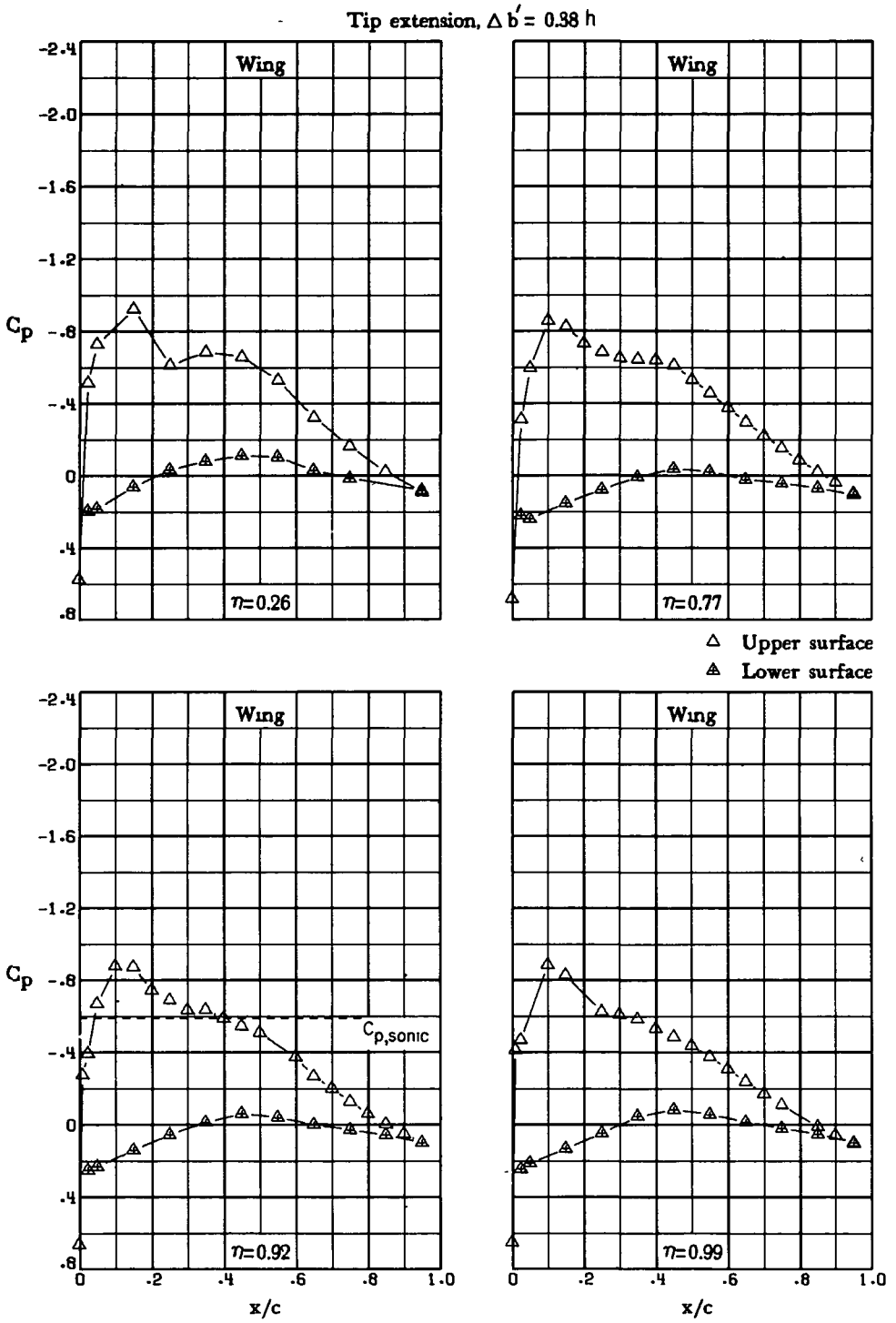

(i) $M_\infty = 0.75$; $\alpha = 2.5^\circ$.

Figure 11.- Continued.

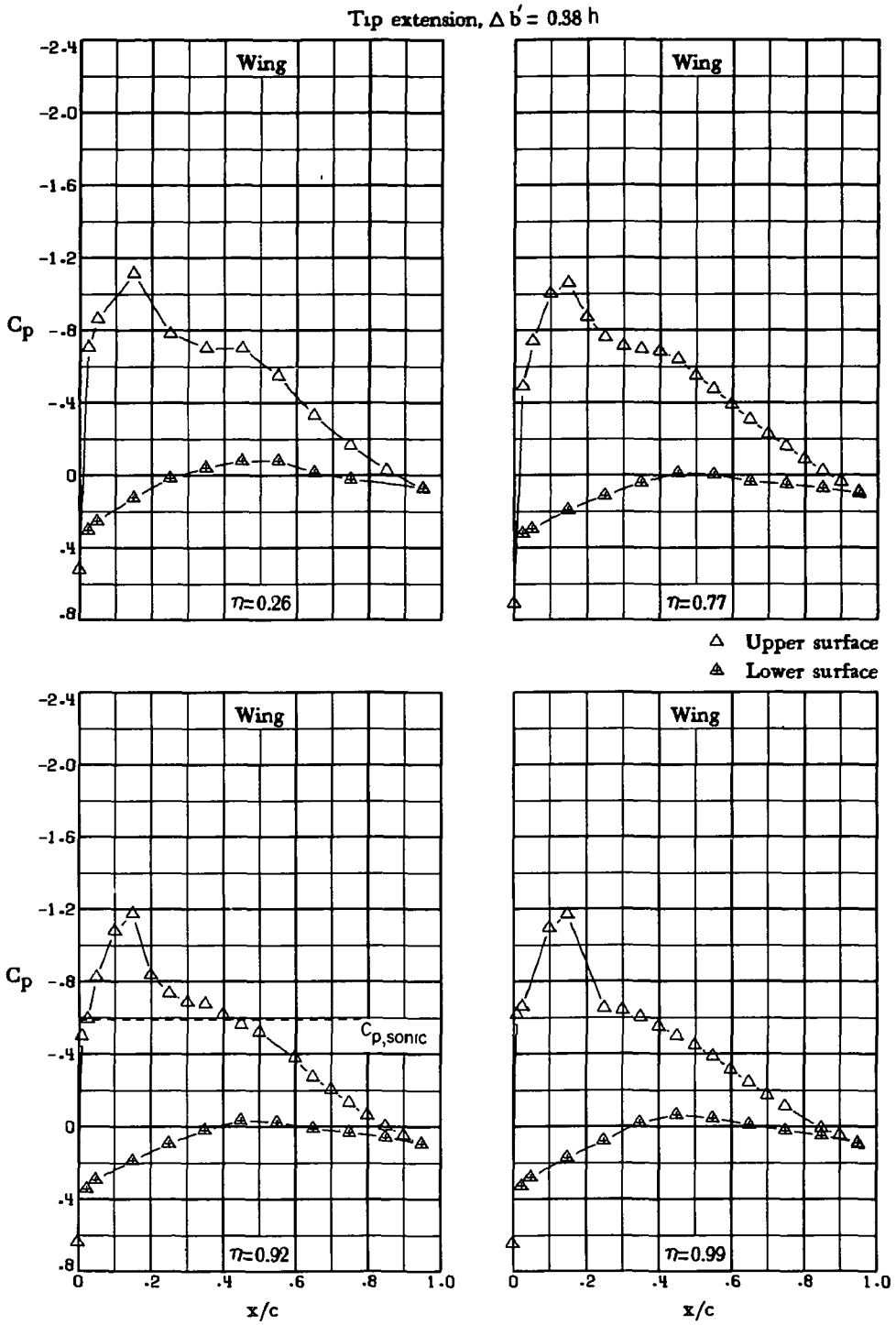

(j) $M_\infty = 0.75$; $\alpha = 3.5^\circ$.

Figure 11.- Continued.

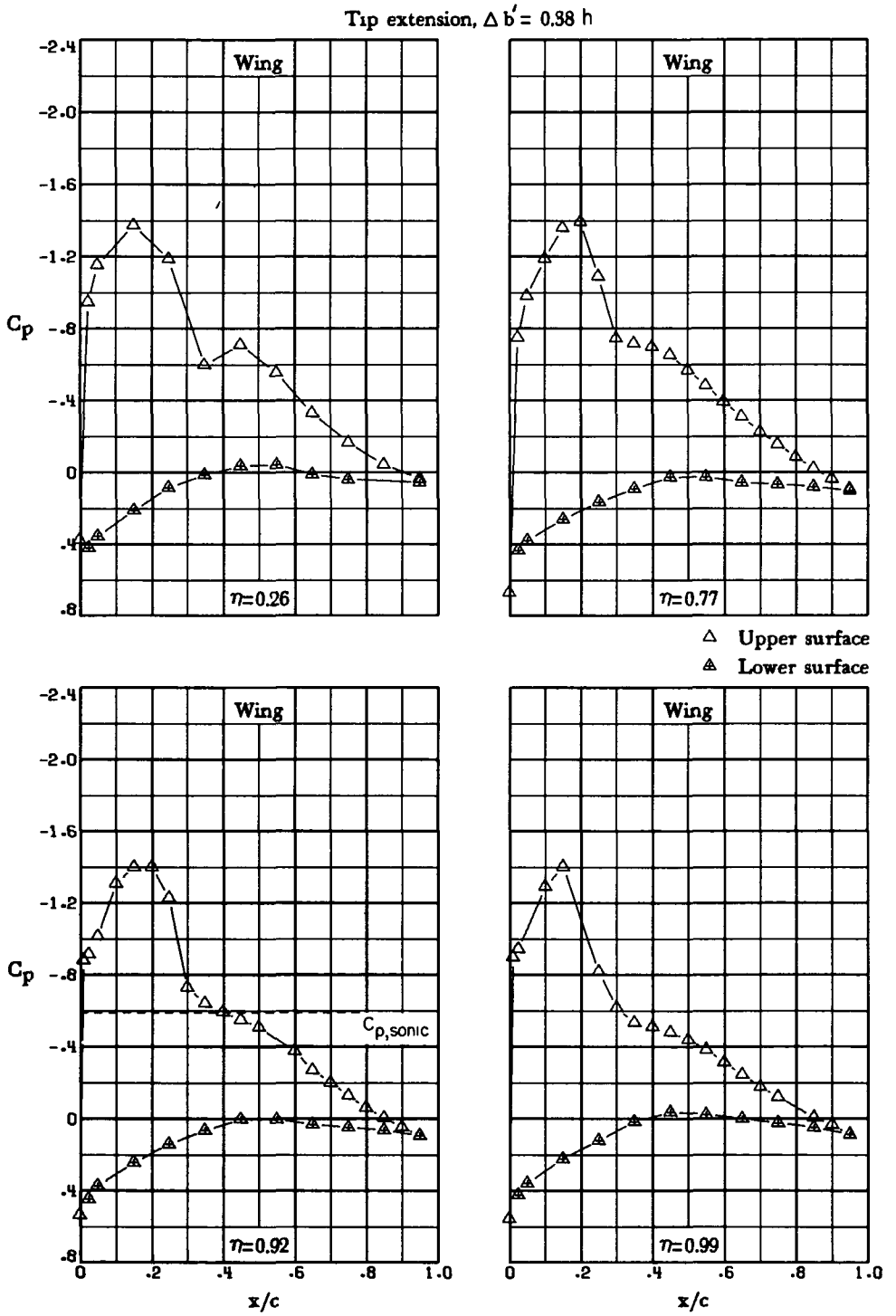

(k) $M_\infty = 0.75$; $\alpha = 5.0^\circ$.

Figure 11.- Continued.

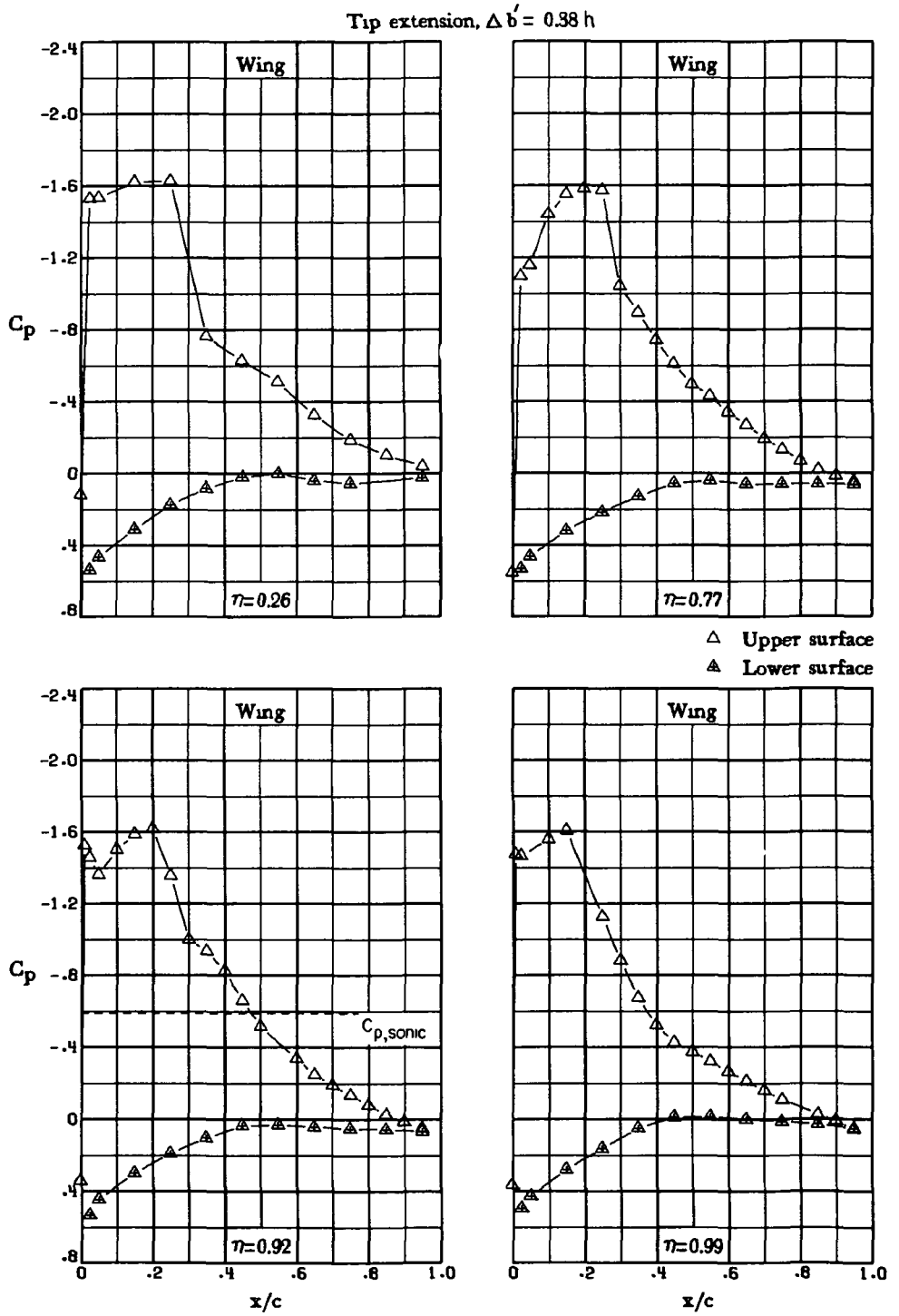

(1) $M_\infty = 0.75$; $\alpha = 7.3^\circ$.

Figure 11.- Continued.

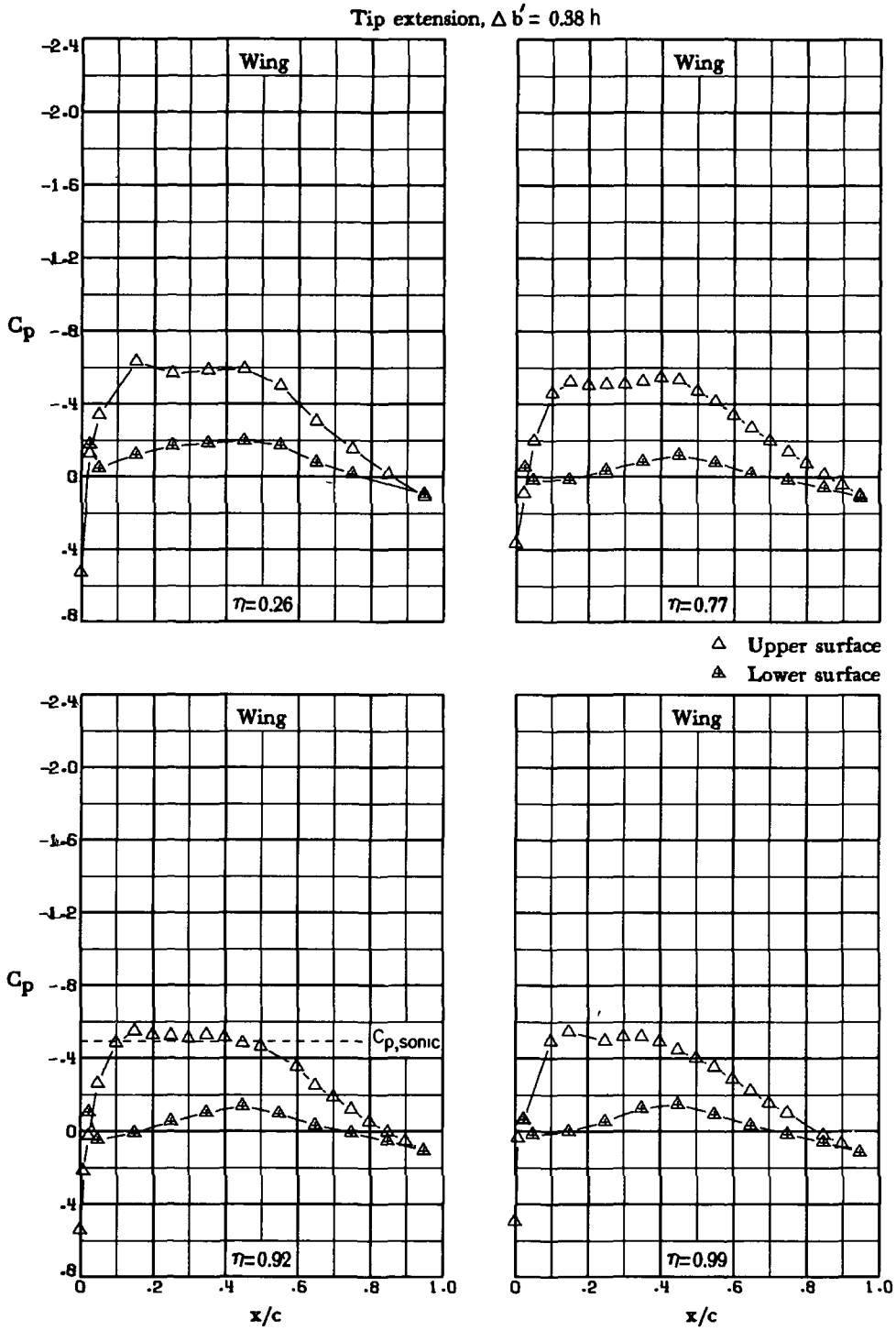

(m) $M_\infty = 0.78$; $\alpha = 0^\circ$.

Figure 11.- Continued.

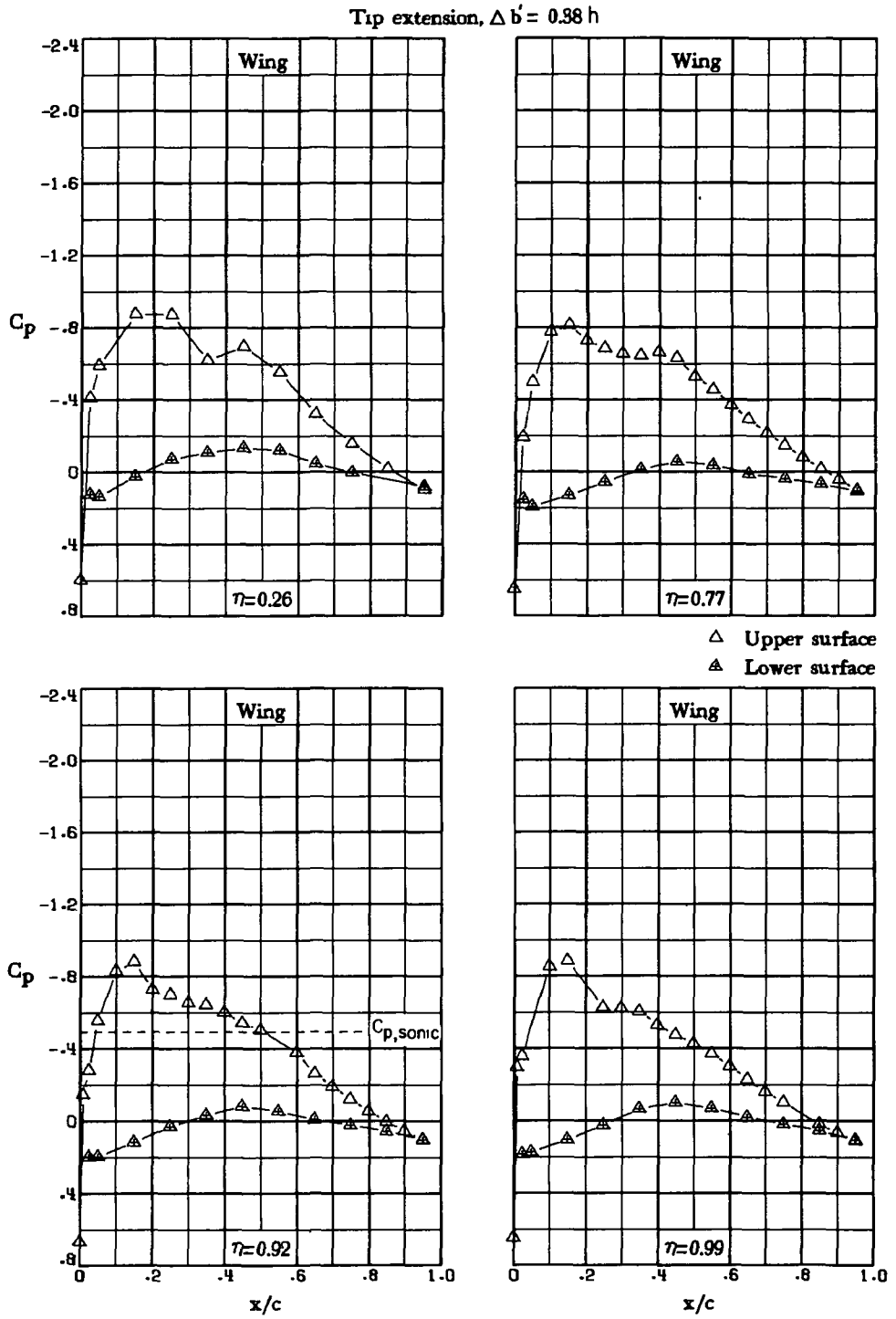

(n) $M_\infty = 0.78$; $\alpha = 2.0^\circ$.

Figure 11.- Continued.

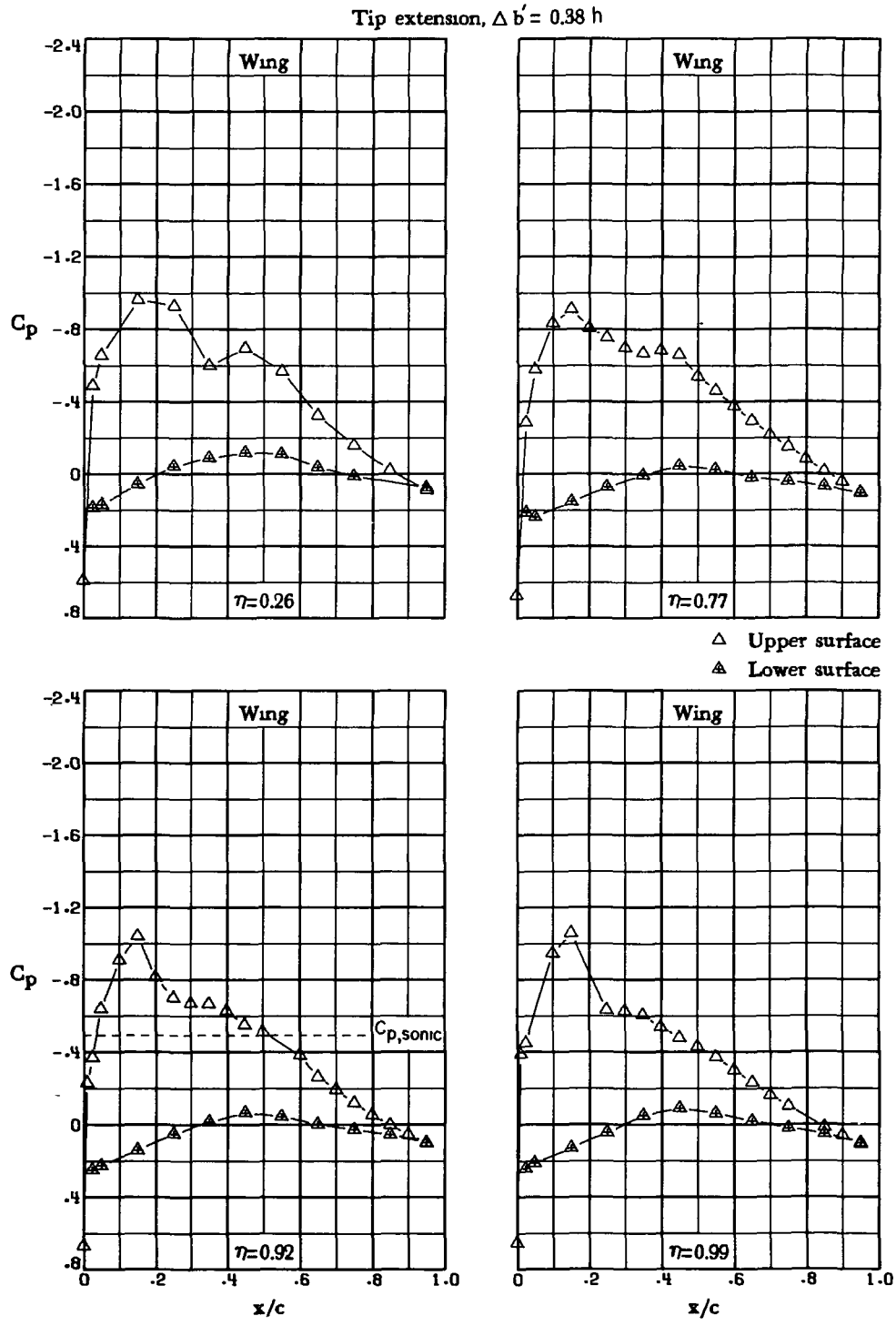

(o) $M_\infty = 0.78$; $\alpha = 2.5^o$.

Figure 11.- Continued.

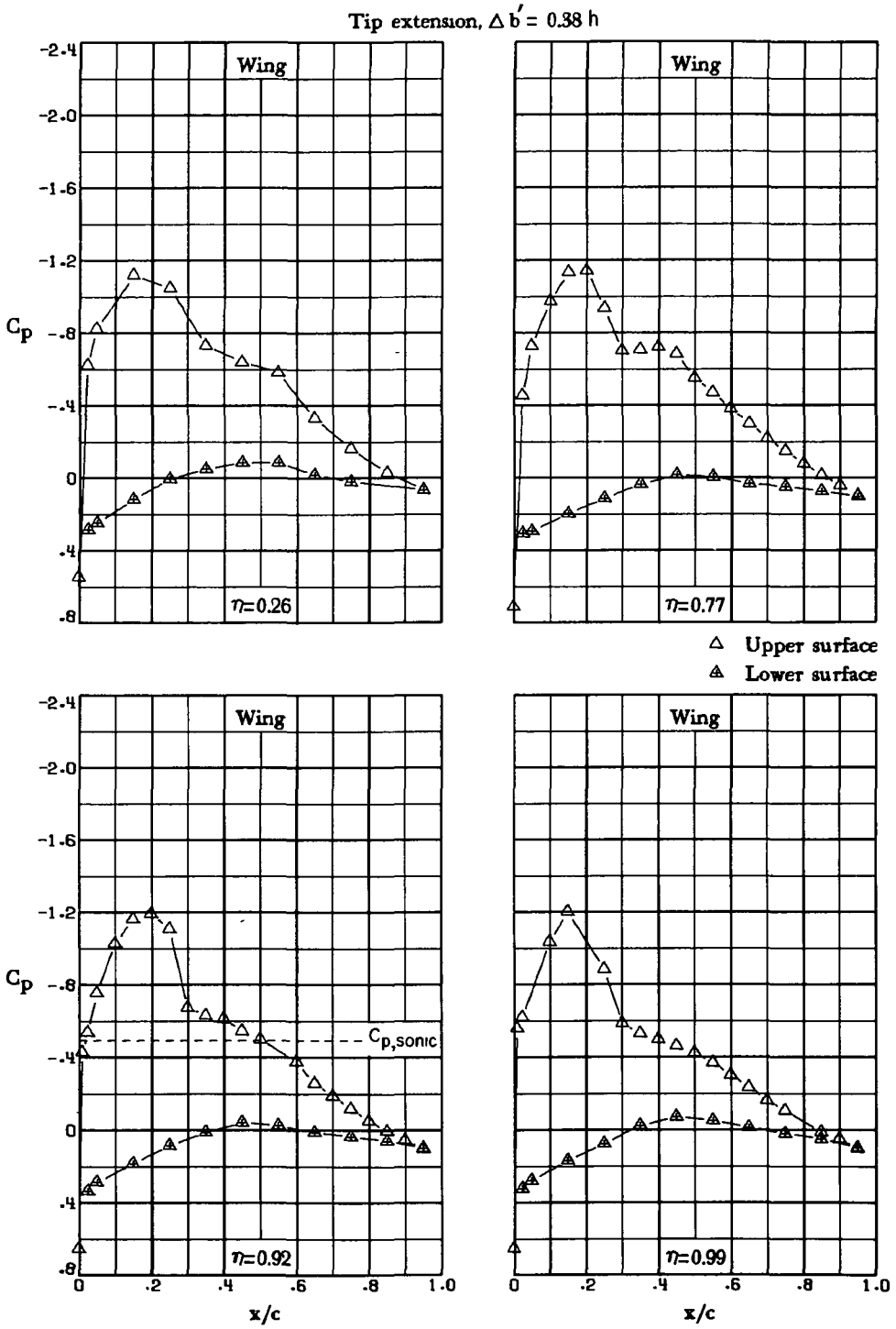

(p) $M_\infty = 0.78$; $\alpha = 3.5^\circ$.

Figure 11.- Continued.

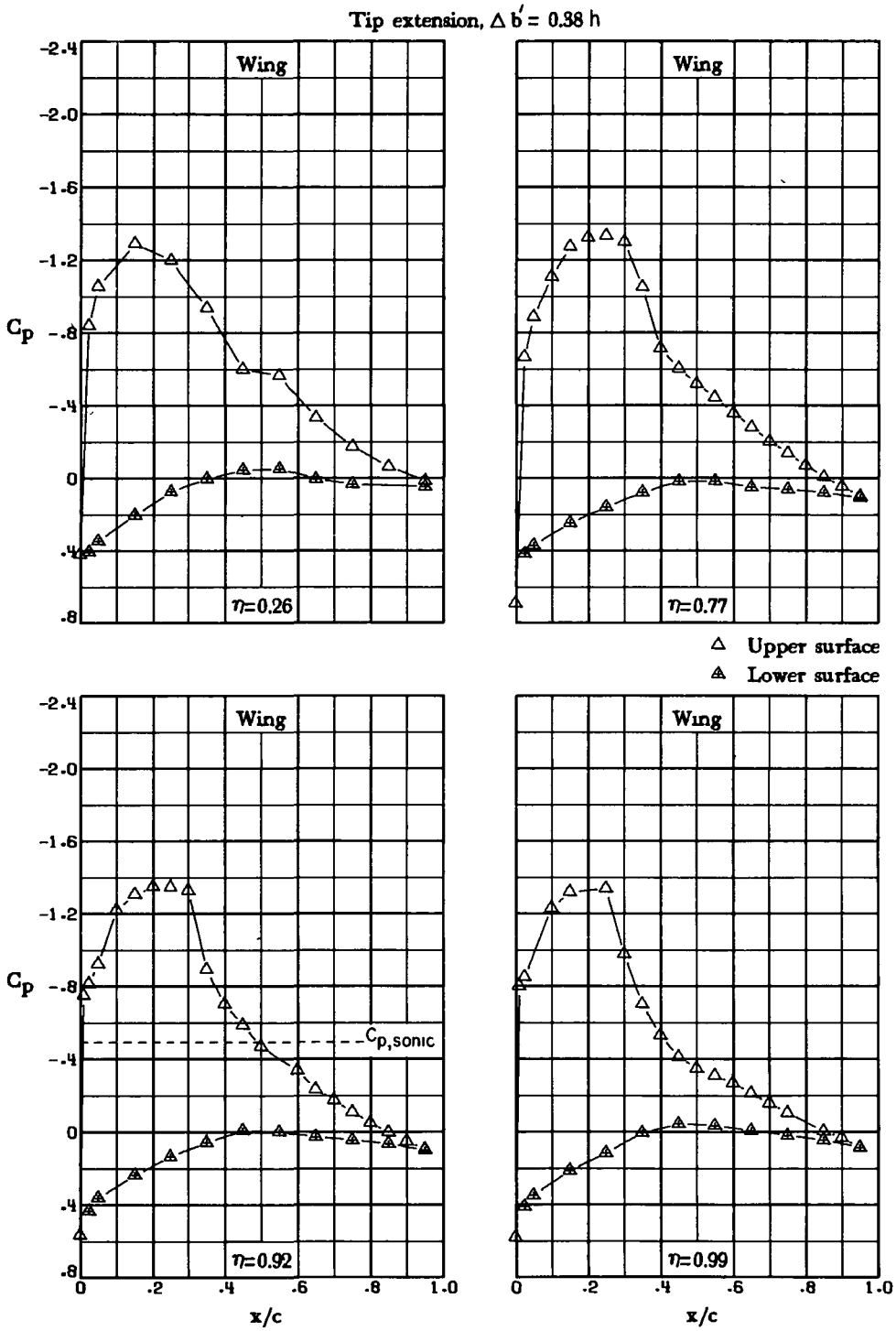

(q) $M_\infty = 0.78$; $\alpha = 5.0^\circ$.

Figure 11.- Continued.

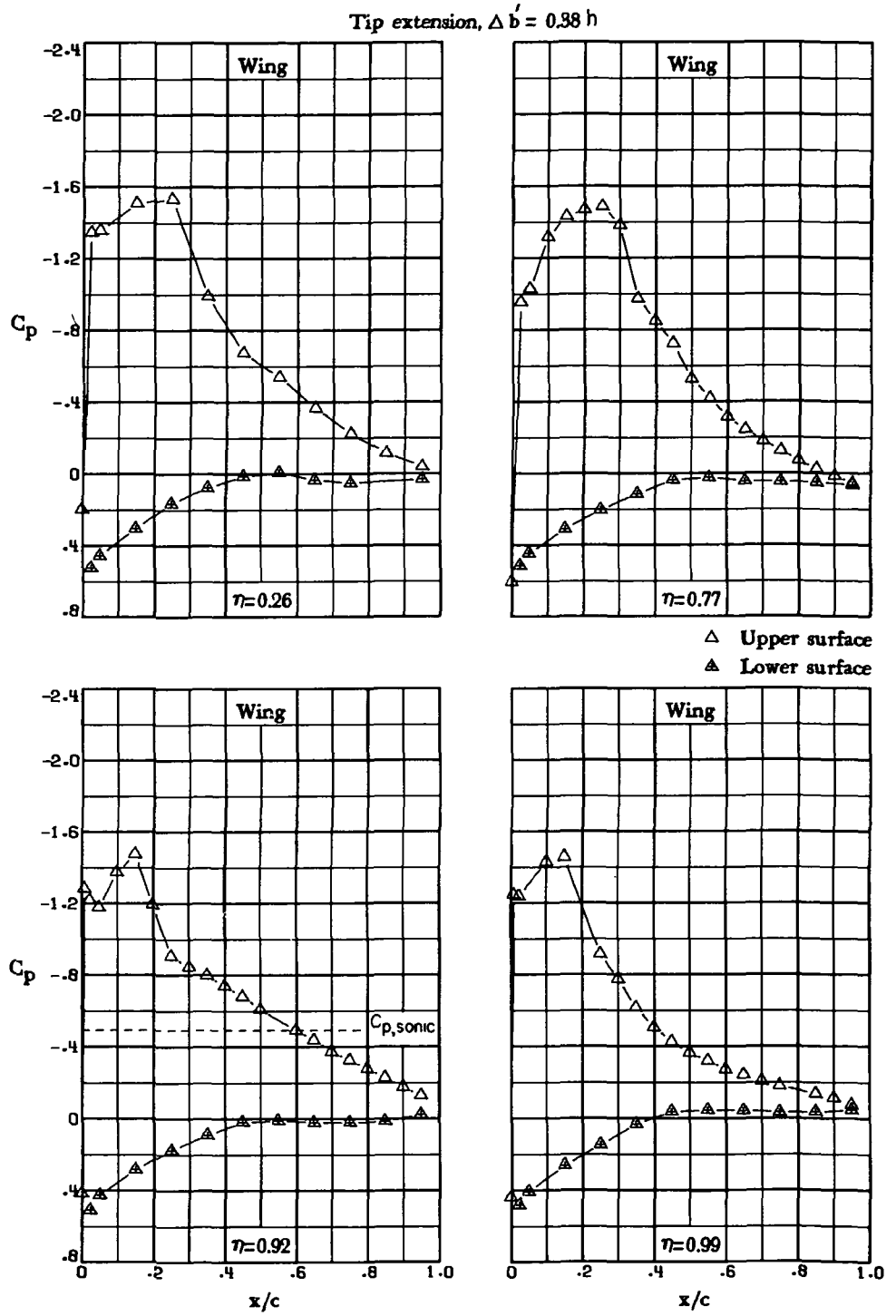

(r) $M_\infty = 0.78$; $\alpha = 7.2^\circ$.

Figure 11.- Continued.

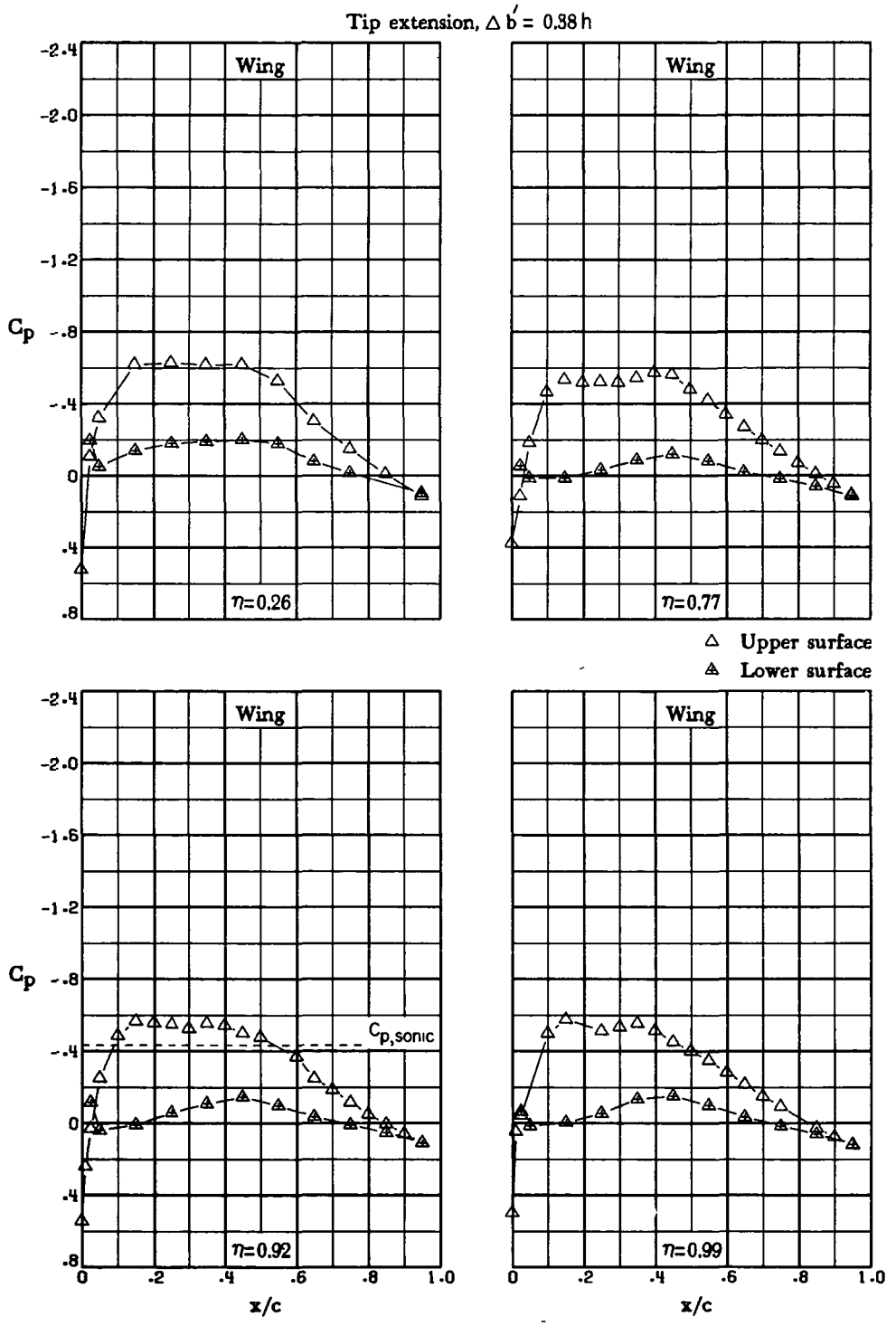

(s) $M_\infty = 0.80$; $\alpha = 0^o$.

Figure 11.- Continued.

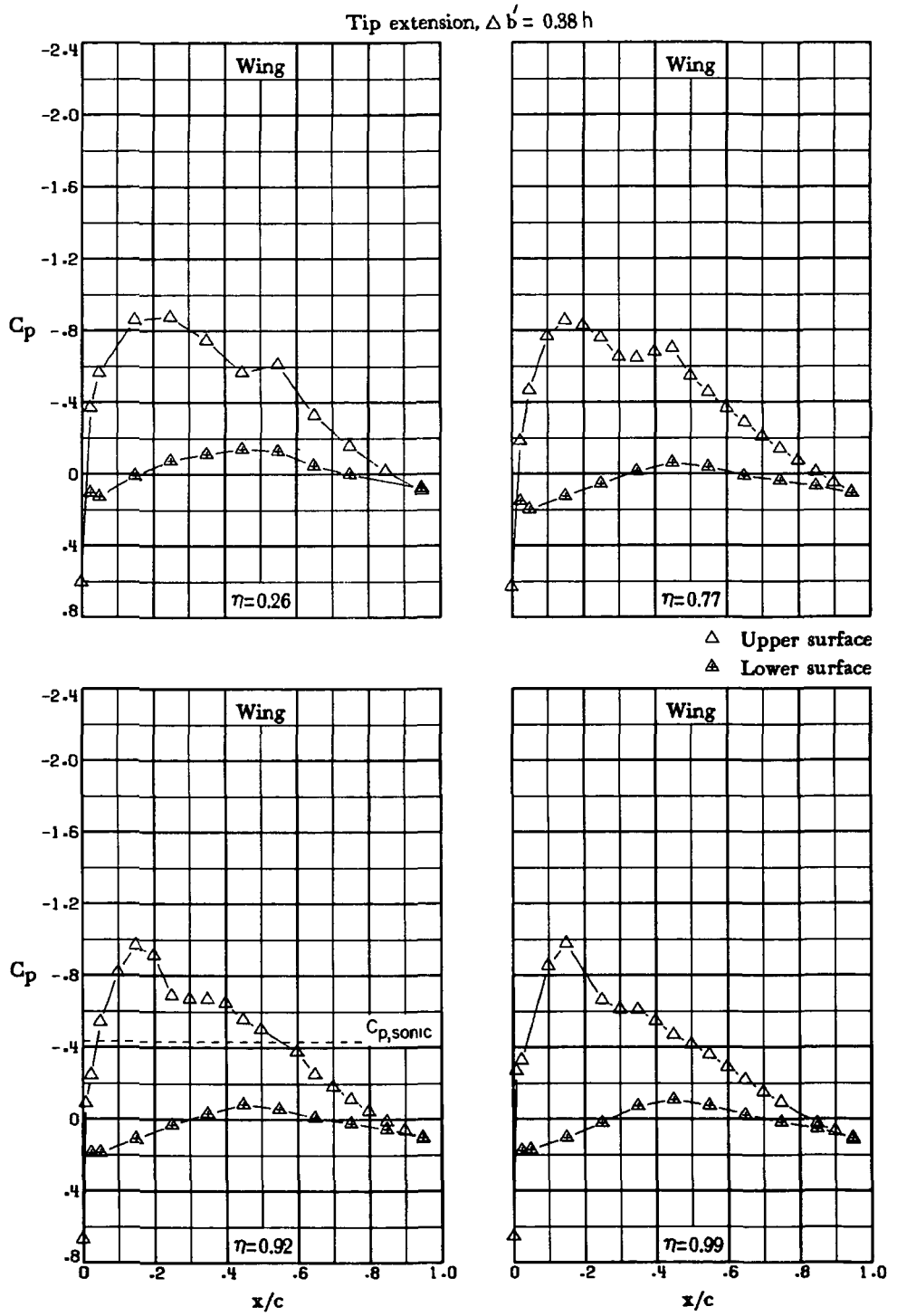

(t) $M_\infty = 0.80$; $\alpha = 2.0^\circ$.

Figure 11.- Continued.

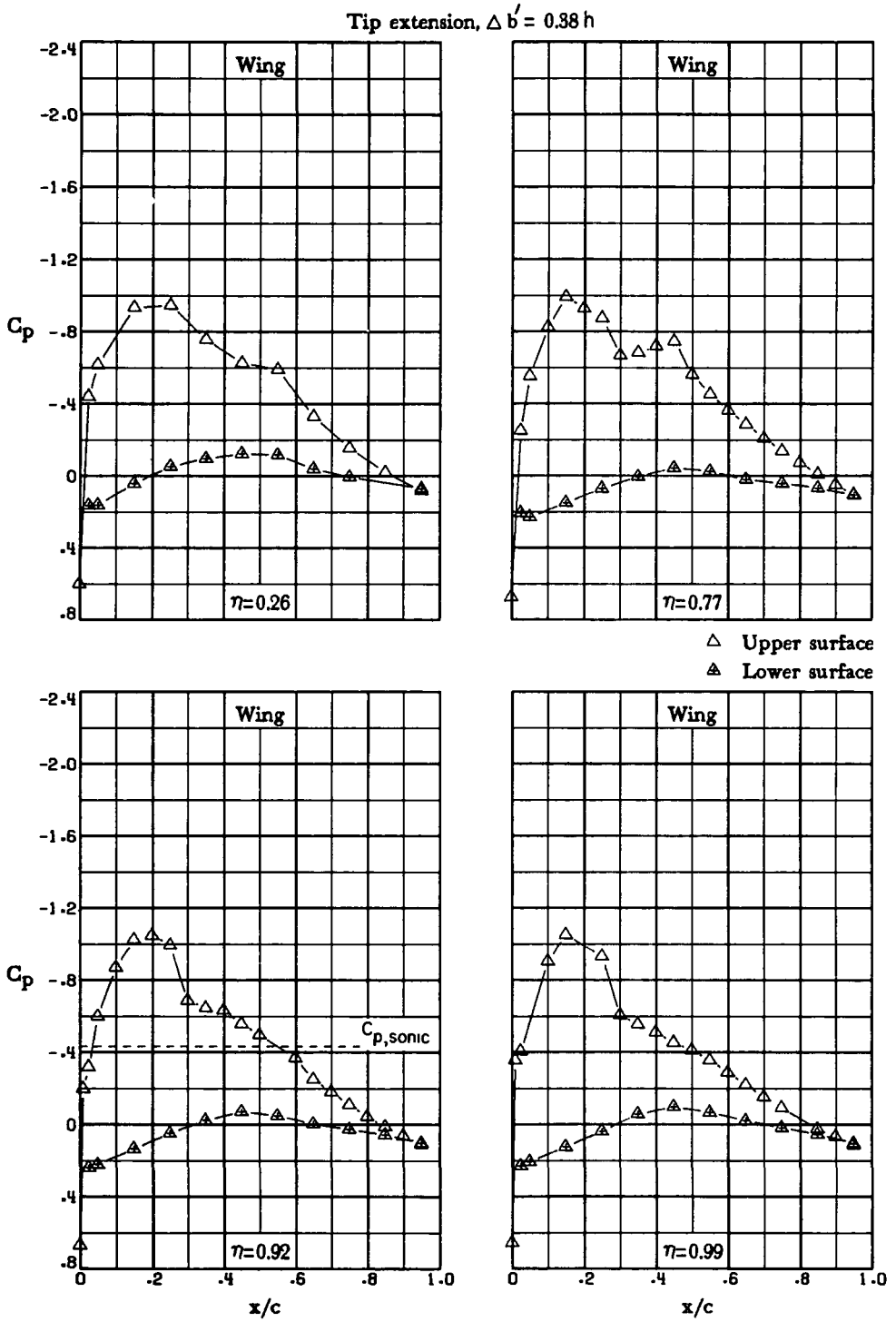

(u) $M_\infty = 0.80$; $\alpha = 2.5^\circ$.

Figure 11.- Continued.

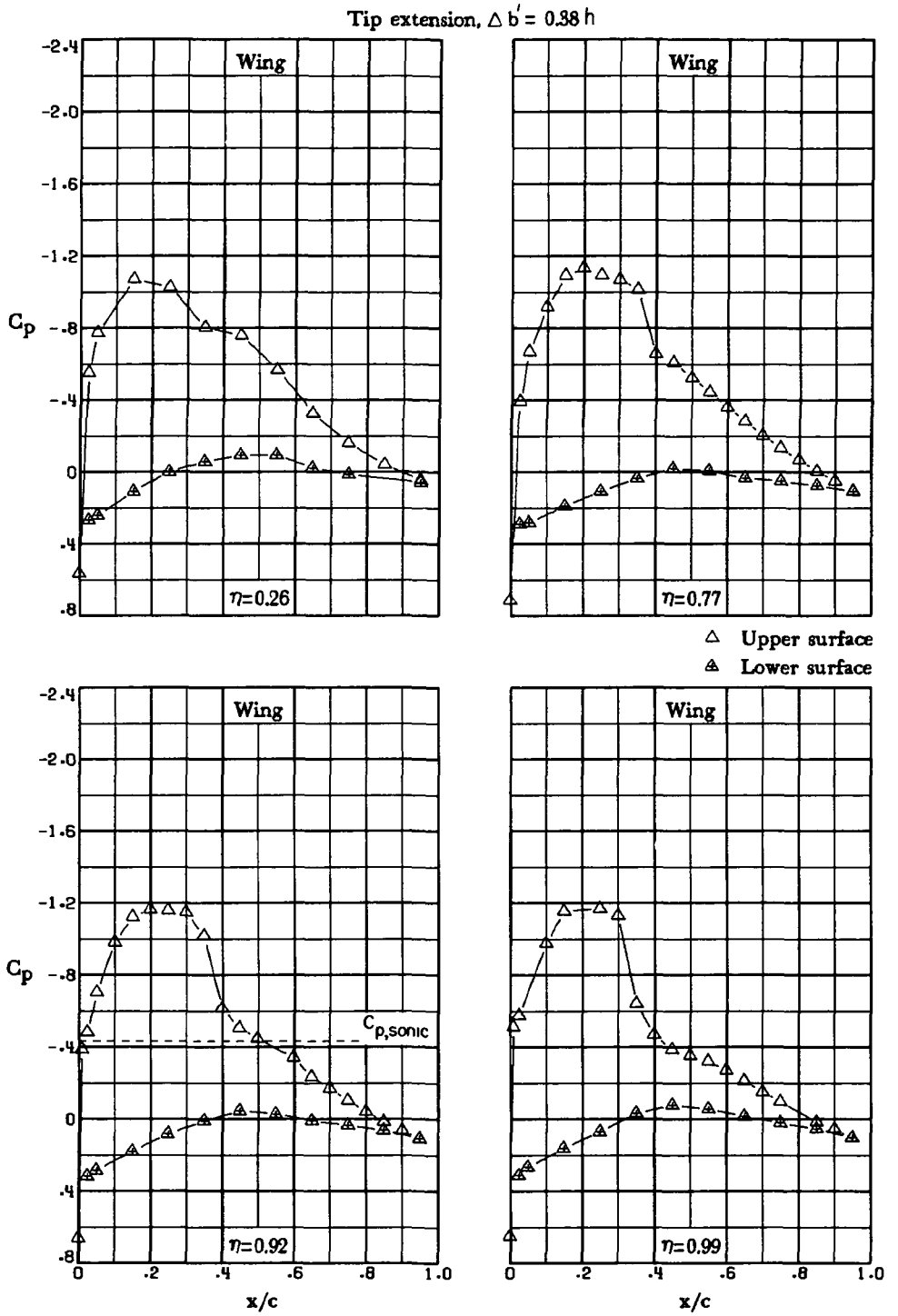

(v) $M_\infty = 0.80$; $\alpha = 3.5^\circ$.

Figure 11.- Continued.

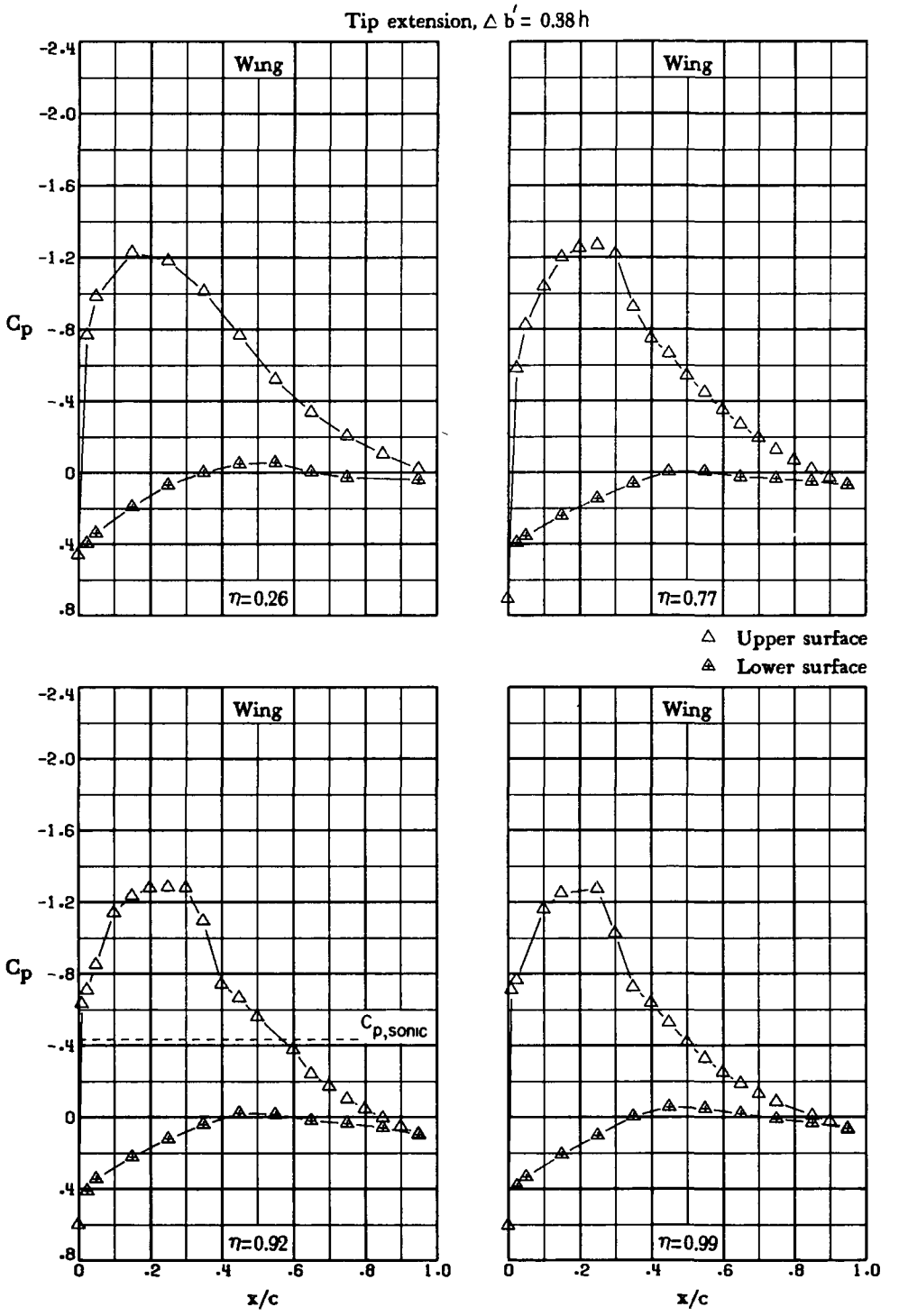

(w) $M_\infty = 0.80$; $\alpha = 5.0^\circ$.

Figure 11.- Continued.

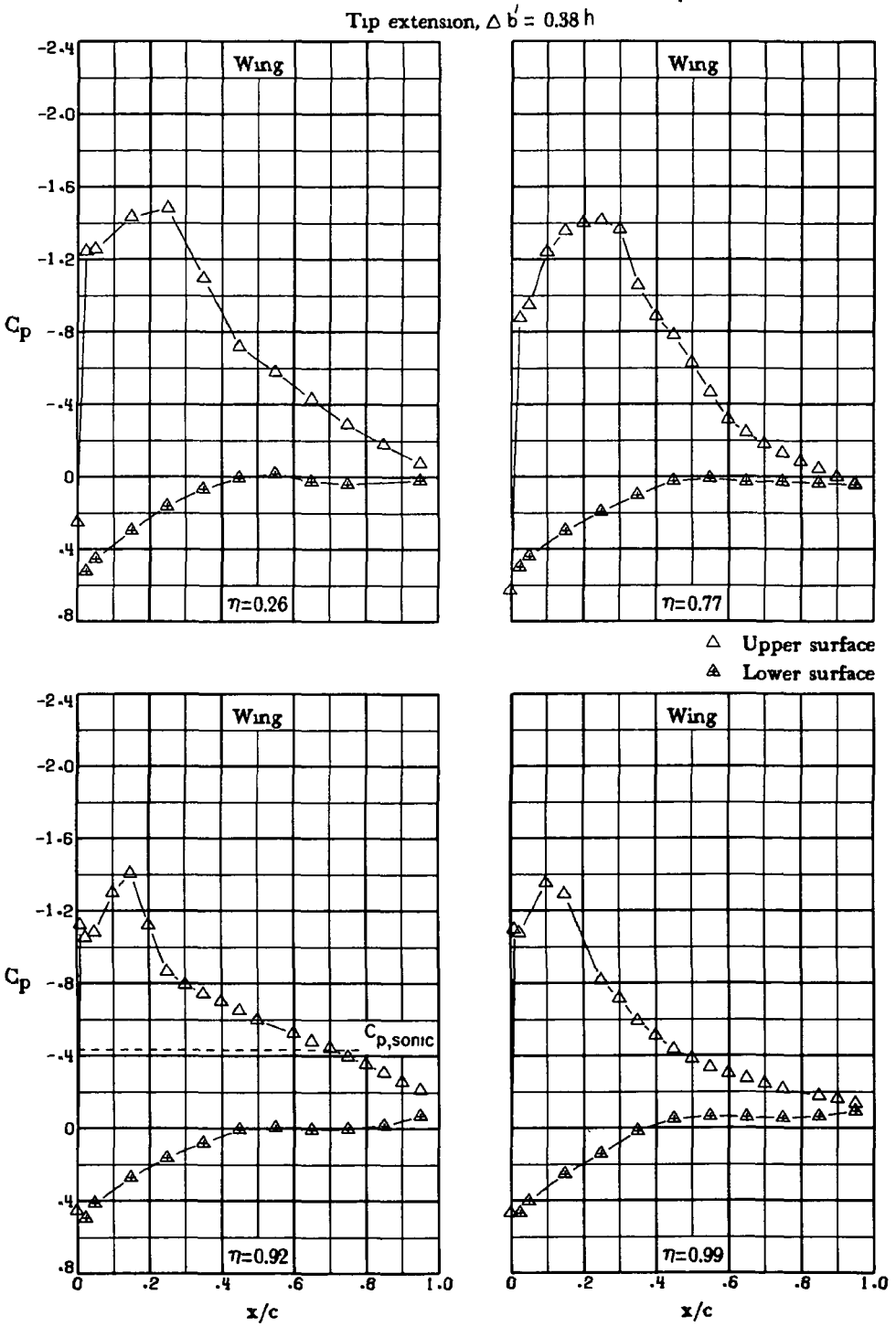

(x) $M_\infty = 0.80$; $\alpha = 7.2^\circ$.

Figure 11.- Concluded.

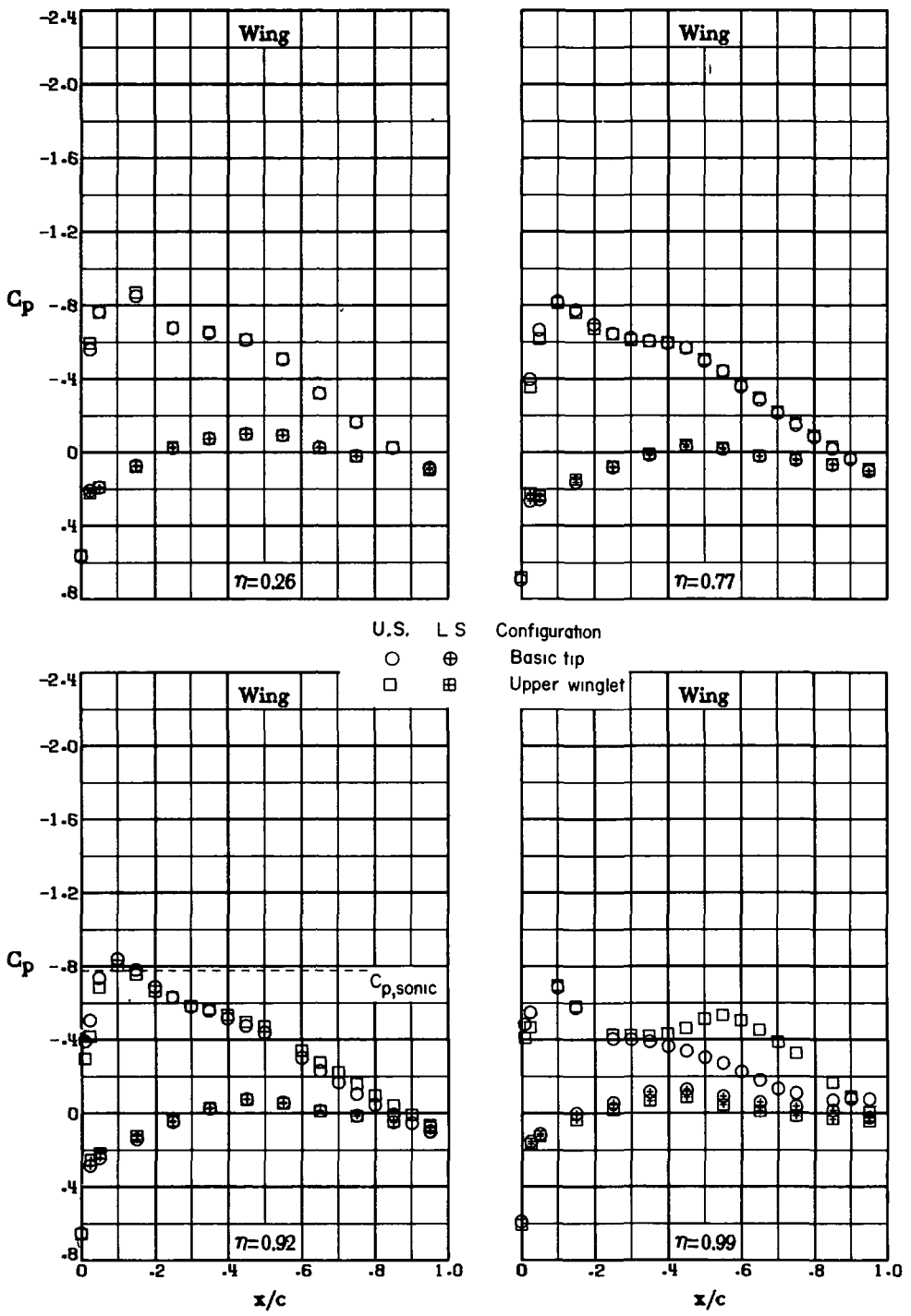

(a) $M_\infty = 0.70$; $\alpha = 2.5^\circ$.

Figure 12.- Comparison of pressure distributions for basic-tip and upper-winglet configurations.

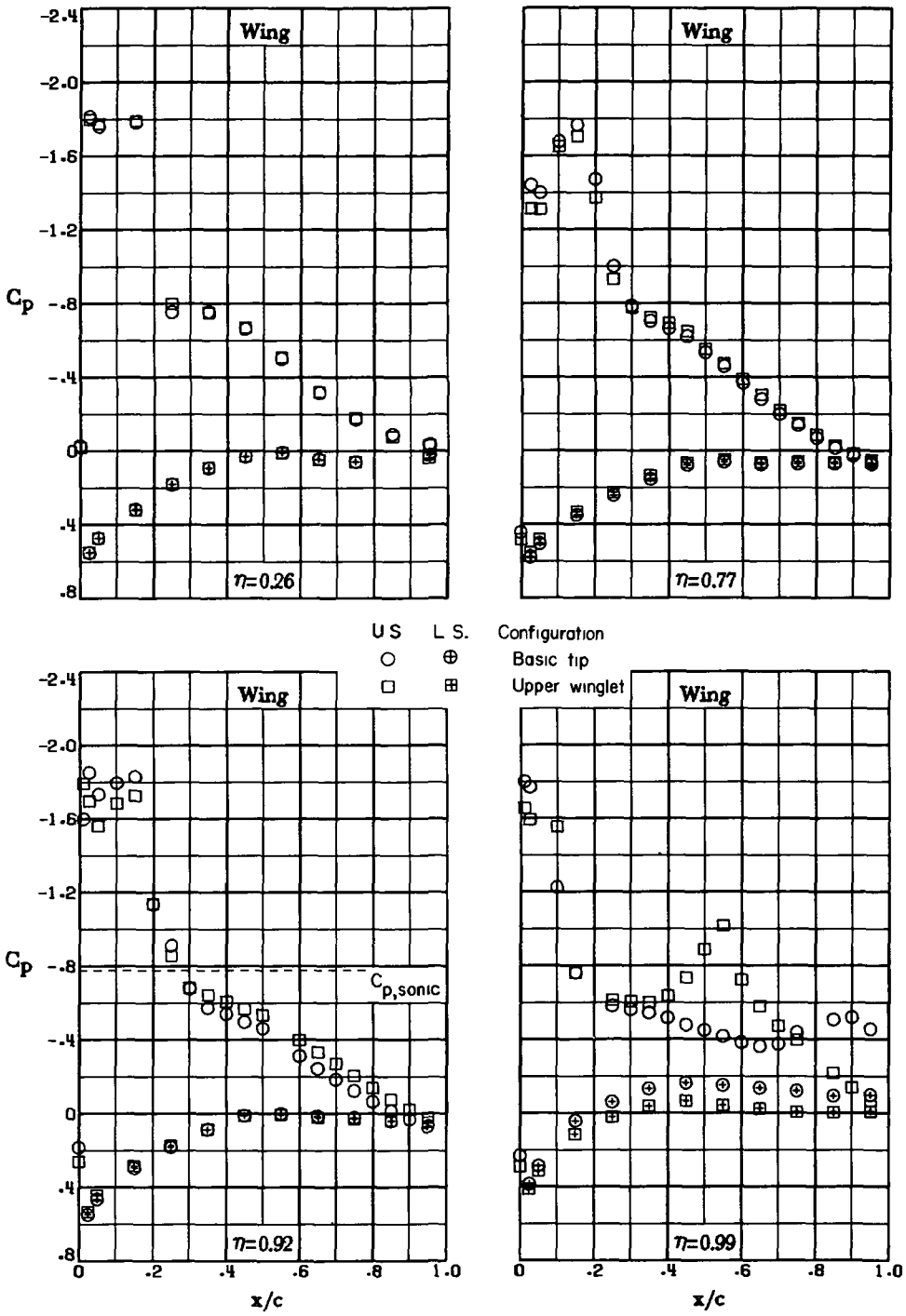

(b) $M_\infty = 0.70$; $\alpha = 7.2^o$.

Figure 12.- Continued.

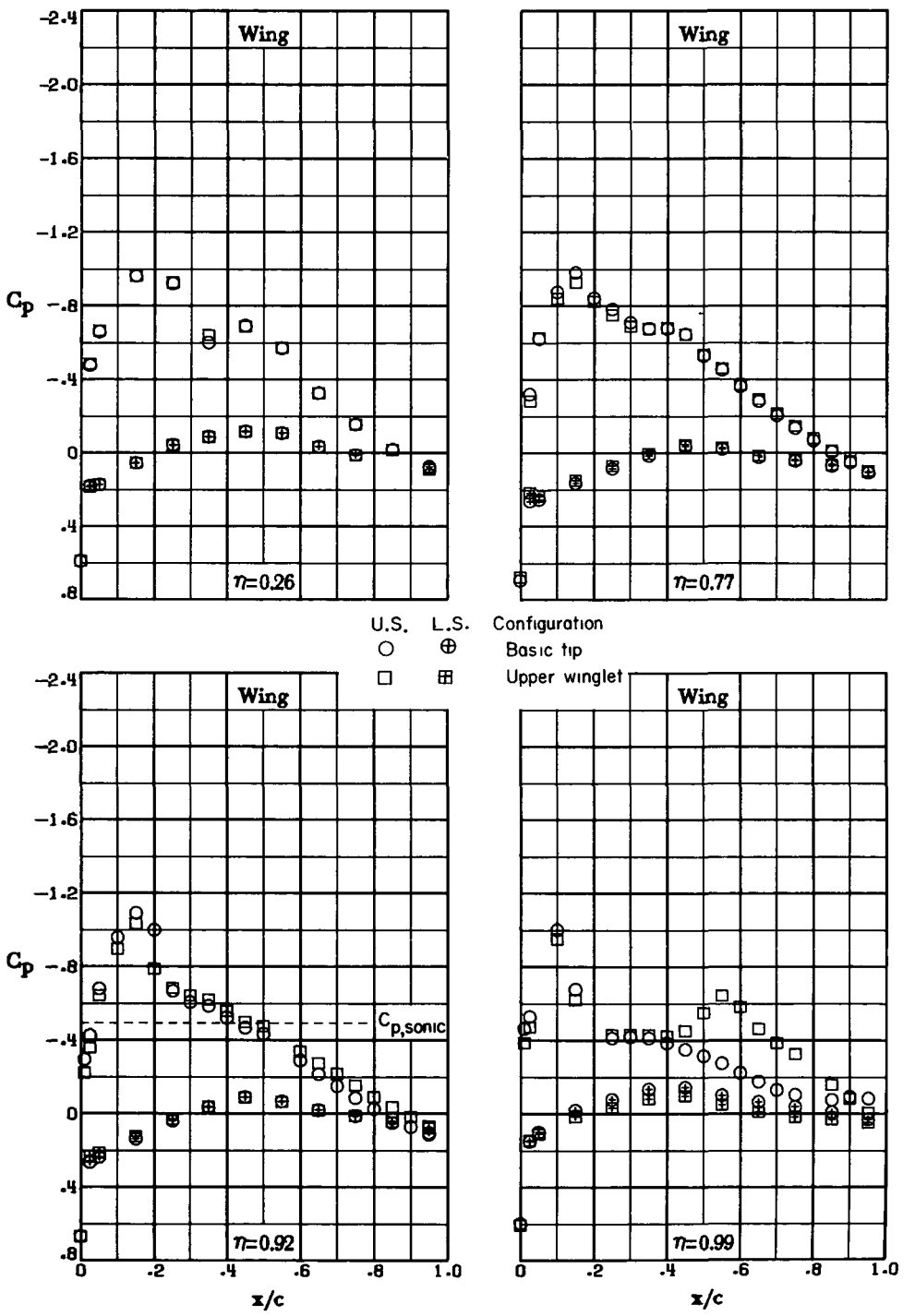

(c) $M_\infty = 0.78$; $\alpha = 2.5^\circ$.

Figure 12.- Continued.

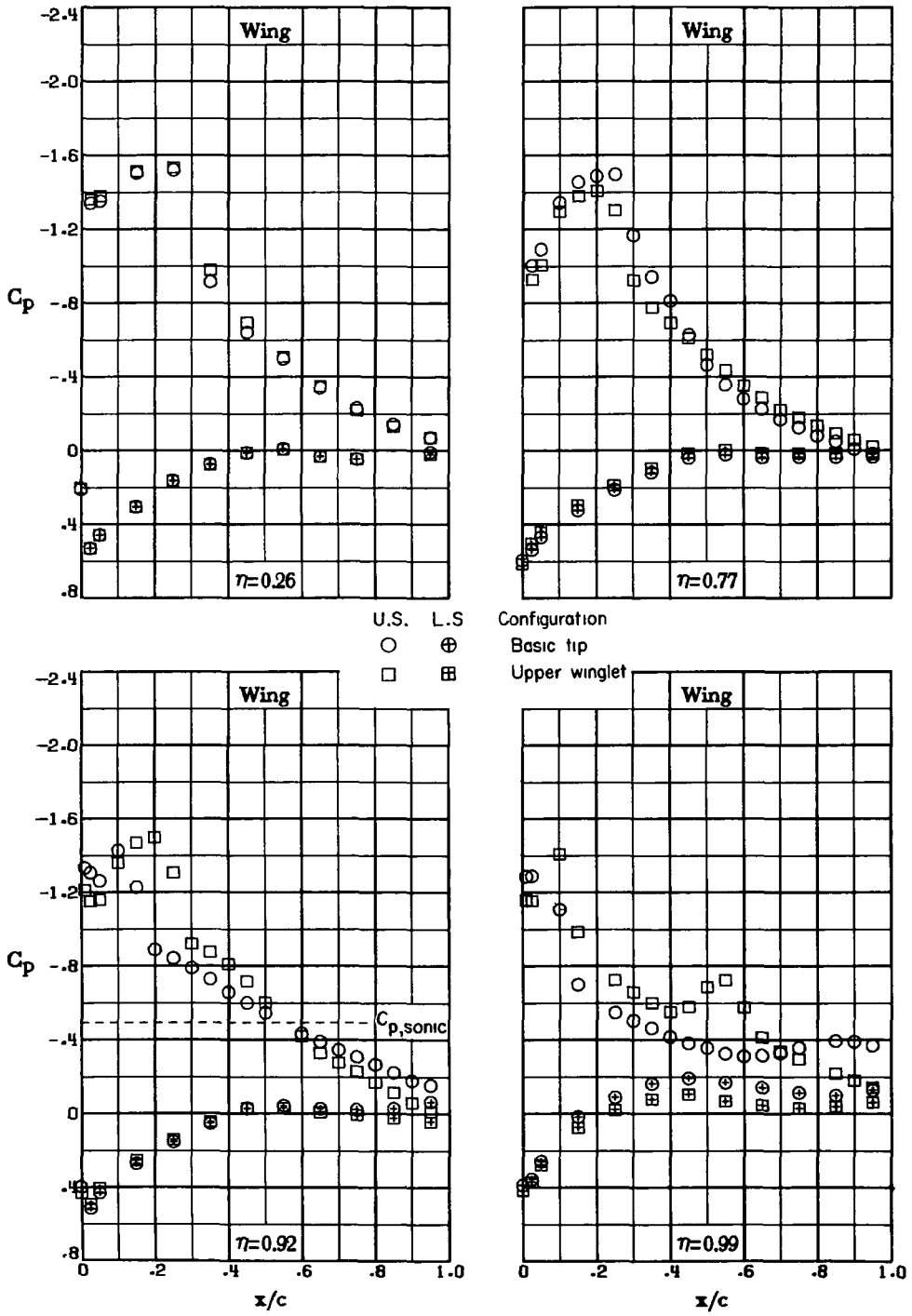

(d) $M_\infty = 0.78$; $\alpha = 7.2^\circ$.

Figure 12.- Concluded.

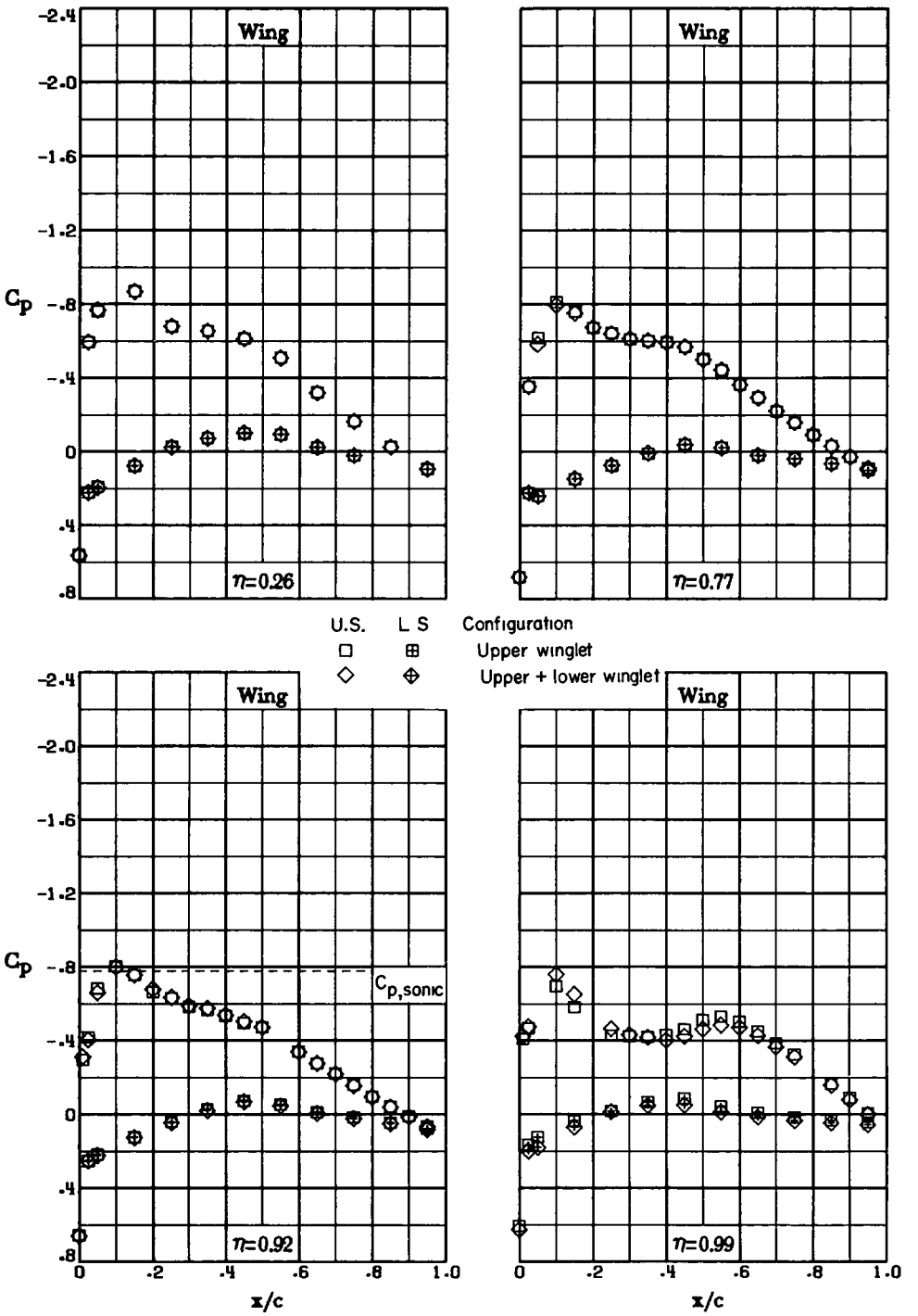

(a) $M_\infty = 0.70$; $\alpha = 2.5^\circ$.

Figure 13.- Comparison of pressure distributions for upper-winglet and upper-and-lower-winglet configurations.

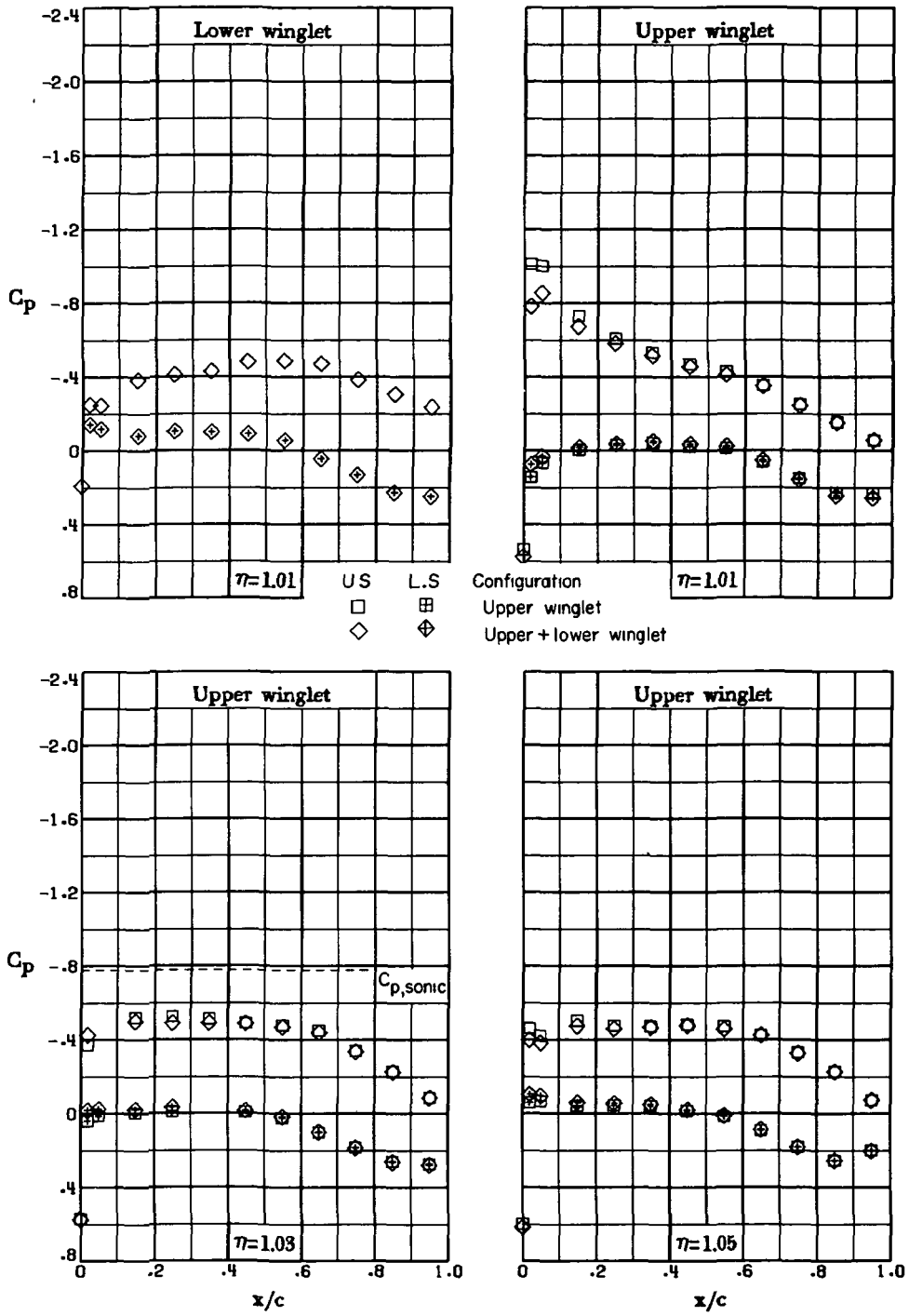

(a) M_∞ = 0.70; α = 2.5°. Concluded.

Figure 13.- Continued.

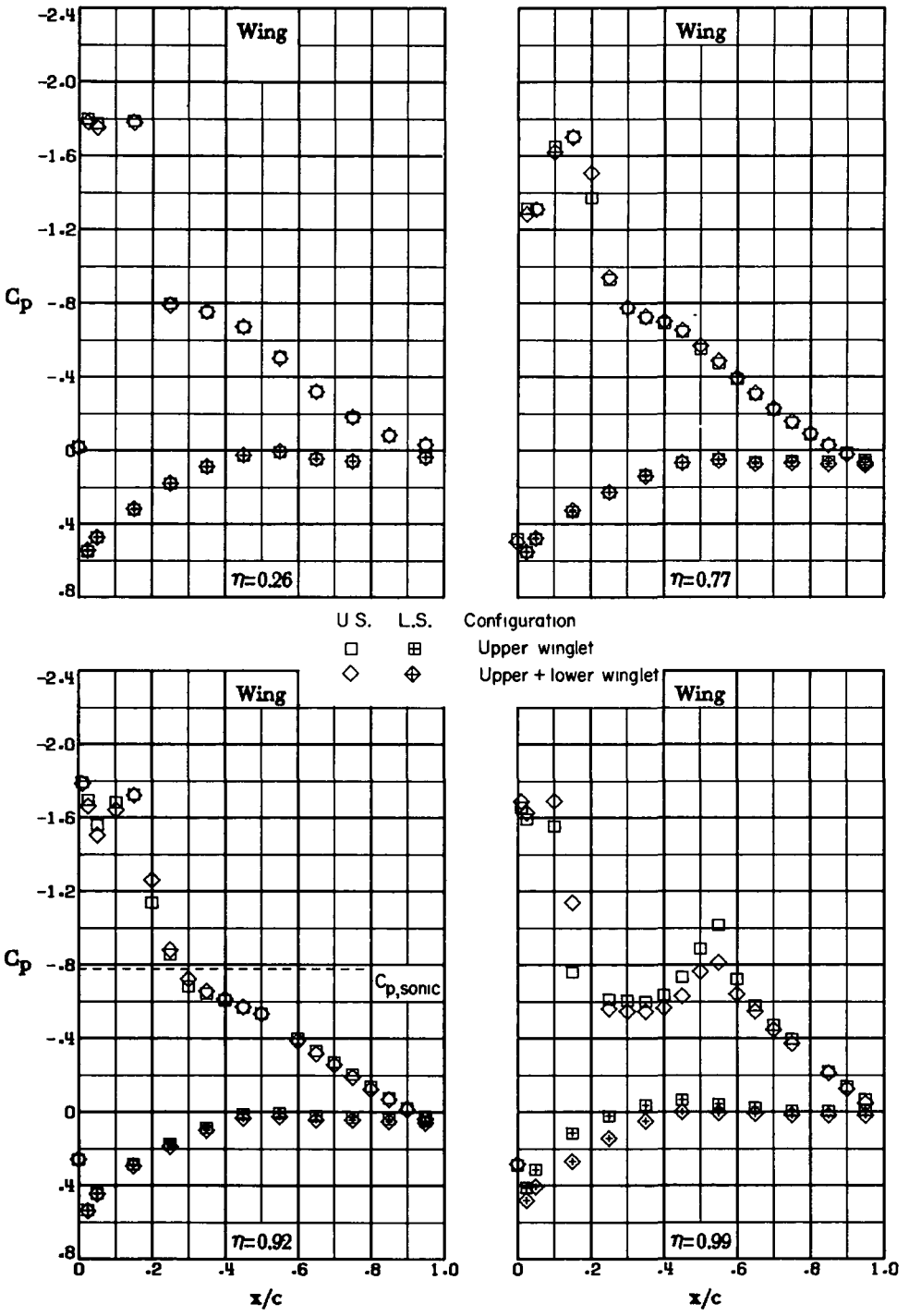

(b) $M_\infty = 0.70$; $\alpha \approx 7.2^\circ$.

Figure 13.- Continued.

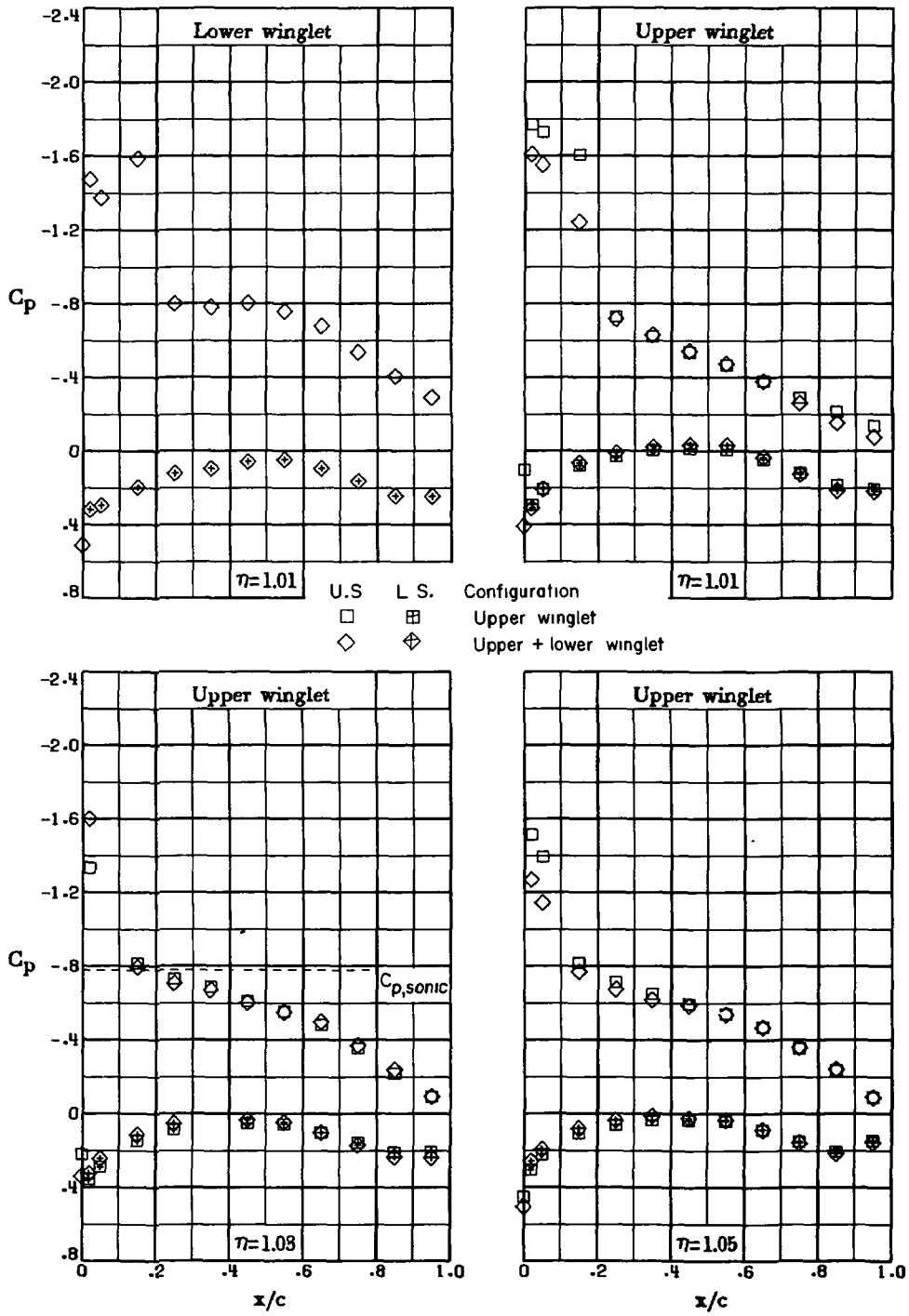

(b) $M_\infty = 0.70$; $\alpha \approx 7.2^o$. Concluded.

Figure 13.- Continued.

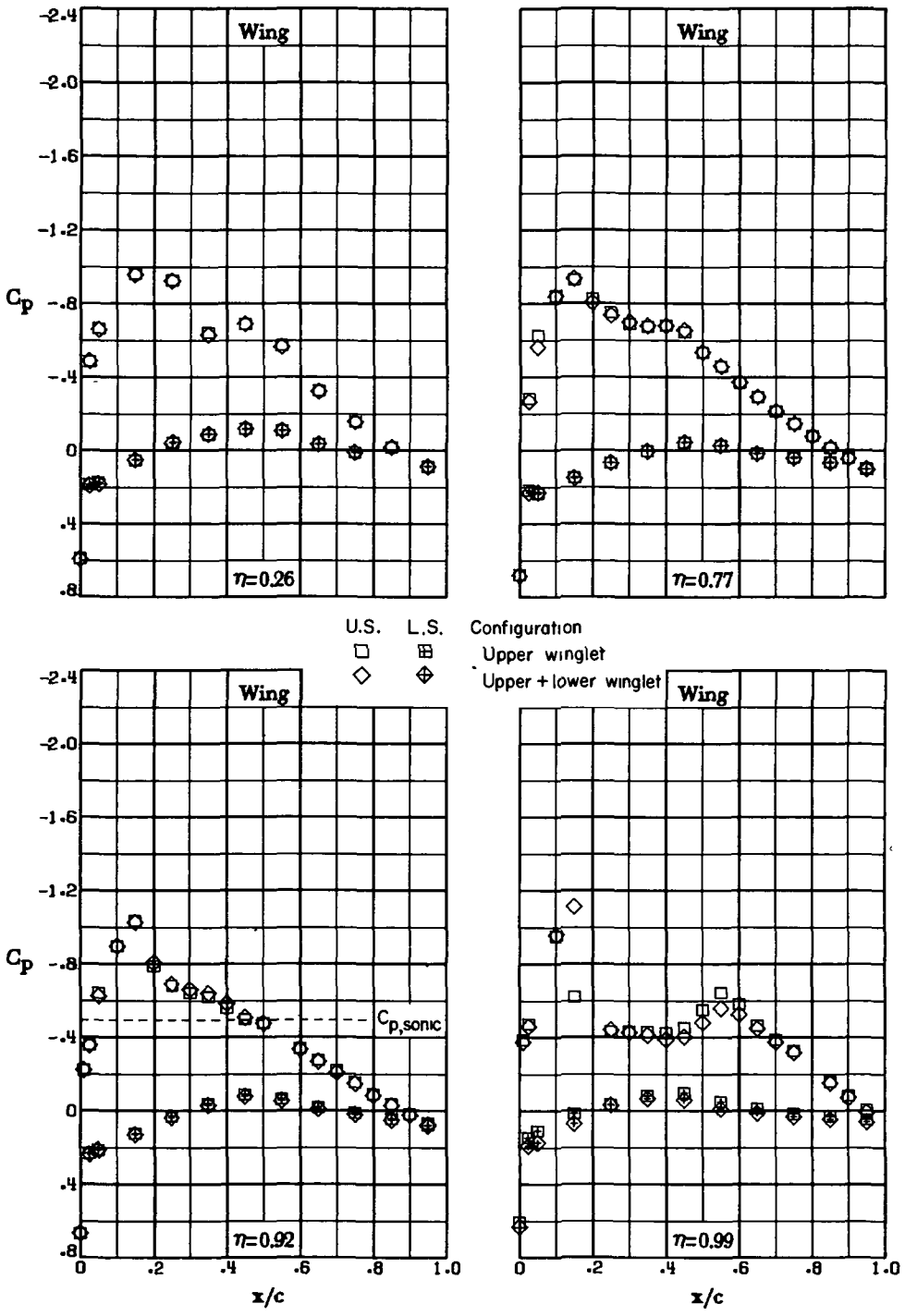

(c) $M_\infty = 0.78$; $\alpha = 2.5^\circ$.

Figure 13.- Continued.

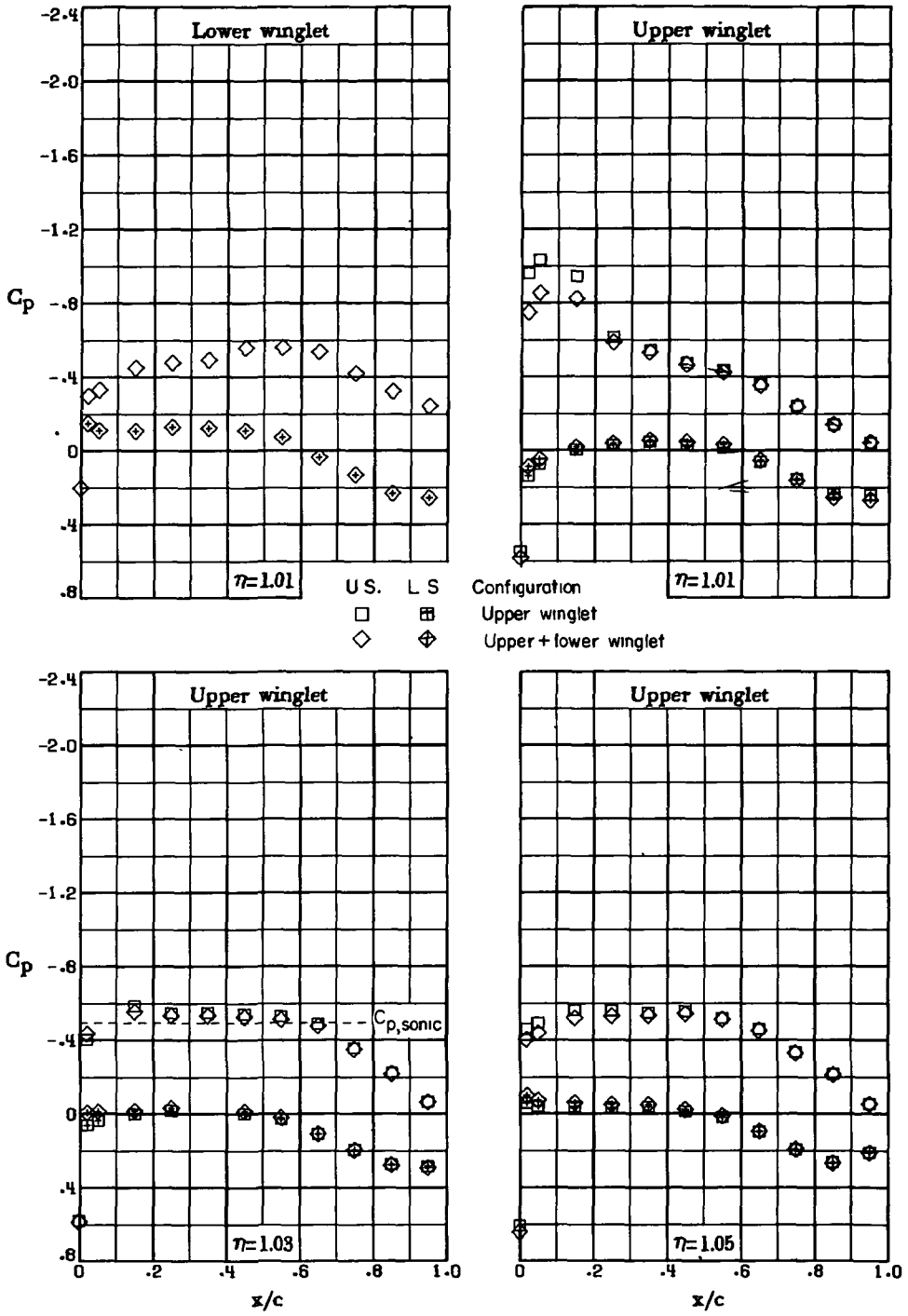

(c) $M_\infty = 0.78$; $\alpha \approx 2.5^\circ$. Concluded.

Figure 13.- Continued.

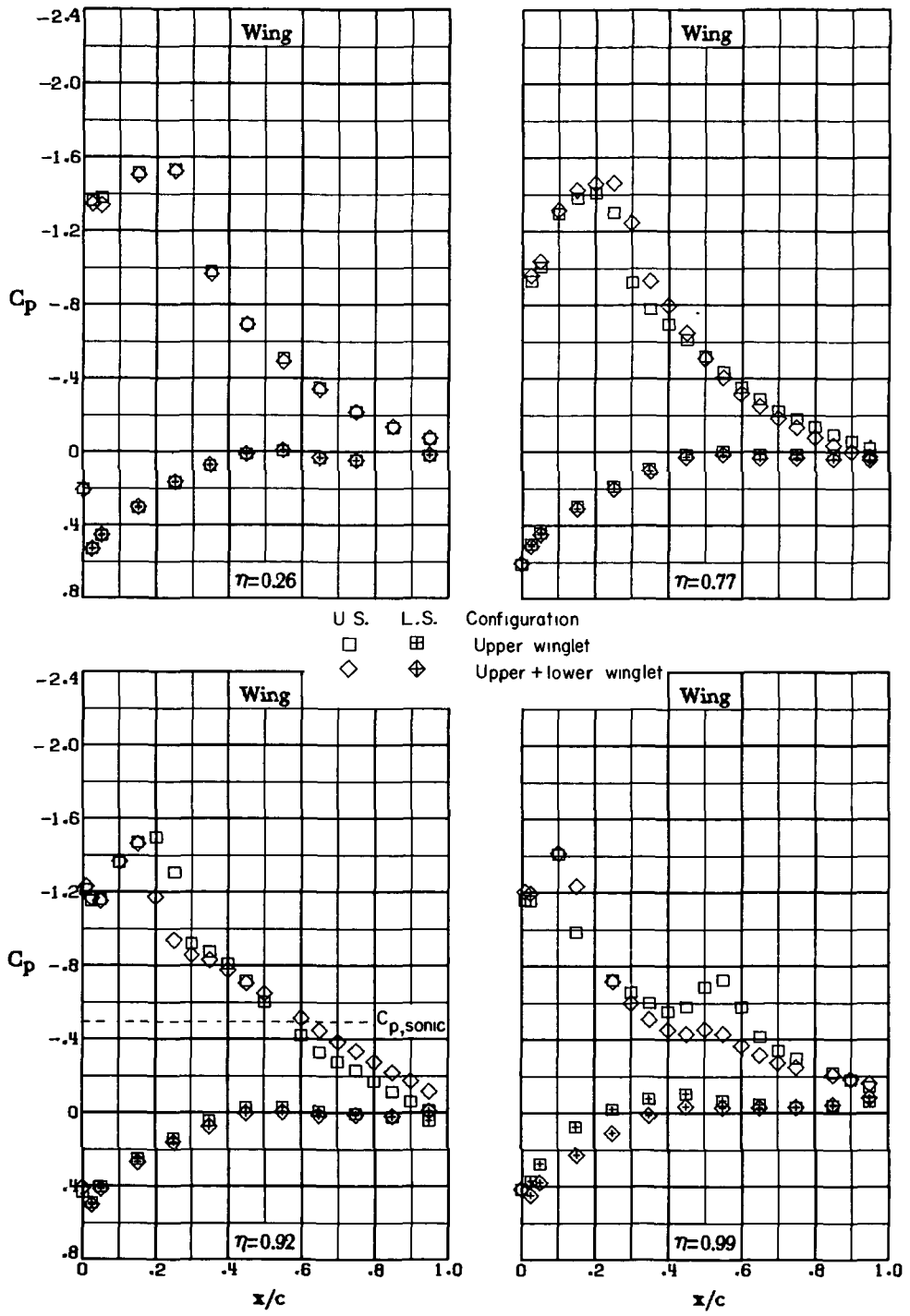

(d) $M_\infty = 0.78$; $\alpha \approx 7.2^\circ$.

Figure 13.- Continued.

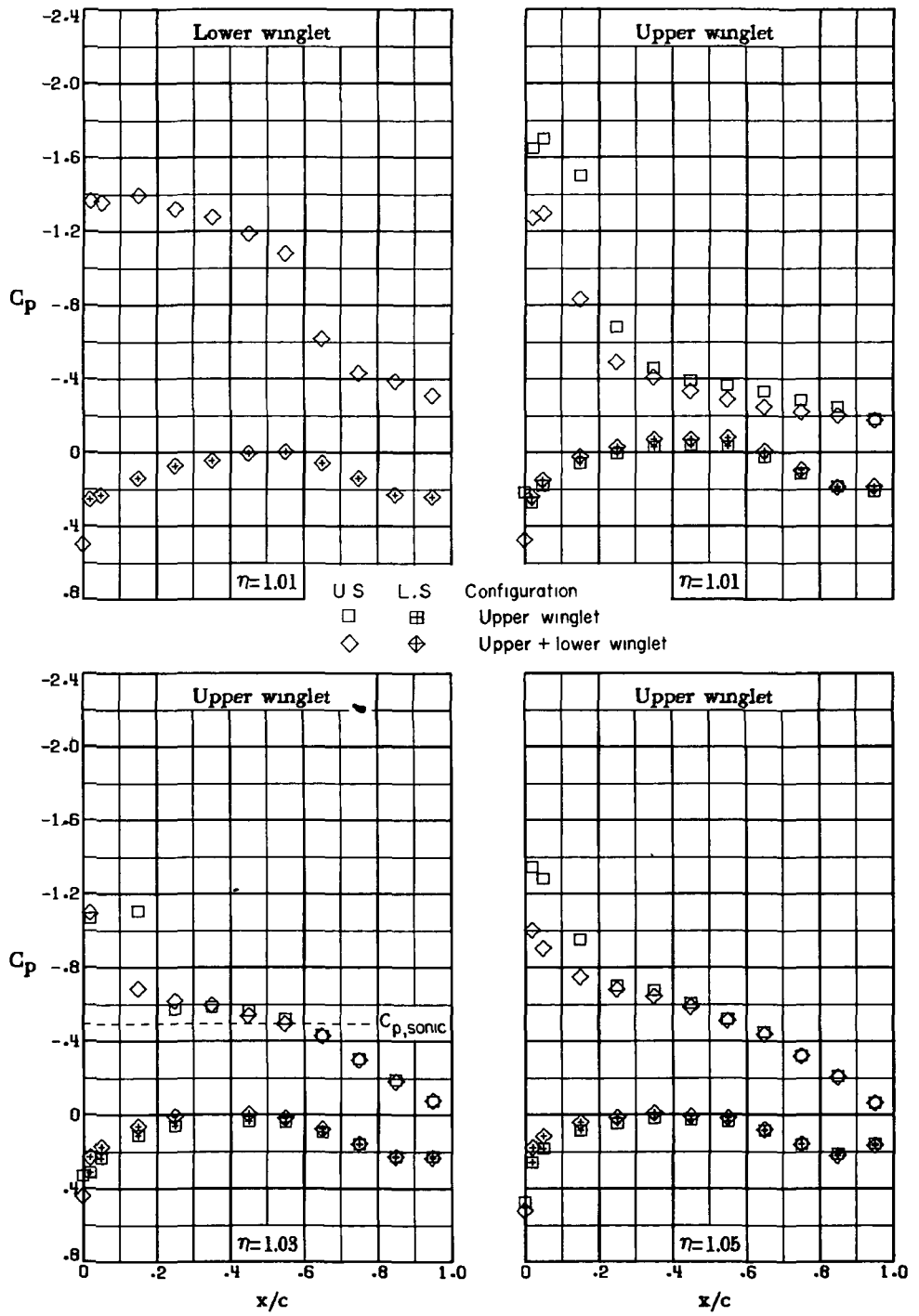

(d) $M_\infty = 0.78$; $\alpha \approx 7.2^\circ$. Concluded.

Figure 13.- Concluded.

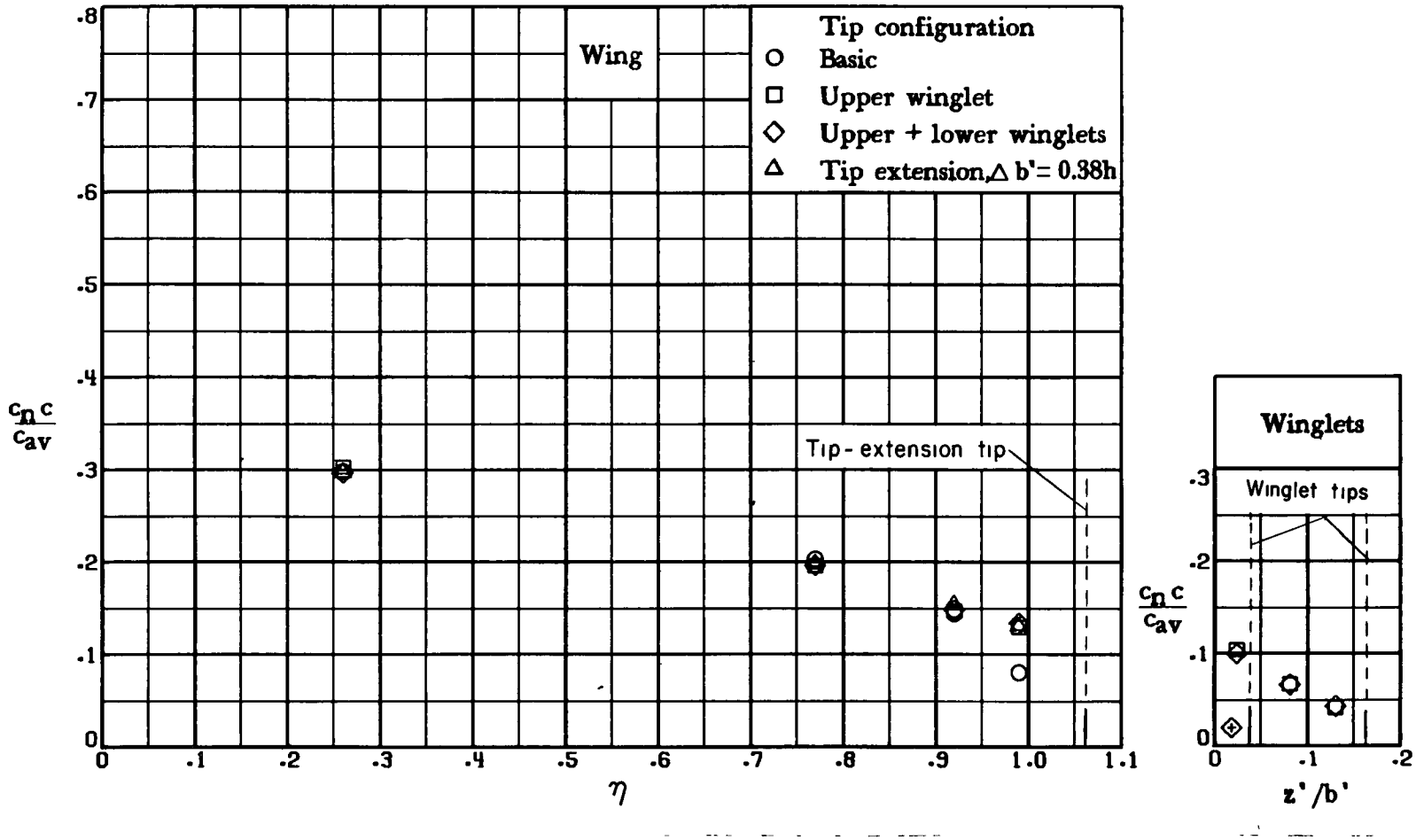

(a) $M_\infty = 0.70$; $\alpha = 0^\circ$.

Figure 14.- Comparison of spanwise load distributions for various configurations. (⊕ indicates lower-winglet data.)

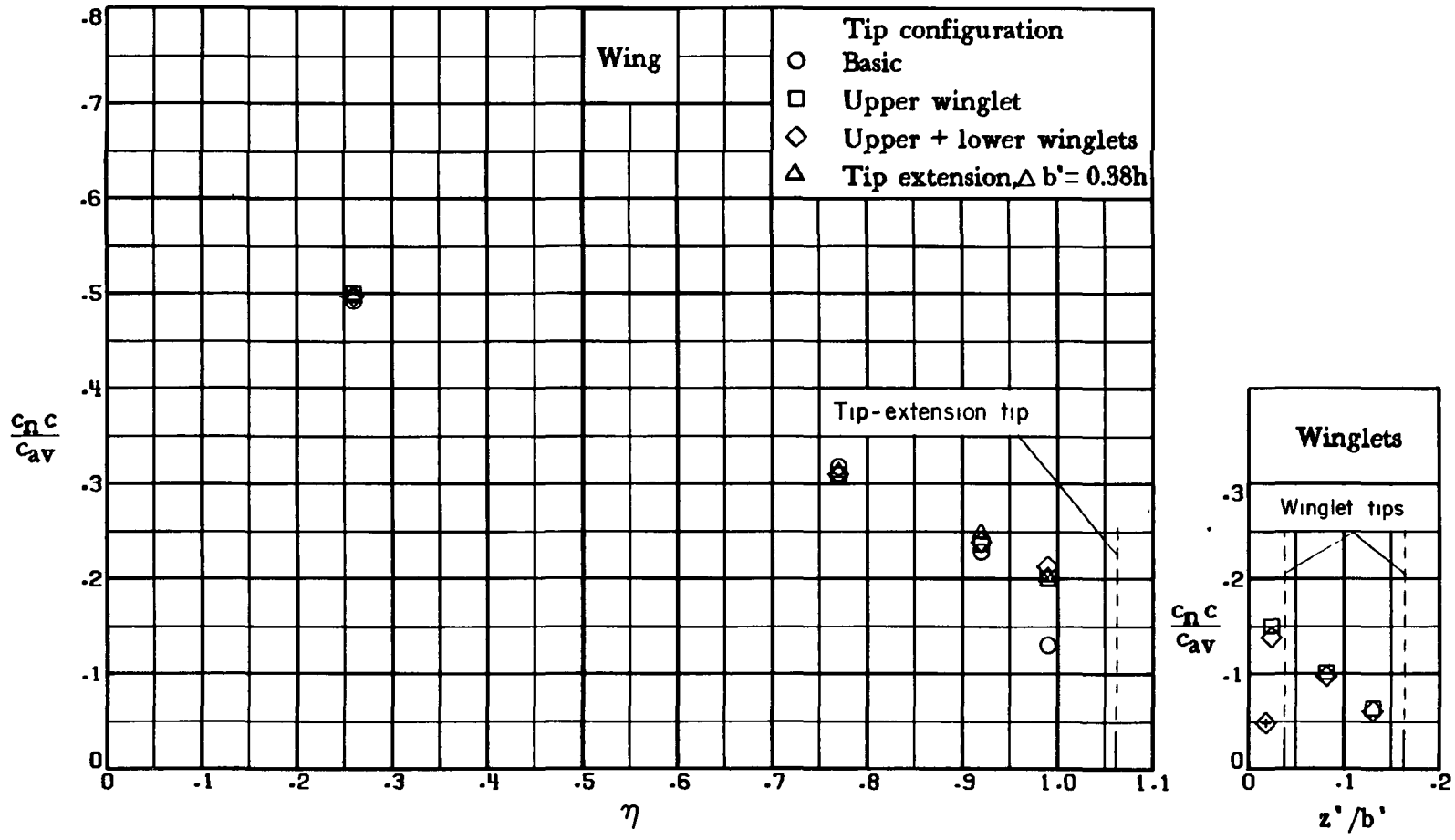

(b) $M_\infty = 0.70$; $\alpha = 2.0^\circ$.

Figure 14.- Continued.

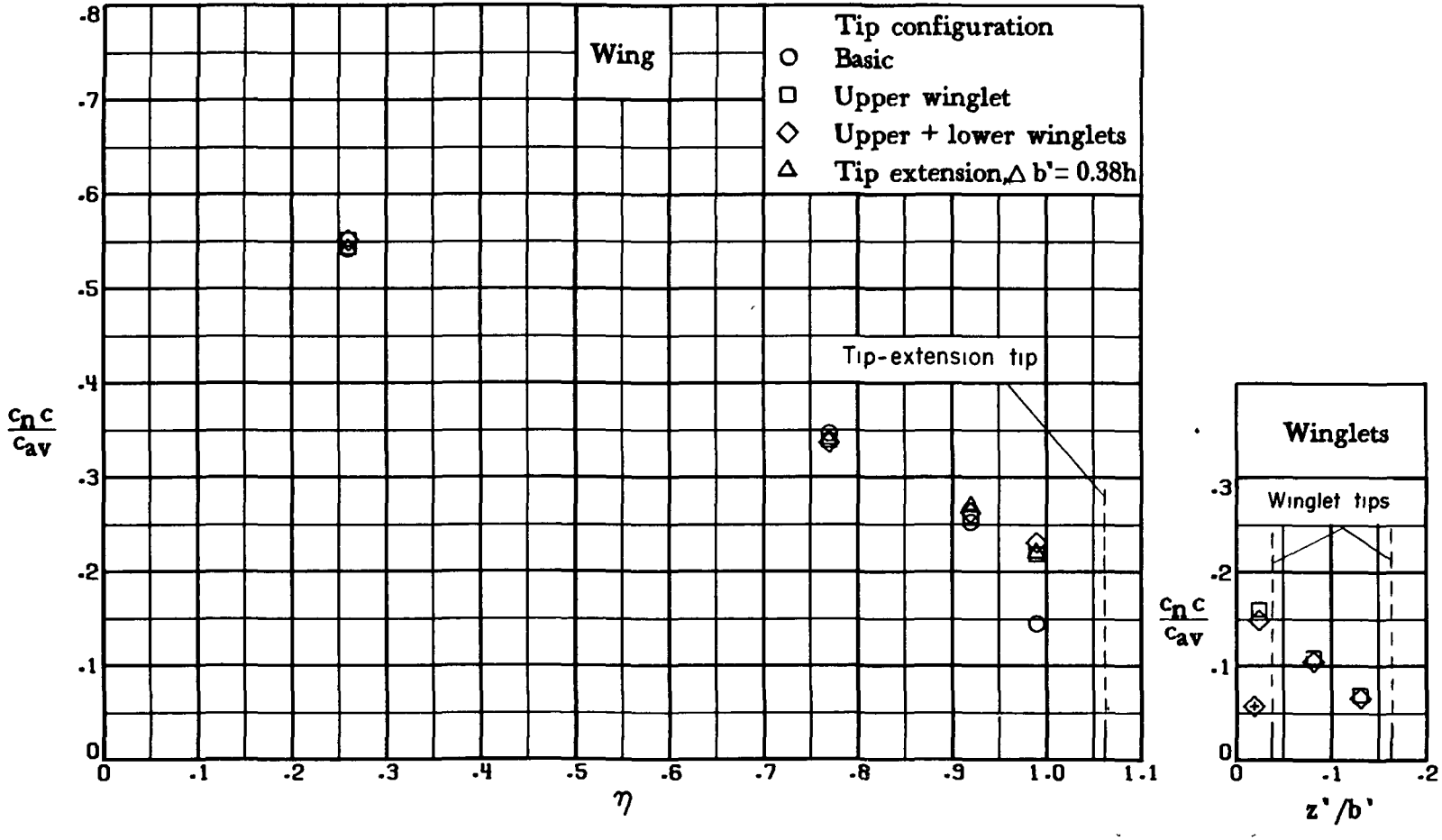

(c) $M_\infty = 0.70$; $\alpha = 2.5^\circ$.

Figure 14.- Continued.

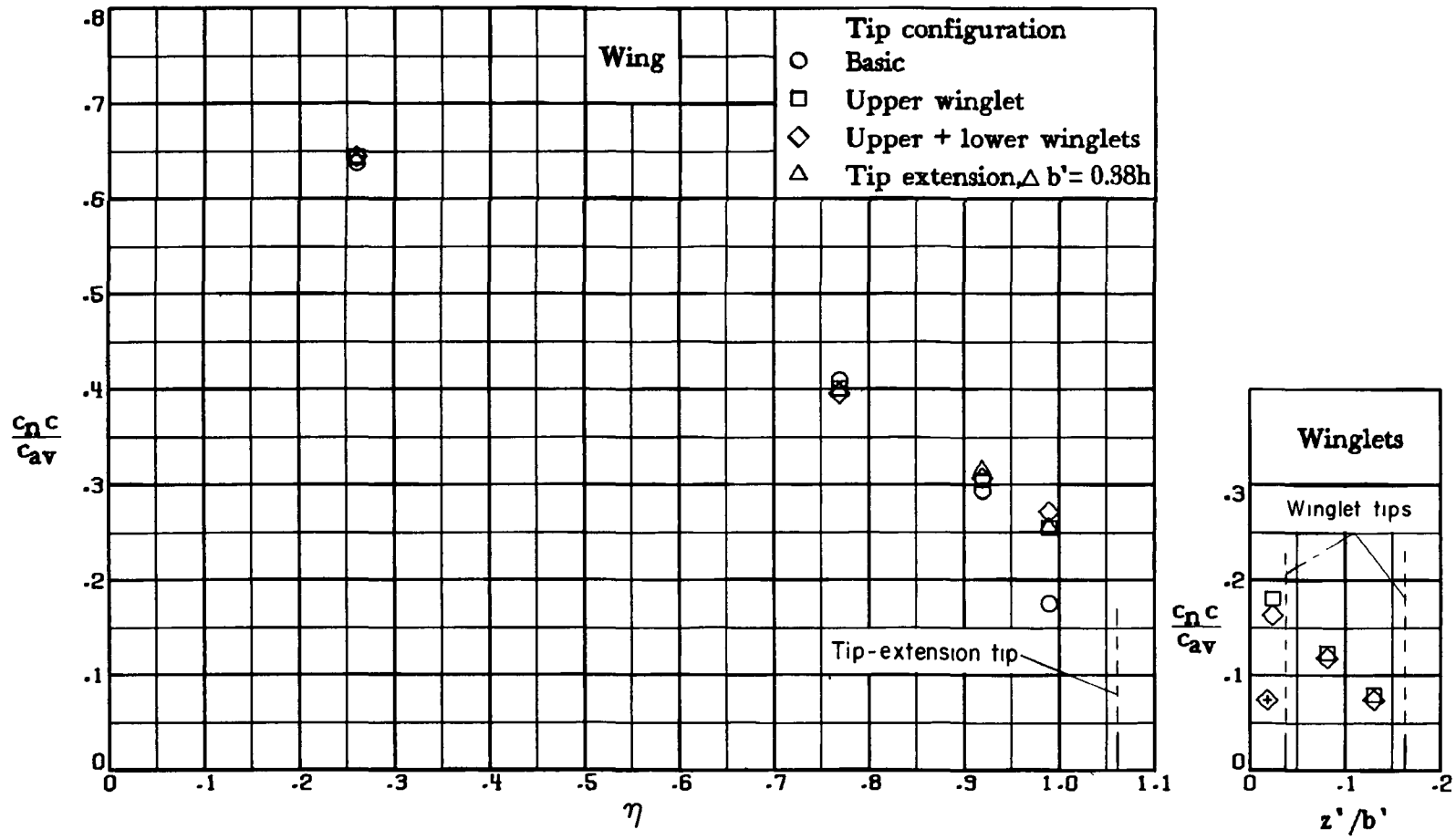

(d) $M_\infty = 0.70$; $\alpha = 3.5^\circ$.

Figure 14.- Continued.

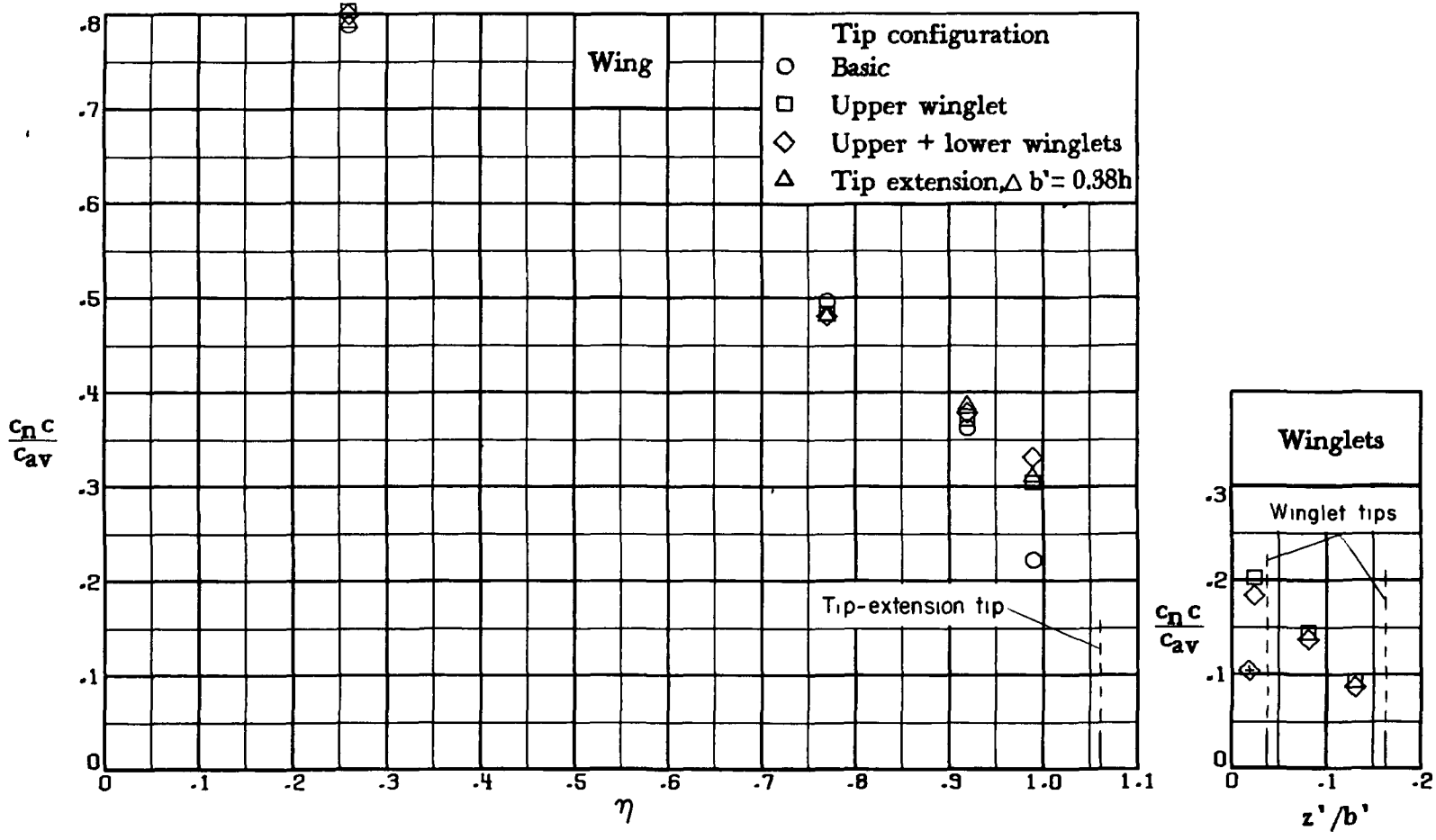

(e) $M_\infty = 0.70$; $\alpha = 5.0^\circ$.

Figure 14.- Continued.

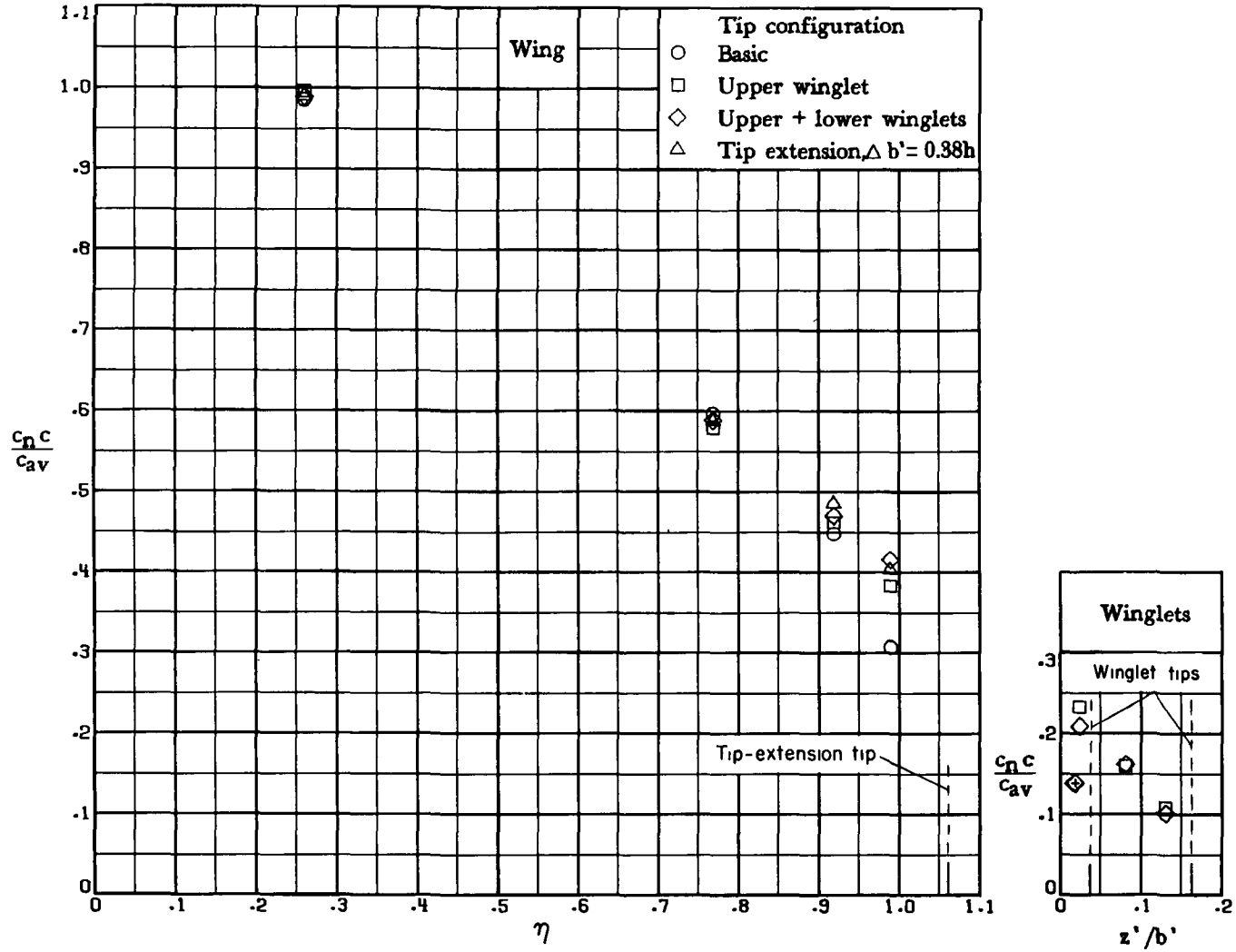

(f) $M_\infty = 0.70$; $\alpha \approx 7.2^\circ$.

Figure 14.- Continued.

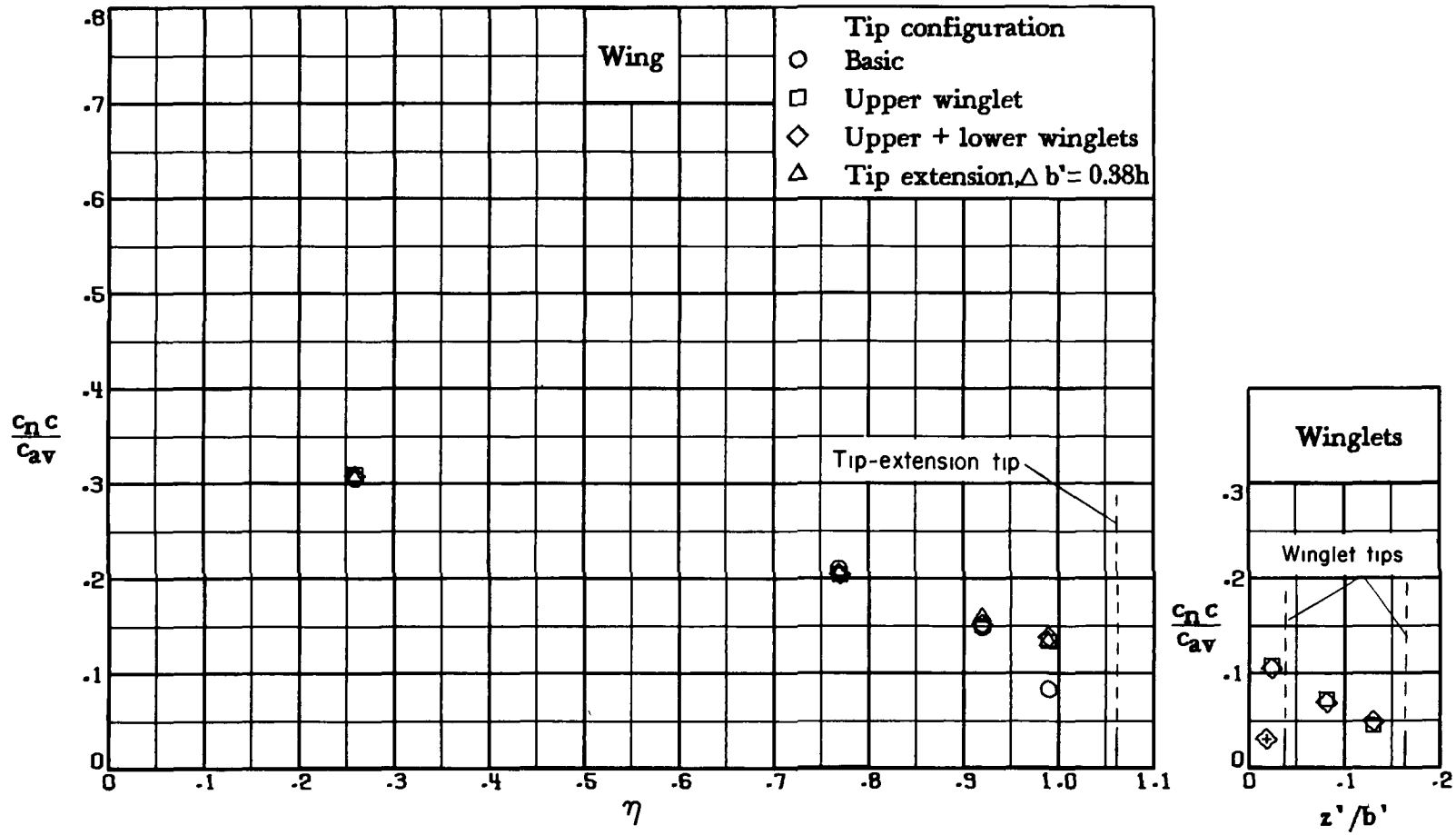

(g) $M_\infty = 0.75$; $\alpha = 0^\circ$.

Figure 14.- Continued.

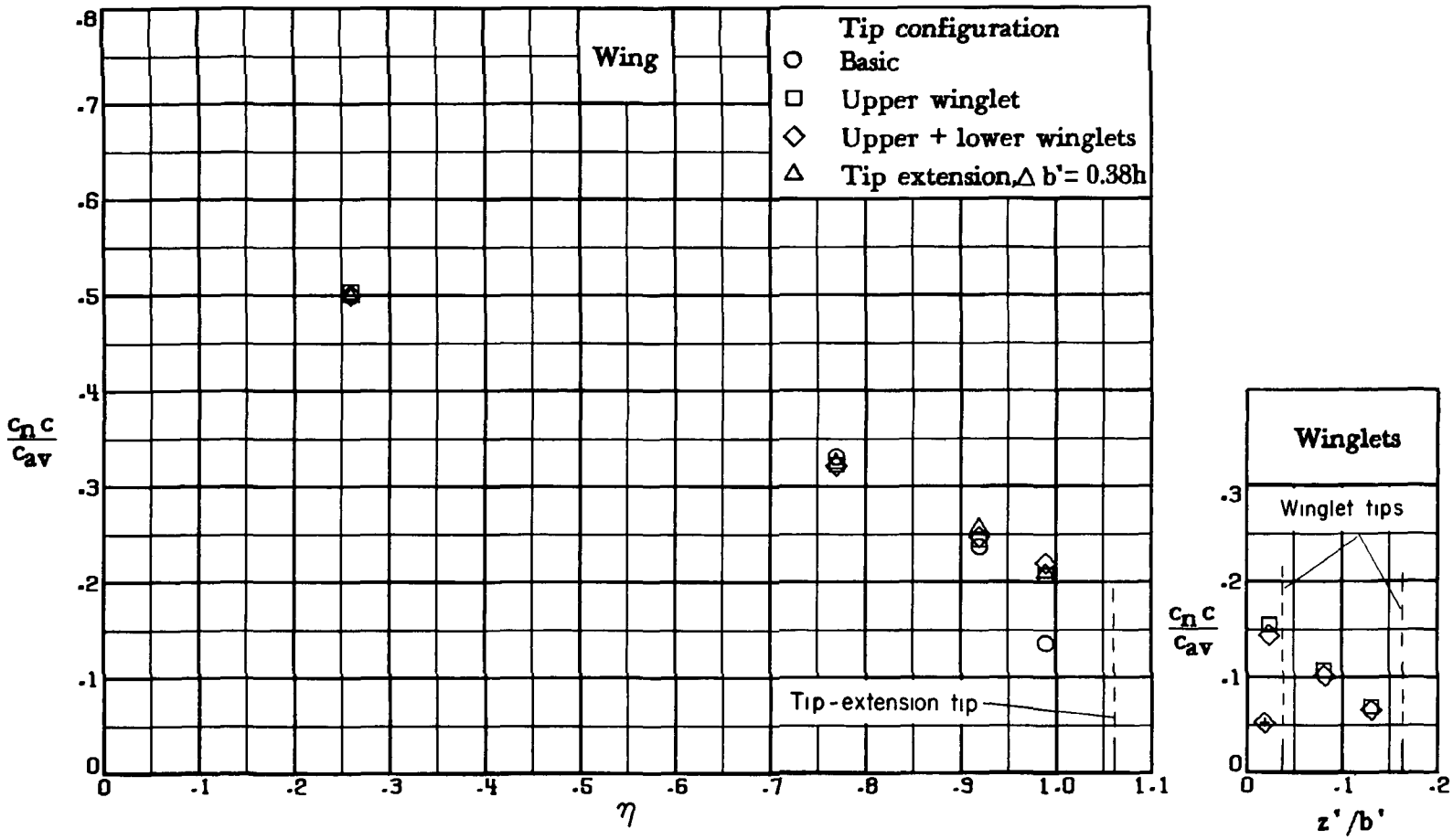

(h) $M_\infty = 0.75$; $\alpha = 2.0^\circ$.

Figure 14.- Continued.

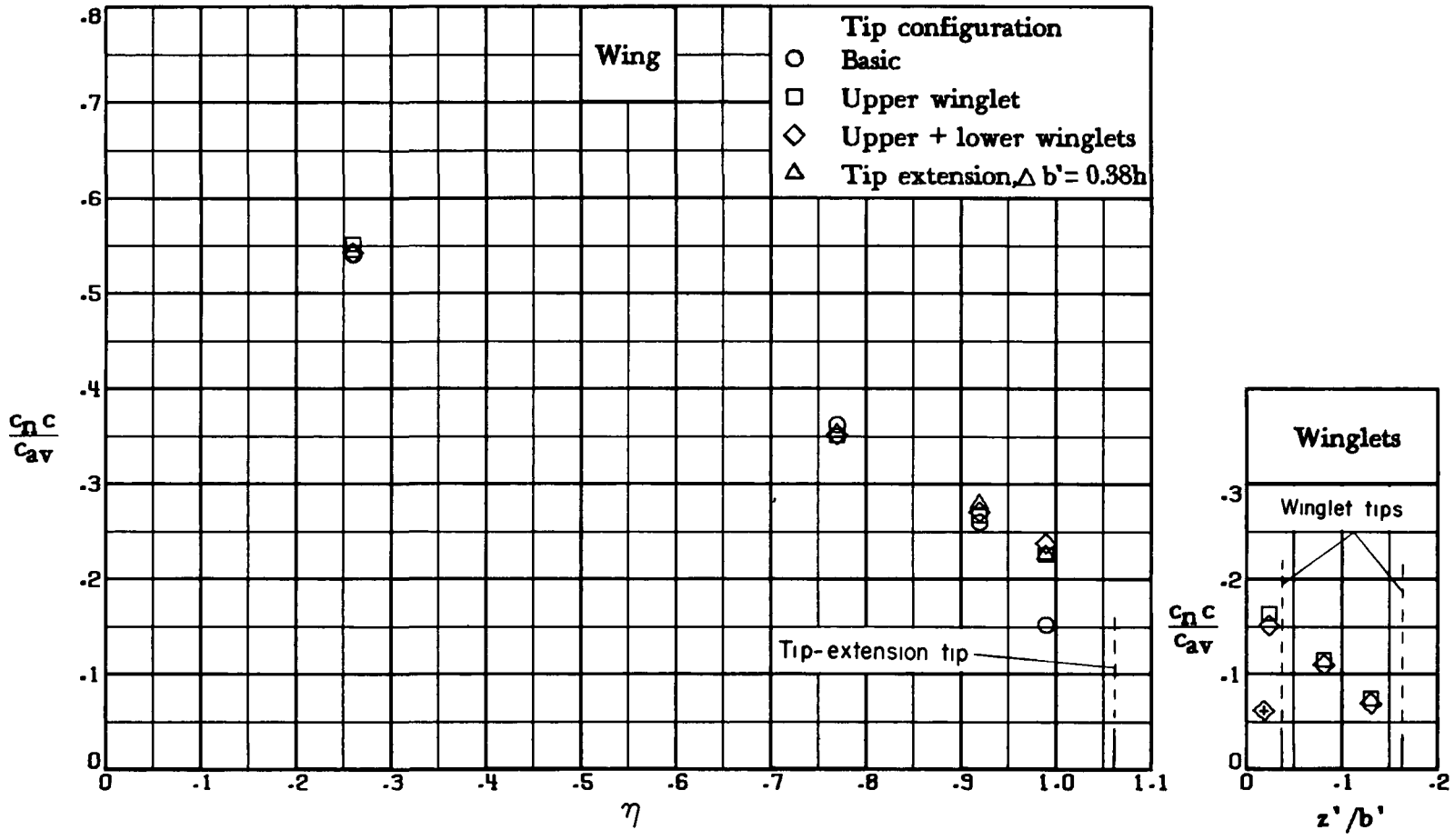

(i) $M_\infty = 0.75$; $\alpha = 2.5^\circ$.

Figure 14.- Continued.

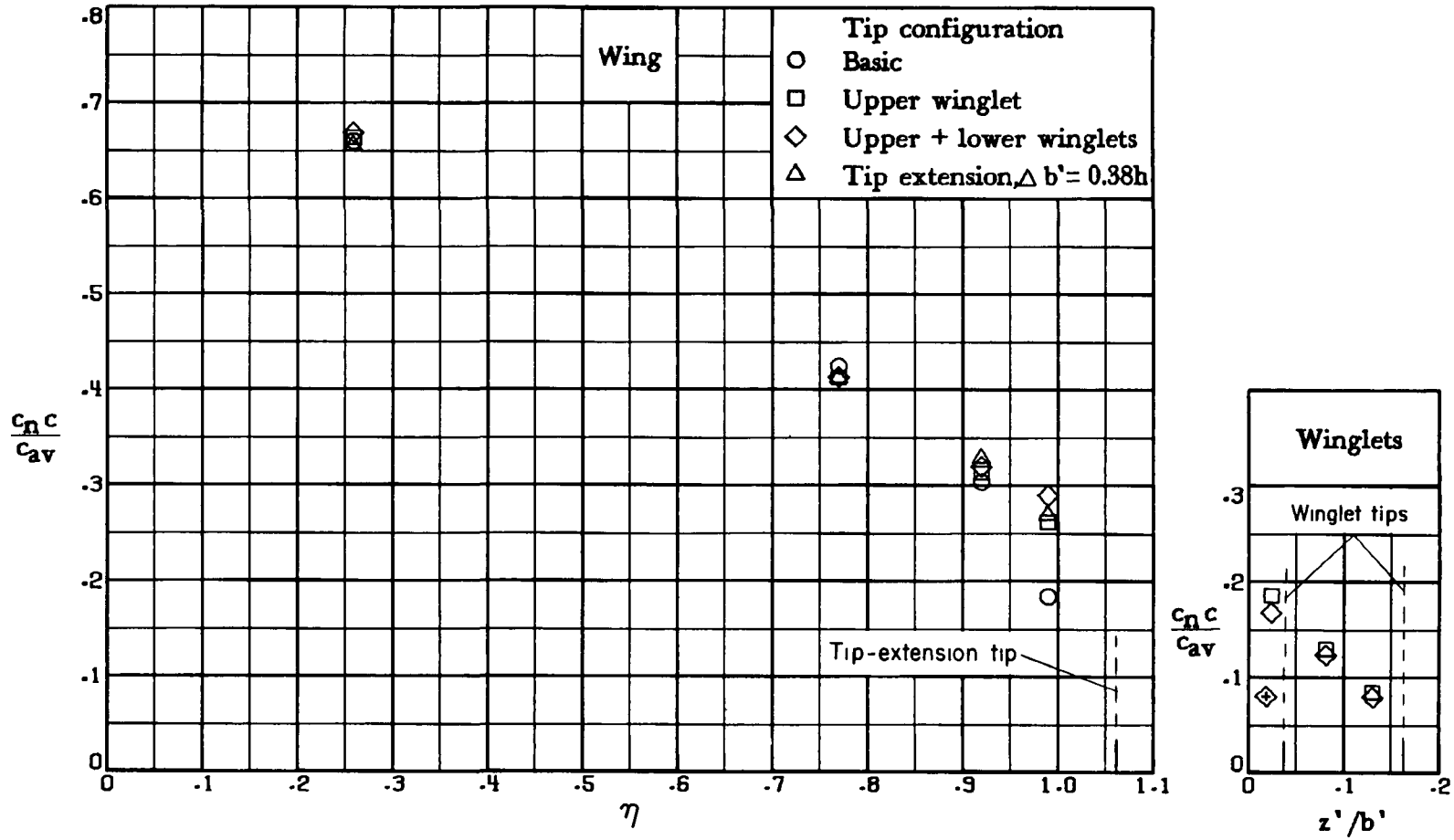

(j) $M_\infty = 0.75$; $\alpha = 3.5^\circ$.

Figure 14.- Continued.

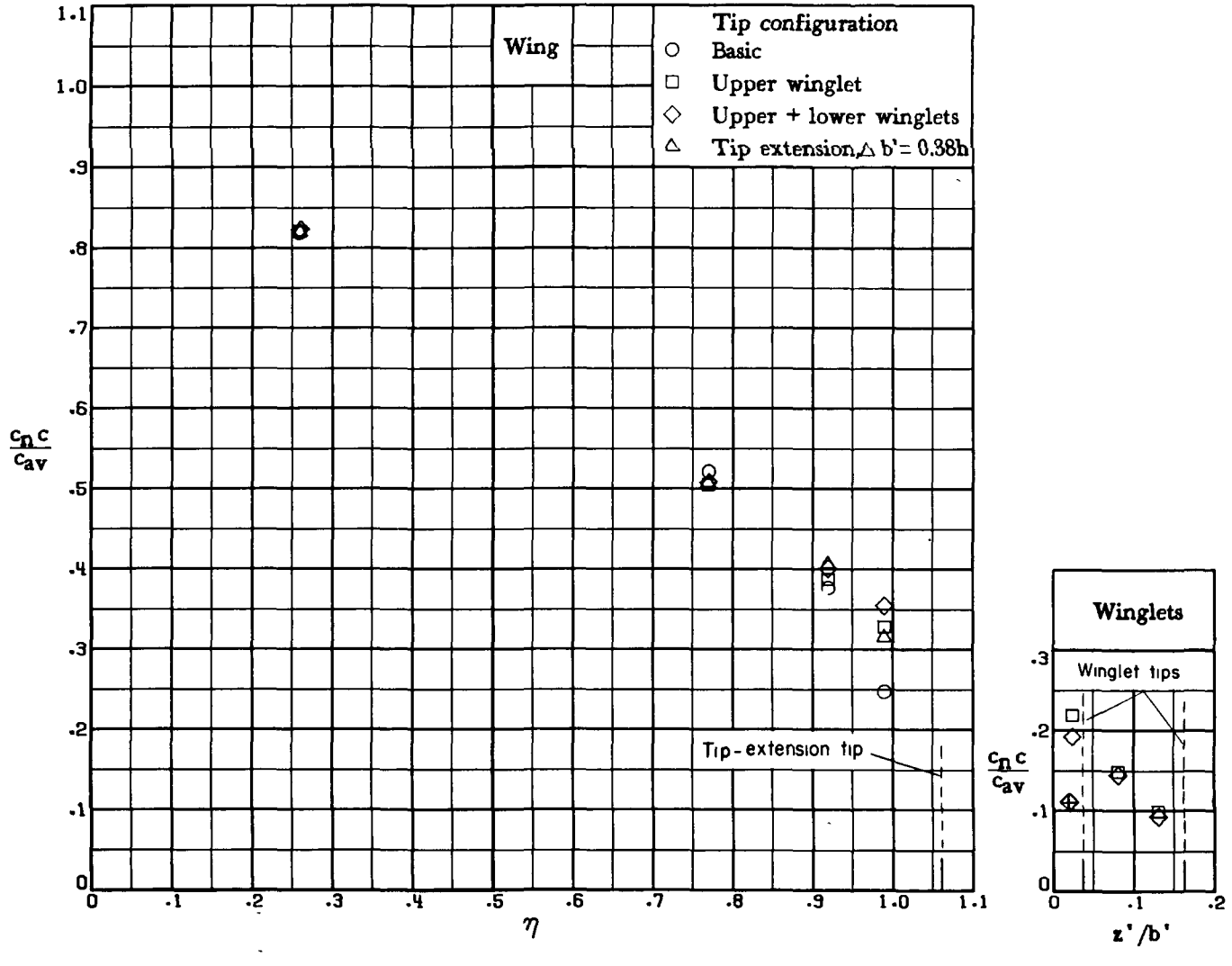

(k) $M_\infty = 0.75$; $\alpha = 5.0^\circ$.

Figure 14.- Continued.

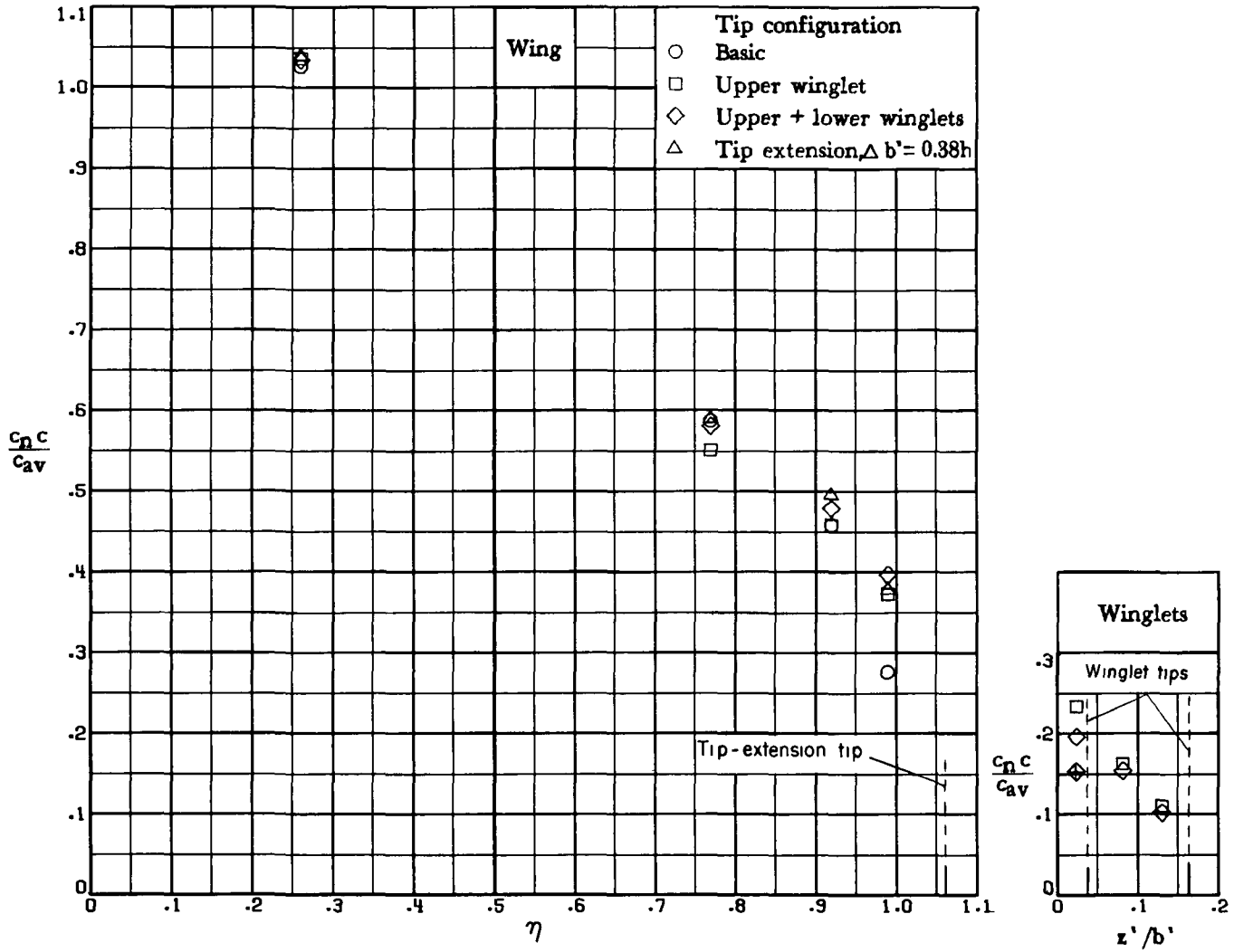

(1) $M_\infty = 0.75$; $\alpha \approx 7.2^\circ$.

Figure 14.- Continued.

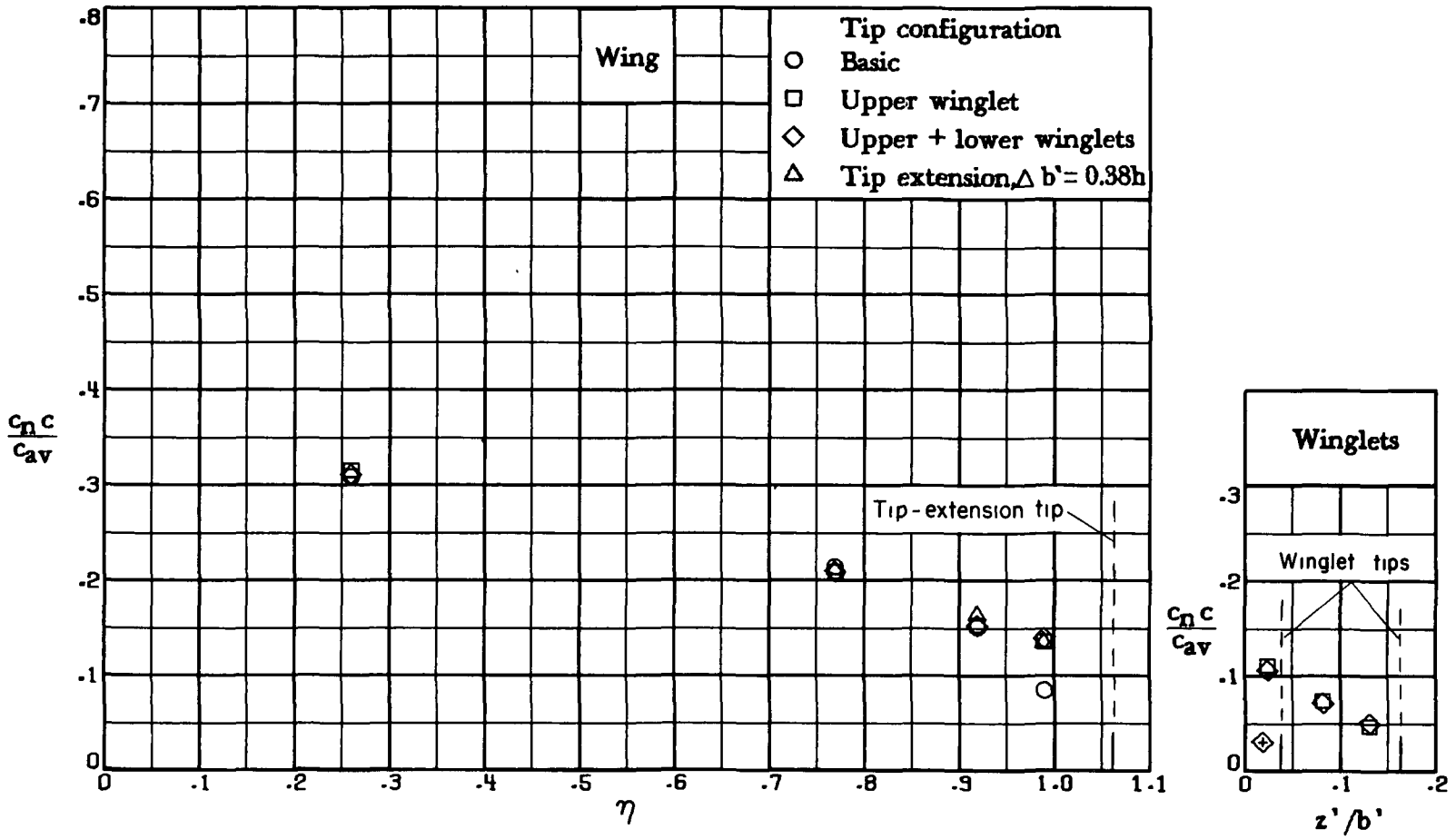

(m) $M_\infty = 0.78$; $\alpha = 0^o$.

Figure 14.- Continued.

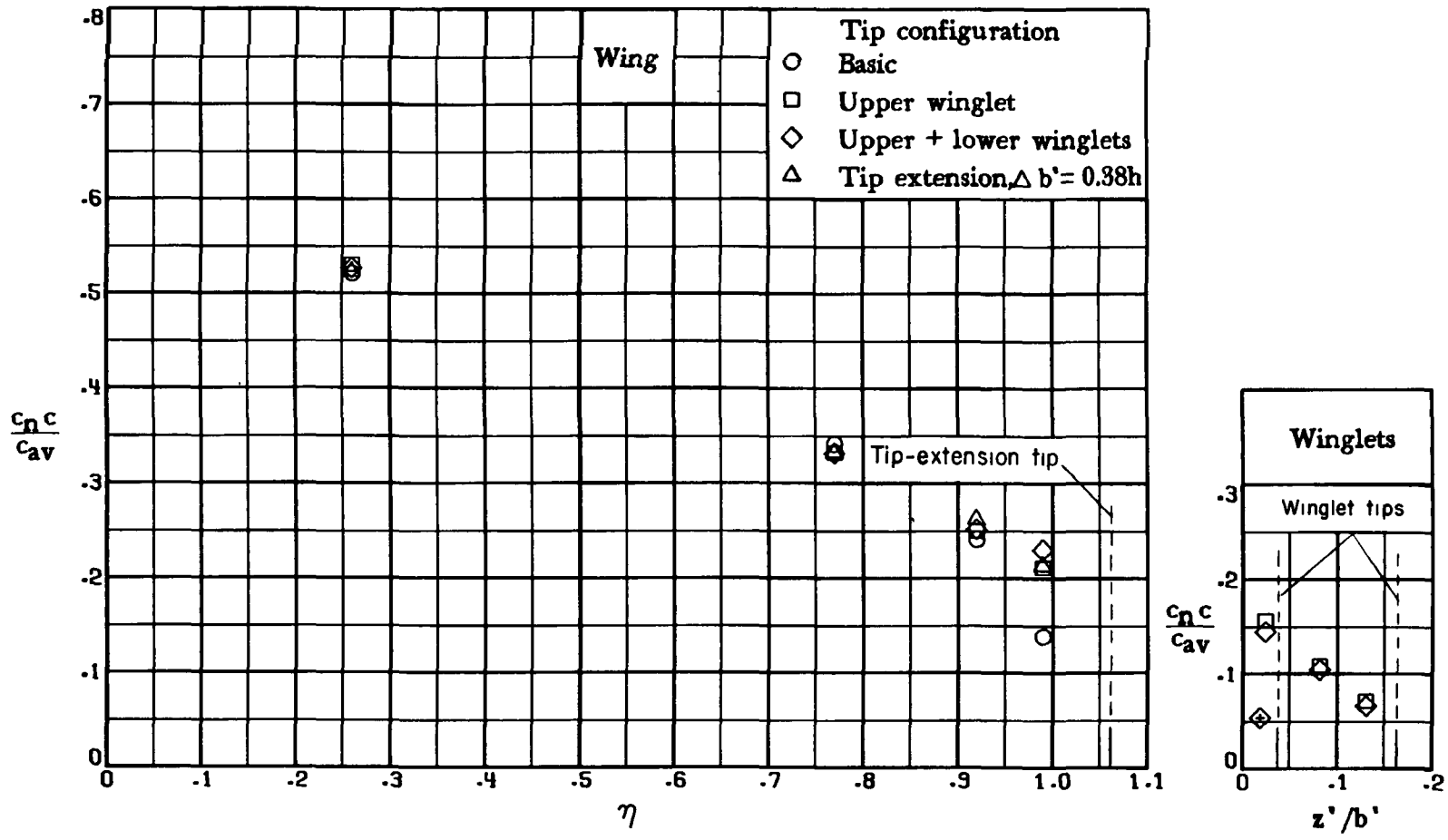

(n) $M_\infty = 0.78$; $\alpha = 2.0^\circ$.

Figure 14.- Continued.

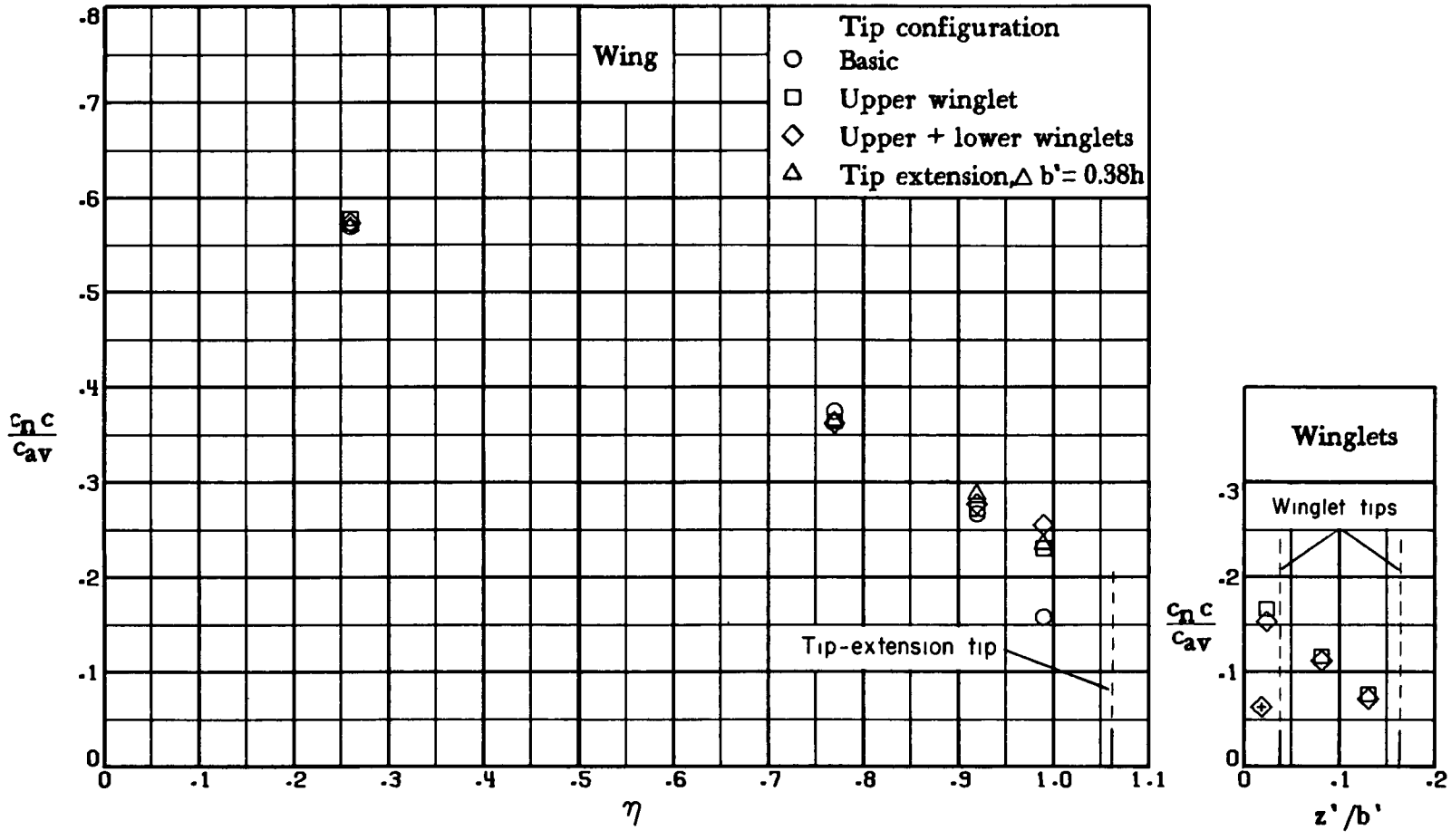

(o) $M_\infty = 0.78$; $\alpha = 2.5^\circ$.

Figure 14.- Continued.

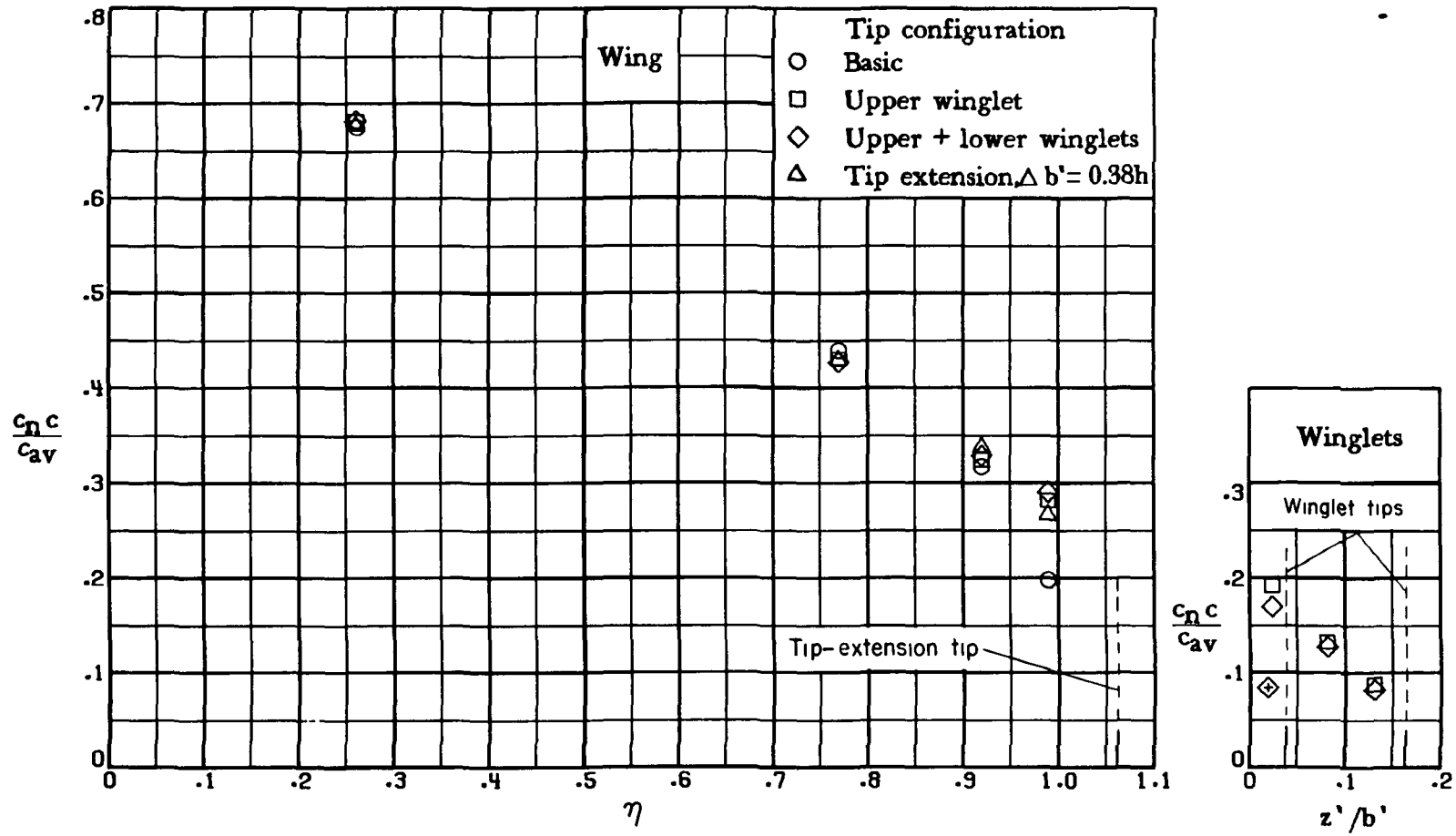

(p) $M_\infty = 0.78$; $\alpha = 3.5^\circ$.

Figure 14.- Continued.

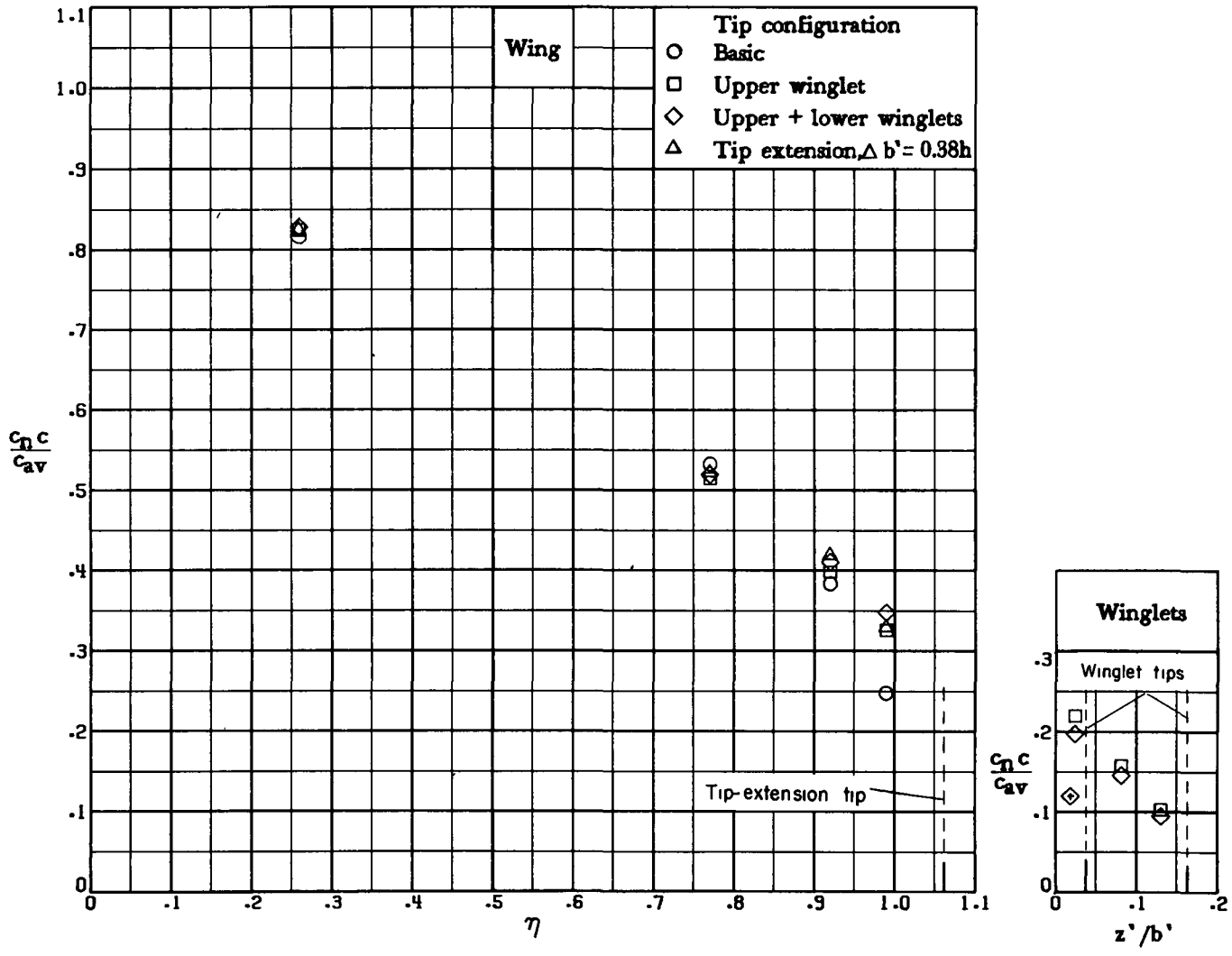

(q) $M_\infty = 0.78$; $\alpha = 5.0^\circ$.

Figure 14.- Continued.

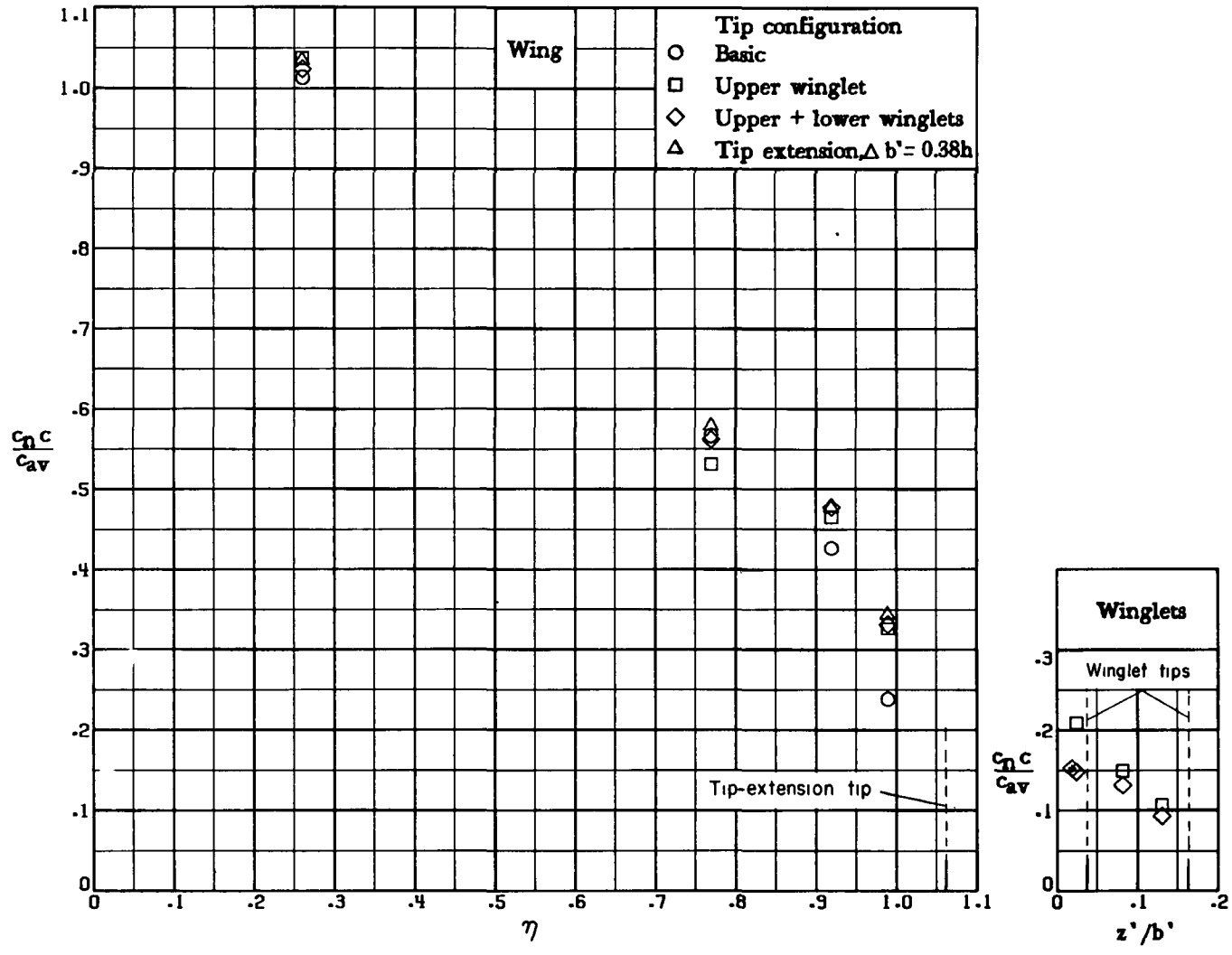

(r) $M_\infty = 0.78$; $\alpha \approx 7.2^\circ$.

Figure 14.- Continued.

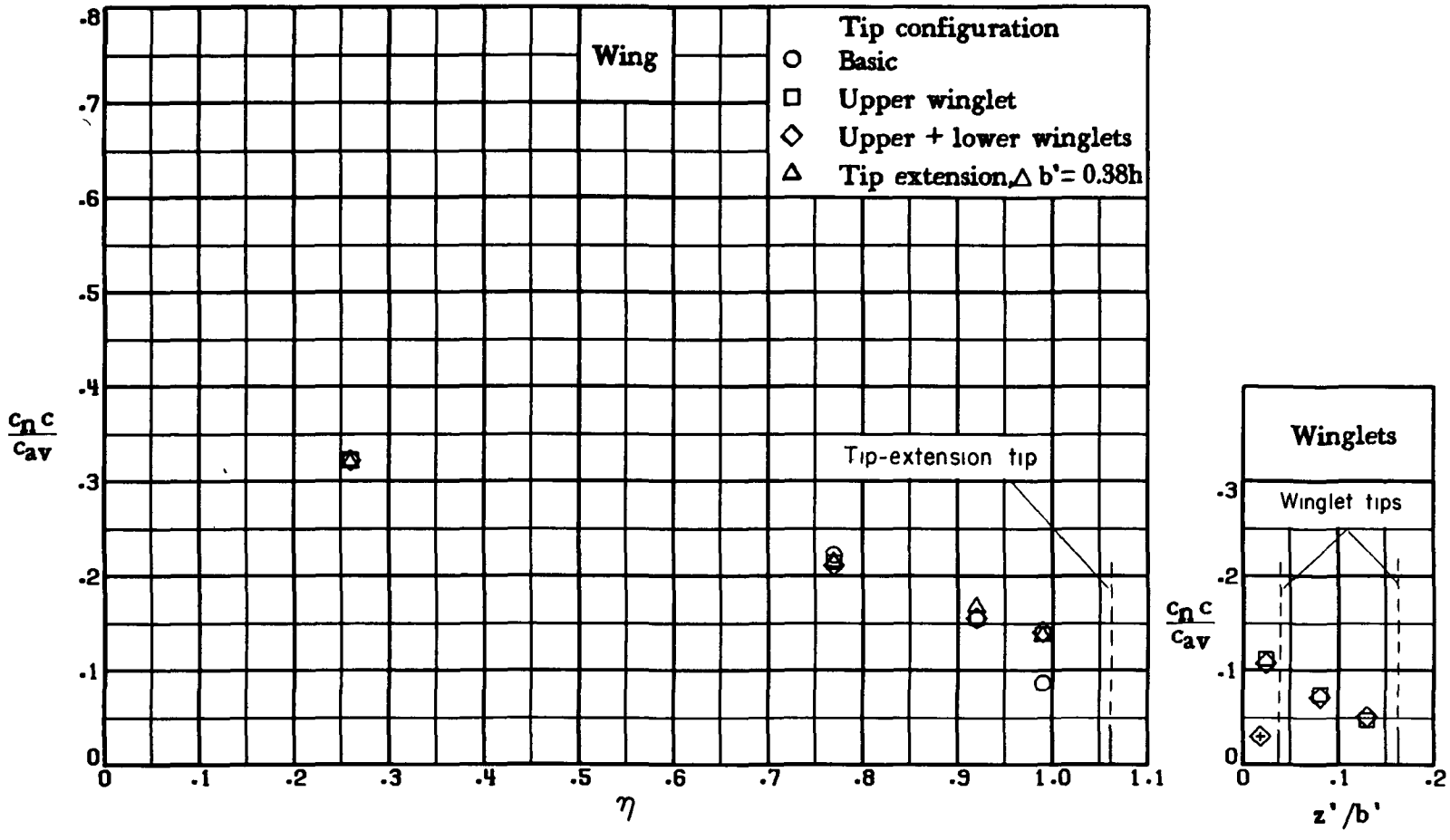

(s) $M_\infty = 0.80$; $\alpha = 0^o$.

Figure 14.- Continued.

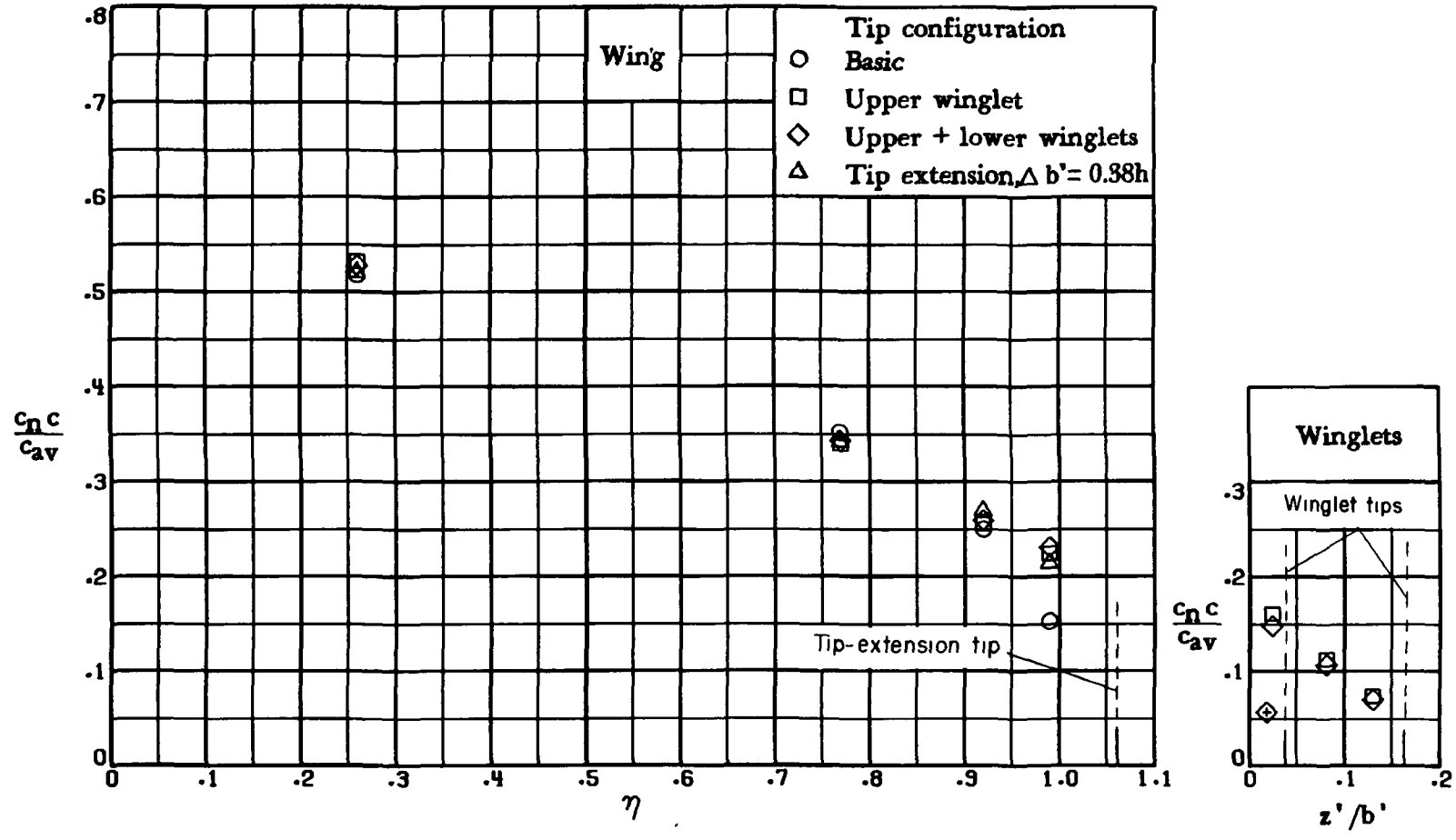

(t) $M_\infty = 0.80$; $\alpha \approx 2.0^\circ$.

Figure 14.- Continued.

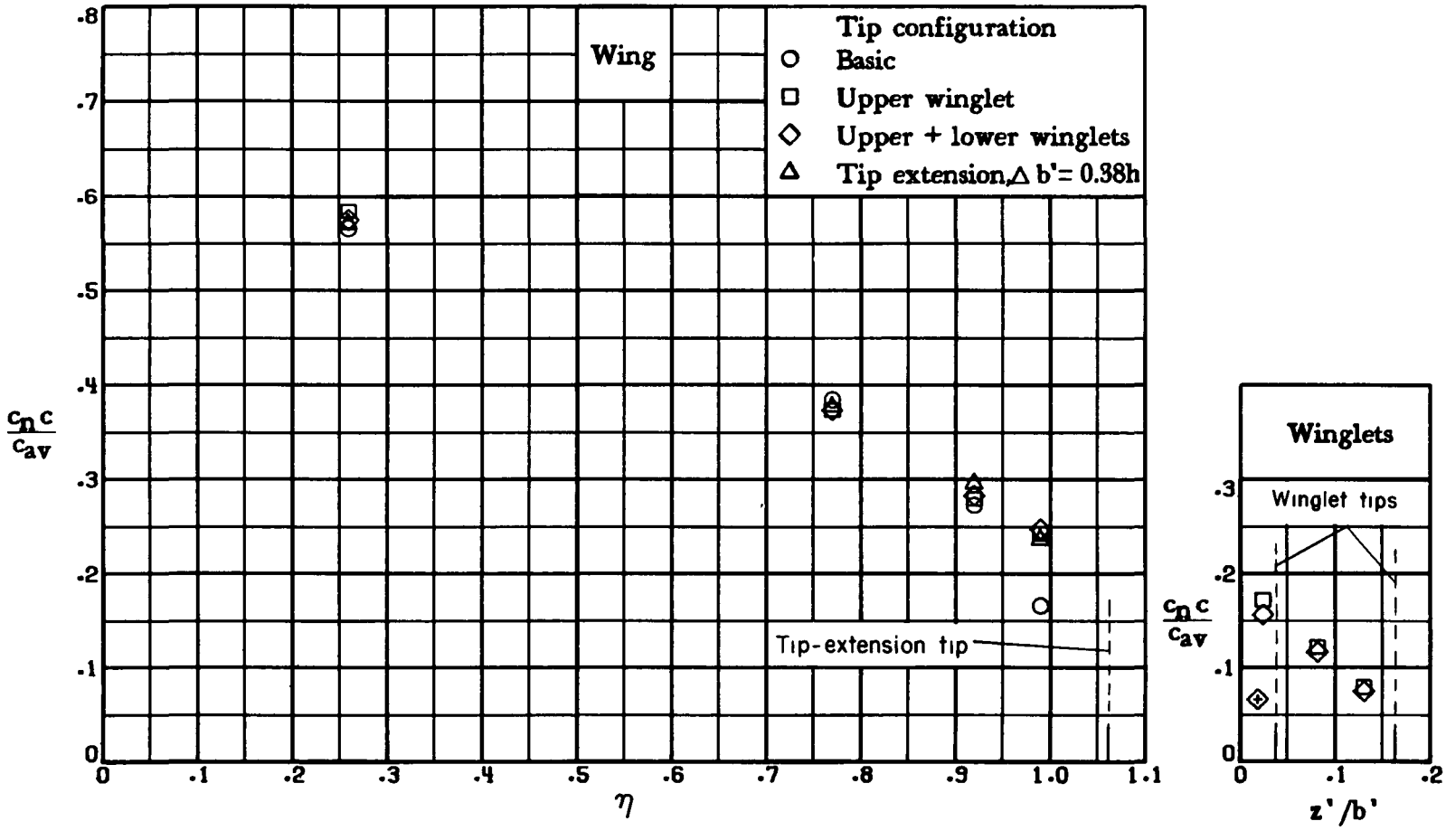

(u) $M_\infty = 0.80$; $\alpha = 2.5^\circ$.

Figure 14.- Continued.

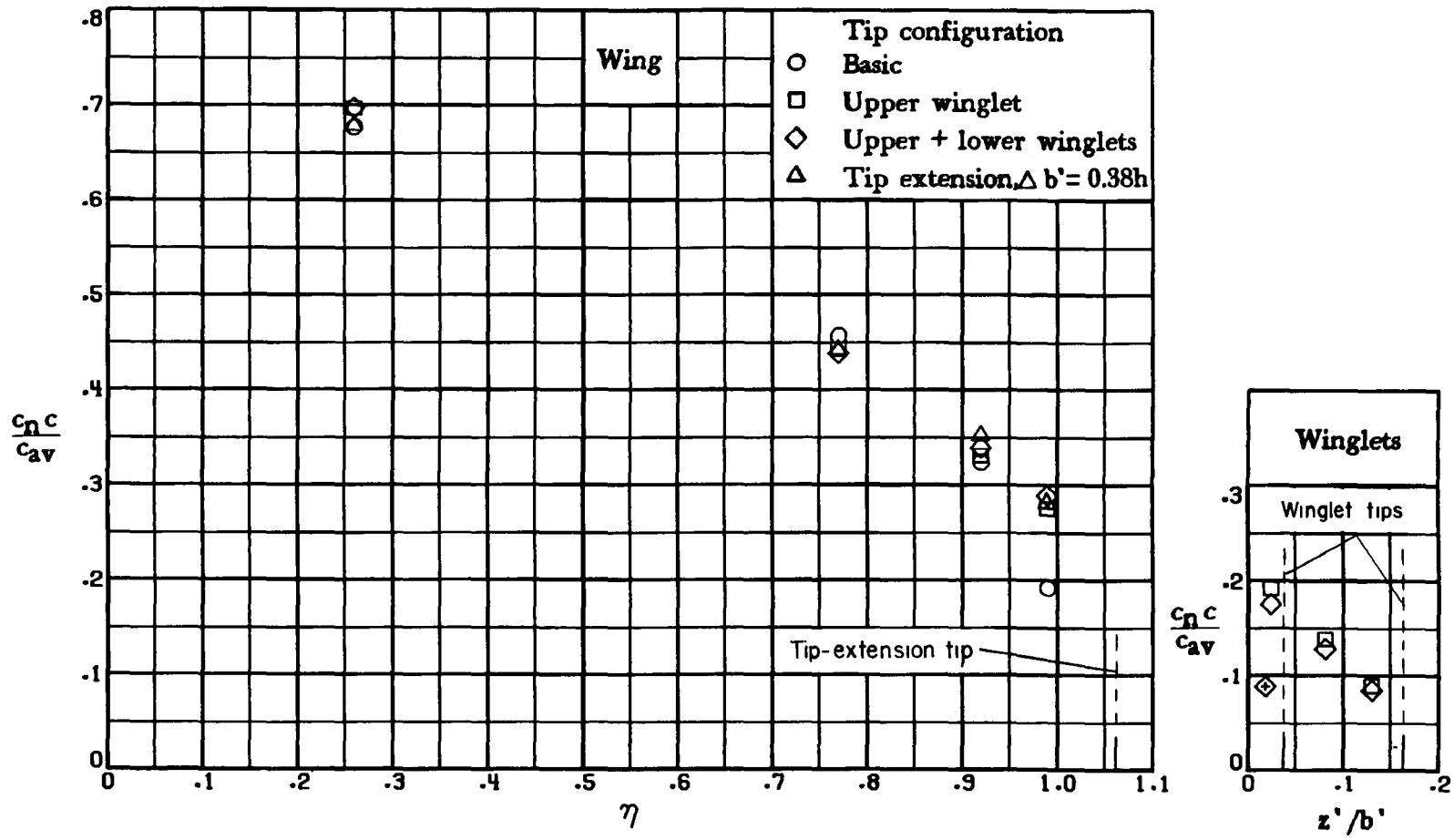

(v) $M_\infty = 0.80$; $\alpha = 3.5^\circ$.

Figure 14.- Continued.

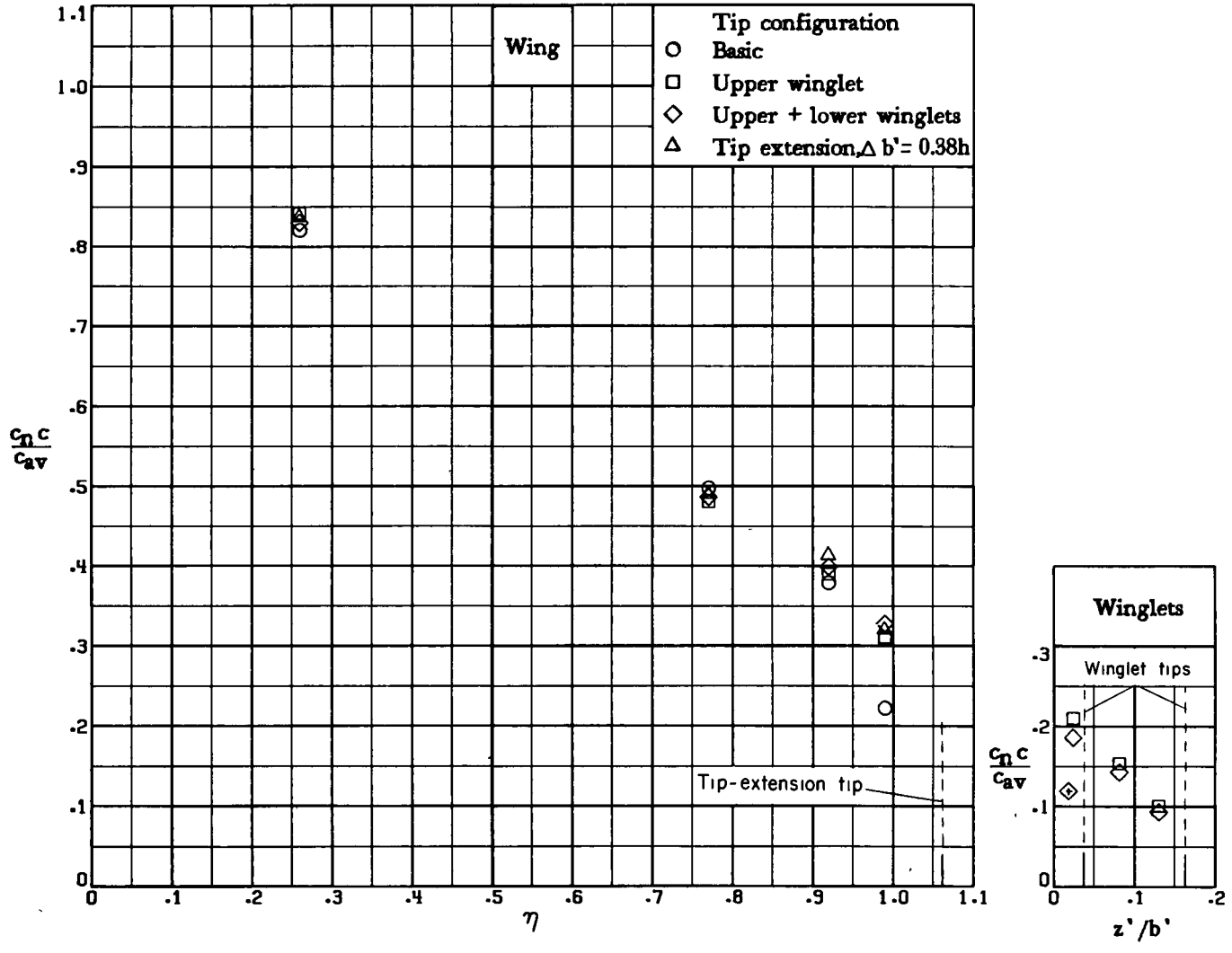

(w) $M_\infty = 0.80$; $\alpha \approx 5.0^\circ$.

Figure 14.- Continued.

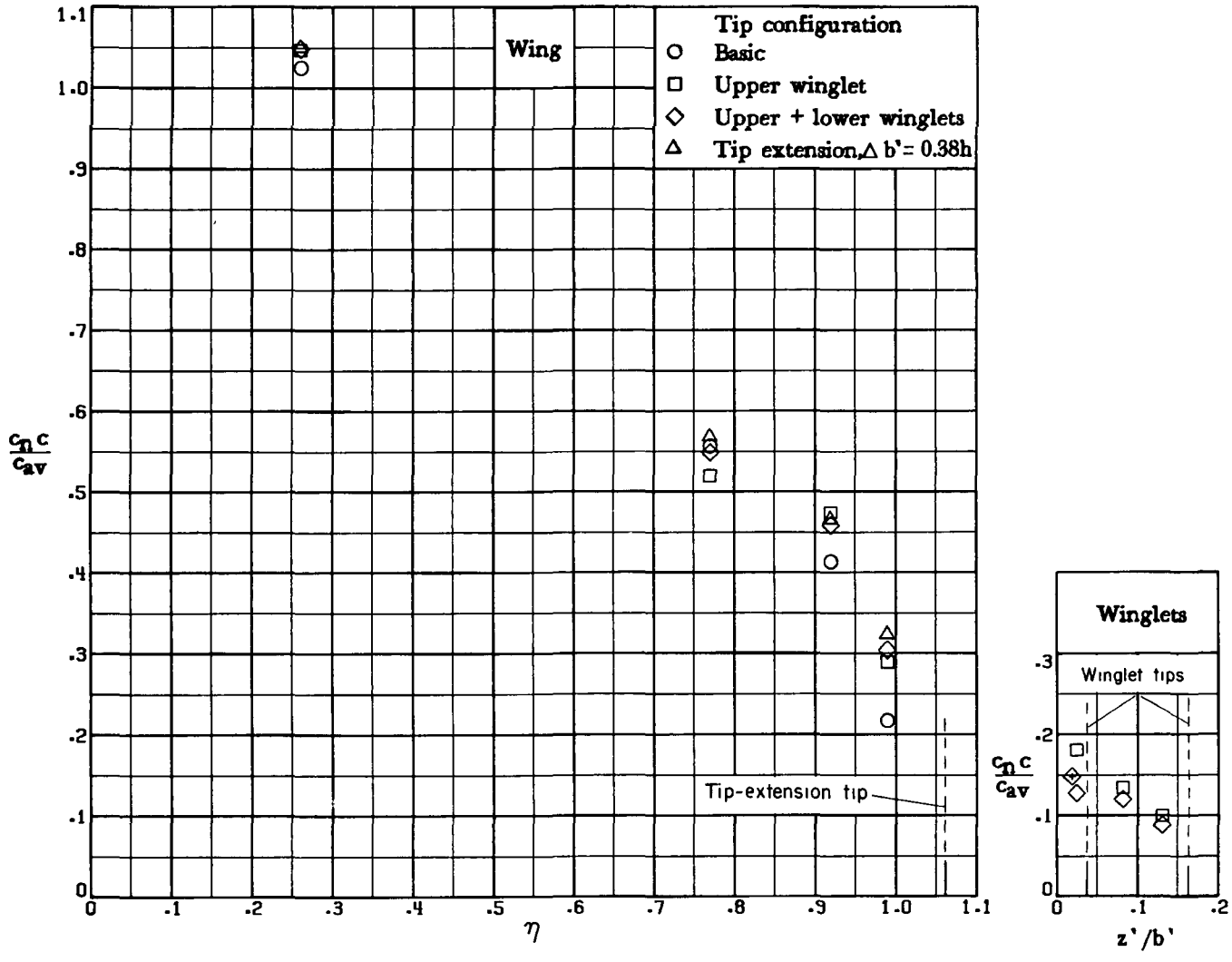

(x) $M_\infty = 0.80$; $\alpha \approx 7.2^\circ$.

Figure 14.- Concluded.

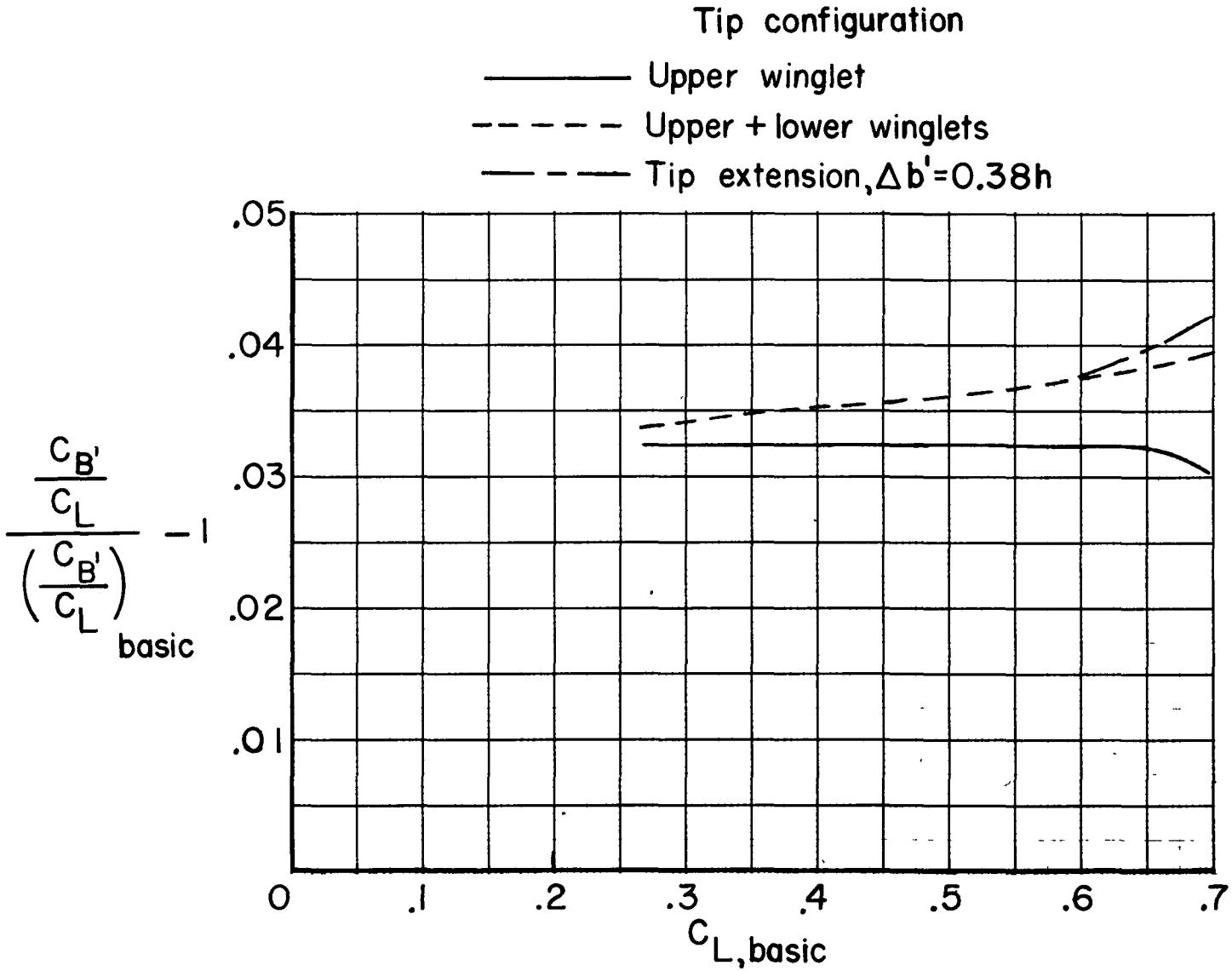

Figure 15.- Variation of incremental bending-moment coefficient with lift coefficient at wing-fuselage juncture. $M_\infty = 0.78$.

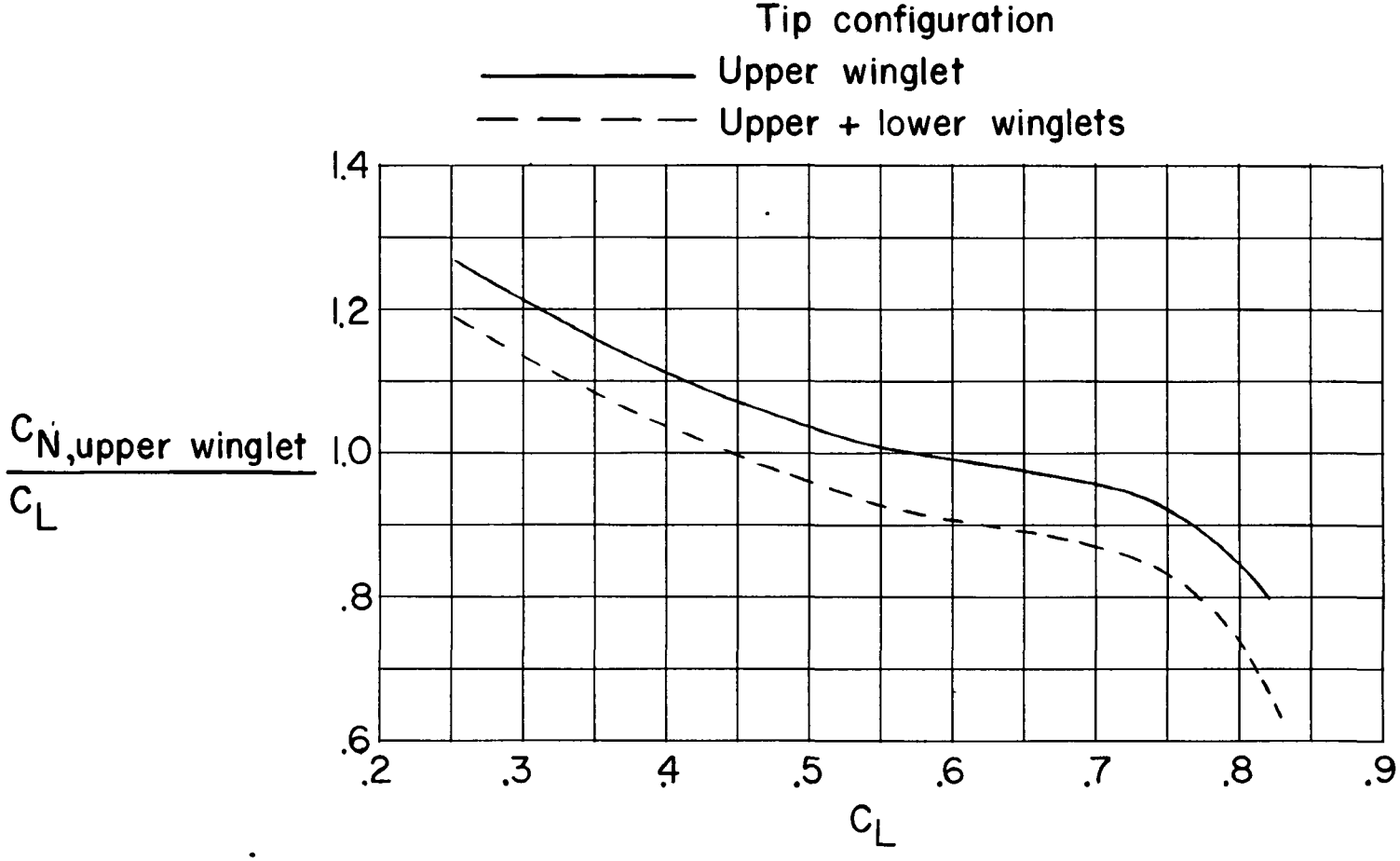

Figure 16.- Variations of ratios of normal-force coefficients for upper winglet to lift coefficient for total configuration. $M_\infty = 0.78$.

"The aeronautical and space activities of the United States shall be conducted so as to contribute . to the expansion of human knowledge of phenomena in the atmosphere and space The Administration shall provide for the widest practicable and appropriate dissemination of information concerning its activities and the results thereof."

—NATIONAL AERONAUTICS AND SPACE ACT OF 1958

NASA SCIENTIFIC AND TECHNICAL PUBLICATIONS

TECHNICAL REPORTS Scientific and technical information considered important, complete, and a lasting contribution to existing knowledge

TECHNICAL NOTES Information less broad in scope but nevertheless of importance as a contribution to existing knowledge

TECHNICAL MEMORANDUMS Information receiving limited distribution because of preliminary data, security classification, or other reasons Also includes conference proceedings with either limited or unlimited distribution.

CONTRACTOR REPORTS Scientific and technical information generated under a NASA contract or grant and considered an important contribution to existing knowledge

TECHNICAL TRANSLATIONS Information published in a foreign language considered to merit NASA distribution in English

SPECIAL PUBLICATIONS Information derived from or of value to NASA activities Publications include final reports of major projects, monographs, data compilations, handbooks, sourcebooks, and special bibliographies

TECHNOLOGY UTILIZATION PUBLICATIONS Information on technology used by NASA that may be of particular interest in commercial and other non-aerospace applications Publications include Tech Briefs, Technology Utilization Reports and Technology Surveys

Details on the availability of these publications may be obtained from:

SCIENTIFIC AND TECHNICAL INFORMATION OFFICE

NATIONAL AERONAUTICS AND SPACE ADMINISTRATION

Washington, D.C. 20546